MULTIPHASE FLOW RATE MEASUREMENT USING A NOVEL CONDUCTANCE VENTURI METER: EXPERIMENTAL AND THEORETICAL STUDY IN DIFFERENT FLOW REGIMES

Abbas Hameed Ali Mohamed Hasan

B.Sc., M.Sc.

A thesis submitted to the University of Huddersfield

in partial fulfilment of the requirements for

the degree of Doctor of Philosophy

The University of Huddersfield

November 2010

Declaration

No portion of the work referred to in this thesis has been submitted in support of an application for another degree or qualification of this or any other university or other institute of learning.

Acknowledgments

There have been a tremendous number of people who have helped me during the course of my PhD study. To name all would be impossible. However, there are a number of people to whom I owe my sincere gratitude.

I would like to express my deep and sincere gratitude to my supervisor, Professor Gary Lucas for his continuous guidance and encouragement and for his valuable advice, comments and suggestions throughout the PhD program at the University of Huddersfield. His wide knowledge and his logical way of thinking have been of great value for me. This thesis could not have been completed without his help and support.

Special thanks are to my parents without whose support and prayers nothing would have possible. I am also obliged to all other members of my family for their support and encouragement.

I owe a special dept of gratitude to my wife for her constructive advice, support and encouragement throughout my study and for understanding why I was so early rise and late to bed for so many months. Particular mention should also be made to my two daughters, in the hope that it will inspire them and others to continue their pursuit of knowledge.

Abstract

Multiphase flows, where two or even three fluids flow simultaneously in a pipe are becoming increasingly important in industry. Although much research has been done to measure the phase flow rates of two-phase flows using a Venturi meter, accurate flow rate measurements of two phase flows in vertical and horizontal pipes at different flow regimes using a Venturi meter remain elusive.

In water continuous multiphase flow, the electrical conductance technique has proven attractive for many industrial applications. In gas-water two phase flows, the electrical conductance technique can be used to measure the gas volume fraction. The electrical conductance is typically measured by passing a known electrical current through the flow and then measure the voltage drop between two electrodes in the pipe. Once the current and the voltage drop are obtained, the conductance (or resistance) of the mixture, which depends on the gas volume fraction in the water, can then be calculated.

The principal aim of the research described in this thesis was to develop a novel conductance multiphase flow meter which is capable of measuring the gas and the water flow rates in vertical annular flows and horizontal stratified gas water two phase flows.

This thesis investigates the homogenous and separated (vertical annular and horizontal stratified) gas-water two phase flows through Venturi meters. In bubbly (approximately homogenous) two phase flow, the universal Venturi meter (non-conductance Venturi) was used in conjunction with the Flow Density Meter, FDM (which is capable of measuring the gas volume fraction at the inlet of the Venturi) to measure the mixture flow rate using the homogenous flow model. Since the separated flow in a Venturi meter is highly complex and the application of the homogenous flow model could not be expected to lead to highly accurate results, a novel conductance multiphase flow meter, which consists of the Conductance Inlet Void Fraction Meter, CIVFM (that is capable of measuring the gas volume fraction at the inlet of the Venturi) and the Conductance Multiphase Venturi Meter, CMVM (that is capable of measuring the gas volume fraction at the throat of the Venturi) was designed and manufactured allowing the new separated flow model to be used to determine the gas and the water flow rates.

A new model for separated flows has been investigated. This model was used to calculate the phase flow rates of water and gas flows in a horizontal stratified flow. This model was also modified to be used in a vertical annular flow. The new separated flow model is based on the measurement of the gas volume fraction at the inlet and the throat of the Venturi meter rather than relying on prior knowledge of the mass flow quality x. Online measurement of x is difficult and not practical in nearly all multiphase flow applications. The advantage of the new model described in this thesis over the previous models available in the literature is that the new model does not require prior knowledge of the mass flow quality which makes the measurement technique described in this thesis more practical.

Contents

List of Figures

List of Tables

Nomenclature

Acronyms

CCCM	Conductance Cross Correlation Meter
CIVFM	Conductance Inlet Void Fraction Meter
CMVM	Conductance Multiphase Venturi Meter
cos	Cosine
DLFLS	Digital Liquid Film Level Sensor
dp	Differential Pressure
GVF	Gas Volume Fraction
I/V	Current-to-Voltage
SCRE	Segmental Conductive Ring Electrode

Symbols

A	Cross sectional area
A_{ste}	Steven constant; equation (2.60)
A_t	Area at the contraction
(BF)	Blockage factor
B_{ste}	Steven constant; equation (2.61)
C	Chisholm constant (Equation (2.40))
C_{Leeuw}	Modified Chisholm parameter defined by de Leeuw (Equation (2.55))
C_{ste}	Steven constant; equation (2.62)
$C_{d,\mathrm{hom}}$	Homogenous mixture discharge coefficient
$C_{dg,st}$	Gas discharge coefficient in a stratified gas-water two phase flow
$C_{dg,wg}$	Gas discharge coefficient in annular (wet gas) flow
$C_{dw,st}$	Water discharge coefficient in a stratified gas-water two phase flow
$C_{dw,wg}$	Water discharge coefficient in annular (wet gas) flow
D	Diameter

D_{ste}	Steven constant; equation (2.63)
D^*	Average diameter between the inlet (vertical pipe) and the throat of the Venturi
f	A single phase friction factor
Fr	Froude number
fq	Rotation frequency in a turbine flow meter
$F_{m,pipe}$	Frictional pressure loss term across a vertical pipe
F_{mv}	Frictional pressure loss (from inlet to the throat of the Venturi)
g	Acceleration of gravity
G_{mix}	Conductance of the mixture
h	Water level
h_c	Heights defined in Figure 3-6
h_i	Heights defined in Figure 3-6
h_p	Pressure tapping separation in a vertical pipe
h_t	Pressure tapping separation in a universal Venturi tube
h_{tt}	Heights defined in Figure 3-6
I	The intensity of a homogenous medium
I_{gas}	Intensity of the beam at the detector when the pipe is full of gas
I_{liq}	The intensity of the beam at the detector when the pipe is full of liquid
I_0	Initial radiation intensity
k	Flow coefficient (including the respective product of the velocity of approach, the discharge coefficient and the net expansion factor)
L	Distance between two sensors (Figure 2-12)
M_m	Relative molecular mass of the air
$\dot{m}$	Mass flow rate
$\dot{m}_T$	Total mass flow rate
n	de Leeuw number (Equations (2.52) and (2.53))
$O.R$	Over-reading factor
P	Static pressure

$\hat{P}$	Pressure ratio (Equation (3-37))
Q	Volumetric flow rate
$Q_{w,c}$	Water volume flow rate at the gas core
R	Radius (Figure 5-5))
r	Specific gas constant
$R_{xy}(\tau)$	Cross-correlation function
S	Slip ratio
S_m	Conductance of the mixture
$\overline{S}_{st}$	Ratio of the slip velocity (throat to inlet)
$\overline{U}$	Average fluid velocity
U	Velocity
U_h	Homogenous superficial velocity
U_h^*	Average homogenous velocity between inlet and the throat of the Venturi
u	Single phase (water) velocity
$U_{f,corr}$	liquid film velocity by cross-correlation technique
V	Dc output voltage
V_{VAF}	Dc output voltage from a Variable Area Flowmeter.
V_{SG}	Superficial gas velocity, Figure 1-2.
V_{SL}	Superficial liquid velocity, Figure 1-2.
x	Mass flow quality
X_{mod}	Modified Lockhart-Martinelli parameter
ΔP	Differential pressure drop
ΔP_{hom}	Differential pressure drop in a homogenous flow
ΔP_H	Magnitude of the hydrostatic head loss between the inlet and the throat of the CMVM in annular (wet gas) flow
ΔP_{TP}	Two phase pressure drop

Greek symbols

$\varepsilon_{Q_m,\text{hom}}$	Percentage error in the predicted mixture volumetric flow rate
$\varepsilon_{\dot{m}_{g,wg}}$	Percentage error in the predicted gas mass flow rate in a wet gas flow
$\varepsilon_{\dot{m}_{w,wg}}$	Percentage error in the predicted liquid film mass flow rate in a wet gas flow
$\varepsilon_{\dot{m}_{w,total,wg}}$	Percentage error in the predicted total water mass flow rate in a wet gas flow
$\varepsilon_{\dot{m}_{g,st}}$	Percentage error in the predicted gas mass flow rate in a stratified flow
$\varepsilon_{\dot{m}_{g,st}}$	Percentage error in the predicted water mass flow rate in a stratified flow
μ	Total attenuation coefficient per unit of length of the fluid
α	Gas volume fraction
τ	Variable time delay in cross-correlation technique
τ_p	Time shift between the maximum similarities in the two measurement signals
ρ	Fluid density
θ	Angle of inclination from vertical
γ	Specific heat ratio (adiabatic index)
$\overline{\alpha}$	Mean gas volume fraction (Equation (3-68))
δ	Water film thickness
σ	Conductivity
θ_{st}	Angle of stratified flow defined by (Figure 5-9))
$\alpha_{1,\text{hom}}\big\vert_{\Delta P_{\text{hom}}=0}$	Inlet gas volume fraction in a homogenous two phase flow when $\Delta P_{\text{hom}} = 0$
$\alpha_{1,\text{hom}}\big\vert_{\Delta P_{pipe}=0}$	Inlet gas volume fraction in a homogenous two phase flow when $\Delta P_{pipe} = 0$

Subscripts

1	inlet of the Venturi in separated flow model
2	throat of the Venturi in separated flow model
a	Upstream position in a vertical pipe (Figure 3-2)
b	Downstream position in a vertical pipe (Figure 3-2)
Chisholm	Chisholm correlation
deLeeuw	de Leeuw correlation
f	liquid (water) film
g	gas phase
g,st	gas in stratified gas water flow
g1	gas at inlet of the Venturi
g2	gas at throat of the Venturi
1,sim,ann	simulating annular flow at the inlet of CMVM
2,sim,ann	simulating annular flow at the throat of CMVM
1,sim,st	simulating stratified flow at the inlet of CMVM
2,sim,st	simulating stratified flow at the throat of CMVM
g1,st	gas phase at the Venturi inlet in a stratified flow
g2,st	gas phase at the Venturi throat in a stratified flow
g1,wg	gas at the inlet of the Venturi in wet gas flow
g2,wg	gas at the throat of the Venturi in wet gas flow
hom	Homogenous
l	liquid phase
Lin	Lin correlation
m	mixture
Murdock	Murdock correlation
o	Oil phase
pipe	Pipeline.
rod	nylon rod
ref	reference
s	superficial
S&L	Smith and Leang correlation
sw	Superficial water

sg	Superficial gas
st	stratified flow
TP	two phase
w	water phase
wg	wet gas
w,wg	water film in wet gas flow
wc	water at the gas core
w,total	total water (i.e. film+core)
w1,st	water phase at the Venturi inlet in a stratified flow
w2,st	water phase at the Venturi throat in a stratified flow

Chapter 1

Introduction

1.1 Introduction

The primary objective of the research described in this thesis was to develop a novel multiphase flow meter which, when combined with appropriate flow models would be capable of measuring the gas and the water flow rates in separated annular and stratified two phase flows. Measurement of the gas and the water flow rates in multiphase flow plays an important role in the oil, gas, chemical and nuclear industries.

In a multiphase flow, different components (e.g. gas and water) flow simultaneously in a pipe. Measurements of multiphase flow have been commonly accomplished by means of a test separator which separates the phases (for example, gas and water in two phase flows, and gas, water and oil in three phase flows) and then single phase flow meters can be used separately to measure the flow rate of each component (see Figure 1-1). This is the traditional solution employed in multiphase flow applications.

In many applications, well designed test separators can achieve accuracies of ±10% of the individual phases flow rates [1]. Although the separation technique is accurate, it is expensive and not practical in many sub-sea applications because it requires considerable space for the equipment and facilities. Nederveen (1989) [2] showed that a saving of up to $30 million would be achieved if the bulk separator on an offshore platform was replaced by a multiphase flow meter. For onshore applications, removing a separator could save up to $600,000.

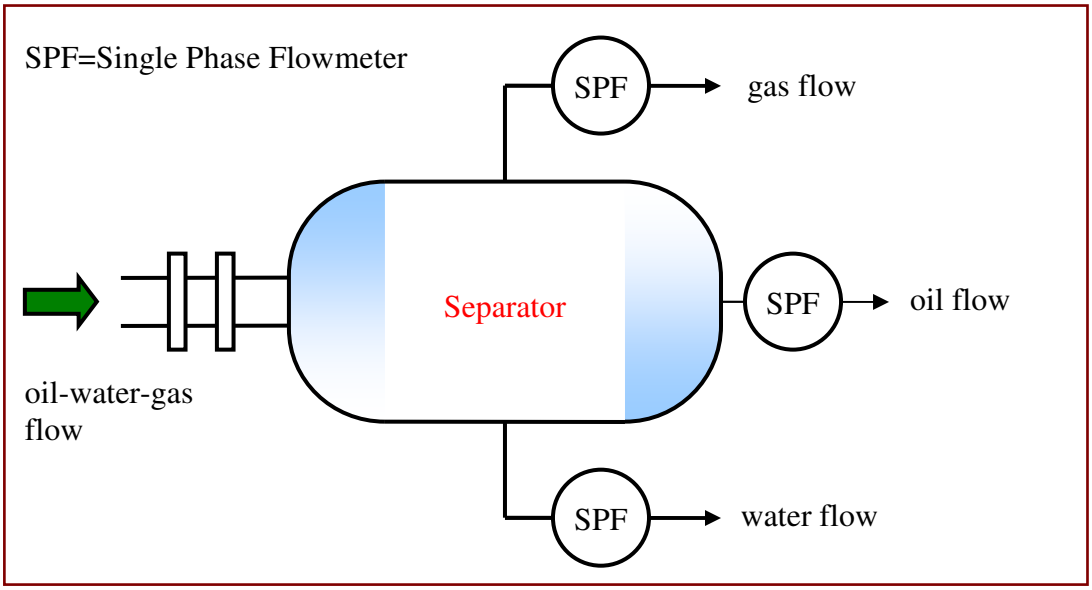

Figure 1-1: Traditional solution to the problem of metering multiphase flows

The phase separation technique has the following limitations:

(i) It is difficult to install on an offshore application where the base of a separator must be mounted on the sea bed (substantial work and effort is needed).

(ii) It takes a considerable time to test the oil or gas well compared with a multiphase flow meter. The response time of a separator may be hours while for a multiphase flow meter it may be minutes [2].

(iii) Maintenance work is quite difficult especially in sub-sea applications.

(iv) It is a very expensive technique.

As a result of the above limitations of the phase separation technique in multiphase flow applications, in-line multiphase flow meters are increasingly being designed for use in multiphase flow measurement applications. As the name suggests, “in-line” measurement techniques replace the test separator and the measurement of phase fractions, and phase flow rates is performed directly in the multiphase flow pipeline [3-5]. In-line measurement of the flow rate components of the multiphase flow is the goal of the current work.

The advantages of employing in-line multiphase flow meters over the phase separation technique in multiphase flow applications are;

(i) Multiphase flow meters (MPFMs) are more suitable for offshore applications because a MPFM is more compact and lighter than a test separator.
(ii) Instantaneous and continuous measurement of the phase fractions and phase flow rates can be achieved using multiphase flow meters. This is very important in detecting the variations in the phase fractions and the phase flow rates, especially, from unstable wells.
(iii) Less materials, equipment and human (oversight, maintenance, etc) resources are needed [6].
(iv) MPFMs can work under different pressure and temperature ranges.
(v) MPFMs can be used to obtain well test data more rapidly than conventional test separators [7].
(vi) MPFMs are cheaper than test separators.

To justify the above claims, in-line multiphase flow meters must satisfy the following criteria in terms of their design, accuracy, maintenance and life, see Table 1-1, [8].

Table 1-1: Desirable parameters of the multiphase flow meters

Range	Accuracy	Life time	Maintenance cost
0-100 % of phase	5% or less per phase	At least 10 years	Reasonable

The criteria for selection of the multiphase flow meters such as, accuracy, consistency, reliability and track record have been discussed in detail by [7,8].

Since the novel multiphase flow meter investigated in this thesis is used in multiphase flows, it is necessary to briefly describe the physics governing multiphase flows including the definition of multiphase flows, the gas-liquid flow patterns and the wet

gas flows. This is done in Section 1.2. Section 1.3 introduces specific areas of multiphase flows and the need for measuring multiphase flow properties. Following this the aim of the current research is presented (see Section 1.4). Finally, the layout of the thesis is given to help readers keep track of the work presented in this thesis.

1.2 Multiphase Flows

1.2.1 What are multiphase flows

Generally speaking, *multiphase flow* is a term used to describe a combination of two or more phases flowing simultaneously in a pipe. The term *phase* generally refers to a flow component rather than a state of matter. For example, gas-water flow is classified as a two phase flow (since two components are present in the flow, namely; the gas and the water) while oil-water-gas flow is classified as a three phase flow. Each phase can be defined in terms of the two main parameters: (i) the mean fractional volume occupied by each phase which is termed the mean *volume fraction*, and (ii) the mean velocity of each phase. Thus the sum of the volume fractions is unity. If the phases are well mixed and the velocities of all of the phases are equal then the mixture can be treated as *homogenous flow*. *Separated flow* is where each phase flows separately with its own velocity and there is little or no mixing of the phases. Examples of such flows are stratified and annular flows [9,10].

Although multiphase flows can take many forms in industrial applications, the term *multiphase flow* in this thesis generally refers to *gas-liquid* two phase flow, or to be specific, it refers to *air-water* two phase flow. The major flow regimes found in vertical and horizontal gas-liquid flows are described in Section 1.2.2.

1.2.2 Gas-liquid flow patterns

The major flow regimes found in 'vertical upward' and 'horizontal' gas-liquid two phase flows are shown in Figures 1-2 and 1-3.

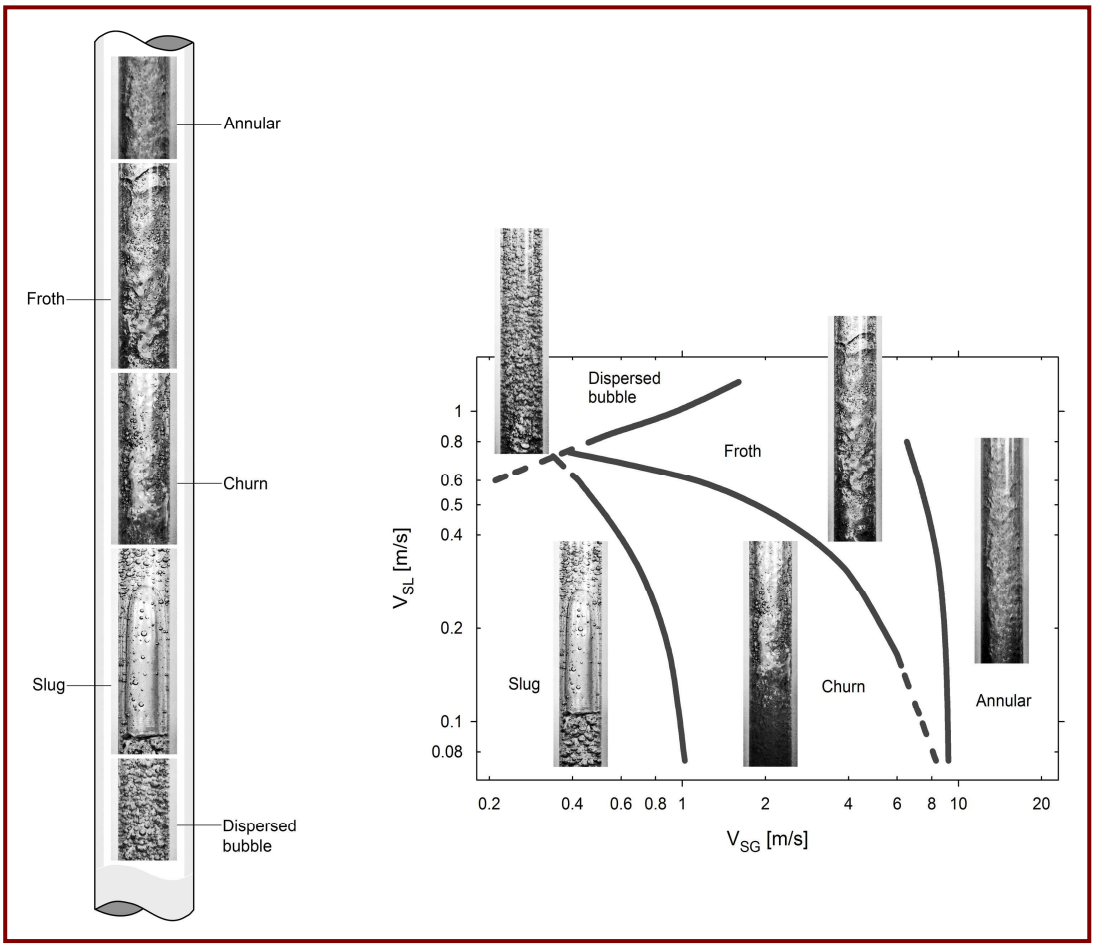

Figure 1-2: Flow regimes in vertical gas-liquid upflows [11]

In vertical gas-liquid flows, at low gas flow rates, the bubble flow regime predominates (see Figure 1-2). As the gas flow rate increases, collisions between bubbles will occur [12]. During these collisions, bubbles will coalesce, forming large gas bubbles (slugs). Small bubbles may be distributed throughout the liquid phase between slugs. A further increase in the gas flow rate causes the slugs to distort and break up to form the churn/froth flow regime. When the gas flow rate is large enough to support a liquid film at the wall of the pipe then the annular flow regime occurs in which a gas core flows at the centre of the pipe with some entrained liquid droplets while liquid film flows at the pipe wall.

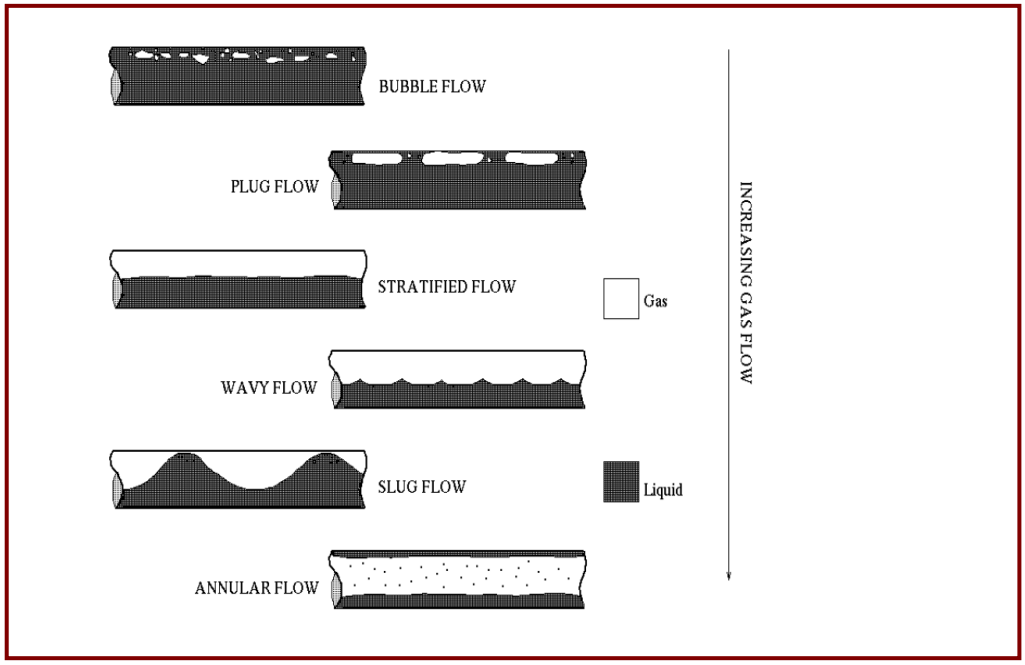

Figure 1-3: Flow regimes in horizontal gas-liquid flows [11]

Unlike the vertical flow regimes, the gas-water flow regimes in a horizontal pipe are affected by gravity which causes the gas phase to flow at the upper side of the horizontal pipe (see Figure-1.3). At low gas flow rates, the flow regime called bubbly flow again predominates. When the gas flow rate increases, the bubbles again coalesce to give rise to the plug flow regime. As the gas flow rate increases further, the plugs coalesce to form a smooth continuous layer, giving rise to the stratified flow regime where the gas phase flows at the top of the pipe and the liquid flows in the bottom portion of the pipe. In real industrial life, the gas-liquid interface in a stratified flow may not always be smooth, ripples may appear on the interface between the phases. If these ripples increase in amplitude due to increases in the gas flow rate then the flow regime moves from stratified flow to the wavy flow regime. A further increase in the gas flow rate causes large waves to occur which may hit the top of the pipe producing slug flow (see Figure 1-3). Annular flow in a horizontal pipe occurs at very high gas flow rates in which a gas core flows at the centre of the pipe and a liquid film at the wall of the pipe. Some entrained liquid droplets may occur within the gas core [13,14]. As can be seen from Figure 1-3, the liquid film in the annular flow regime is thicker at the bottom of the pipe than that at the top. This is due to the effects of gravity.

In the current research, the flow regimes that were studied in gas-water flows were the "vertical bubbly" flow regime, "vertical annular" flow regime and "horizontal stratified" flow regime. It should be noted that the vertical bubbly air-water two phase flows studied in this thesis were approximately homogenous (i.e. the average properties on the scale of a few bubble diameters were approximately the same everywhere in the flow). Therefore, whenever the readers come across the term "homogenous flow" throughout this thesis, it refers to vertical bubbly two phase flow, allowing the homogenous flow model described in Chapter 3 to be used.

1.2.2.1 Wet gas flows

The term '*wet gas flow*' has many definitions in the literature. Some researchers define a wet gas flow in terms of the gas volume fraction. Steven (2002) [15], for example, defines the '*wet gas flow*' as the flow with gas volume fraction greater than 95%. Others [16,17] state that the gas volume fraction in wet gas flow should be greater than 90%. Some authors define wet gas flows in terms of the Lockhart-Martinelli parameter, X, the ratio of the frictional pressure drop when the liquid phase flows alone to the frictional pressure drop when the gas phase flows alone in the pipe [18-20]. Mehdizadeh and Williamson (2004) [18] divided 'wet gas flow' into three types as shown in Table 1-2.

Table 1-2: Types of wet gas [18]

Type of Wet Gas	Lockhart-Martinelli parameter, X	Typical Applications
Type 1	$X \leq 0.025$	Type 1 wet gas measurement represents measurement systems at production wellheads, unprocessed gas pipelines, separators, allocation points, and well test facilities. Liquid measurement is necessary to make correction for improved gas measurements.

Type 2	$0.025 < X \leq 0.30$	Type 2 wet gas-metering systems cover higher liquid flow ranges so that the users often require more accurate gas and liquid flow rates. Applications include the flow stream at the production wellhead, co-mingled flow line, or well test applications.
Type 3	$X > 0.30$	Type 3 meter must make an oil, gas and water rate determination at relatively high GVF > 80% or $X \geq 0.3$. Typical application is gas condensate wells and gas lift wells.

In general [17], '*wet gas flow'* is defined as a gas flow which contains some liquid. The liquid volume fraction may vary between one application and another, though generally, the gas volume fraction should be greater than 90%. More information about wet gas flows and wet gas flow meters can be found, for example, in [21-26].

1.3 Existence of multiphase flows and the need for measuring their properties

Two phase or even three phase flows are commonly found in industry. The purpose of this section is merely to show the range of areas in which the current research could be applicable. The main industries and fields where multiphase flows exist are;

- Oil and gas industry
- Chemical industry

The relevant applications for multiphase flows are described below.

1.3.1 Oil and gas industry

The fluids extracted from oil wells are found as a mixture of liquid and gaseous hydrocarbons. In other words, the fluid produced from an oil well is a mixture of natural gas and oil but, in many applications, water is also present. Solid components (e.g. sand) may also be present in the mixture. Multiphase flows can be also found in natural gas gathering (from wellheads) and both onshore and offshore transmission pipelines. The term gathering refers to the transport process of the gas stream from its source (e.g. wellhead) to the processing facility. Multiphase flows are found in all

stages of the oil-gas production. These stages are drilling, extracting and also refining (the drilling and extracting operations are described later in this section). Therefore, various multiphase flow configurations may occur in the oil and gas production.

At this point, it is worthwhile to understand the fundamentals of an oil-gas-water production well. Fossil fuels are, essentially, made from the fossilized remains of plants, animals and microorganisms that lived millions of years ago. The question now is how do these living organisms turn into liquid or gaseous hydrocarbon mixtures?

There are many different theories which exist to describe the formation of oil and natural gas under the ground. The most widely accepted theory states that when the remains of plants and animals or any other organic materials are compressed under the earth at very high pressure for a long time (millions of years), fossil fuels are formed. With the passage of time, mineral deposits formed on top of the organisms and effectively buried them under rock. The pressure and temperature then increased. For these conditions, and possibly other unknown factors, organic materials broke down into fossil fuels.

Some people think that the oil under the earth is found in pools of liquid oil. In fact, oil reservoirs are made up of layers of porous, sedimentary rock with a denser, impermeable layer of rock on top which trap the oil and the gas (see Figure 1-4). Oil marinades into the porous rocks making them saturated like a wet sponge [27]. Water may also exist underneath the oil in the oil reservoir.

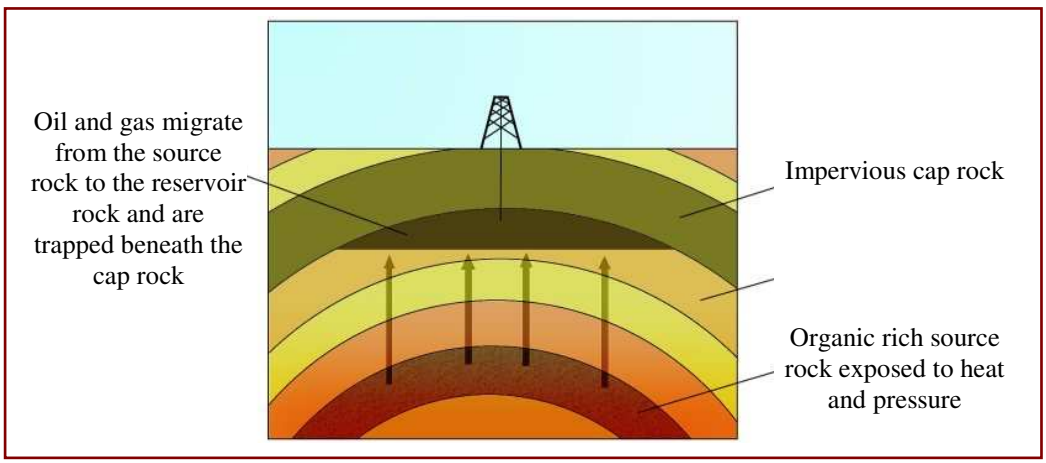

Figure 1-4: Conventional oil reservoir

To extract the oil from an oil reservoir, an oil well must be drilled. This process is called 'drilling process' and is illustrated below.

A drilling mud is a fluid which is pumped into the well during the oil well drilling process. The purpose of pumping this fluid into the well during the drilling operation is to lift the drilling cuttings, which accumulate at the bottom of the well, up to the well bore (see Figure 1-5).

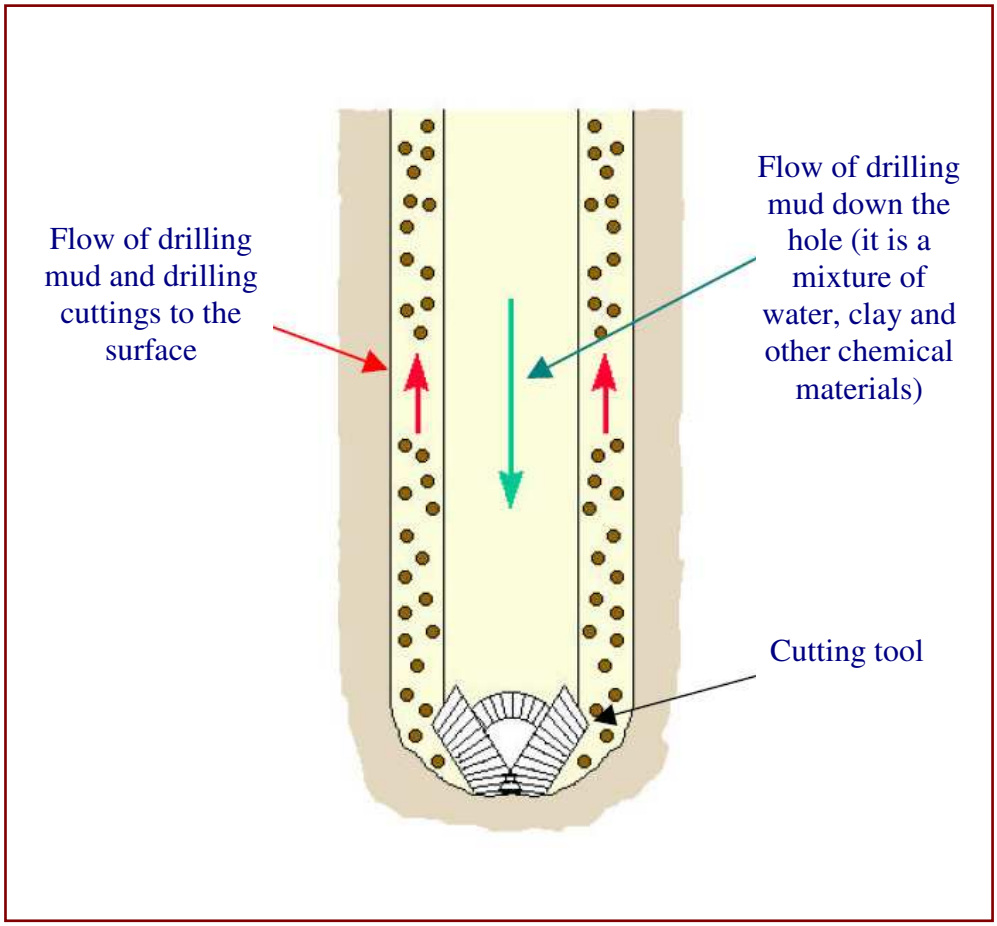

Figure 1-5: Schematic diagram of the oil well drilling process

Once the drilling operation is finished, oil can then be extracted using one of the oil extraction techniques. There are many techniques used in oil extraction, and the two most common are described below [27].

(i) Oil pump extraction

Once the drilling process is completed (see Figure 1-5) the drilling rig is removed and a pump is placed on the well head as shown in Figure 1-6. The principle of operation of this system is that an electric motor which is placed on the ground surface drives a gear box that moves a lever (pitman arm) which is connected to the polishing rod through the walking beam. Any movement on the lever will move the polishing rod up and down (see Figure 1-6). The polishing rod is attached to a sucker rod, which is attached to a pump (placed underground). The purpose of this pump is to lower the pressure above the oil and so allow the oil to be forced up through the well head.

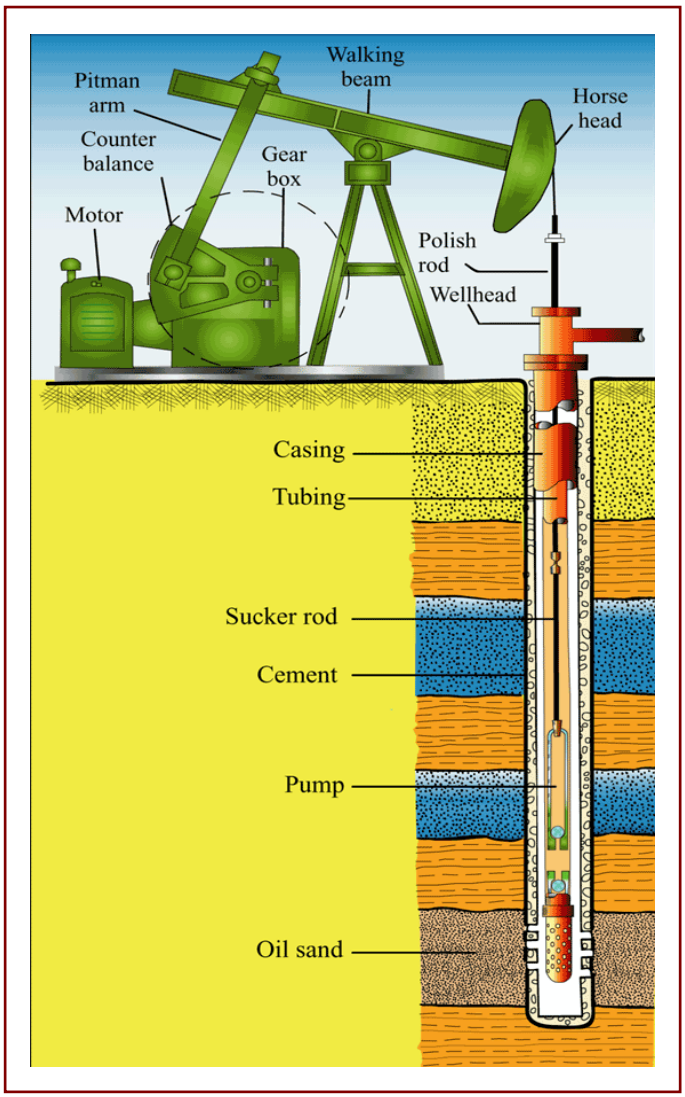

Figure 1-6: Oil pump extraction technique

(ii) Thermally enhanced oil recovery method (TEOR)

In some cases, the oil is too heavy to flow up the well. To overcome this problem another well can be drilled adjacent to the production well, and through which steam under high pressure is injected into the second well (see Figure 1.7). Injection of steam into the reservoir also creates high pressure which helps push the oil up the well [27,28].

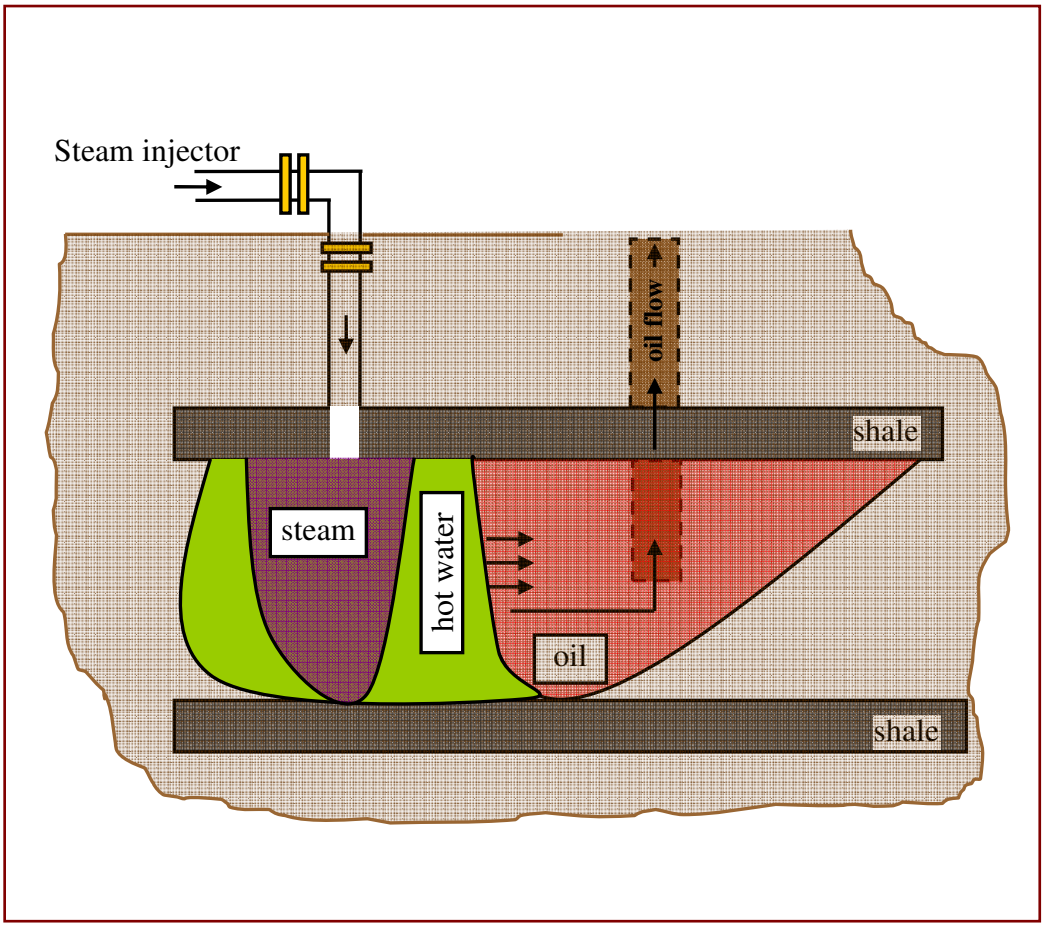

Figure 1-7: TEOR method

It should be noted that during the oil extraction processes, gas and water may be present in the flow. To measure the individual phase flow rates in such flows,

measurement of the multiphase flow properties (e.g. the mean volume fraction and the mean velocity of each phase) in the oil and gas industry is necessary.

1.3.2 Chemical industry

Multiphase flows occur in many chemical processes. In chemical processes that involve gas-liquid reactions, the contact between phases has to be sufficient to achieve optimal performance [29]. Gas-liquid two phase flows can be found in many chemical reactions such as chlorination, oxidation and aerobic fermentation reactions. To achieve optimal performance in chemical processes which involve such reactions, an accurate measurement of the mass transfer rate of the two phases and the interfacial area per unit volume must be performed [30].

One of the most important devices in the chemical industry which involves multiphase flow is the bubble column reactor. Bubble column reactors provide several advantages in terms of design and operation over other reactors such as, excellent heat and mass transfer rate characteristics [31,32], high thermal stability, lack of mechanical moving parts, high durability of the catalyst material, online flexibility for catalyst addition/withdrawal during the process, little maintenance and low operational costs.

In bubble column reactors, the gas volume fraction, bubble characteristics, local and mean heat transfer characteristics and mass transfer characteristics are all important in design and operation of the bubble columns. Therefore, measurements of multiphase flow parameters are important in order to achieve optimal performance in bubble column reactors [33-38].

The other two types of multiphase reactors are fluidized bed reactor and fixed or packed trickle bed reactor. A comprehensive description of these types of reactors can be found in [39-46].

1.4 Aims of the present work

The main aim of the research described in this thesis is to develop new techniques for accurate phase flow rate measurement in separated annular and stratified flows. The intention is to design a novel multiphase flow meter which is capable of measuring the gas and the water flow rates in two phase, water-gas, water continuous, vertical annular flows and horizontal stratified flows. A further aim is to investigate the use of the Universal Venturi Tube (UVT) in bubbly (approximately homogenous) gas-water two phase flows. The objectives, providing the solution to achieve the aims, are outlined below.

Objectives

1. To investigate a mathematical flow model for bubbly (approximately homogenous) gas-water two phase flows through a UVT, predicting the mixture (homogenous) flow rate.

2. To develop an integrated system comprising the UVT and the flow density meter, allowing the homogenous flow model to be used to determine the mixture flow rate in bubbly (approximately homogenous) gas-water two phase flows.

3. To develop a novel mathematical flow model for separated horizontal stratified gas-water two phase flows through a Venturi meter, predicting the gas and the water flow rates.

4. To investigate a new mathematical flow model for separated vertical (wet gas) flows through a Venturi meter, predicting the gas and the water flow rates.

5. To design a novel conductance multiphase flow meter, allowing the separated annular and stratified flow models (which will be investigated to achieve the objectives (3) and (4) above) to be used to determine the gas and the water flow rates.

6. To calibrate the conductance multiphase flow meter in simulated annular and stratified flows.

1.5 Thesis Overview

The underlying theme of the work described in this thesis is that of the use of Venturi meters in bubbly, stratified and annular gas-water two phase flows. This section gives the reader a brief description of the contents of each subsequent chapter of this thesis.

CHAPTER 2 This chapter describes previous relevant research. A review of existing techniques for measuring multiphase flows is presented. The correlations that are used in calculating two phase flow rates using Venturi meters and orifice plates (i.e. Murdock, Chisholm, Smith and Leang, Lin, de Leeuw and Steven correlations) are also discussed in this chapter.

CHAPTER 3 This chapter describes the mathematical modelling of the Venturi meter in bubbly (that are assumed to be approximately homogenous), stratified and annular two phase flows. This chapter introduces a homogenous gas-water two phase flow model through a UVT (non-conductance Venturi). A novel stratified and annular flow model which depends on the measurement of the gas volume fraction at the inlet and the throat of the Venturi is described.

CHAPTER 4 The design and construction of the flow density meter, UVT, the conductance multiphase flow meter (Conductance Inlet Void Fraction Meter, CIVFM, and Conductance Multiphase Venturi Meter, CMVM) is described in this chapter. The UVT is used in conjunction with the flow density meter to study the homogenous two phase flow while the conductance multiphase

flow meter is used to study separated (vertical annular and horizontal stratified) gas-water two phase flows.

CHAPTER 5 In this chapter, the bench tests on the CIVFM and the CMVM are performed. To simulate the film thickness (and hence the liquid volume fraction) in annular flow through a conductance multiphase flow meter different diameter nylon rods were inserted through the CIVFM and the throat section of the CMVM whilst the gap between the outer surface of the nylon rod and the inner surface of the pipe wall was filled with water, representing the water film in a real annular flow situation. For simulated horizontal stratified flows, the conductance multiphase flow meter was mounted horizontally and was statically calibrated by varying the level of water at the inlet and the throat of the Venturi. The height of water at the inlet of the Venturi was then related to the inlet water volume fraction while the water volume fraction at the throat of the Venturi was obtained from the height of the water at the throat section of the CMVM. Once the value of the water volume fraction at a given position in the Venturi was known the gas volume fraction could easily be found since the sum of the gas and liquid volume fractions is always unity.

CHAPTER 6 This chapter introduces the experimental apparatus and procedures to carry out flow measurement of two phase flows using a Venturi meter in different horizontal and vertical flow regimes. The calibration procedures for the reference equipment are also described.

CHAPTER 7 The results from the bubbly (approximately homogenous) gas-water two phase flow experiments using the UVT and the flow density meter are discussed.

CHAPTER 8 This chapter discusses the results obtained from the conductance multiphase flow meter in annular gas-water two phase flows. An alternative technique of measuring the liquid flow rate using wall conductance sensors is also presented.

CHAPTER 9 This chapter presents the experimental results obtained from the conductance multiphase flow meter in horizontal stratified gas-water two phase flows. Predicted gas and water flow rates in a stratified gas-water two phase flow were obtained from the conductance multiphase flow meter and compared with reference gas and water flow rates.

CHAPTER 10 The conclusions of the thesis are presented in this chapter.

CHAPTER 11 This chapter presents recommendations and suggestions for further work.

Chapter 2

Previous Relevant Research on Multiphase Flow Measurement

Introduction

In industrial processes, the need for measuring the fluid flow rate arises frequently. Accurate and repeatable flow rate measurements are necessary for process development and control.

Differential pressure devices (e.g. orifice plate and Venturi meter) have been widely used as two phase flow meters and considerable theoretical and experimental studies have been published. The study of multiphase flow through Venturi and orifice meters are described for example by; Murdock (1962) [47], Chisholm (1967,1977) [48,49], Smith and Leang (1975) [50], Lin (1982) [51], de Leeuw (1994,1997) [52,53] and Steven (2002) [15].

In this chapter, a review of existing techniques for measuring multiphase flows is presented in Section 2.1. Following this, the previous correlations listed above with their flow conditions, assumptions and limitations are described (see Section 2.2).

It should be noted that the purpose of presenting the previous correlations for the differential pressure devices (Venturis and orifice plates) in this chapter is mainly to show that all of them depend on prior knowledge of the mass flow quality, x, which is defined as the ratio of the gas mass flow rate to the total mass flow rate. Therefore, the study of the previous correlations described in Section 2.2 is not intended to give more details about how the gas and the water mass flow rates are derived. For more

details regarding the derivation of the gas and the water mass flow rates presented in Section 2.2, refer to the author's M.Sc. dissertation [54]. In fact, online measurement of the mass flow quality, x, is difficult and not practical in nearly all multiphase flow applications. Therefore, the presentation of these correlations in this chapter is to assist the study and development of the new separated flow model (see Chapter 3) which depends on the measurement of the gas volume fraction at the inlet and the throat of the Venturi instead of relying on prior knowledge of the mass flow quality, x, as in previous correlations.

2.1 A review of existing techniques for measuring multiphase flows

Existing multiphase flow measurement techniques can be classified into two main categories; 'invasive techniques' and the 'non-invasive techniques'. The difference between these two categories is that with an invasive technique, the sensor is placed (physically) in a direct contact with the fluid flow to measure the flow parameters. For a non-invasive technique, the sensing element does not directly interfere with the flow. For example, a hot film anemometer is an invasive technique while the differential pressure technique in multiphase flows is classified as non-invasive.

Measuring techniques for multiphase flow can be accomplished either locally or globally. 'Local measurement' is a term used to describe the measurement of a specific parameter in a multiphase flow at a predefined position (single point) in a pipeline. 'Global measurements' give mean values of the multiphase flow (e.g. the mean volume fraction and the mean velocity and hence, the mean flow rate). For example, the conductive needle probes in bubbly two phase flow can be regarded as a local measurement. The ultrasound attenuation method is an example of global measurement.

This section is not intended to describe all multiphase flow measurement techniques available in the literature but only to highlight the most common principles used for measuring the phase velocity and the phase fraction in multiphase flow technologies.

2.1.1 Phase fraction measurement

In general, most of the multiphase flow meters available on the market today use one of the following methods to measure the phase volume fraction.

2.1.1.1 Differential pressure technique

The differential pressure technique is a non-invasive technique and can be considered as a global measurement. The differential pressure technique has proven attractive in the measurement of volume fraction. It is simple in operation, easy to handle and low cost. In a multiphase flow, differential pressure techniques can be used to measure the mean volume fraction in vertical and inclined flows. Differential pressure techniques may also provide information on the flow regime, especially, the slug flow regime where the fluctuations in the pressure drop can be easily indentified [55-57]. Detailed information about the numerical techniques used in multiphase flows to study the fluctuations in the differential pressure signal can be found in [58-61].

In the current research, the differential pressure technique is used to measure the gas volume fraction $\alpha_{1,\mathrm{hom}}$ in bubbly (approximately homogenous) gas-water two phase flows at the upstream section of the UVT. This technique is discussed, in detail, in Section 3.1.1.

In bubbly gas-water two phase flows, the gas volume fraction $\alpha_{1,\mathrm{hom}}$ obtained from the differential pressure technique is given by (see Section 3.1.1 for full derivations);

$$\alpha_{1,\mathrm{hom}} = \frac{\left(\Delta P_{pipe} + F_{m,pipe}\right)}{g h_P \cos\theta(\rho_w - \rho_g)}$$

Equation (2.1)

where ΔP_{pipe} is the pressure drop across the pipe (between the pressure tappings), $F_{m,pipe}$ is the frictional pressure loss term between the pressure tappings, h_p is the pressure tapping separation, ρ_w and ρ_g are the water and the gas densities respectively, g is the acceleration of the gravity and θ is the angle of inclination from vertical.

The flow density meter (FDM) which is based on the differential pressure technique was designed as part of the current study to measure the mean gas volume fraction at the inlet of the UVT (see Chapter 4, Section 4.1 for more information).

2.1.1.2 Electrical conductance technique

Electrical conductance technique is used to measure the phase volume fraction in water continuous, multiphase flows. This technique has proven attractive for many industrial applications due to its fast response and relative simplicity in operation. Early work on this technique was proposed by Spigt (1966) [62] and Olsen (1967) [63] who studied the method and the design of electrodes. Olsen (1967) [63] showed that the ring electrodes were preferable for fixed field application rather than using electrodes which interfered with the flow. Barnea et al. (1980) [14], Tsochatzidis et al. (1992) [64], Zheng et al. (1992) [65], Fossa (1998) [66] are some of the many who used the conductance technique in multiphase flows.

In multiphase flow applications, electrical conductance varies with concentration and distribution of the phases. The electrical conductance is typically measured by passing a known electrical current through the flow and then measuring the voltage drop between two electrodes in the pipe. Once the current and the voltage drop are obtained, the conductance (or resistance) of the mixture can be calculated [67].

The conductance technique is the basis of the current research. In other words, the gas volume fractions at the inlet and the throat of the Venturi in horizontal stratified gas-water two phase flows and annular (wet gas) flows were measured using two ring electrodes flush mounted with the inner surface of the Venturi inlet, and two ring electrodes flush mounted with inner surface of the Venturi throat (see Chapter 4 for more details). The design and calibration of the novel conductance multiphase flow meter investigated in this thesis is described, in detail, in Chapters 4, and 5.

The basic operation of the electrical conductance technique in gas-water two phase flows is that the conductance of the mixture depends on the gas volume fraction in the

water. The conductance of the mixture G_{mix} can be calculated using the circuit shown in Figure 2-1 (see also the full diagram of the electronic circuit in Section 4.5).

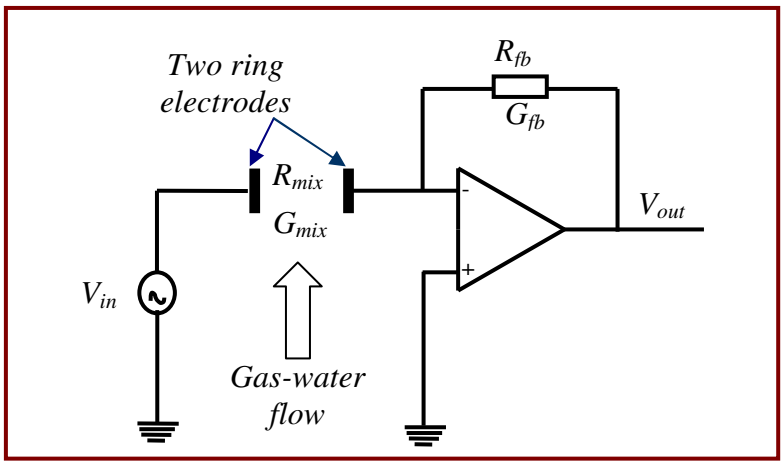

Figure 2-1: Fluid conductance circuit

From Figure 2-1, the output voltage V_{out} can be written as;

$$V_{out} = -\frac{R_{fb}}{R_{mix}} V_{in}$$

Equation (2.2)

where R_{mix} is the resistance of the mixture.

By definition the conductance *G* is the reciprocal of the resistance. Therefore, Equation (2.2) can be re-written as;

$$V_{out} = -\frac{G_{mix}}{G_{fb}} V_{in}$$

Equation (2.3)

where G_{mix} is the conductance of the mixture.

The conductance decreases with increasing gas volume fraction and increases with increasing water volume fraction as shown in Figure 2-2.

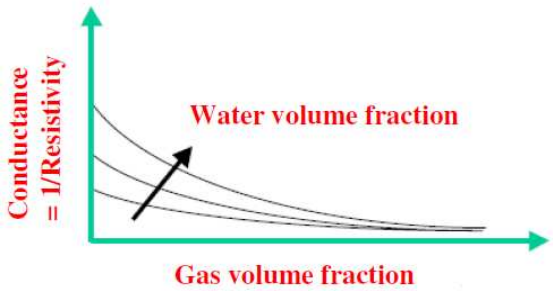

Figure 2-2: Variation of the conductance with gas and water volume fractions

The choice of excitation frequency is very important because it can affect the operation of the conductance sensor. At low frequencies, the conductance between the electrodes is affected by a number of capacitive and resistive elements that arise at the electrode-electrolyte interface. This is commonly referred to the 'double layer' effect [33]. The excitation frequency should be high enough to eliminate this double layer effect [68]. Considerable studies have been published to study the influence of frequency of the signal on the measurement of the conductance system. It has generally been concluded that frequencies of at least 10kHz should be used [69]. In the current research, the amplitude and frequency of the excitation voltage were 2.12V p-p and 10kHz respectively.

2.1.1.3 Electrical capacitance technique

The first systematic study of the capacitance technique in multiphase flow measurement was carried out by Abouelwafa et al. (1980) [70]. Electrical capacitance is a non-invasive technique and can be used for volume fraction measurement in multiphase flows only when the continuous phase is non-conducting (e.g. oil continuous, oil-water two phase flow).

A typical capacitance system consists of two electrodes (different configurations and more than two sensors might be used, refer for example, to [71]) placed on each side of the flowing medium. The basic physics behind the capacitance technique is that the capacitance depends on the permittivity (dielectric) of the mixture between two electrodes. The permittivity of the mixture varies with the amount of oil, gas and water in the mixture.

From Maxwell's equations [72], the formula which describes the relationship between permittivity (also known as dielectric constant) of an oil-gas mixture and the gas volume fraction α is given by;

$$\varepsilon_{m,o-g} = \varepsilon_o \frac{2\varepsilon_o + \varepsilon_g - 2\alpha(\varepsilon_o - \varepsilon_g)}{2\varepsilon_o + \varepsilon_g + \alpha(\varepsilon_o - \varepsilon_g)}$$

Equation (2.4)

where $\varepsilon_{m,o-g}$ is the permittivity of the oil-gas mixture, α is the gas volume fraction, ε_o is the permittivity of oil and ε_g is the permittivity of gas.

Maxwell's equation can also be used for oil-water flows. Equation (2.5a) gives the relationship which expresses the permittivity of the oil-water mixture $\varepsilon_{m,o-w}$ in terms of the permittivity ε_w of the dispersed phase (water), the permittivity ε_o of the continuous phase (oil) and the volume fraction α_w of dispersed phase (water).

$$\varepsilon_{m,o-w} = \varepsilon_o \frac{2\varepsilon_o + \varepsilon_w - 2\alpha_w(\varepsilon_o - \varepsilon_w)}{2\varepsilon_o + \varepsilon_w + \alpha_w(\varepsilon_o - \varepsilon_w)}$$

Equation (2.5a)

In oil-water-gas mixtures, the formula which expresses the permittivity ε_m of the oil-water-gas mixture in terms of the permittivity ε_{liq} of the liquid (oil and water), the permittivity ε_g of the gas and the gas volume fraction α is [73];

$$\varepsilon_m = \varepsilon_{liq} \frac{2\varepsilon_{liq} + \varepsilon_g - 2\alpha(\varepsilon_{liq} - \varepsilon_g)}{2\varepsilon_{liq} + \varepsilon_g + \alpha(\varepsilon_{liq} - \varepsilon_g)}$$

Equation (2.5b)

It should be noted that, the capacitance technique is used only when the continuous phase is non-conducting. However, if the continuous phase is conducting (e.g. gas–water two-phase flow), the Maxwell equation is given by;

$$\sigma_m = \frac{2\sigma_w(1-\alpha)}{\alpha + 2}$$

Equation (2.6)

where σ_m and σ_w are the conductivities of the mixture and water respectively and α is the gas volume fraction.

An extensive review of the electrical capacitance technique in multiphase flows was provided, for example, by Beek (1967) [74], Ramu and Rao (1973) [75], Shu et al. (1982) [76] and May et al. (2008) [77].

2.1.1.4 Gamma ray attenuation

The gamma ray attenuation technique has been extensively used to measure the average gas and liquid volume fraction of gas-liquid two phase flows [78]. The idea behind this technique is that gamma rays are absorbed at different rates by different materials. The measurement of component ratios in multiphase flow using gamma-ray attenuation was first suggested by Abouelwafa and Kendall (1980) [79].

A gamma-ray densitometer consists of a radioactive source and a detector placed in a way so that the beam of gamma rays passes through the flow and is monitored on the opposite side of the multiphase mixture. The amount of radiation that is absorbed or scattered by the fluid is a function of both the density and the energy level of the source (see Figure 2-3).

For a homogenous medium, the intensity *I*, of the received beam at the detector is given by;

$$I = I_0 e^{-\mu z}$$

Equation (2.7)

where I_0 is the initial radiation intensity, μ is the total attenuation coefficient per unit of length of the fluid and *z* is the gamma ray path length through the medium.

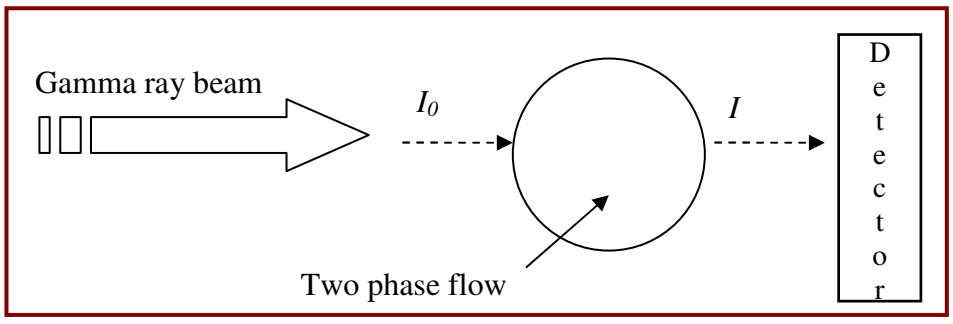

Figure 2-3: Gamma ray attenuation

Petrick and Swanson (1958) [80] studied how the distribution of the phases within the flow effects the measurement of the void fraction. In this study, two hypothetical flows were studied as described below.

(i) In the first case, they proposed a hypothetical flow where the phases (i.e. gas and liquid) are arranged in layers at right angles to the radiation beam as shown in Figure 2-4 (see also Lucas (1987) [81]).

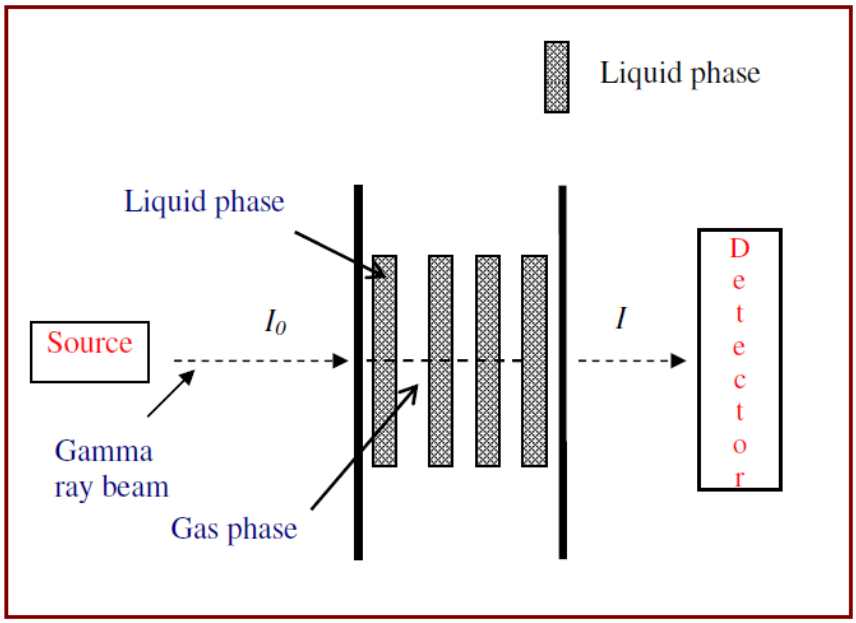

Figure 2-4: Gamma ray densitometer: A hypothetical flow where the liquid and gas phases are in Layers perpendicular to the radiation beam

For the above case, the void fraction is given by;

$$\alpha = \frac{\ln\left(\frac{I}{I_{liq}}\right)}{\ln\left(\frac{I_g}{I_{liq}}\right)}$$

Equation (2.8)

where I is the intensity of the received beam at the detector in the presence of the homogeneous mixture, I_{liq} is the intensity of the received beam at the detector with the pipe full of liquid only and I_g is the intensity of the received beam at the detector with the pipe full of gas only.

(ii) In the second case, they considered a hypothetical flow where the phases are arranged in layers parallel to the beam as shown in Figure 2-5.

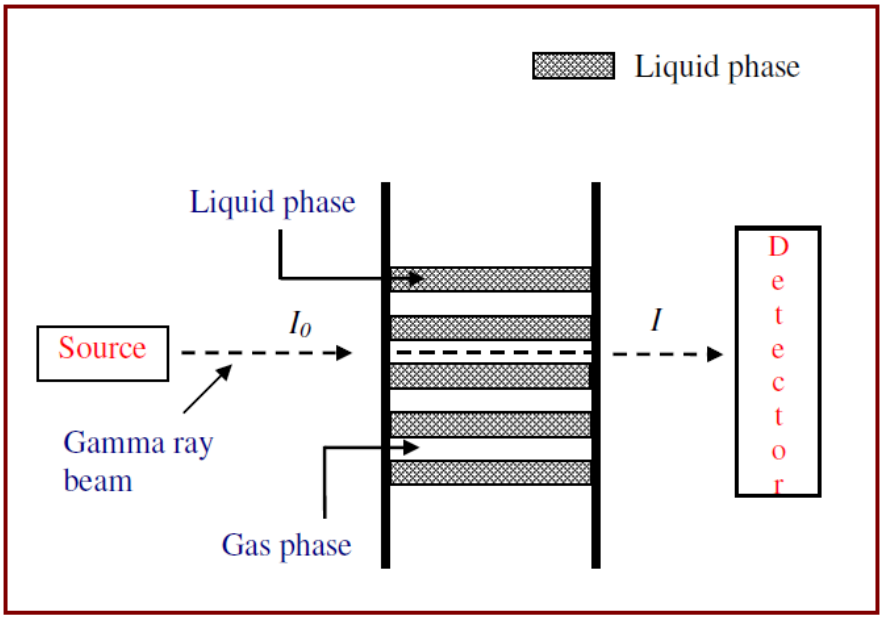

Figure 2-5: Gamma ray densitometer: A hypothetical flow where the phases are arranged in Layers parallel to the radiation beam

If the beam applied is horizontal to the fluid layers then the void fraction is given by;

$$\alpha = \frac{I - I_{liq}}{\mathrm{I_g} - I_{liq}}$$

Equation (2.9)

The Gamma-ray detector can be calibrated by performing a static test on the known single phase fluid. This can be achieved by isolating the multiphase flow meter first and then performing a static single test measurement on a single phase flow.

One of the major limitations of the single beam gamma ray attenuation technique described above is that the average void fraction is measured across a single pipe diameter. In other words, the estimated value of the void fraction may not represent the true value of the actual mean void fraction within the mixture. To overcome this problem, dual or multiple energy gamma ray attenuation methods can be used. For

more information on dual and multiple gamma ray attenuation techniques refer for example, to [80,82-87].

2.1.1.5 Quick closing valve technique

This technique is a common technique for measuring the average gas volume fraction in gas-liquid two phase flows. The basic idea behind this technique is that, by simultaneously closing valves at either end of the test section the gas and the liquid can be trapped see Figure 2-6.

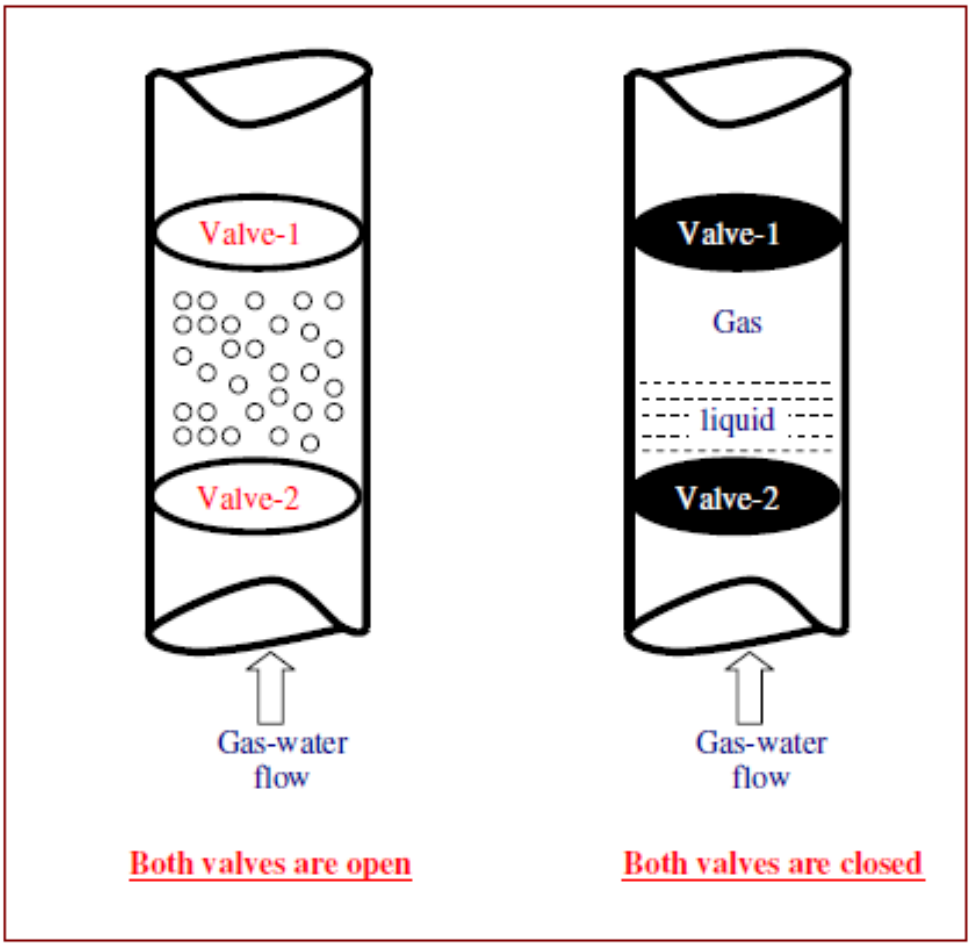

Figure 2-6: Quick closing valve technique

The mean gas volume fraction α can then be calculated using;

$$\alpha = \left[\frac{\text{volume of the gas trapped in the test section}}{\text{total volume of the test section (i.e.total volumes between the valves)}} \right]$$

Equation (2.10)

Once the mean gas volume fraction α is obtained, the mean liquid volume fraction α_{liq} can be easily determined using;

$$\alpha_{liq} = 1 - \alpha$$

Equation (2.11)

For more information about quick closing valve technique, see for example, [88,89]

2.1.1.6 Electrical impedance tomography (EIT)

Electrical impedance tomography (EIT) is a non- invasive visualisation technique that allows imaging of the distribution of electrical properties (e.g. capacitance and resistance) of a multiphase flow within a medium (e.g. a pipe). The idea of EIT is to reconstruct an image of a component based on its spatial distribution of electrical properties [90,91]. This enables the phase fractions to be measured.

The main electrical properties measured with EIT are resistance and capacitance. The electrical properties of multiphase flows will specify the type of the electrical impedance tomography system. Therefore, if the measured property is resistance then the electrical resistance tomography (ERT) is used but if the measured property is capacitance then the electrical capacitance tomography is used (ECT). It should be noted that ERT is appropriate for a conductive multiphase mixture where the continuous phase is a conductive phase while ECT is used in a non-conductive multiphase mixture. More information regarding EIT can be found in [92-97]

2.1.1.7 Sampling technique

One of the sampling techniques in a multiphase flow technology is called ‘internal’ or ‘grab’ sampling. As the name indicates, internal or grab sampling is a process

whereby part (a sample) of a multiphase flow is periodically extracted from the main stream in order to provide information on the composition of the main flow. This technique is usually used in oil industry, where the oil-gas-water flow is present, to give information on the amount of water present in the oil.
The idea behind this technique is that a tubular probe with an orifice plate is inserted inside the pipe. The orifice plate is used to homogenise the flow. A valve is installed on the sampling line which is opened for a short time at regular intervals. When suction is applied to the tube, the small volume of fluid can be extracted periodically into the collection vessel. The relative amounts of each component can then be measured. The composition of the entire flow in a pipeline is then determined by taking the average value of these samples over appropriate periods of time.

The major limitation of this technique is that the flow must be homogenised since only one single probe is used. In other words, the water and oil must be well mixed upstream of the sampling probe otherwise significant error might occur. An extensive review on this technique was given by [98,99].

Another sampling technique used in multiphase flow is 'Isokinetic sampling'. This technique is used for extracting a sample from a multiphase flowing stream at the same velocity as the fluid being sampled. The purpose of using this technique is to obtain a sample which represents the actual local composition of the bulk fluid in multiphase flows. The sampling probe is smaller than that used in the 'grab' sampling. Again, the major limitation of this technique is that the fluid needs to be homogenised. For non-homogenous two phase flows, the phases have different velocities and the use of isokinetic sampling in such cases is difficult [100-103].

2.1.2 Phase velocity measurement

2.1.2.1 Venturi meter

A Venturi is basically designed to be used in a single phase flow. The use of a Venturi meter in a single phase flow is well understood and described in ISO 5167:2003. However, the equations described by ISO standard for the Venturi in a single phase flow cannot be directly applied to multiphase flows without correction.

Considerable theoretical and experimental studies have been published to describe mathematical models of Venturi meters in multiphase flow applications including its use in vertical and horizontal flows. The study of multiphase flow through contraction meters are described for example by; [47,104,48-50,105-107,51,108-112,52,53,113,15,114-116].

Venturi meters are often used to measure the velocity of the multiphase flow. The Venturi meter, see Figure 2-7, consists of an upstream section (a), a convergent section (b), a throat section (c), a divergent section (d) and an outlet section (e). The principle of operation of the Venturi meter is that the fluid entering the Venturi is accelerated to a higher velocity as the flow area is decreased. In other words, at the throat, the pressure decreases to a minimum where the velocity increases to a maximum. If the area between an upstream section and the throat section are well designed, the relationship between the differential pressure across the Venturi meter and the velocity of the fluid (and hence the mass/volume flow rate) can be expressed in terms of Bernoulli's equation. It should be noted that in multiphase flow measurements, the relationship between the flow rate and the pressure drop across the Venturi meter is complex and not simple as in single phase flow and should include the flow quality or the phase holdups.

The Venturi meter is essential to the current research. Two Venturis were used in this thesis. The first one was the Universal Venturi Tube, UVT, which was used to study the bubbly gas-water flows, and the second one was the conductance Venturi meter which was used in vertical annular (wet gas) flows and horizontal stratified two phase flows. For more information regarding the design and the flow model of these Venturis, see Chapters 3 and 4.

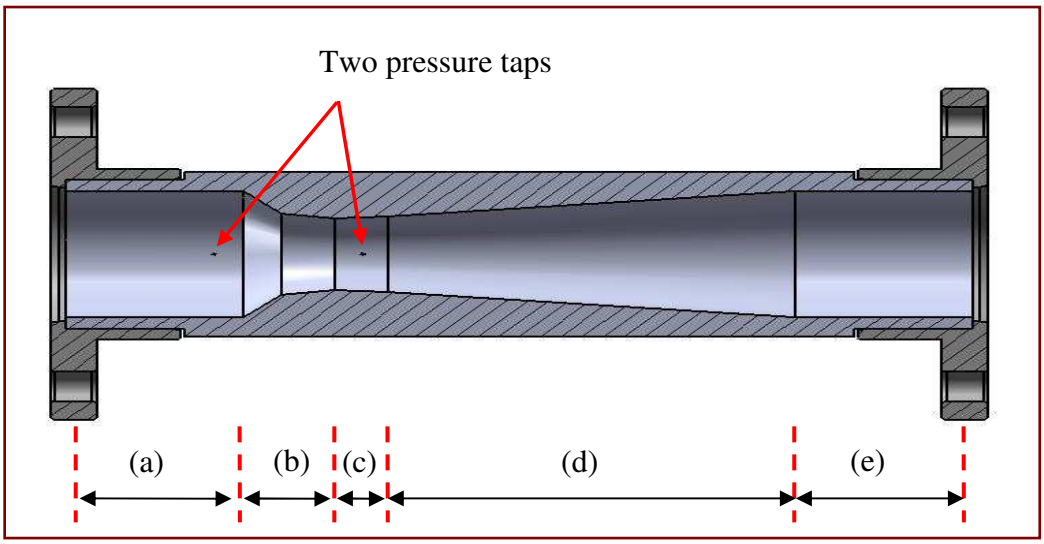

Figure 2-7: A Venturi meter

2.1.2.2 Acoustic pulse technique

Acoustic techniques are widely used in multiphase flow applications. The principle of operation of this technique is that an acoustic pulse is sent through the fluid between two transducers placed on either side of the pipe as shown in Figure 2-8. First of all, the pulse is sent from the downstream transducer to the upstream transducer and then from the upstream transducer to the downstream transducer. The travel time of the pulse in both directions is a function of the flow velocity. This technique is also known as pulse and return method.

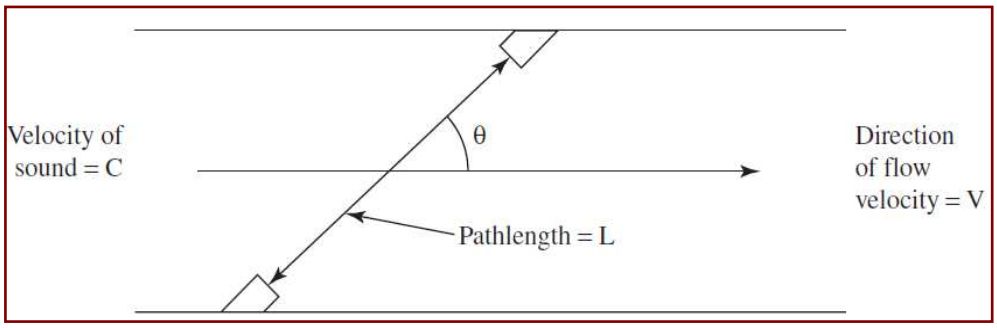

Figure 2-8: Principle of acoustic technique for measuring the velocity of the flow[99]

This technique is usually used in homogenous flow where the velocities of the phases in the mixture are equal. For more information regarding this technique, see [117,118].

2.1.2.3 Ultrasonic flow meter

Ultrasound waves are sound waves with a frequency higher than the upper limit of human hearing. The basic idea behind ultrasonic techniques is that the required information about the measured medium can be obtained by using the reflection, absorption, and scattering effects of the medium on the incident ultrasonic waves. The ultrasonic signals are transmitted and received using a number of transducers. The transducers convert an electrical signal (voltage pulse) into acoustic signal and vice-versa. Figure 2-9 shows a schematic diagram of a common configuration of the ultrasonic flow meter.

The ultrasonic flow meters are highly accurate, fast response, suitable for a wide range of fluids. In addition, there are no mechanical moving parts.

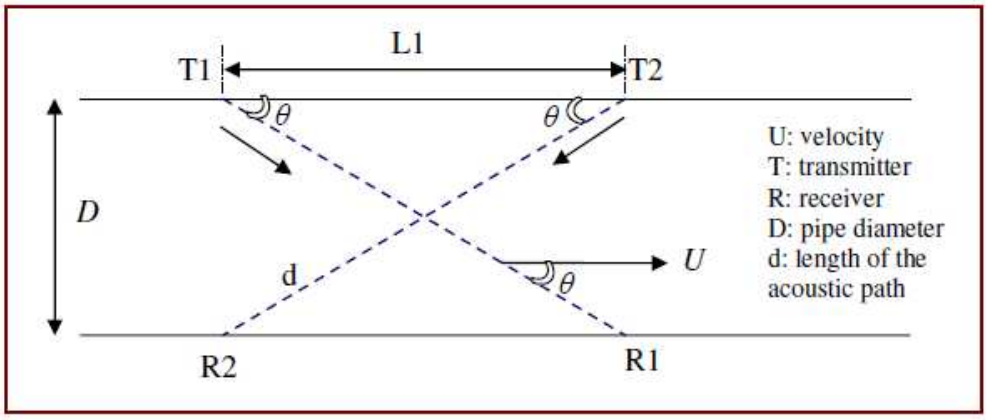

Figure 2-9: A schematic diagram of a commonly used configuration for an ultrasonic flow meter

In order to determine the fluid velocity U the following assumptions are made; (i) the acoustic path length, d is constant. (ii) the speed of sound, c is constant. The acoustic distance which is travelled by the ultrasonic beam can be expressed as;

$$d = \frac{D}{\sin\theta}$$

Equation (2.12)

The velocity u_d of the ultrasonic beam along the downstream path (from T1 to R1) and the velocity u_u of ultrasonic beam along the upstream path (from T2 to R2) are respectively expressed as;

$$u_d = c + U\cos\theta$$

Equation (2.13)

and;

$$u_u = c - U\cos\theta$$

Equation (2.14)

where U is the fluid velocity and θ is the angle shown in Figure 2-9.

For more information regarding this technique, refer to [119-121].

2.1.2.4 Turbine flow meters

A turbine flow meter is one of the most important instruments used in the process industries for the measurement of liquid flow rate. A turbine flow meter consists of a multi-bladed rotor mounted on free running bearings. Usually two sets of bearings are used, one upstream and one downstream of the rotor. A typical turbine flow meter is shown in Figure 2-10.

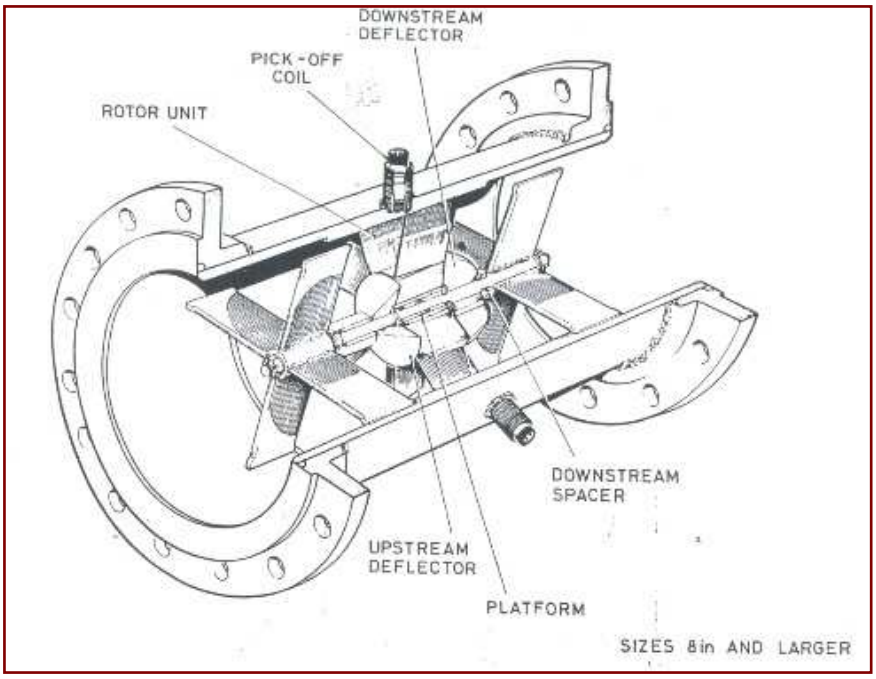

Figure 2-10: Layout of a typical turbine flow meter

The kinetic energy of the flowing liquids turns the rotor. For an ideal linear turbine flow meter, the angular speed of the rotor is proportional to the mean liquid velocity U through the turbine meter. Therefore,

$$f_{turbine} = k_{turbine} U$$

Equation (2.15)

where $f_{turbine}$ is the frequency in revolutions per second, U is the mean liquid velocity in ms^{-1} and $k_{turbine}$ is the constant of proportionality.

The volumetric flow rate Q is given by;

$$Q = AU$$

Equation (2.16)

where A is the 'effective' cross sectional area of the turbine meter.

Combining Equations (2.15) and (2.16) gives;

$$f_{turbine} = KQ$$

Equation (2.17)

where K is the meter constant (or K-factor) and is given by;

$$K = \frac{k}{A}$$

Equation (2.18)

It should be noted that K also represents the number of rotor revolutions per unit volume of liquid passing through the turbine flow meter.

A pick-up coil is mounted in the casing of the turbine flow meter so that each time a specific rotor blade passes the coil, an output pulse is produced. These output pulses are transmitted to a frequency counter and/or totaliser, from which the instantaneous liquid flow rate and/or totalised liquid flow can be deduced, using Equation (2.17). It should be noted that some turbine flow meters have pick-ups which are sensitive to all of the rotor blades, whilst other turbine meters have more than one pick-up.

Many attempts have been made to use turbine flow meters in two-phase flows. There are several models describing the turbine velocity, $U_{turbine}$ in a two phase flow. For example, Rouhani (1964, 1974) [122,123] derived a model for the turbine velocity $U_{turbine}$ as follows;

$$U_{turbine} = U_L \frac{\left(S^2 + \frac{\rho_L}{\rho_G} \frac{(1-\alpha)}{\alpha} \right)}{\left(S + \frac{\rho_L}{\rho_G} \frac{(1-\alpha)}{\alpha} \right)}$$

Equation (2.19)

where U_L is the liquid velocity, S is the slip ratio, ρ_L and ρ_G are the liquid and gas densities respectively and α is the gas volume fraction.

Aya (1975) [124] modified the Rouhani model to obtain;

$$U_{turbine} = \frac{U_L \sqrt{S + \frac{\rho_L}{\rho_G} \frac{(1-\alpha)}{\alpha}}}{\sqrt{1 + \frac{\rho_L}{\rho_G} \frac{(1-\alpha)}{\alpha}}}$$

Equation (2.20)

The Rouhani and Aya models are based on the analysis of the different forces acting on the turbine blades. The assumptions that were made are; a steady state flow, a flat velocity profile and a flat void fraction profile.

One of the major limitations of using a turbine flow meter in two phase flows is that for intermittent flow conditions, changes in angular momentum of the rotor and the fluid rotating within the rotor will occur. Therefore, the speed of the rotation does not truly represent the instantaneous value of the mass flux in a turbine flow meter [99]. Considerable theoretical and experimental studies have been published on the behaviour of the turbine flow meters in two phase flows, see for example; [125,126,124,127-129].

2.1.2.5 Vortex shedding meters

Vortex shedding flow meters are widely used for measuring the liquid flow rate in a single phase flow. In common with the turbine flow meter discussed in Section 2.1.2.4, vortex shedding meters produce a frequency that is proportional to the volumetric flow rate. Unlike the turbine flow meter however, the vortex shedding flow meter relies on the oscillation of a portion of the fluid, not on the motion of a mechanical element as in turbine flow meters.

Vortex shedding is a natural phenomenon which arises when any (long) two dimensional body (e.g. 2-D bluff body) is placed in a cross-flow. Therefore, when a bluff body is placed in a rapidly moving flow stream it produces a disturbance called 'vortex shedding' which is dependent on the fluid velocity and the properties of the fluid. Under certain conditions (e.g. an adverse pressure gradient or the presence of sharp discontinuities), the boundary layers can separate flow from the two dimensional body to form two free shear layers (see Figure 2-11). The free shear layers then roll up into vortices, alternately, on either side of the body and are shed into the wake. The vortices thus shed proceed downstream in a staggered procession known as a Karman vortex street.

The frequency f_v at which the vortices in the Karman vortex street pass a fixed point in the wake is proportional to the fluid velocity U_{vortex}, for a wide range of values of fluid velocity. For a vortex shedding meter, in a pipe flow, a meter constant K_{vortex} is given by;

$$K_{vortex} = \frac{f_v}{Q}$$

Equation (2.21)

where Q is the fluid volumetric flow rate ($Q = AU_{vortex}$).

The meter constant K_{vortex} can also be expressed in terms of Strouhal number, St using;

$$K_{vortex} = \frac{St}{WA}$$

Equation (2.22)

where W is the bluff body base width and A is the effective cross-sectional area of the vortex shedding meter. St in Equation (2.22) is given by;

$$St = \frac{f_v W}{U_{vortex}}$$

Equation (2.23)

The volumetric flow rate Q through the vortex shedding meter is given by;

$$Q = \frac{R_e \mu A}{\rho \mathrm{D}}$$

Equation (2.24)

where R_e is the pipe Reynolds number, μ is the viscosity of the fluid and D is the pipe internal diameter.

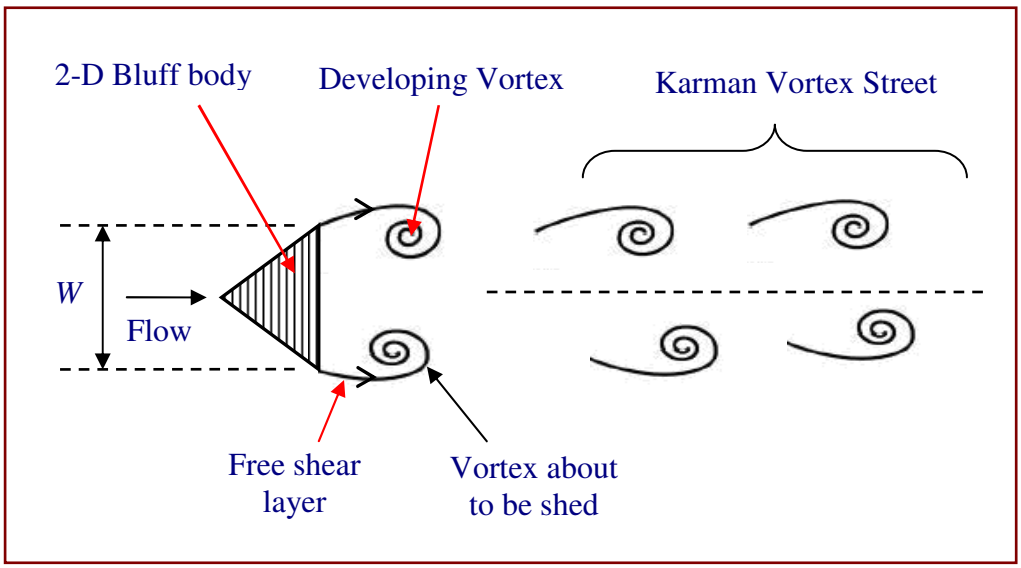

Figure 2-11: A schematic diagram of Vortex shedding

Vortex shedding meters are also used in two phase flows, but here the operation of the vortex shedding flow meter is complex because the frequency of shedding is strongly dependent on the gas void fraction. Foussat and Hulin (1983) [130] studied

the conditions in which vortex shedding flow meter can be used in two phase flows. They concluded that at higher gas void fractions and low velocities, the implementation of vortex shedding techniques becomes very difficult. They recommend that the gas void fraction should be less than 10% and the velocity should be higher than $0.45 ms^{-1}$.

It should be also noted that, in two phase flows, whilst the meter constant K_{vortex} is approximately constant over a wide range of flow rates, its value can change with the fluid volumetric flow rate, Q. Also the repeatability of the vortex shedding meters in two phase flows is not quite as good as that of turbine flow meters. These facts have implications for the level of accuracy that can be expected from vortex shedding meters in multiphase flow applications. More details on the use of vortex shedding flow meters in two phase flows can be found in [131-133].

2.1.2.6 Cross correlation technique

A fluid velocity in a pipe can be measured using cross-correlation techniques and signal processing methods (see Figure 2-12). A full review of the cross-correlation flow meters is given by [134]. The idea behind the cross-correlation technique is that some properties of the flow are measured by two identical sensors separated by a known distance. As the flow passes between the two sensors the output signal pattern x(t) from the first sensor will be repeated after a short period of time (dt) at the second sensor y(t). The time lag between y(t) and x(t) corresponds to the time taken for discontinuities in the flow to travel between sensor (x) and sensor (y). A cross-correlation algorithm is then applied to x(t) and y(t). These signals are compared to find the time elapsed between the maximum similarities in the two signals. This time shift corresponds to the time it takes the flow to travel from sensor (x) to sensor (y). If the distance between the sensors is known then the velocity of the flow can easily be determined.

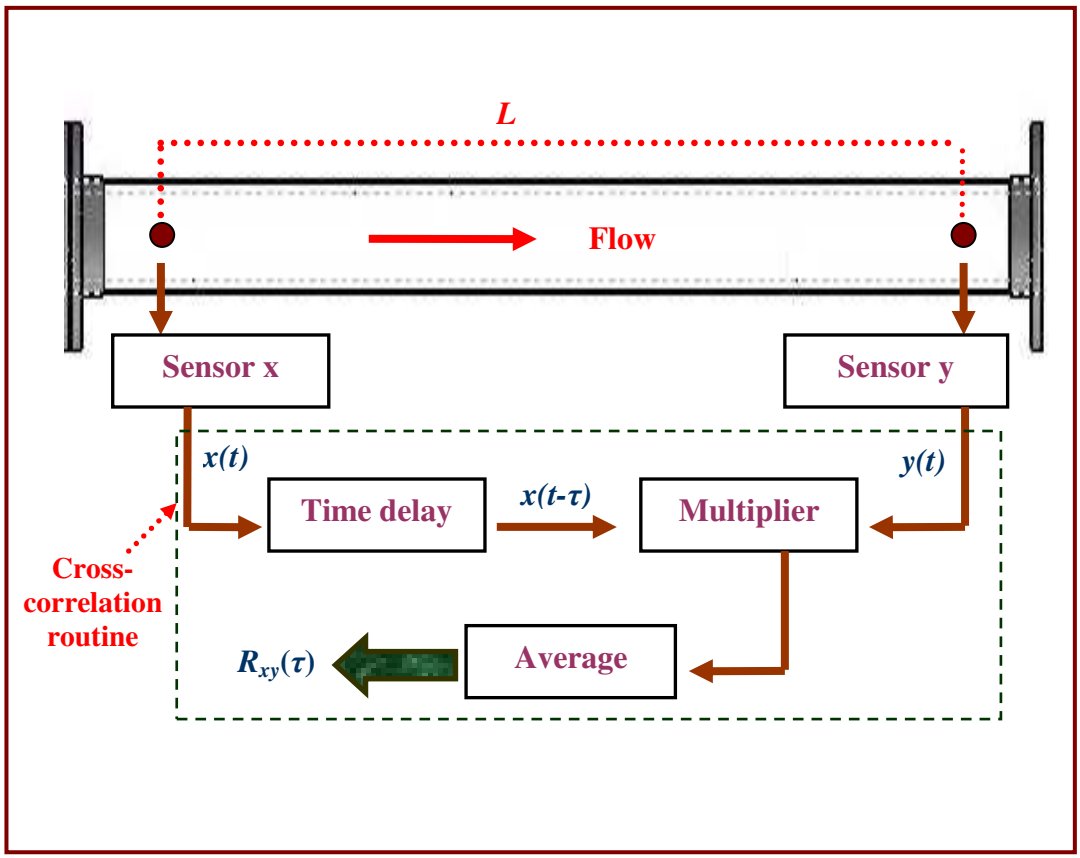

Figure 2-12: A schematic diagram of a Cross-correlation flow meter

The sensing (detecting) techniques where the cross-correlation method is often used are (for example); electrical impedance techniques [135,136], optical probes [137], ultrasound sensors [138] and X-or-gamma ray densitometers [139,140].

The cross-correlation function, $R_{xy}(\tau)$ of two random signals, $x(t)$ and $y(t)$ can be mathematically expressed as;

$$R_{xy}(\tau) = \lim_{T\to\infty} \frac{1}{T} \int_0^T x(t-\tau).y(t)\, dt$$

Equation (2.25)

where τ is variable time delay and T is time period over which the signals $x(t)$ and $y(t)$ are sampled.

The cross-correlation function, $R_{xy}(\tau)$ is plotted as a function of τ. The maximum value (peak) of $R_{xy}(\tau)$ will occur at $\tau = \tau_p$ (where τ_p is the time shift between the maximum similarities in the two measurement signals). Thus τ_p can be measured by obtaining the value of τ which gives a maximum value of $R_{xy}(\tau)$. Since the distance between two sensors, *L* is known, the average fluid velocity, $\overline{U}$ can be expressed as;

$$\overline{U} = \frac{L}{\tau_p}$$

Equation (2.26)

For more information on multiphase flow metering techniques including phase fraction measurement methods (such as; neutron absorption and scattering, infrared, ultrasound, and others) and the phase velocity measurement methods (such as; laser doppler anemometry (LDA), positive displacement meter, magnetic flow meter and others), refer to [18,19,99,69].

2.2 Previous models on Venturis and Orifice meters used for multiphase flow measurement

As mentioned earlier, the purpose of studying the previous models for the Venturi and orifice meters in this section is to show the dependency of these correlations on the mass flow quality, *x*. Therefore, this section is not intended to give more details about the derivation of these models. For more details about the derivation of the models, refer to the author's M.Sc. dissertation [54].

The previous models for Venturi and orifice meters presented in this section include; Murdock (1962) [47], Chisholm (1967,1977) [48,49], Smith and Leang (1975) [50], Lin (1982) [51], de Leeuw (1994,1997) [52,53] and Steven (2002) [15]. At the end of this section it will be seen that all of the above correlations, which play an important role in the literature, depend on the mass flow quality, *x*. In practice, online measurement of *x* is difficult and not practical in nearly all multiphase flow applications. This demonstrates the need for investigating a new model which is not dependent on the mass flow quality *x*. This new model is one of the main objectives

in the current research and is described, in detail, in the next chapter (specifically, in Section 3.2).

2.2.1 Murdock correlation

2.2.1.1 Summary of Murdock correlation

Murdock (1962) [47] carried out a study on the general case of two phase flow through an orifice plate meter which was not restricted to only wet gas flows. Murdock developed a rational equation modifying the single phase equation by introducing an experimental constant (correction factor). He considers a two phase flow to be a separated flow (stratified flow) and he computed the total mass flow rate using an experimentally obtained constant (constant=1.26) and assumed that the quality of the mixture was known. He stated that the two phase flow might be computed with a tolerance of 1.5 percent.

The correction factor in Murdock correlation was a function of the modified version of Lockhart-Martinelli parameter defined as the ratio of the superficial flows momentum pressure drops and not the friction pressure drops as in the original definition of Lockhart-Martinelli parameter. The modified Lockhart-Martinelli parameter X_{mod} was given by;

$$X_{\mathrm{mod}} = \sqrt{\frac{\Delta P_w}{\Delta P_g}} = \left(\frac{\dot{m}_w}{\dot{m}_g}\right)\left(\frac{k_g}{k_w}\right)\sqrt{\frac{\rho_g}{\rho_w}} = \left(\frac{1-x}{x}\right)\left(\frac{k_g}{k_w}\right)\sqrt{\frac{\rho_g}{\rho_w}}$$

Equation (2.27)

where ΔP is the pressure drop, $\dot{m}$ is the mass flow rate, k is the flow coefficient (including the respective product of the velocity of approach, the discharge coefficient and the net expansion factor), ρ is the density and x is the mass flow quality. The subscripts w and g refer to the water and gas phases flowing alone respectively.

The gas mass flow rate in Murdock correlation is given by;

$$\dot{m}_g = \frac{A_t k_g \sqrt{2\Delta P_{TP}\rho_g}}{1+1.26\dfrac{1-x}{x}\dfrac{k_g}{k_w}\sqrt{\dfrac{\rho_g}{\rho_w}}} = \frac{(\dot{m}_g)_{apparent}}{1+1.26\dfrac{1-x}{x}\dfrac{k_g}{k_w}\sqrt{\dfrac{\rho_g}{\rho_w}}}$$

Equation (2.28)

where x is the mass flow quality, A_t is the area at the constriction, ΔP_{TP} is the two phase pressure drop and $(\dot{m}_g)_{apparent}$ is the gas mass flow rate under two phase differential pressure [$(\dot{m}_g)_{apparent} = A_t k_g \sqrt{2\Delta P_{TP}\rho_g}$]

Equation (2.28) can be written in terms of modified Lockhart-Martinelli parameter when Equation (2.27) is substituted into Equation (2.28);

$$\dot{m}_g = \frac{(\dot{m}_g)_{apparent}}{1+1.26X_{\text{mod}}}$$

Equation (2.29)

When the Venturi is used in water-gas annular flows the measured differential pressure ΔP_{TP} will be higher than if the flow was gas phase alone, ΔP_g [141]. If this additional pressure drop is not corrected for then it will lead to an over-reading of the gas mass flow rate, $O.R_{Murdock}$ (see Equation (2.30)).

$$O.R_{Murdock} = \frac{(\dot{m}_g)_{apparent}}{(\dot{m}_g)} = \sqrt{\frac{\Delta P_{TP}}{\Delta P_g}} = 1+1.26X_{\text{mod}}$$

Equation (2.30)

where $(\dot{m}_g)$ is the corrected gas mass flow rate.

It is well known that;

$$\frac{1-x}{x} = \frac{\dot{m}_w}{\dot{m}_g}$$

Equation (2.31)

The water mass flow rate $\dot{m}_w$ in the Murdock correlation can be obtained by substituting Equations (2.31) into (2.28) and solving for $\dot{m}_w$. Then;

$$\dot{m}_w = \frac{A_t k_w \sqrt{2\Delta P_{TP}\rho_w}}{\frac{k_w}{k_g}\frac{\dot{m}_g}{\dot{m}_w}\sqrt{\frac{\rho_w}{\rho_g}}+1.26}$$

Equation (2.32)

Equation (2.32) can be written in terms of modified Lockhart-Martinelli parameter by substituting Equations (2.27) into (2.32);

$$\dot{m}_w = \frac{A_t k_w \sqrt{2\Delta P_{TP} \rho_w}}{1.26 + \frac{1}{X_{\text{mod}}}}$$

Equation (2.33)

It is well known that the mass flow quality x is given by;

$$x = \frac{\dot{m}_g}{\dot{m}_T}$$

Equation (2.34)

where $\dot{m}_T$ is the total mass flow rate.

Substituting Equations (2.34) into (2.28) and solving for $\dot{m}_T$ gives the total mass flow rate in the Murdock correlation (see Equation (2.35)).

$$\dot{m}_T = \frac{A_t k_g \sqrt{2\Delta P_{TP} \rho_g}}{x + 1.26(1-x)\frac{k_g}{k_w}\sqrt{\frac{\rho_g}{\rho_w}}}$$

Equation (2.35)

2.2.1.2 Conditions and assumptions of the Murdock correlation

The conditions and assumptions of Murdock correlation can be summarized as;

(i) The model assumes zero interfacial shear stress.

(ii) Orifice diameter (mm): 25.4, 31.7

(iii) Pipe diameter (mm): 63.5, 102.

(iv) The diameter ratio (β): 0.25 and 0.5.

(v) The standard taps locations of radius: (1*D* and 1/2*D*).

(vi) The range of X_{mod} ($X_{\text{mod}} = \sqrt{\frac{\Delta P_w}{\Delta P_g}}$): 0.41 – 0.25

(vii) The range of $\sqrt{\frac{\rho_w}{\rho_g}}$: 3.9 – 34.7

(viii) The minimum liquid Reynolds number: $\mathrm{Re}_w = 50$.

(ix) The minimum gas Reynolds number: $\mathrm{Re}_g = 10{,}000$, for more details, refer to [47,54]

2.2.1.3 Limitations of Murdock correlation

(i) The Murdock correlation is based on prior knowledge of the mass flow quality, x (prior knowledge of gas and liquid flow rates). Therefore, measuring the mass flow quality online is difficult and not practical.

(ii) The Murdock correlation uses a simplified model of a two phase flow through the constriction meter in which it assumes that there is no friction between the phases. The friction influences can be neglected only when (i) the viscosities of the phases are small and (ii) the slip ratio between phases is negligible. Due to neglecting the influence of the friction between the phases, Agar and Farchy (2002) [142] showed that the Murdock correlation is not expected to give highly accurate results in wet gas flow applications.

2.2.2 Chisholm correlation

2.2.2.1 Summary of Chisholm correlation

The Chisholm correlation [48,49] is a function of pressure and the modified Lockhart-Martinelli parameter, X_{mod}. The flow is assumed stratified flow. Chisholm uses the modified Lockhart-Martinelli parameter and the effect of interfacial shear force between the phases is also considered. Chisholm studied a general two phase flow through an orifice plate and then later modified his correlation for higher quality conditions. Chisholm stated that when the modified Lockhart-Martinelli parameter $X_{\mathrm{mod}} > 1$, then the slip ratio, S, is given by;

$$S = \left(\frac{\rho_w}{\rho_g} \right)^{\frac{1}{4}}$$

Equation (2.36)

and when $X_{\mathrm{mod}} < 1$, the slip ratio is given by;

$$S = \left(\frac{\rho_w}{\rho_h} \right)^{\frac{1}{2}}$$

Equation (2.37)

where ρ_h is the homogenous density.

The gas mass flow rate in Chisholm correlation is given by, (Steven, 2002);

$$\dot{m}_g = \frac{k_g A_t \sqrt{2\Delta P_{TP} \rho_g}}{\sqrt{1 + CX_{\text{mod}} + X_{\text{mod}}^2}} = \frac{k_g A_t \sqrt{2\Delta P_{TP} \rho_g}}{\sqrt{1 + \left[\left(\frac{\rho_w}{\rho_g} \right)^{\frac{1}{4}} + \left(\frac{\rho_g}{\rho_w} \right)^{\frac{1}{4}} \right] X_{\text{mod}} + X_{\text{mod}}^2}}$$

Equation (2.38)

Equation (2.38) can be re-written in terms of the over-reading factor, $O.R_{Chisholm}$

$$O.R_{Chisholm} = \frac{(\dot{m}_g)_{apparent}}{(\dot{m}_g)} = \sqrt{\frac{\Delta P_{TP}}{\Delta P_g}} = \sqrt{1 + \left[\left(\frac{\rho_w}{\rho_g} \right)^{\frac{1}{4}} + \left(\frac{\rho_g}{\rho_w} \right)^{\frac{1}{4}} \right] X_{\text{mod}} + X_{\text{mod}}^2}$$

Equation (2.39)

The Chisholm constant *C* in Equation (2.38) is defined as;

$$C = \frac{1}{S} \sqrt{\frac{\rho_w}{\rho_g}} + S \sqrt{\frac{\rho_g}{\rho_w}}$$

Equation (2.40)

where S is the velocity ratio (slip velocity) and is defined by Equations (2.36) or (2.37).

2.2.2.2 Conditions and assumptions of the Chisholm correlation

The conditions and assumptions of the Chisholm correlation are as follows;

(i) Orifice diameter (mm): 9.5 – 25.4

(ii) Pipe diameter (mm): 51.

(iii) Range of modified Lockhart-Martinelli parameter, X_{mod} : 0.5 - 5.0

(iv) Range of $\sqrt{\frac{\rho_w}{\rho_g}}$: ~ 29.

(v) Value of C (X_{mod} , from experiment): 5.3

(vi) Value of C (X_{mod} <1, from theoretical { $C = \left(\frac{\rho_w}{\rho_g}\right)^{\frac{1}{4}} + \left(\frac{\rho_g}{\rho_w}\right)^{\frac{1}{4}}$ }): 5.57

(vii) The flow is assumed to be stratified flow.

(viii) The shear force of boundary is considered, for more details see [48,49,54].

2.2.2.3 Limitations of Chisholm correlation

(i) The velocity ratio throughout the orifice meter is assumed constant.

(ii) Again, the Chisholm correlation is based on prior knowledge of the mass flow quality, *x*.

2.2.3 Lin correlation

2.2.3.1 Summary of Lin correlation

The Lin correction factor K_{Lin} is a function of the velocity ratio *S*, and the density ratio ρ_g / ρ_w . Lin (1982) [51] also uses the simplified Lockhart-Martinelli parameter. Lin includes the effect of the shear force between the phases in his correlation. He developed his model based on a separated flow model (i.e. for general stratified two phase flow) and he compared his model against the experimental data. This comparison showed that the Lin model can be used to calculate the flow rate or the quality of vapour-liquid (or steam-water) mixture in the range 0.00455 to 0.328 of the density ratio ρ_g / ρ_w , and in pipe sizes ranging from 8 to 75 mm (β = 0.25 to 0.75).

The corrective coefficient K_{Lin} in Lin correlation is given by;

$$K_{Lin} = 1.48625 - 9.26541\left(\frac{\rho_g}{\rho_w}\right) + 44.6954\left(\frac{\rho_g}{\rho_w}\right)^2 - 60.6150\left(\frac{\rho_g}{\rho_w}\right)^3 - 5.12966\left(\frac{\rho_g}{\rho_w}\right)^4 - 26.5743\left(\frac{\rho_g}{\rho_w}\right)^5$$

Equation (2.41)

The gas mass flow rate in the Lin correlation is given by;

$$\dot{m}_g = \frac{k_w A_t x\sqrt{2\Delta P_{TP}\rho_w}}{K_{Lin}(1-x) + x\sqrt{\frac{\rho_w}{\rho_g}}} = \frac{k_w A_t \sqrt{2\Delta P_{TP}\rho_g}}{K_{Lin}\left(\frac{\dot{m}_w}{\dot{m}_g}\right)\sqrt{\frac{\rho_g}{\rho_w}} + 1} = \frac{k_w A_t \sqrt{2\Delta P_{TP}\rho_g}}{K_{Lin}X_{\text{mod}} + 1} = \frac{(\dot{m}_g)_{apparent}}{K_{Lin}X_{\text{mod}} + 1}$$

Equation (2.42)

In terms of an over-reading factor, $O.R_{Lin}$, Equation (2.42) can be written as;

$$O.R_{Lin} = \frac{(\dot{m}_g)_{apparent}}{(\dot{m}_g)} = \sqrt{\frac{\Delta P_{TP}}{\Delta P_g}} = K_{Lin}X_{\text{mod}} + 1$$

Equation (2.43)

The water mass flow rate in Lin correlation can be expressed as;

$$\dot{m}_w = \frac{k_w A_t \sqrt{2\Delta P_{TP}\rho_w}}{K + \left(\frac{1}{X_{\text{mod}}}\right)}$$

Equation (2.44)

2.2.3.2 Conditions and assumptions of Lin correlation

(i) The gas and liquid (water) phases flow separately through an orifice.

(ii) The pipe diameter (mm): 32.

(iii) The diameter ratio (β): 0.321 – 0.624

(iv) The density ratio ρ_g/ρ_w : 0.1425 – 0.328

(v) The range of the mass flow quality x: (0 – 1.0).

(vi) The orifice diameter (mm): 10.0, 20.0

(vii) Lin assumes that the superficial flow coefficients k_g and k_w (including the respective product of the velocity of approach, the discharge coefficient and the net expansion factor. Note: expansion factor for water is 1) are equal.

(viii) Line uses the modified Lockhart-Martinelli parameter.

(ix) The mass velocity passing through orifice ranged from 917.16 to 1477.42 kg/m^2.s.

(x) The tested pressure ratios (P/P_c) were: 0.5698, 0.7108, 0.7401 and 0.8319, and the respective density ratios (ρ_g/ρ_w) were: 0.1425, 0.2150, 0.2450 and 0.3280. (P_c is the critical pressure), for more information, refer to [51,54] .

2.2.3.3 Limitation of Lin correlation

i) Again, prior knowledge of the gas and liquid mass flow rates is needed (i.e. mass flow quality must be known).

2.2.4 The Smith and Leang correlation

2.2.4.1 Summary of Smith and Leang correlation

In general, two correlation approaches are used in two-phase flow. The first uses a function to relate the pseudo single-phase flow to the two-phase flow rate. The other uses a blockage factor (*BF*) to determine the gas mass flow rate. Smith and Leang (1975) [50] developed a model which accounts for the liquid presence by introducing a parameter called a blockage factor (*BF*) that takes account of the partial blockage of the pipe area by the liquid phase [15]. The Smith and Leang correlation can be used for orifice plates and Venturi meters. The (*BF*) is given by;

$$(BF) = 0.637 + 0.4211x - \frac{0.00183}{x^2}$$

Equation (2.45)

where x is the mass flow quality.

It is well known that, the single gas mass flow rate $\dot{m}_g$ through a Venturi/orifice is given by;

$$\dot{m}_g = A_t k_g \sqrt{2\rho_g \Delta P_g}$$

Equation (2.46)

where A_t is the area at the constriction, k_g is the gas flow coefficient (including the respective product of the velocity of approach, the discharge coefficient and the net expansion factor), ΔP_g is the gas pressure drop and ρ_g is the gas density.

The Smith and Leang correlation solves for the single phase flow rate directly rather than a pseudo rate (i.e. introducing the (*BF*) directly into Equation (2.46) and taking into accounts the gas flow area A_g). Therefore;

$$\dot{m}_g = k_g A_g (BF) \sqrt{2\Delta P_g \rho_g}$$

Equation (2.47)

The over-reading factor, $O.R_{S\&L}$ in Smith and Leang correlation can be expressed as;

$$O.R_{S\&L} = \frac{1}{(BF)} = \frac{1}{0.637 + 0.4211x - \dfrac{0.00183}{x^2}}$$

Equation (2.48)

2.2.4.2 Conditions and assumptions of Smith and Leang correlation

The conditions and assumptions of the Smith and Leang correlation can be summarised as;

(i) Higher quality region is defined as $x > 0.1$.

(ii) Lower quality region is defined as $x < 0.1$.

(iii) BF would be linear at higher quality values.

(iv) Smith and Leang (1975) used the same experimental data as James (1965), Murdock (1962) and Marriott (1970), for more details, see [50,54].

2.2.4.3 Limitations Smith and Leang correlation

i) Again, Smith and Leang correlation is based on prior knowledge of the mass flow quality.

ii) The model uses empirical method to define the blockage factor.

2.2.5 The de Leeuw correlation

2.2.5.1 Summary of de Leeuw correlation

The de Leeuw correlation [52,53] uses the Venturi in wet gas applications. This correlation is a modified form of Chisholm correlation and is used to predict the effect of the presence of the liquid phase on Venturi meter reading for a wet gas horizontal flow application. The correction is based on experimental data. de Leeuw claimed that the deviations between his correlation and the experimental data was less than 2%. The major difference between the de Leeuw correlation and the other well known orifice plate correlations (e.g. Murdock and Chisholm) is that the de Leeuw correlation is not only a function of the Lockhart-Martinelli parameter and pressure drop as with the Murdock and Chisholm correlations but does depend on the gas and liquid densiometric Froude numbers.

de Leeuw mentioned that the best representation for the wet gas flow conditions should be through using the gas and liquid densiometric Froude numbers Fr_g and Fr_l which are respectively expressed as;

$$Fr_g = \frac{U_{sg}}{\sqrt{gD}}\sqrt{\frac{\rho_g}{\rho_w - \rho_g}}$$

Equation (2.49)

and;

$$Fr_l = \frac{U_{sw}}{\sqrt{gD}}\sqrt{\frac{\rho_w}{\rho_w - \rho_g}}$$

Equation (2.50)

where D, g, U_{sg} and U_{sw} are the pipe diameter, 9.81ms^{-2}, the superficial gas velocity, and the superficial liquid (water) velocity.

It should be noted that the Froude numbers (Equations (2.49) and (2.50)) are purely empirical, no mathematical model was used.

de Leeuw stated that the ratio of the liquid Froude number to the gas Froude number equals the Lockhart-Martinelli parameter X. de Leeuw used the simplified version of the modified Lockhart-Martinelli parameter, X_{simp} by substituting $k_g = k_w$ in Equation (2.27). Therefore;

$$X_{simp} = \sqrt{\frac{\Delta P_w}{\Delta P_g}} = \left(\frac{\dot{m}_w}{\dot{m}_g}\right)\sqrt{\frac{\rho_g}{\rho_w}} = \left(\frac{1-x}{x}\right)\sqrt{\frac{\rho_g}{\rho_w}} = \frac{Fr_l}{Fr_g}$$

Equation (2.51)

The de Leeuw correlation is given in the form of Chisholm correlation (Equation (2.38)) with the constant 1/4 replaced by a parameter denoted as n, where n is a function of the gas densiometric Froude number, Fr_g (i.e. a function of the gas flow rate, the fluid density and the meter geometry) and can be expressed as;

$$n = 0.41 \qquad \text{for} \quad 0.5 \le Fr_g \le 1.5$$

Equation (2.52)

$$n = 0.606(1 - e^{-0.746 Fr_g}) \quad \text{for} \quad Fr_g \ge 1.5$$

Equation (2.53)

Replacing the constant term 1/4 in Equation (2.38) by n gives;

$$\dot{m}_g = \frac{k_g A_t \sqrt{2\Delta P_{TP} \rho_g}}{\sqrt{1 + C_{Leeuw} X_{simp} + X_{simp}^2}} = \frac{k_g A_t \sqrt{2\Delta P_{TP} \rho_g}}{\sqrt{1 + \left[\left(\frac{\rho_w}{\rho_g}\right)^n + \left(\frac{\rho_g}{\rho_w}\right)^n\right] X_{simp} + X_{simp}^2}}$$

Equation (2.54)

where k_g is the gas flow coefficient (including the respective product of the velocity of approach, the discharge coefficient and the net expansion factor), A_t is the area at the constriction, ΔP_{TP} is the two phase pressure drop and C_{Leeuw} is the modified Chisholm parameter defined by de Leeuw and can be written as;

$$C_{Leeuw} = \left(\frac{\rho_w}{\rho_g}\right)^n + \left(\frac{\rho_g}{\rho_w}\right)^n$$

Equation (2.55)

where *n* is defined by Equations (2.52) and (2.53)

The gas mass flow rate over-reading factor in de Leeuw correlation can be expressed as;

$$O.R_{deLeeuw} = \frac{(\dot{m}_g)_{apparent}}{(\dot{m}_g)} = \sqrt{\frac{\Delta P_{TP}}{\Delta P_g}} = \sqrt{1 + \left[\left(\frac{\rho_w}{\rho_g}\right)^n + \left(\frac{\rho_g}{\rho_w}\right)^n\right] X_{simp} + X_{simp}^2}$$

Equation (2.56)

The water mass flow rate in de Leeuw correlation is given by;

$$\dot{m}_w = \frac{k_w A_t \sqrt{2\Delta P_{TP} \rho_w}}{\sqrt{1 + \left[\left(\frac{\rho_w}{\rho_g}\right)^n + \left(\frac{\rho_g}{\rho_w}\right)^n\right] \frac{1}{X_{simp}} + \frac{1}{X_{simp}^2}}}$$

Equation (2.57)

where k_w is the water flow coefficient (including the respective product of the velocity of approach and the discharge coefficient).

2.2.5.2 Conditions and assumptions of de Leeuw correlation

The experimental data for a Venturi meter in the de Leeuw correlation is summarised in Table 2-1.

Table 2-1: Summary of experimental data (de Leeuw correlation) [52-54]

P bar	Gas vel. [m/s]	Gas Froude number	Liq. vel. [m/s]	Liquid Froude number	Lockhart-Martinelli parameter	LGR [$m^3/10^6$ nm^3]	GVF [%]
90	12	4.8	0-1.2	0-1.31	0-0.3	0-1000	100-90
	8	3.2	0-0.9	0-0.97	0-0.3	0-1000	100-90
	4	1.6	0-0.4	0-0.44	0-0.3	0-1000	100-90
45	11.4	3.2	0-0.8	0-0.85	0-0.3	0-1500	100-92
	5.8	1.6	0-0.4	0-0.42	0-0.3	0-1500	100-92
30	14.5	3.2	0-0.8	0-0.83	0-0.3	0-1800	100-94
	7.3	1.6	0-0.4	0-0.41	0-0.3	0-1800	100-94
15	17	2.5	0-0.7	0-0.71	0-0.3	0-2500	100-96
	10	1.5	0-0.4	0-0.41	0-0.3	0-2500	100-96

2.2.5.3 Limitations of de Leeuw correlation

(i) The Froude number in de Lueew correlation is purely empirical, no mathematical model was used.

(ii) de Leeuw uses the simplified definition of the modified Lockhart-Martinelli parameter which is a function of the mass flow quality *x*. In other words, prior knowledge of the mass flow quality is needed.

2.2.6 Steven correlation

2.2.6.1 Summary of Steven correlation

Steven (2002) [15] found that, the de Leeuw correlation which is based on 4 inches (100mm) as the Venturi diameter with $\beta = 0.40$, was not suitable for NEL wet gas loop, (i.e. for the Venturi of a diameter of 6 inches and $\beta = 0.55$). Steven investigated a new correlation with new independent data from the NEL wet gas loop that would

give a better fit for a 6 inch Venturi and 0.55 diameter ratio geometry. The Steven correlation is also based on the Froude number. The experiment was conducted for three pressures (20, 40 and 60 bar). The Steven correlation is based on the form;

$$\sqrt{\frac{\Delta P_{TP}}{\Delta P}} = f(X, Fr_g)$$

Equation (2.58)

The particular form of equation found to be the overall best fit for each of the three pressures used in Steven correlations is given by;

$$\sqrt{\frac{\Delta P_{TP}}{\Delta P_g}} = \frac{1 + A_{Ste} X_{\mathrm{mod}} + B_{Ste} Fr_g}{1 + C_{Ste} X_{\mathrm{mod}} + D_{Ste} Fr_g}$$

Equation (2.59)

where the constants A_{Ste}, B_{Ste}, C_{Ste} and D_{Ste} are respectively given by;

$$A_{Ste} = 2454.51\left(\frac{\rho_g}{\rho_w}\right)^2 - 389.568\left(\frac{\rho_g}{\rho_w}\right) + 18.146$$

Equation (2.60)

$$B_{Ste} = 61.695\left(\frac{\rho_g}{\rho_w}\right)^2 - 8.349\left(\frac{\rho_g}{\rho_w}\right) + 0.223$$

Equation (2.61)

$$C_{Ste} = 1722.917\left(\frac{\rho_g}{\rho_w}\right)^2 - 272.92\left(\frac{\rho_g}{\rho_w}\right) + 11.752$$

Equation (2.62)

$$D_{Ste} = 57.387\left(\frac{\rho_g}{\rho_w}\right)^2 - 7.679\left(\frac{\rho_g}{\rho_w}\right) + 0.195$$

Equation (2.63)

The gas mass flow rate in Steven correlation can be expressed as;

$$\dot{m}_g = k_g A_t \sqrt{2\Delta P_{TP} \rho_g} \left(\frac{1 + C_{Ste} X_{\mathrm{mod}} + D_{Ste} Fr_g}{1 + A_{Ste} X_{\mathrm{mod}} + B_{Ste} Fr_g} \right)$$

Equation (2.64)

The gas mass flow rate over-reading factor, $O.R_{Steven}$, can be written as;

$$O.R_{Steven} = \frac{(\dot{m}_g)_{apparent}}{(\dot{m}_g)} = \sqrt{\frac{\Delta P_{TP}}{\Delta P_g}} = \left(\frac{1 + A_{Ste} X_{\mathrm{mod}} + B_{Ste} Fr_g}{1 + C_{Ste} X_{\mathrm{mod}} + D_{Ste} Fr_g} \right)$$

Equation (2.65)

2.2.6.2 Conditions and assumptions of the Steven correlation

The conditions and assumptions of Steven correlation can be summarised as follows;

(i) The experiment was conducted for three pressures (20, 40 and 60 bar).

(ii) The experiment has been run under four gas flow rates (400, 600, 800 and 1000 m^3/h).

(iii) At a gas flow rate of 1000 m^3/h, the desired upper range of the liquid flow rate could not be reached.

(iv) The maximum liquid flow rate at which the blower could maintain a gas flow rate of 1000m^3/h was at the upper end of the equipment range.

(v) The lower liquid flow rate limits were close to zero as possible.

(vi) The Venturi diameter: 6 inches.

(vii) The diameter ratio, β: 0.55.

(viii) The system fluid was nitrogen and kerosene, (substitute as the fluids simulating wet natural gas flows).

(ix) Minimum value of X_{mod} : 0.001312.

(x) Maximum value of X_{mod} : $X_{\max} = \dfrac{0.108 + 2.251\left(\dfrac{\rho_g}{\rho_w}\right) - 0.06 Fr_g}{1 + 3.552\left(\dfrac{\rho_g}{\rho_w}\right) - 0.418 Fr_g + 0.039 Fr_g^2}$

(xi) The liquid flow coefficient K_l is assumed to be the product of the Venturi meter's velocity of approach and the standard discharge coefficient when t Re < 10^6, i.e $C_d = 0.995$. In other words; $k_w = (\frac{1}{\sqrt{1-\beta^4}}) \times (C_d)$

(xii) Gas flow coefficient k_g : due to the high value of Re for the superficial gas flow rates, the Venturi meter had to be calibrated at the three test pressures:

For 20 bar; $k_g = -0.001583806\dot{m}_g + 1.046511$

For 40 bar; $k_g = -0.00125486\dot{m}_g + 1.051785$

For 60 bar; $k_g = -0.0009251669\dot{m}_g + 1.05646$

2.2.6.3 Limitations

(i) The Steven correlation is a function of the modified Lockhart-Martinelli parameter which is a function of the mass flow quality.

(ii) Steven applied the data using a surface fit software package. The limits of Steven correlation are the limits of the data set used to create it.

Summary

A review of existing techniques for measuring multiphase flows was presented in Section 2.1. Different measurement principles were described which include phase fraction measurements (such as, differential pressure technique, electrical conductance technique, electrical capacitance technique, gamma ray attenuation, quick closing valve, EIT tomography, internal (grab) sampling and isokinetic sampling techniques) and the phase velocity measurements (such as, a Venturi meter, acoustic pulse, ultrasound flow meter, turbine flow meter, vortex shedding meter and cross-correlation technique).

Considerable theoretical and experimental studies have been published to describe mathematical models of the Venturi and orifice meters in multiphase flow applications such as, Murdock, Chisholm, Lin, Smith and Leang, de Leeuw and Steven correlations (see Section 2.2).

These correlations are based on the mass flow quality, x. In other words, prior knowledge of the mass flow quality is needed. In fact, online measurement of the mass flow quality is difficult and not practical in nearly all multiphase flow applications.

The difficulty that arises from the online measurement of the mass flow quality for the previous correlations reflects the need to investigate a new model which is not dependent on the mass flow quality x. The development of such a model is one of the main objectives in the current research and is described, in detail, in the next chapter (specifically in Section 3.2). The new model depends on the measurement of the gas volume fraction at the inlet and the throat of the Venturi rather than requiring prior knowledge of the mass flow quality as in previous correlations, which makes the measurement technique described in this thesis more practical. The measurement of the gas volume fraction at the inlet and the throat of the Venturi was achieved by using a conductance multiphase flow meter.

The main aim of the research described in this thesis is to develop a novel conductance multiphase flow meter which is capable of measuring the gas and the water flow rates in two-phase, water-gas, water continuous, vertical annular flows and horizontal stratified flows. The separated annular and stratified flows are complex and the accurate measurement of the phase flow rate in such flows constitutes a major challenge in multiphase flow applications. The conductance multiphase flow meter consists of the Conductance Inlet Void Fraction Meter with two ring electrodes flush mounted with the inner surface of the pipe, which is capable of measuring the gas volume fraction at the inlet of the Venturi and the Conductance Multiphase Venturi Meter (CMVM), with two ring electrodes flush mounted with the inner surface of the throat section, which is capable of measuring the gas volume fraction at the throat of the Venturi meter. The reason for choosing the Venturi meters over other common differential pressure devices (e.g. orifice plates) in the current research is that the Venturi meter has a smooth flow profile that reduces the frictional losses which in turn, increases the reliability, repeatability and predictability of the device.

Chapter 3

Mathematical Modelling of a Multiphase Venturi Meter

Introduction

Differential pressure devices can be used in multiphase flow metering. The most common differential pressure device is the Venturi meter, but orifice plates have also been used widely. The advantage of the Venturi meter over the orifice plate is that the Venturi meter is much more predictable and repeatable than the orifice plate for a wide range of flow conditions. Further, the smooth flow profile in a Venturi meter reduces frictional losses which (i) increases the reliability of the device and (ii) improves the pressure recovery [143].

In multiphase flow measurements, the relationship between the flow rate and the pressure drop across the Venturi meter is not simple as in single phase flow and should include the flow quality or the phase holdups. In a homogenous flow model where the slip is zero, the mixture densities at the inlet and the throat can be assumed equal and substitution of the mixture density at the inlet of the Venturi into the Bernoulli equation would be reasonably expected to lead to accurate results. This assumption is valid for low gas flow rates where the homogenous flow can be treated as a single phase flow. In some cases of two phase flow, the two- phases are normally well mixed and behave as a homogenous flow. The two phases are also assumed to have unity slip ratio S (i.e. the ratio of the water velocity to the gas velocity is unity) and therefore travel with the same velocities.

Separated flow in a Venturi meter is highly complex (where the velocity ratio, $S \neq 1$) and the application of a homogenous flow model could not reasonably be expected to lead to highly accurate results. In other words, the gas volume fraction at the inlet is

not the same as that at the throat of the Venturi. If this is the case, a gas volume fraction measurement technique at the throat must also be introduced instead of just relying on the gas volume fraction measurement at the inlet of the Venturi.

This chapter describes new mathematical models through a Venturi meter including;

(i) a vertical/inclined homogenous gas-water two phase flow model (see Section 3.1).

(ii) a horizontal stratified gas-water two phase flow model (see Section 3.2.1).

(iii) a vertical separated (annular) gas-water two phase flow model (see Section 3.2.2).

3.1 A homogenous gas-water two phase flow model through a Venturi meter

In the case of homogenous flow where the two phases are normally well mixed, the gas and water are assumed to have the same velocity. That is, the velocity ratio or slip ratio is unity (S=1). Figure 3-1 is intended to illustrate homogenous gas-water two phase flow for the general case of an inclined Venturi meter.

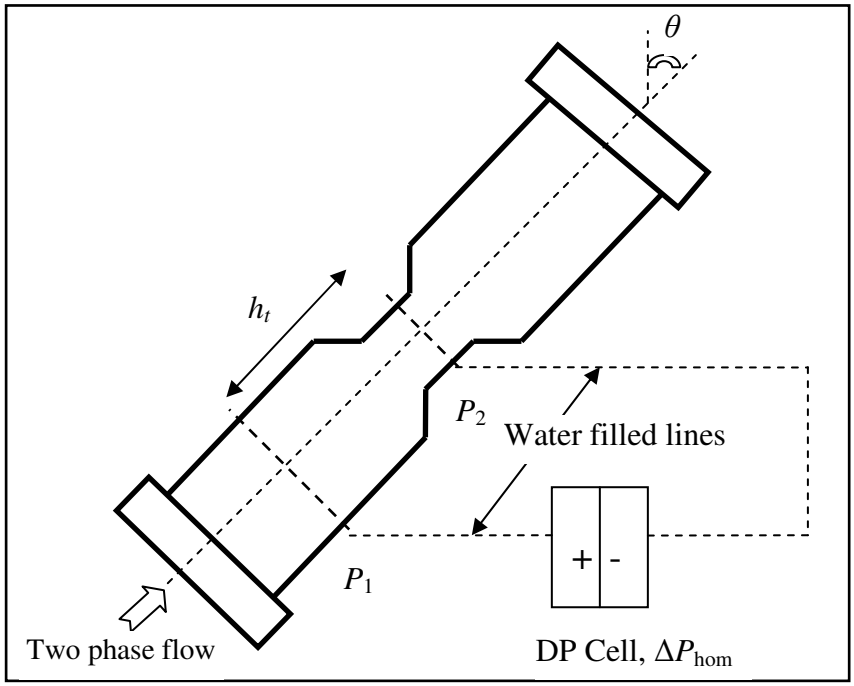

Figure 3-1: Homogenous gas-water two phase flow in a Venturi meter

From figure 3-1, it is possible to write;

$$\Delta P_{\text{hom}} = P_1 - P_2 - \rho_w g h_t \cos\theta$$

Equation (3.1)

where ΔP_{hom} is the differential pressure measured, using a dp cell, which is connected to the Venturi inlet and throat via water filled lines in a homogenous flow, P_1 and P_2 are the static pressure at the inlet and the throat of the Venturi, ρ_w is the water density, g is the acceleration of the gravity, h_t and θ are the pressure tapping separation and the angle of inclination from vertical respectively.

From Bernoulli's equation, it is possible to write that;

$$P_1 - P_2 = \frac{1}{2}\rho_m (U_2^2 - U_1^2) + \rho_m g h_t \cos\theta + F_{mv}$$

Equation (3.2)

where ρ_m is the mixture density, F_{mv} is the frictional pressure loss (from inlet to the throat of the Venturi) and U is the fluid velocity. The subscripts 1 and 2 refer to the inlet and the throat of the Venturi respectively.

Substituting Equation (3.2) into (3.1) gives;

$$\Delta P_{\text{hom}} + g h_t \cos\theta(\rho_w - \rho_m) - F_{mv} = \frac{1}{2}\rho_m \left(U_2^2 - U_1^2\right)$$

Equation (3.3)

Assuming constant mixture density the mass conservation equation is given by;

$$U_1 = U_2 \frac{A_2}{A_1}$$

Equation (3.4)

where A_1 and A_2 are the cross sectional areas at inlet and the throat of the Venturi.
From Equations (3.3) and (3.4), it is possible to write;

$$U_2^2 = \frac{2A_1^{\,2}}{\rho_m\left(A_1^{\,2} - A_2^{\,2}\right)}\left(\Delta P_{\text{hom}} + gh_t\cos\theta(\rho_w - \rho_m) - F_{mv}\right)$$

Equation (3.5)

It is well known that the volumetric flow rate of the homogenous mixture, $Q_{m,\text{hom}}$ can be expressed as;

$$Q_{m,\text{hom}} = (U_2 A_2)$$

Equation (3.6)

Combining Equations (3.5) and (3.6) gives;

$$Q_{m,\text{hom}} = \frac{A_2}{\sqrt{1-\left(\frac{A_2}{A_1}\right)^2}}\sqrt{\frac{2}{\rho_m}}\sqrt{\Delta P_{\text{hom}} + gh_t\cos\theta(\rho_w - \rho_m) - F_{mv}}$$

Equation (3.7)

ρ_m in Equation (3.7) is given by;

$$\rho_m = \alpha_{1,\text{hom}}\rho_g + (1-\alpha_{1,\text{hom}})\rho_w \approx \rho_w(1-\alpha_{1,\text{hom}})$$

Equation (3.8)

where $\alpha_{1,\text{hom}}$ is the inlet gas volume fraction in the homogenous gas-water two phase flow through the Venturi meter and ρ_g is the gas density.

Instead of using the frictional pressure loss term F_{mv}, a discharge coefficient can be used. Involving a homogenous discharge coefficient, $C_{d,\text{hom}}$ and combining Equations (3.7) and (3.8) gives;

$$Q_{m,\text{hom}} = \frac{C_{d,\text{hom}} A_2}{\sqrt{1-\left(\frac{A_2}{A_1}\right)^2}} \sqrt{\frac{2}{\rho_w (1-\alpha_{1,\text{hom}})}} \sqrt{\Delta P_{\text{hom}} + \alpha_{1,\text{hom}} \rho_w g h_t \cos\theta}$$

Equation (3.9)

It is clear from Equation (3.9) that, in order to determine $Q_{m,\text{hom}}$, the gas volume fraction, $\alpha_{1,\text{hom}}$ must be known. The gas volume fraction $\alpha_{1,\text{hom}}$ in Equation (3.9) can be measured by a differential pressure technique also known as an "online flow density meter".

3.1.1 Measurement of the gas volume fraction in a homogenous gas-water flow using the differential pressure technique

The differential pressure technique has proven attractive in the measurement of volume fraction. It is simple in operation, easy to handle, non intrusive and low cost. This differential pressure technique can be used only in vertical or inclined pipelines.

With reference to Figure 3-2, it is possible to write;

$$P_a = P_b + \rho_m g h_p \cos\theta + F_{m,pipe}$$

Equation (3.10)

where $F_{m,pipe}$ is the frictional pressure loss term between the pressure tappings in the parallel pipe section, and where h_p is the pressure tapping separation.

The differential pressure ΔP_{pipe} measured by a differential pressure sensor which is connected to the tappings via water filled lines can be expressed as;

$$\Delta P_{pipe} = P_b + \rho_w g h_p \cos\theta - P_a$$

Equation (3.11)

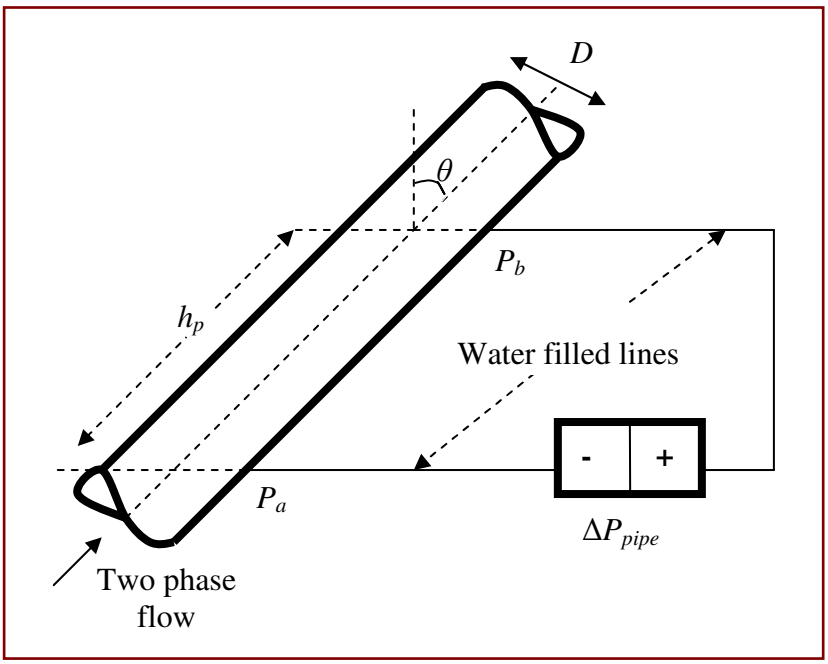

Figure 3-2: Measurement of the gas volume fraction using the differential pressure technique

Combining Equations (3.10) and (3.11) gives;

$$\Delta P_{pipe} + F_{m,pipe} = g h_p \cos\theta(\rho_w - \rho_m)$$

Equation (3.12)

The frictional pressure loss term, $F_{m,pipe}$ can be expressed as [144];

$$F_{m,pipe} = \frac{2\rho_w h_p f U_h^2}{D}$$

Equation (3.13)

where f is a single phase friction factor (see Equation (3.27) and Section 7.2), U_h is the homogenous velocity (or mixture superficial velocity), D is the inner pipe diameter and h_p is the axial pressure tapping separation.

Substituting Equation (3.8) into equation (3.12) and solving for $\alpha_{1,\text{hom}}$ gives;

$$\alpha_{1,\text{hom}} = \frac{\left(\Delta P_{pipe} + F_{m,pipe}\right)}{g h_P \cos\theta(\rho_w - \rho_g)}$$

Equation (3.14)

Once the gas volume fraction, $\alpha_{1,\text{hom}}$ from Equation (3.14) is obtained, the total mixture volumetric flow rate in a homogenous flow, $Q_{m,\text{hom}}$ can then be easily determined. The gas volumetric flow rate Q_g and the water volumetric flow rate Q_w may also be needed individually (therefore, $Q_g = \alpha_{1,\text{hom}} Q_{m,\text{hom}}$ and $Q_w = (1 - \alpha_{1,\text{hom}})Q_{m,\text{hom}}$).

3.1.2 A prediction model for the pressure drop sign change in a homogenous two phase flow through a Venturi meter

Many differential pressure cells can not read negative differential pressure drops (i.e. they can not read a differential pressure if the pressure at the '+' input is less than the pressure at the '-' input (see Figure 3-1)). The two phase air-water pressure drop across a Venturi meter may change its sign from positive to negative. In other words, in a two phase flow through a Venturi, in which the inlet and throat are connected to the dp cell via water filled lines, because the mixture density is lower than the density of water the pressure at the '+' input of the dp cell can be lower than the pressure at the '-' input (see Figure 3-1). This situation can never arise in a single phase flow. A new model has been developed to predict the sign change in the pressure drop across the dp cell for a vertical and inclined Venturis. This section describes how the sign change of the measured pressure drop can be predicted. The prediction model for the pressure drop sign change in two phase flow through a vertical and inclined pipe is described in Section 3.1.3.

It is important that the pressure drop sign change in two phase flow can be predicted so that the differential pressure cell can be correctly installed.

In terms of the homogenous velocity, U_h the mass conservation equation (see Equation (3.4)) can be re-written as;

$$U_2 = U_h \frac{A_1}{A_2}$$

Equation (3.15)

where $U_h = U_1$

Combining Equations (3.3), (3.8) and (3.15) gives;

$$\Delta P_{\text{hom}} = \frac{1}{2}\rho_w (1-\alpha_{1,\text{hom}}) U_h^2 \left\{ \left(\frac{A_1}{A_2} \right)^2 - 1 \right\} - \alpha_{1,\text{hom}} \rho_w g h_t \cos\theta + F_{mv}$$

Equation (3.16)

The frictional pressure loss (from the inlet to the throat of the Venturi) F_{mv} can be written as;

$$F_{mv} = \frac{2\rho_w h_t f U_h^{2*}}{D^*}$$

Equation (3.17)

where D^* is the average diameter between the inlet and the throat of the Venturi and U_h^* is the average homogenous velocity between inlet and the throat of the Venturi and can expressed as;

$$U_h^* = \frac{1}{2}(U_h + U_2)$$

Equation (3.18)

Combining Equations (3.15) and (3.18) gives;

$$U_h^* = U_h \left\{ 0.5 + \frac{A_1}{2A_2} \right\}$$

Equation (3.19)

The homogenous velocity can be expressed in terms of the reference homogenous mixture volumetric flow rate, $Q_{m,\hom,ref}$ using;

$$U_h = \frac{Q_{m,\hom,ref}}{A_1} = \frac{Q_{g,ref,\hom} + Q_{w,ref,\hom}}{A_1}$$

Equation (3.20)

where $Q_{g,ref,\hom}$ and $Q_{w,ref,\hom}$ are the reference gas and water volumetric flow rates respectively.

Re-arranging Equation (3.16) gives;

$$\Delta P_{\hom} = K_1(1-\alpha_{1,\hom})U_h^2 - \alpha_{1,\hom}K_2 + F_{mv}$$

Equation (3.21)

where;

$$K_1 = \frac{1}{2}\rho_w\left\{\left(\frac{A_1}{A_2}\right)^2 - 1\right\}$$

Equation (3.22)

and;

$$K_2 = \rho_w g h_t \cos\theta$$

Equation (3.23)

Equation (3.21) can be re-written as;

$$\Delta P_{\hom} = -C_1 + C_2$$

Equation (3.24)

where;

$$C_1 = \alpha_{1,\hom}K_2$$

Equation (3.25)

and;

$$C_2 = K_1(1-\alpha_{1,\hom})U_h^2 + F_{mv}$$

Equation (3.26)

It is clear from Equation (3.24) that the measured differential pressure across the dp cell is negative when;

$$C_1 > C_2$$

and positive when;

$$C_2 > C_1$$

3.1.3 Prediction model for the pressure drop sign change across the dp cell for homogenous two phase flow through a vertical or inclined pipe section

The single phase friction factor, f in Equation (3.13) can be expressed as;

$$f = \frac{\Delta P_w D}{2\rho_w h_p u^2}$$

Equation (3.27)

where ΔP_w is the pressure drop across a parallel pipe section in a single phase flow (water only) and u is the single phase (water) velocity.

Combining Equations (3.13) and (3.14) and solving for ΔP_{pipe} gives;

$$\Delta P_{pipe} = \alpha_{1,\hom} g h_p \cos\theta(\rho_w - \rho_g) - \frac{2\rho_w h_p f U_h^2}{D}$$

Equation (3.28)

It is clear from equation (3.28) that the pressure drop across the dp cell in two phase flow ΔP_{pipe} becomes negative if;

$$U_h^2 > \hat{K}$$

Equation (3.29)

where;

$$\hat{K} = \frac{\alpha_{1,\hom} g \cos\theta(\rho_w - \rho_g) D}{2 f \rho_w}$$

Equation (3.30)

Equation (3.30) can be re-arranged so that;

$$\hat{K} = k^* \frac{\alpha_{l,\text{hom}}}{f}$$

Equation (3.31)

where;

$$k^* = \frac{g \cos\theta(\rho_w - \rho_g)D}{2\rho_w}$$

Equation (3.32)

It should be noted that the constant, k^* depends on the flow and experimental conditions.

3.2 A novel separated two phase flow model

In a separated flow, the assumption of equal velocities for the different phases is no longer valid. In other words, the slip ratio *S*, is not unity. Stratified gas-water two phase flow is a separated flow where the gas and water travel with different velocities. A new stratified horizontal two phase flow model is described in Section 3.2.1. A new annular flow model where the liquid film flows at the wall of the pipe and the gas core flows at the centre of the pipeline is described in Section 3.2.2.

3.2.1 Stratified gas-water two phase flow model

In horizontal stratified flow, the water phase flows at the bottom of the pipe while the gas flows at the top. Each phase travels with its own velocity.

Figure 3-3 shows a horizontal stratified gas-water two phase flow through a Venturi meter. Due to the substantial difference between the water and the gas differential pressures across the Venturi in a stratified two phase flow, another low differential pressure device (i.e. an inclined manometer) may be used at the top of the Venturi to measure the differential pressure drop of the gas phase.

It should be noted that the horizontal interface in Figure 3-3 is symbolic only and it may not be horizontal in practice. This does not however affect the calculations-even if a non-horizontal interface is considered-since the measurement of the gas volume fraction at the inlet and the throat of the Venturi is exist.

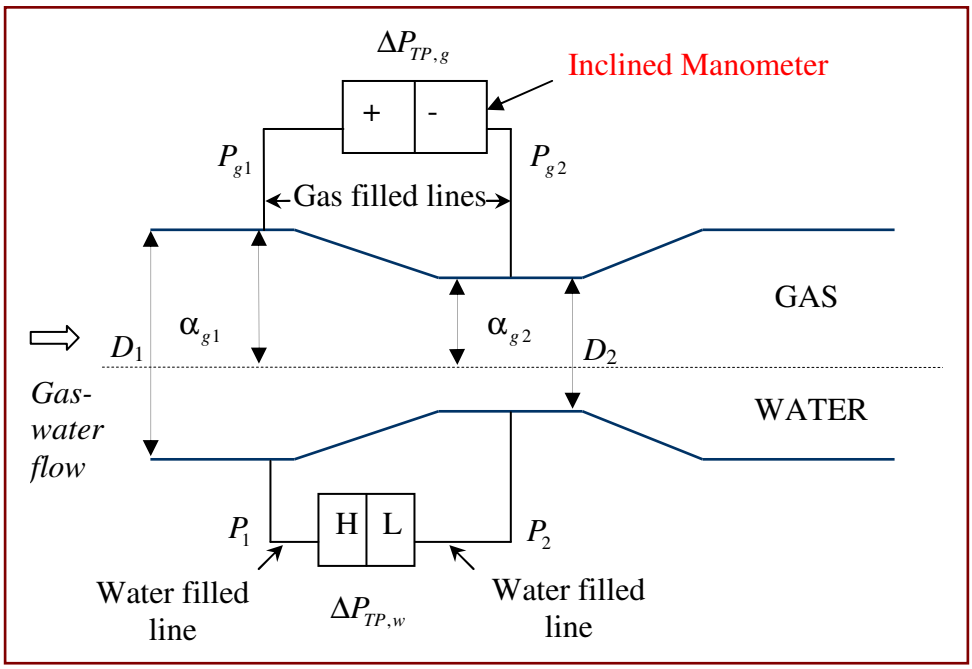

Figure 3-3: Stratified gas-water two phase flow through a Venturi meter

For the gas phase, the Bernoulli equation can be written as;

$$P_{g1}+\frac{1}{2}\rho_{g1}U_{g1}^2=P_{g2}+\frac{1}{2}\rho_{g2}U_{g2}^2$$

Equation (3.33)

where P, ρ and U are the static pressure, the density and the velocity respectively. The subscripts 1, 2 and g refer to the inlet, throat of the Venturi and the gas phase respectively.

The continuity equation of the gas phase is given by;

$$U_{g1}A_1\alpha_1\rho_{g1}=U_{g2}A_2\alpha_2\rho_{g2}=\dot{m}_g$$

Equation (3.34)

where $\dot{m}_g$ is the gas mass flow rate.

The gas density at the inlet of the Venturi ρ_{g1} is related to the gas density at the throat of the Venturi, ρ_{g2} by the following equation;

$$\frac{P_1}{\rho_{g1}^{\gamma}} = \frac{P_2}{\rho_{g2}^{\gamma}}$$

Equation (3.35)

where γ is the specific heat ratio or adiabatic index. ($\gamma = \frac{c_p}{c_v}$) where c_p and c_v are the specific heats at constant pressure and volume respectively.

Equation (3.35) can be re-arranged to give;

$$\rho_{g2} = \rho_{g1}(\hat{P})^{1/\gamma}$$

Equation (3.36)

where;

$$\hat{P} = \frac{P_2}{P_1}$$

Equation (3.37)

Combining Equations (3.34) and (3.36) gives;

$$U_{g1}\alpha_1 A_1 = U_{g2}\alpha_2 A_2(\hat{P})^{1/\gamma}$$

Equation (3.38)

Equation (3.38) can be re-written as;

$$U_{g2}^2(\hat{P})^{2/\gamma} = U_{g1}^2\left\{\frac{\alpha_1 A_1}{\alpha_2 A_2}\right\}^2$$

Equation (3.39)

Combining Equations (3.33) and (3.36) gives;

$$P_{g1} - P_{g2} = \frac{1}{2}\rho_{g1}\left\{(\hat{P})^{1/\gamma}U_{g2}^2 - U_{g1}^2\right\}$$

Equation (3.40)

Substituting Equation (3.39) into (3.40) gives;

$$P_{g1} - P_{g2} = \Delta P_{TP,g} = \frac{1}{2}\rho_{g1} U_{g1}^2 \left\{ \left(\frac{\alpha_1 A_1}{\alpha_2 A_2} \right)^2 (\hat{P})^{-1/\gamma} - 1 \right\}$$

Equation (3.41)

where $\Delta P_{TP,g}$ is the measured gas pressure drop under two phase flow. The pressure lines are gas filled and any differential pressure at the dp cell due to hydrostatic effect in the gas lines is negligible and so will be ignored.

Equation (3.41) can be re-written as;

$$U_{g1} = \sqrt{\frac{2\Delta P_{TP,g}}{\rho_{g1}}} \frac{1}{\sqrt{\left(\frac{\alpha_1 A_1}{\alpha_2 A_2} \right)^2 (\hat{P})^{-1/\gamma} - 1}}$$

Equation (3.42)

Substituting Equation (3.42) into (3.34) and introducing a discharge coefficient $C_{dg,st}$ for the gas phase in a horizontal stratified gas-water two phase flow gives;

$$\dot{m}_{g,st} = \rho_{g1} U_{g1} A_1 \alpha_1 = \sqrt{2\rho_{g1}\Delta P_{TP,g}} \frac{C_{dg,st} A_1 \alpha_{1,st}}{\sqrt{\left(\frac{\alpha_{1,st} A_1}{\alpha_{2,st} A_2} \right)^2 (\hat{P})^{-1/\gamma} - 1}}$$

Equation (3.43)

where $\dot{m}_{g,st}$ is the gas mass flow rate in a horizontal stratified gas-water two phase flow through a Venturi meter. The subscript *st* in Equation (3.43) is added to distinguish between a horizontal stratified flow and other flow regimes.

The gas density ρ_{g1} in Equation (3.43) can be written as;

$$\rho_{g1} = \frac{P_1}{rT_1}$$

Equation (3.44)

where P_1 and T_1 are the absolute pressure and absolute temperature at the inlet section respectively and *r* is the specific gas constant and is given by;

$$r = \frac{1000R}{M_m}$$

Equation (3.45)

where R is the universal gas constant and M_m is the relative molecular mass of the air.

For the liquid phase, the Bernoulli equation can be expressed as;

$$P_1 + \frac{1}{2}\rho_w U_{w1}^2 = P_2 + \frac{1}{2}\rho_w U_{w2}^2$$

Equation (3.46)

where the subscript *w* refers to the water phase.

The continuity equation of the water phase in a stratified gas-water two phase flow is given by;

$$U_{w1}(1-\alpha_1)A_1\rho_w = U_{w2}(1-\alpha_2)A_2\rho_w = \dot{m}_w$$

Equation (3.47)

Re-arranging Equation (3.47) gives;

$$U_{w2} = U_{w1}\frac{(1-\alpha_1)A_1}{(1-\alpha_2)A_2}$$

Equation (3.48)

Substituting Equation (3.48) into (3.46) gives;

$$(P_1 - P_2) = \frac{1}{2}\rho_w U_{w1}^2\left\{\left[\frac{(1-\alpha_1)A_1}{(1-\alpha_2)A_2}\right]^2 - 1\right\}$$

Equation (3.49)

Re-arranging Equation (3.49) gives;

$$U_{w1} = \sqrt{\frac{2(P_1 - P_2)}{\rho_w}}\frac{1}{\sqrt{\left\{\frac{(1-\alpha_1)A_1}{(1-\alpha_2)A_2}\right\}^2 - 1}}$$

Equation (3.50)

Substituting Equation (3.50) into (3.47) gives;

$$\dot{m}_{w,st} = \sqrt{2\rho_w (P_1 - P_2)} \frac{(1-\alpha_{1,st})A_1}{\sqrt{\left\{\frac{(1-\alpha_{1,st})A_1}{(1-\alpha_{2,st})A_2}\right\}^2 - 1}}$$

Equation (3.51)

The subscript *st* is added in Equation (3.51) just to distinguish between a horizontal stratified flow and other flow regimes.

Figure 3-4 shows the real shape of the gas-water boundary in the horizontal Venturi meter that has been observed in the current investigation. The boundary undergoes a step change in height from the inlet to the throat of the Venturi meter.

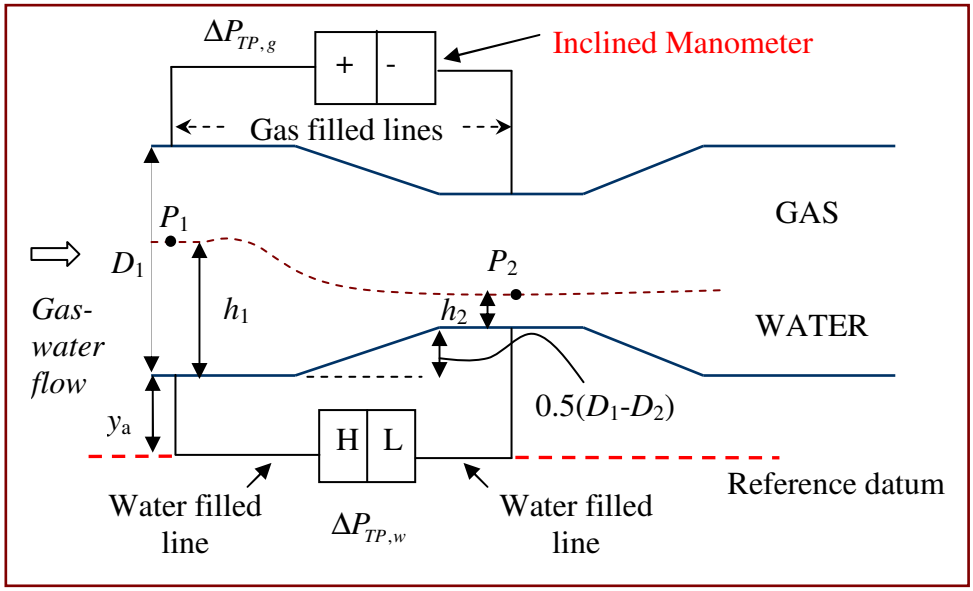

Figure 3-4: A real (approximated) air-water boundary through a Venturi meter

By basing the analysis on the water boundary at the interface, the influence of the change in water height on the expression of the water mass flow rate through the Venturi can be eliminated. With reference to Figure 3-4, Bernoulli's equation for a particle of the water phase at the boundary can be written as;

$$P_1 + \frac{1}{2}\rho_w U_{w1}^2 + \rho_w g h_1 = P_2 + \frac{1}{2}\rho_w U_{w2}^2 + \rho_w g(h_2 + 0.5(D_1 - D_2))$$

Equation (3.52)

Re-arranging Equation (3.52) gives;

$$(P_1 - P_2) = \frac{1}{2}\rho_w (U_{w2}^2 - U_{w1}^2) - \rho_w g\{(h_1 - h_2) - 0.5(D_1 - D_2)\}$$

Equation (3.53)

Equation (3.53) can be re-written as;

$$(P_1 - P_2) - \Delta\tilde{P} = \frac{1}{2}\rho_w (U_{w2}^2 - U_{w1}^2)$$

Equation (3.54)

where;

$$\Delta\tilde{P} = -\rho_w g\{(h_1 - h_2) - 0.5(D_1 - D_2)\}$$

Equation (3.55)

From Figure 3-4, it is possible to write;

$$P_1 + \rho_w g(y_a + h_1) - \{P_2 + \rho_w g(y_a + 0.5(D_1 - D_2) + h_2)\} = \Delta P_{TP,w}$$

Equation (3.56)

where $\Delta P_{TP,w}$ is the measured pressure drop across the lower differential pressure sensor in Figure 3-4. Note that this dp cell is connected to the Venturi by water filled lines.

Re-arranging Equation (3.56) gives;

$$(P_1 - P_2) = \Delta P_{TP,w} - \rho_w g\{(h_1 - h_2) - 0.5(D_1 - D_2)\}$$

Equation (3.57)

Substituting Equation (3.55) into (3.57) gives;

$$(P_1 - P_2) = \Delta P_{TP,w} + \Delta\tilde{P}$$

Equation (3.58)

Combining Equations (3.48), (3.54) and (3.58) and introducing a discharge coefficient $C_{dw,st}$ for the water phase in a stratified gas-water two phase flow enables derivation of the following expression for the water mass flow rate, $\dot{m}_{w,st}$ in stratified gas-water two phase flow;

$$\dot{m}_{w,st} = C_{dw,st} \frac{(1-\alpha_{1,st})A_1}{\sqrt{\left\{\frac{(1-\alpha_{1,st})A_1}{(1-\alpha_{2,st})A_2}\right\}^2 - 1}} \sqrt{2\rho_w \Delta P_{TP,w}}$$

Equation (3.59)

In a separated flow, the slip ratio, *S* is not unity as in homogenous flow. The slip ratio, *S* at the inlet and the throat of the Venturi can be expressed respectively as;

$$S_1 = \frac{U_{g1}}{U_{w1}}$$

Equation (3.60)

and;

$$S_2 = \frac{U_{g2}}{U_{w2}}$$

Equation (3.61)

Dividing Equation (3.34) by (3.47) and combining Equations (3.36), (3.60) and (3.61) gives;

$$\frac{\alpha_2}{\alpha_1} = \frac{(\hat{P})^{-1/\gamma}}{\left\{\frac{S_2}{S_1}(1-\alpha_1) + \alpha_1(\hat{P})^{-1/\gamma}\right\}}$$

Equation (3.62)

3.2.2 Vertical annular gas-water flow model through a Venturi meter

The new model of a vertical annular gas-water flow through a Venturi meter depends on the measurements of the gas volume fractions at the inlet and the throat of the

Venturi rather than relying on prior knowledge of the mass flow quality as in previous models (see Section 2.2). This model is based on the fact that each phase flows separately as shown in Figure 3-5.

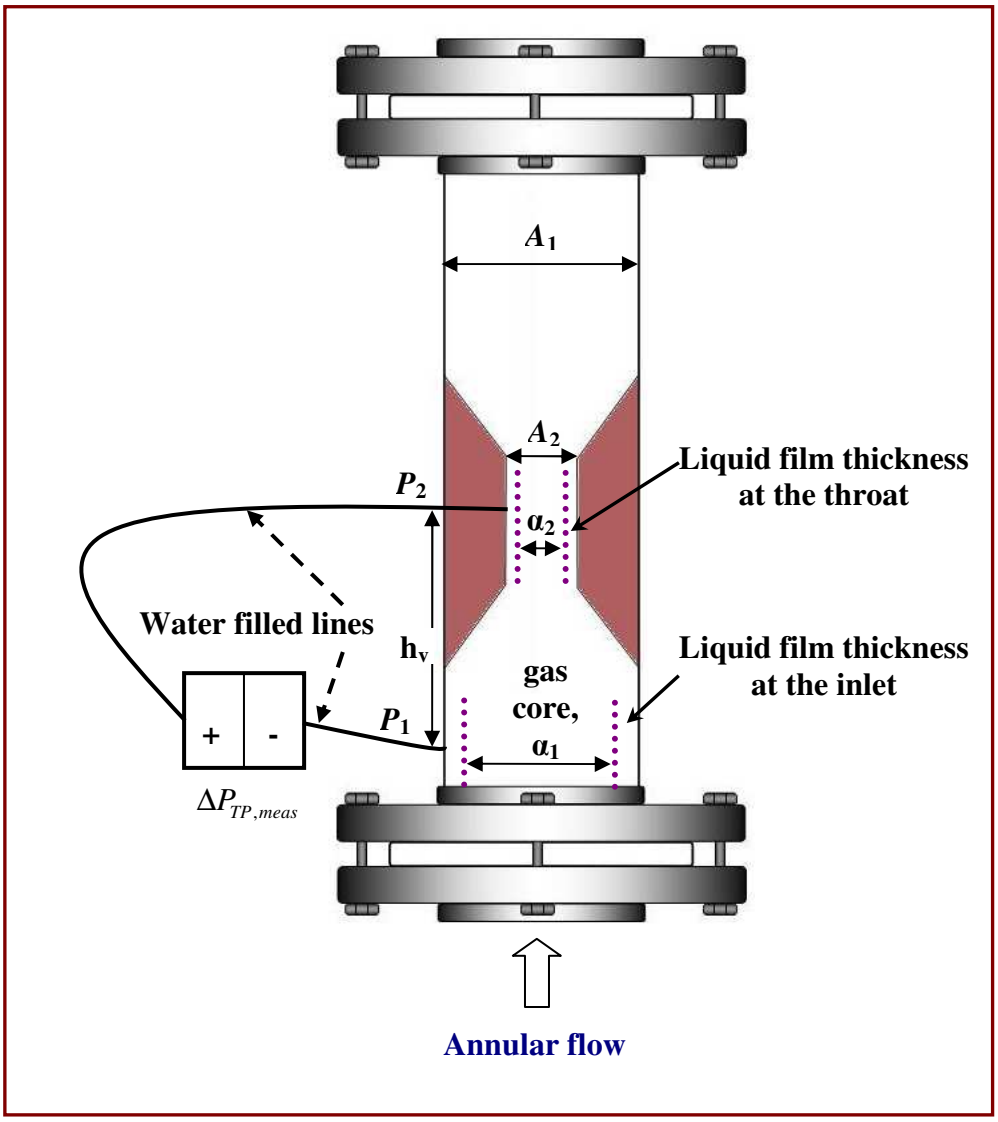

Figure 3-5: Annular gas-water flow through a Venturi meter

For the gas phase in vertical annular flow, the Bernoulli equation can be written as;

$$P_1 + \frac{1}{2}\rho_{g1}U_{g1}^2 = P_2 + \frac{1}{2}\rho_{g2}U_{g2}^2 + \Delta P_H$$

Equation (3.63)

where ΔP_H is the magnitude of the hydrostatic head loss between the inlet and the throat of the Venturi (i.e. between the pressure tappings shown in Figure 3-5).
From Equations (3.34), (3.36) and (3.63) the following relationship is obtained;

$$(\Delta P_{TP,wg} - \Delta P_H) = \frac{1}{2}\rho_{g1}U_{g1}^2\left\{\left(\frac{\alpha_1 A_1}{\alpha_2 A_2}\right)^2 (\hat{P})^{-1/\gamma} - 1\right\}$$

Equation (3.64)

where $\Delta P_{TP.wg}$ is the gas-water two phase differential pressure drop across the Venturi in annular flow and is equal to $(P_1 - P_2)$.

Equation (3.64) can be re-arranged to give;

$$U_{g1} = \frac{1}{\sqrt{\left(\frac{\alpha_1 A_1}{\alpha_2 A_2}\right)^2 (\hat{P})^{-1/\gamma} - 1}}\sqrt{\frac{2(\Delta P_{TP,wg} - \Delta P_H}{\rho_{g1}}}$$

Equation (3.65)

Combining Equations (3.34) and (3.65) and introducing a discharge coefficient for the gas phase in annular flow gives;

$$\dot{m}_{g,wg} = C_{dg,wg}\frac{\left(2\rho_{g1}\left\{\Delta P_{TP,wg} - \Delta P_H\right\}\right)^{\frac{1}{2}} A_1 A_2 \alpha_{1,wg}\alpha_{2,wg}}{\left\{\left(\alpha_{1,wg}A_1\right)^2\left(\hat{P}\right)^{\frac{-1}{\gamma}} - \left(\alpha_{2,wg}A_2\right)^2\right\}^{\frac{1}{2}}}$$

Equation (3.66)

where $\dot{m}_{g,wg}$ and $C_{dg,wg}$ are the predicted gas mass flow rate in annular gas-water flow through the Venturi and the gas discharge coefficient in annular flow respectively. The subscript *wg* in Equation (3.66) is added to α_1 and α_2 to distinguish between the gas volume fraction in annular gas-water flow and other flow regimes.

With reference to Figure 3-5 and given that the lines joining the pressure tappings to the dp cell are water filled, $\Delta P_{TP,wg}$ in Equation (3.66) can be written as;

$$\Delta P_{TP,wg} = \rho_w g h_v - \Delta P_{wg,meas}$$

Equation (3.67)

where $\Delta P_{wg,meas}$ is the differential pressure in annular gas-water flow measured by the dP cell.

The hydrostatic head loss term ΔP_H in Equation (3.66) can be calculated by making the assumption that the mean gas volume fraction in the converging section of the Venturi is $\overline{\alpha}$ (see Figure 3-6) where;

$$\overline{\alpha} = \frac{\alpha_{1,wg} + \alpha_{2,wg}}{2}$$

Equation (3.68)

where $\alpha_{1,wg}$ and $\alpha_{2,wg}$ are the gas volume fractions at the inlet and the throat of the Venturi in annular flow.

The hydrostatic head loss term ΔP_H can now be expressed as follows (using the position of the pressure tappings shown in Figure 3-6);

$$\Delta P_H = g h_i \left\{\rho_w (1-\alpha_{1,wg}) + \rho_{g1}\alpha_{1,wg}\right\} + g h_c \left\{\rho_w (1-\overline{\alpha}) + \overline{\rho}_g \overline{\alpha}\right\} + g h_{tt} \left\{\rho_w (1-\alpha_{2,wg}) + \rho_{g2}\alpha_{2,wg}\right\}$$

Equation (3.69)

where h_i, h_c and h_{tt} are the heights defined in Figure 3-6.

The gas discharge coefficient $C_{dg,wg}$ can be expressed as;

$$C_{dg,wg} = \frac{\dot{m}_{g,ref,wg}}{\dot{m}_{g,wg}}$$

Equation (3.70)

where $\dot{m}_{g,ref,wg}$ is the reference gas mass flow rate in annular flow.

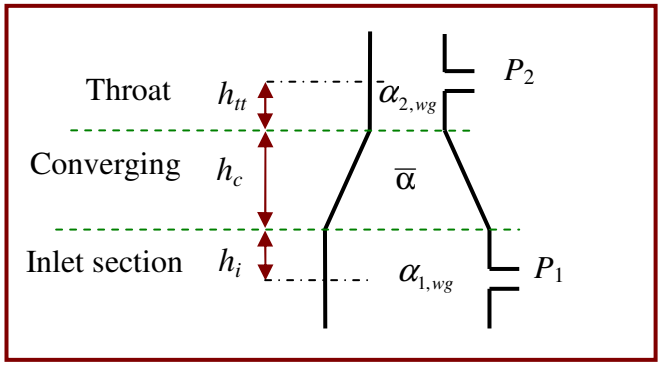

Figure 3-6: Inlet, converging and throat sections of the Venturi meter

For the water phase in vertical annular flow, the Bernoulli equation can be written as;

$$P_1 + \frac{1}{2}\rho_w U_{w1}^2 = P_2 + \frac{1}{2}\rho_w U_{w2}^2 + \Delta P_H$$

Equation (3.71)

Equations (3.47), (3.48) and (3.71) can now be combined to give the water mass flow rate in annular gas-water flow $\dot{m}_{w,wg}$;

$$\dot{m}_{w,wg} = C_{dw,wg}\sqrt{2\rho_w(\Delta P_{TP,wg} - \Delta P_H)}\,\frac{A_1(1-\alpha_{1,wg})A_2(1-\alpha_{2,wg})}{\sqrt{(1-\alpha_{1,wg})^2 A_1^2 - (1-\alpha_{2,wg})^2 A_2^2}}$$

Equation (3.72)

where $C_{dw,wg}$ is the water discharge coefficient in annular flow. $\Delta P_{TP,wg}$ and ΔP_H are defined by Equations (3.67) and (3.69) respectively. Again the subscript wg in Equation (3.72) is added to α_1 and α_2 to distinguish between the gas volume fraction in annular flow and the gas volume fraction in other flow regimes.

It should be noted that for a given phase, the mass flow rate, $\dot{m}$ is related to the volumetric flow rate, Q by;

$$\dot{m} = \rho\, Q$$

Equation (3.73)

where ρ is the density of the phase in question. Hence, the gas and water volumetric flow rates can be calculated using Equations (3.66), (3.72) and (3.73).

Summary

A mathematical model of a homogenous gas-water two phase flow through a Venturi meter has been developed. In homogenous flow, the slip velocity can be assumed to be unity. The gas volume fraction throughout the Venturi meter in a homogenous flow can be assumed constant. The gas volume fraction at the inlet of the Venturi in a homogenous gas-water two phase flow $\alpha_{1,\text{hom}}$ can be measured by a differential pressure technique also known as an "online flow density meter". The measurement of the gas volume fraction at the inlet of the Venturi meter enables the volumetric flow rate of the homogenous mixture, $Q_{m,\text{hom}}$ to be determined (see Equation (3.9)).

In a separated flow, the assumption of equal phase velocities is no longer valid and relying only on measurement of the gas volume fraction at the inlet of the Venturi would not reasonably be expected to lead to highly accurate results. New models were investigated to measure the gas/water mass flow rate in a stratified/annular two phase flows through a Venturi meter. The measurements of the differential pressure across the Venturi meter and the gas volume fractions at the inlet and the throat of the Venturi enable the gas and the water mass flow rates in separated flows (i.e. horizontal stratified and vertical annular flows) to be determined using Equations (3.43), (3.59), (3.66) and (3.72).

It is clear that, the advantage of the new separated flow models (see Section 3.2) over the previous models described in Section 2.2 is that they do not require prior knowledge of mass flow quality, x. In other words, the new models depend only on the measurement of α_1 ***and*** α_2 ***which makes the measurement technique more practical than those used previously.***

Chapter 4

Design and Construction of a Flow Density Meter (FDM), Universal Venturi Meter and a Conductance Multiphase flow Meter

Introduction

Two Venturis were used in the research described in this thesis. The first Venturi which is a Universal Venturi Tube (UVT) (interchangeably called a non-conductance UVT in this thesis) was used to study a bubbly (gas-water two phase flow while the second Venturi was used to study separated flows (i.e. annular and stratified flows). The second Venturi used in this research is called a Conductance Multiphase Venturi Meter (CMVM) because it contains apparatus for measuring the electrical conductance of flowing mixtures. The CMVM is combined with the Conductance Inlet Void Fraction Meter (CIVFM) to form the conductance multiphase flow meter.

In a homogenous gas-water flow, the gas volume fraction at the inlet and the throat of the Venturi can be assumed equal. Therefore, measurement of the gas volume fraction $\alpha_{1,\text{hom}}$ at the inlet of the Venturi enables estimation of the mixture volume flow rate $Q_{m,\text{hom}}$ in a homogenous gas-water two phase flow through a Venturi meter

using Equation (3.9). A Flow Density Meter (FDM) was designed and constructed to measure the gas volume fraction $\alpha_{l,\mathrm{hom}}$ at the inlet of the non-conductance Venturi meter. The UVT was designed and constructed principally to study homogenous gas-water two phase flows (see Section 4.2).

Separated flow in a Venturi meter is highly complex and, therefore, to measure $\dot{m}_{g,wg}$, $\dot{m}_{w,wg}$, $\dot{m}_{g,st}$ and $\dot{m}_{w,st}$ (see Equations (3.43), (3.59), (3.66) and (3.72)) in such conditions a gas volume fraction measurement technique must also be introduced at the throat of the Venturi instead of just relying on the gas volume fraction measurement at the Venturi inlet.

An advanced conductance multiphase flow meter which is capable of measuring the gas volume fractions at the inlet and the throat of the Venturi was designed and constructed. This device combined the CIVFM and the CMVM.

The CIVFM measured the gas volume fraction at the inlet of the Venturi while the CMVM measured the gas volume fraction at the throat of the Venturi meter. This arrangement enables gas volume fraction measurements to be made in horizontal flows unlike the FDM technique, described in Sections 3.1.1 and 4.1, which relies on some vertical separation between the pressure tappings. Two ring electrodes at the inlet and two ring electrodes at the throat of the Venturi were used to obtain the gas volume fraction at the inlet and the throat of the Venturi [145].

In this chapter, the design and construction of the FDM which is capable of measuring the gas volume fraction at the inlet of the UVT in a bubbly (approximately homogenous) gas-water two phase flow is presented in Section 4.1. The FDM cannot be used in horizontal flows but homogenous air-water flows are normally only encountered in vertical or near vertical pipelines (and with gas volume fraction less than about 17%).

This chapter also presents the design and construction of the UVT and the conductance multiphase flow meter which can be used to study homogenous and

separated flows respectively (see Sections 4.2 and 4.3). The design of the wall conductance sensors that can be used to measure the liquid film flow rate in annular gas-water two phase flow is also presented in Section 4.4.

4.1 Design of the Flow Density Meter (FDM)

A combination of the FDM and the non-conductance Venturi meter (or UVT) enables the mixture volumetric flow rate in a homogenous gas-water two phase flow to be determined (see Equation (3.9)). The design of the UVT is discussed in Section 4.2. Figure 4-1 shows the design of the online FDM.

The gauge pressure sensor was used as shown in Figure 4-1. Measured gauge pressure was added to atmospheric pressure (from a barometer) to give absolute pressure in the FDM. The absolute pressure together with the measured temperature (from a thermocouple) in ^{o}K were used to correct the measured reference gas mass flow rate from a thermal mass flow meter to a reference gas volumetric flow rate.

In order to determine the gas volume fraction at the inlet of the UVT using the FDM, the differential pressure ΔP_{pipe} (see Equation (3.11)) must be measured. A Yokogawa dp cell connected to the pressure tappings via water filled lines was installed to do this task. The pressure tapping separation in the vertical pipe section is 1m. It should be noted that the FDM can be used in vertical and inclined flows (but not horizontal). For the current study, it was only used in vertical flows (i.e. $\theta = 0$ in Equation (3.14)).

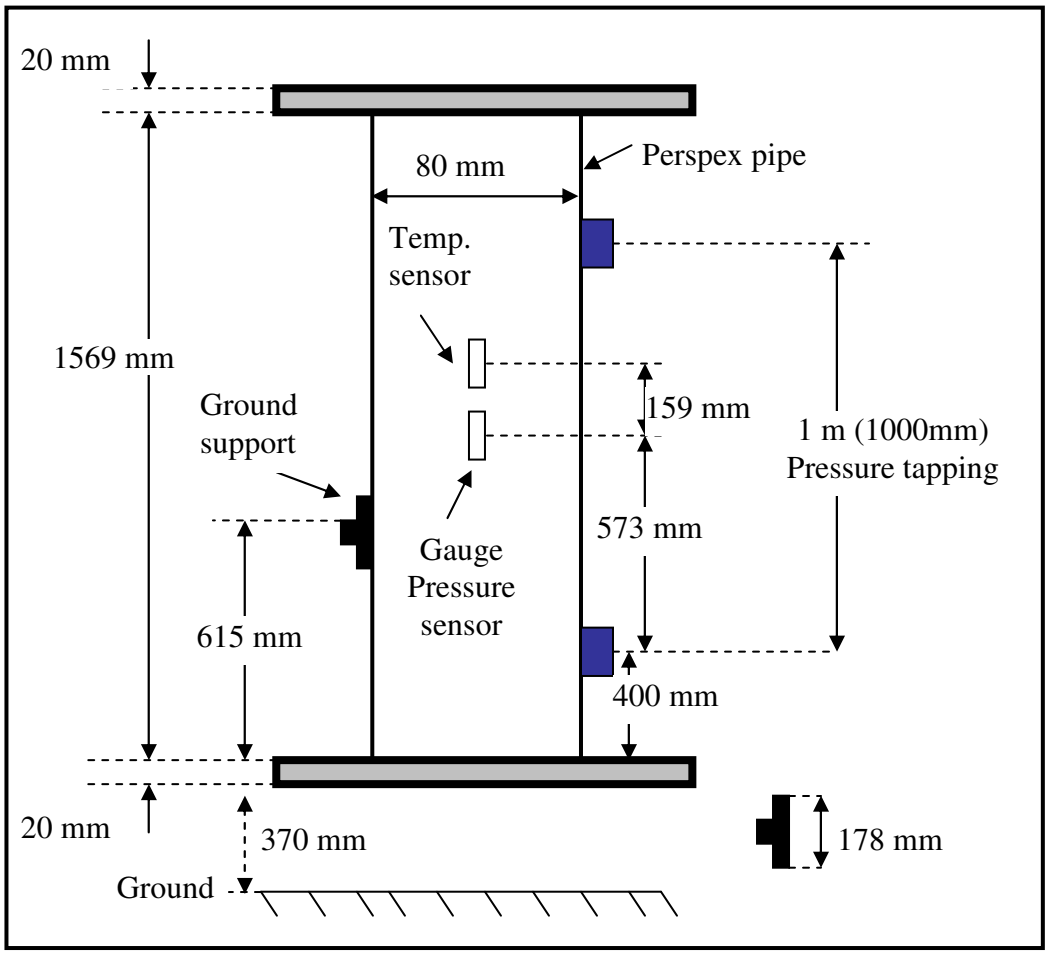

Figure 4-1: The design of the FDM

4.2 Design of the Universal Venturi Tube (UVT)

The UVT was used to study vertical bubbly (approximately homogenous) gas-water two phase flows, and Figure 4-2 shows the dimensions of the UVT. Basically, this Venturi meter was originally designed at the University of Huddersfield to measure the water or gas flow rate alone (i.e. single phase flow rate). Since a homogenous flow can be treated as a single phase flow, this Venturi design was used in conjunction with the FDM described in Section 4.1 to study vertical, bubbly (approximately homogenous) gas water two phase flows.

The angles and dimensions of the UVT are identical to the hydraulic shape designed by [146]. This Venturi meter is composed of the transition section (which consists of

a 40^o inlet and a 7^o throat cone), the throat section and the 5^o outlet section (see Figure 4-2). The Venturi meter and its 2D drawing were designed using "Solid Works" package.

A differential pressure ΔP_{hom} measured by a dp cell connected between the inlet and throat of the Venturi meter via water filled lines was necessary to calculate the mixture volumetric flow rate $Q_{m,\text{hom}}$ (see Equation (3.9)). This differential pressure was measured using a Honeywell differential pressure transmitter.

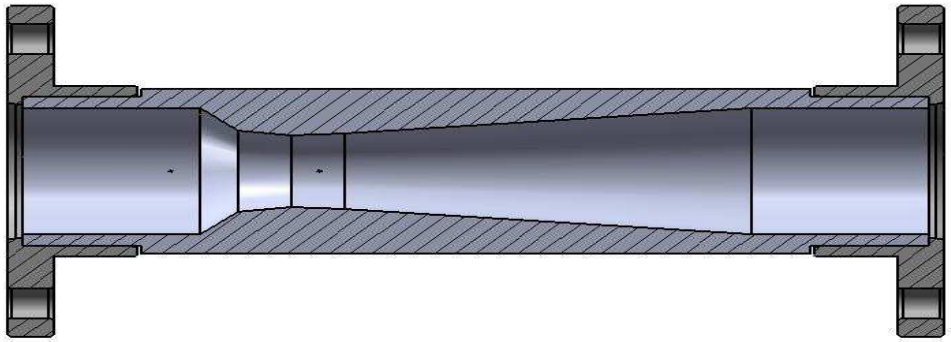

(a) Assembly of the non-conductance Venturi meter (UVT)

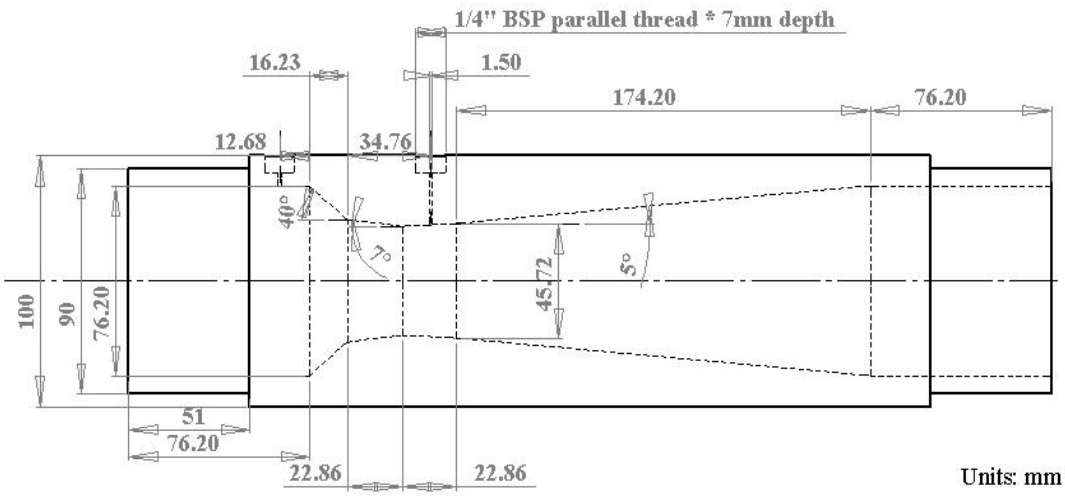

(b) 2D drawing of the non-conductance Venturi meter (UVT)

Figure 4-2: The design of the non-conductance Venturi meter (UVT)

A schematic diagram of the combined FDM section and the UVT which represents the test section used to investigate vertical, bubbly (approximately homogenous) gas water two phase flows is shown in Figure 4-3.

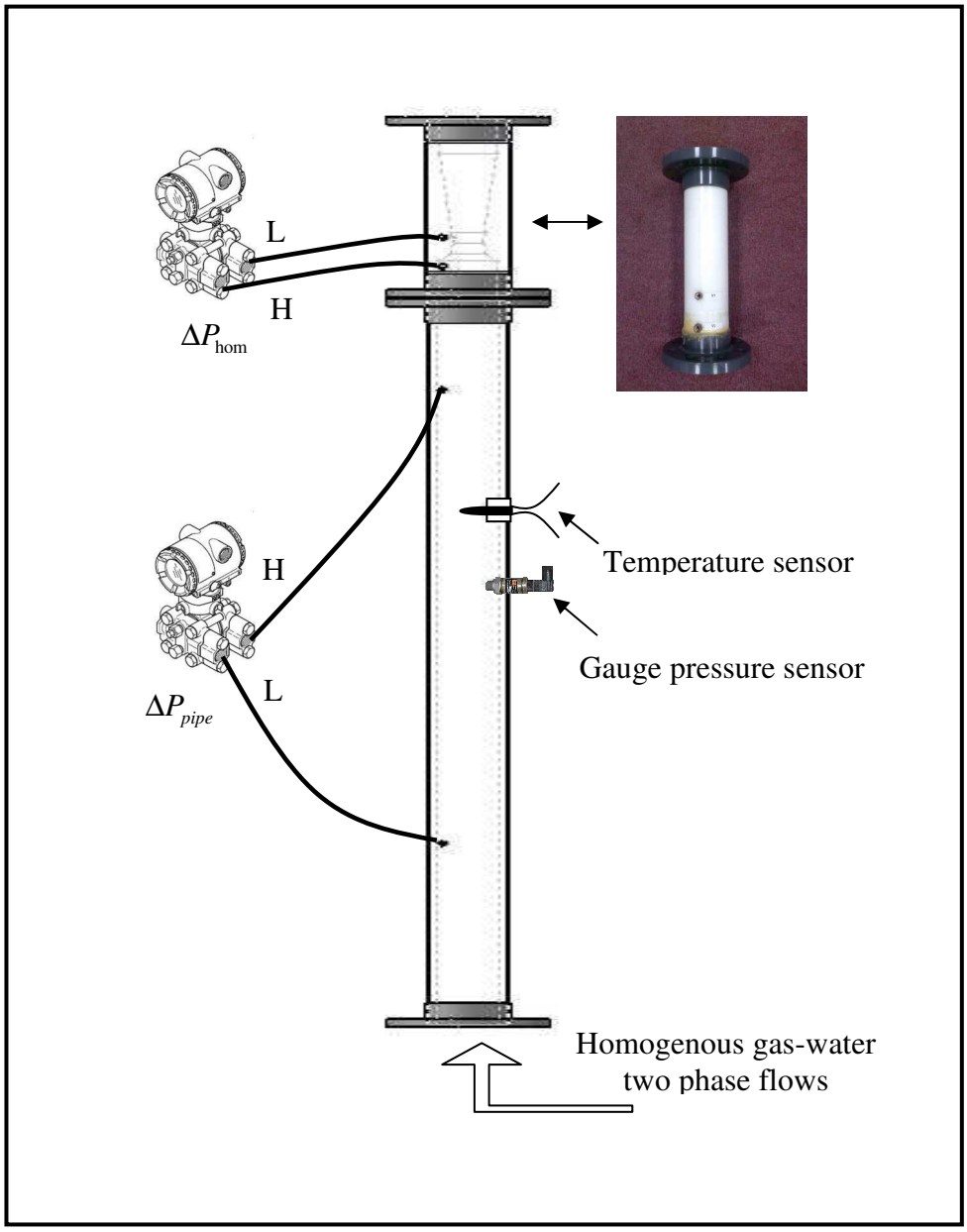

Figure 4-3: A schematic diagram of the FDM and the UVT (insert photo shows-the UVT)

4.3 Design of the conductance multiphase flow meter

The reason for designing the novel conductance multiphase flow meter is to enable measurement of the gas volume fraction at the inlet and the throat of the Venturi using an electrical conductance technique. This, in turn, enables the gas and the water flow rates to be measured in separated flows (i.e. annular (wet gas) and stratified gas-water two phase flows) using the theory outlined in Chapter 3. The use of electrical conductance techniques means that gas volume fraction measurement is possible even in horizontal flows. The FDM technique described in Section 4.1 relies on differential pressure measurement and so cannot be used in horizontal flows. Measurement of the gas volume fraction at the inlet and the throat of the Venturi gives an advantage over previous work because it is not necessary to know the mass flow quality, x (see the new mathematical model in Sections 3.2.1 and 3.2.2). This makes the measurement technique described in this thesis more reliable and practical.

The conductance multiphase flow meter consists of two parts;

(i) The Conductance Inlet Void Fraction Meter, CIVFM (see Section 4.3.1), and
(ii) The Conductance Multiphase Venturi Meter, CMVM (see Section 4.3.2).

The CIVFM is used to measure the gas volume fraction at the inlet of the Venturi. Electrodes at the throat section of the CMVM are used to measure the gas volume fraction at the throat of the Venturi.

4.3.1 Design of the conductance inlet void fraction meter (CIVFM)

The CIVFM was designed to measure the gas volume fraction at the inlet of the Venturi by measuring the electrical conductance of the water-air mixture between two electrodes (denoted 'Electrode-1' and 'Electrode-2' in Figure 4-4). Figure 4-4 shows the assembly of the CIVFM. The 2D drawing of the CIVFM is shown in Figure 4-5. Figure 4-6 shows some photos of the CIVFM.

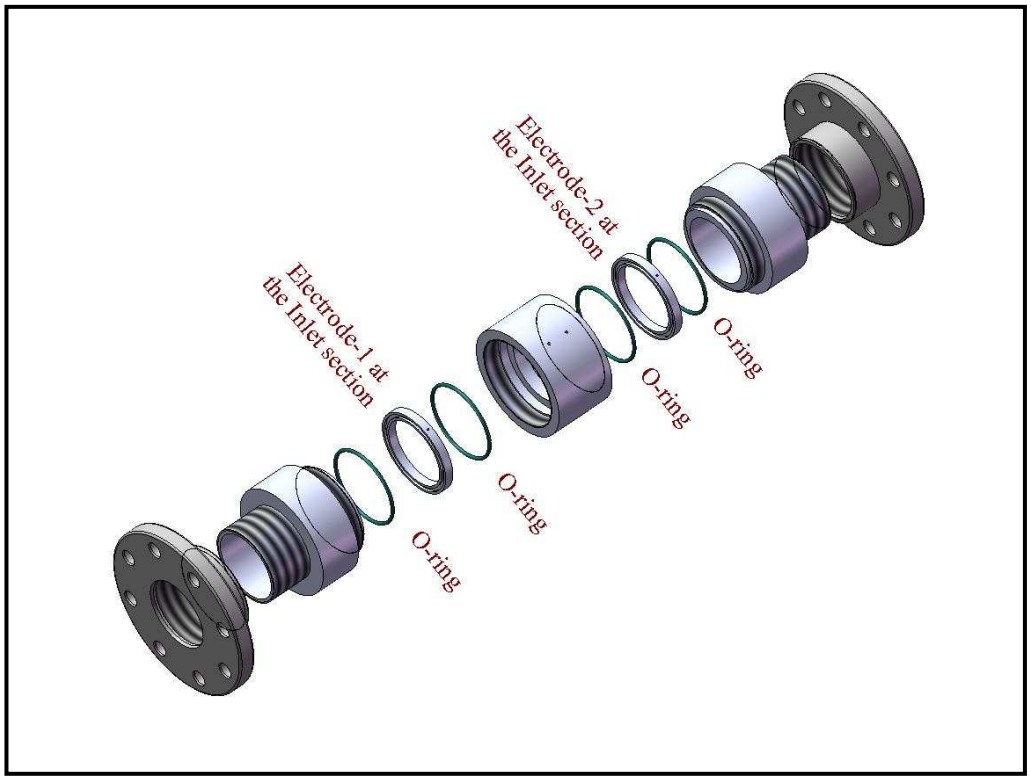

Figure 4-4: Assembly parts of the conductance inlet void fraction meter CIVFM)

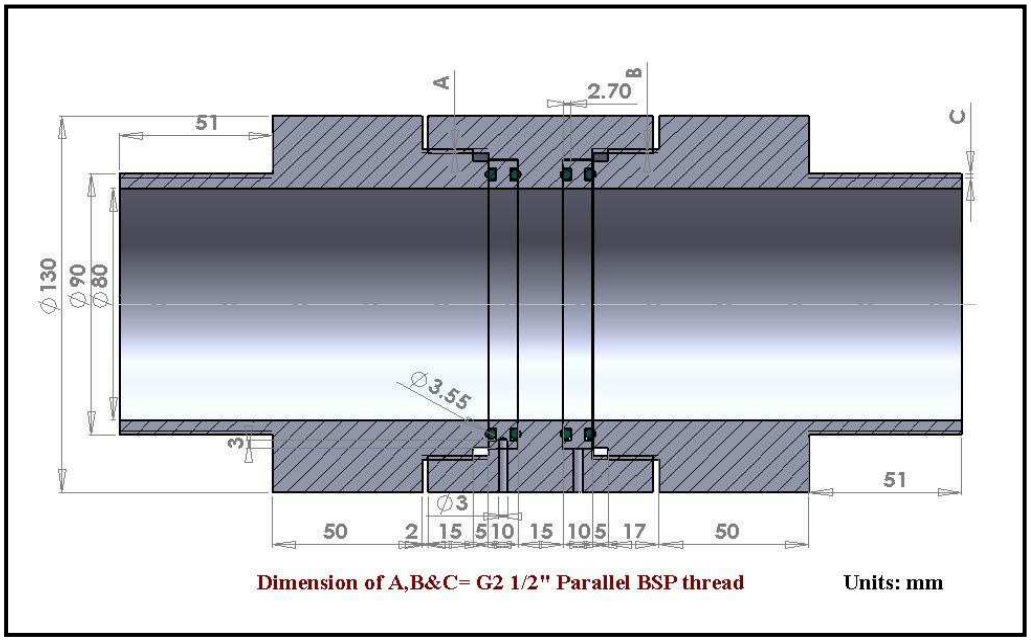

Figure 4-5: 2D drawing of the conductance inlet void fraction meter (CIVFM)

Figure 4-6: Photos of the conductance inlet void fraction meter (CIVFM)

4.3.2 Design of the Conductance Multiphase Venturi Meter (CMVM)

The CMVM shown in Figure 4-7 consists of eleven elements; two threaded flanges, four O-rings, two stainless steel electrodes, and Venturi, inlet, throat, and outlet sections. The two stainless steel electrodes flush mounted with the inner surface of the Venturi throat are used for measuring the gas volume fraction at the throat by measuring the electrical conductance of the water-air mixture, as described in Sections 5.1 and 5.3. One of the most advanced features of this design is that all parts can be assembled/disassembled easily including the threaded flanges. Another advantage of this design is that it is very straightforward to change the throat section [145]. Changing the throat section with four electrodes enables the velocity of the water film in annular flow to be determined using a cross-correlation technique.

2-D drawings of the inlet, electrode, throat and the outlet of the conductance Venturi section are shown in Figures 4-8 to 4-11. The complete 2-D drawing of the CMVM including all eleven parts; the inlet, four electrodes with eight o-rings, the throat and the outlet sections is shown in Figure 4.12.

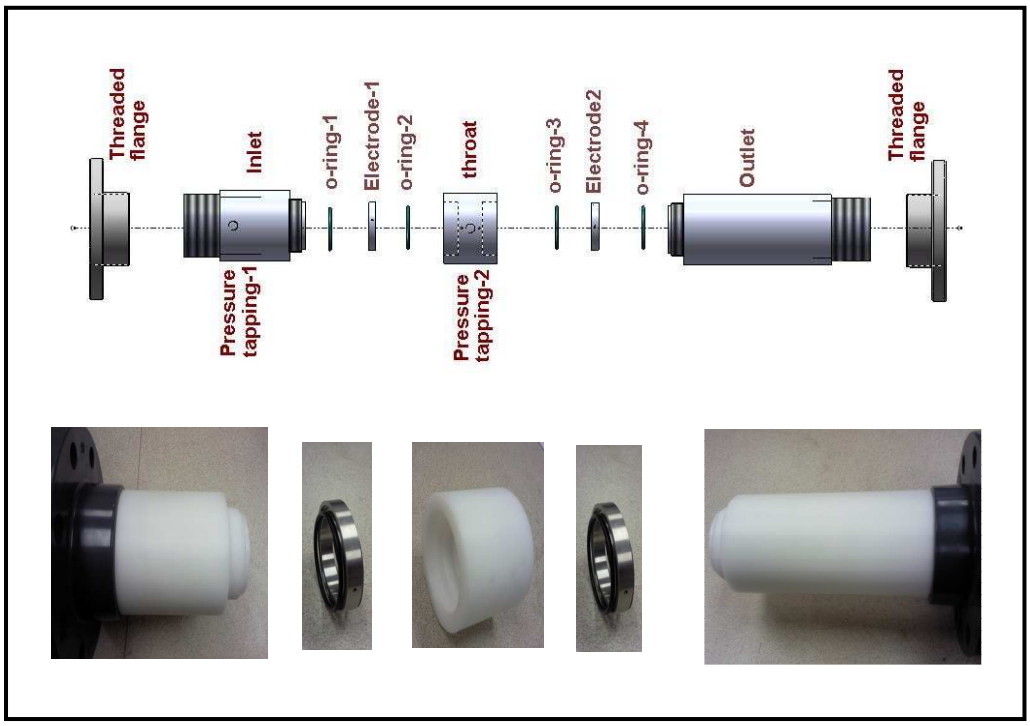

Figure 4-7: The assembly parts of the conductance multiphase Venturi meter (CMVM)

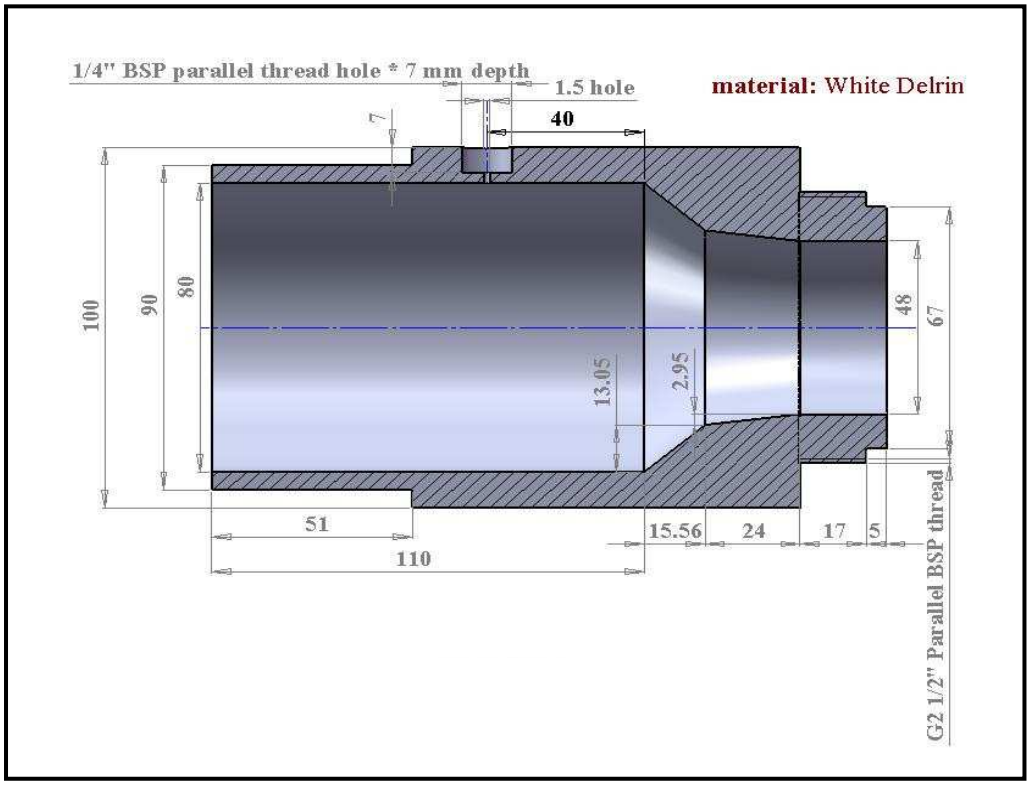

Figure 4-8: Inlet section of the CMVM

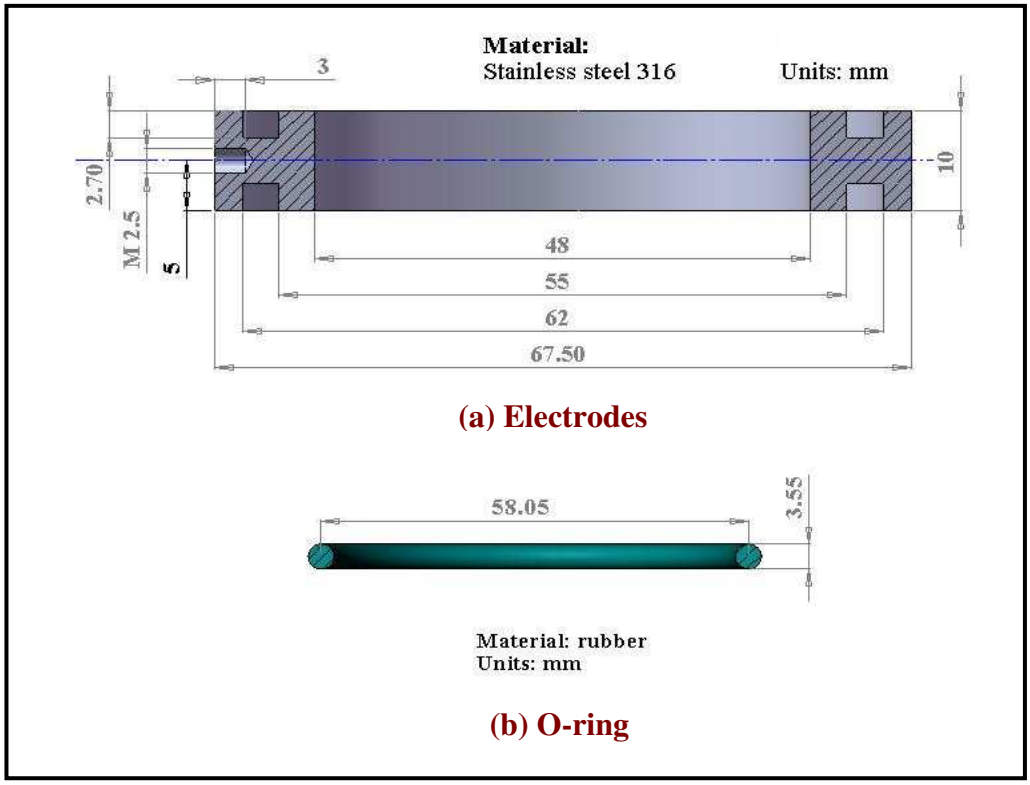

Figure 4-9: Design of the electrode and O-ring

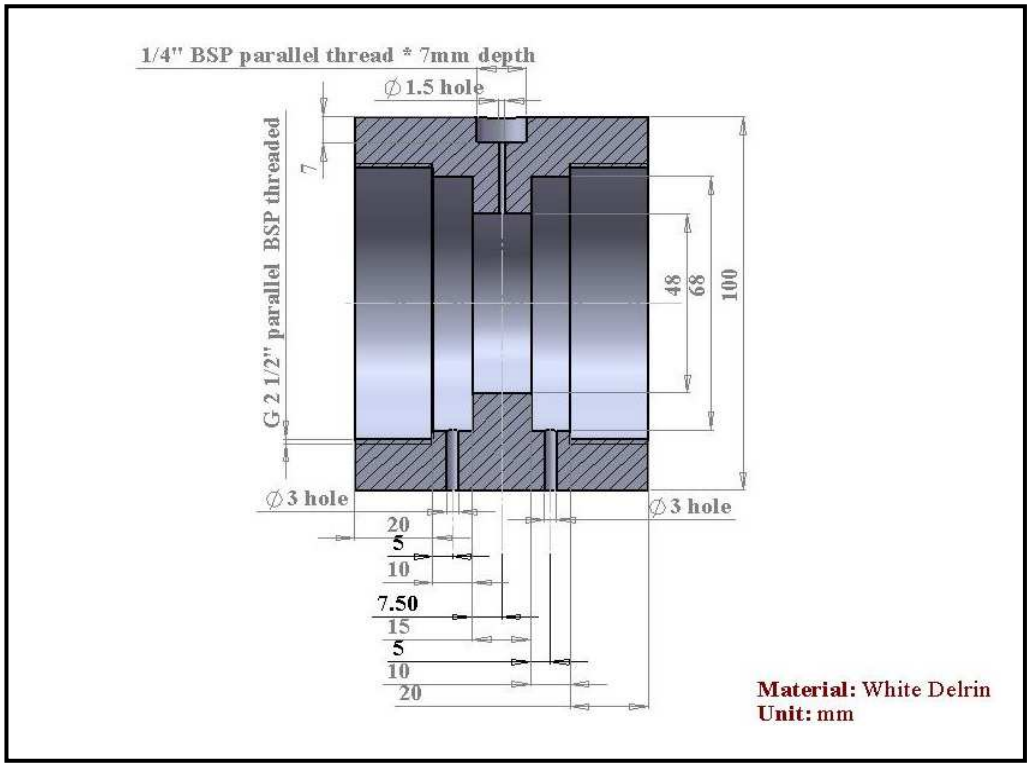

Figure 4-10: Design of the throat section

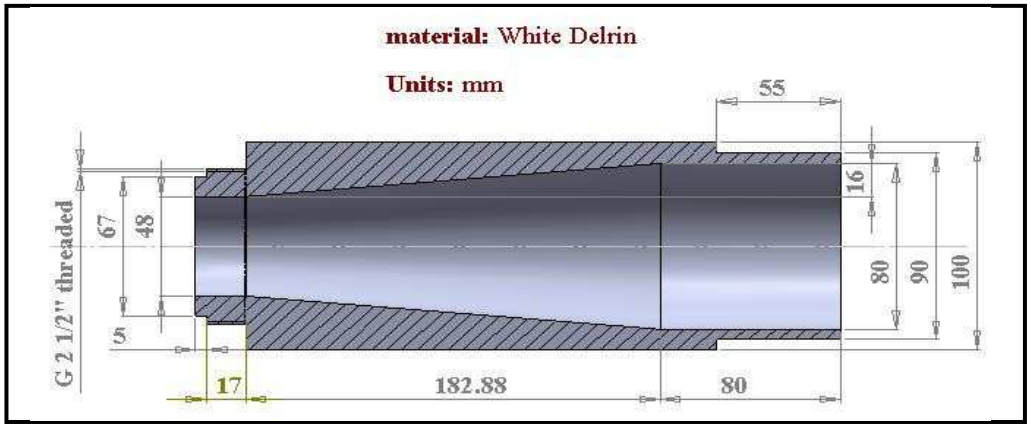

Figure 4-11: Design of the outlet section

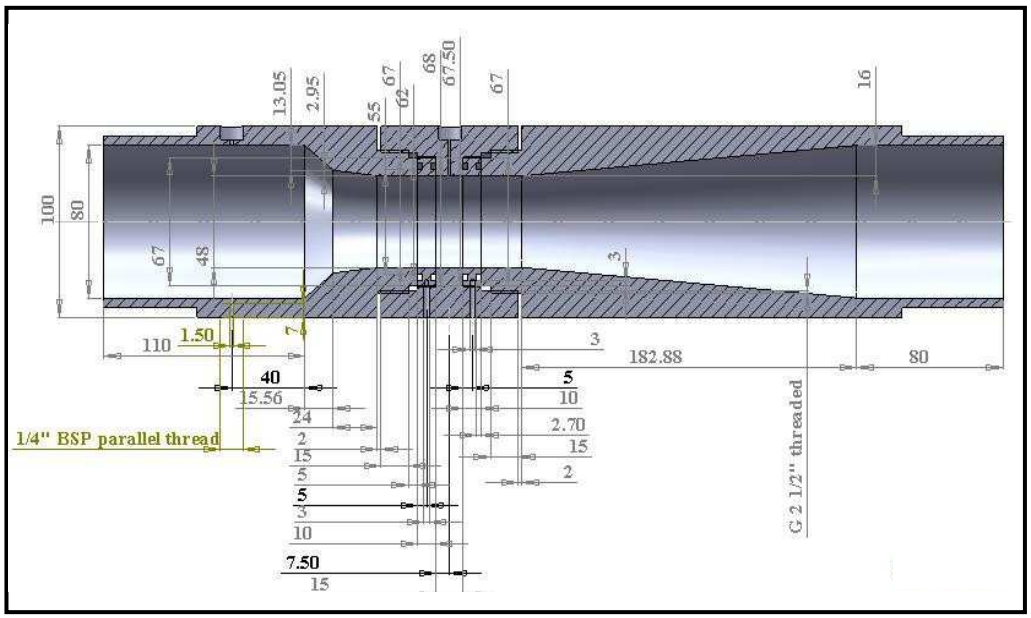

Figure 4-12: Full 2D drawing of the CMVM after assembly

4.4 Design of the conductance wall sensor

Wall Conductance Sensors (WCSs) were used as an alternative method of measuring the liquid film thickness and velocity in annular gas-water two phase flow (see Section 8.11). Figure 4-13 shows the design of the test section which includes two WCSs. The electrodes in the WCS are made from stainless steel. Figure 4-14 shows the non-scale 2-D drawing of the WCS [147]. The picture of the test section is also shown in Figure 4-14.

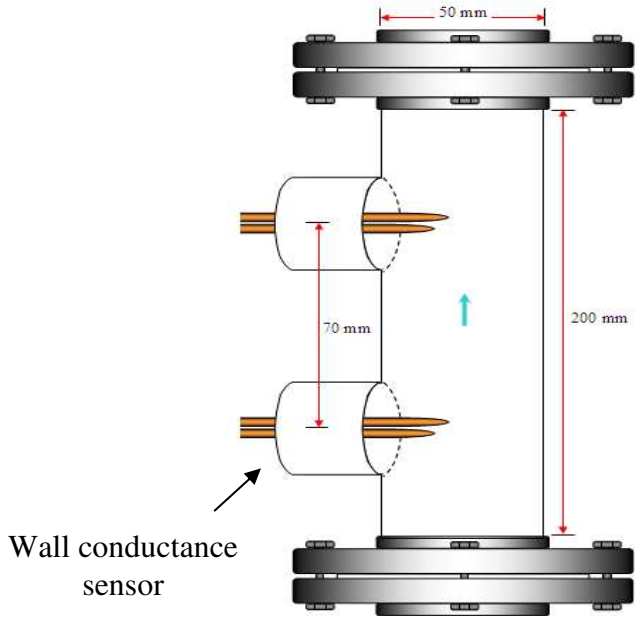

Source of the picture: Al-Yarubi (2010)

Figure 4-13: Test section with wall conductance sensors

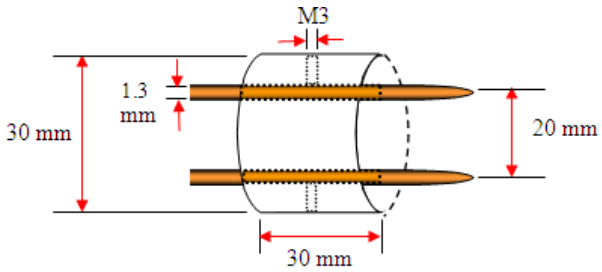

(a) 2-D (non-scale) drawing of the wall conductance sensor

(b) Picture of the wall conductance sensor

Source of the figure: Al-Yarubi (2010)

Figure 4-14: Design of the wall conductance flow meter

4.5 The measurement electronics system

Conductance electronics circuits were built to measure the water film thickness in annular flow (and hence the gas volume fraction at the inlet and the throat of the Venturi). In horizontal stratified flows these circuits can be used to measure the water level at the inlet and the throat of the Venturi (and hence the gas volume fraction at the inlet and the throat of the Venturi meter in horizontal stratified flows).

Two similar electronics circuits were built to measure the gas volume fraction at the inlet and the throat of the Venturi in annular and stratified flows respectively. The first circuit was connected to the electrodes at the CIVFM in which the inlet gas volume fraction can be measured in both vertical annular and horizontal stratified gas-water two phase flows. The second electronic circuit was connected to the electrodes at the throat of the CMVM in order to measure the gas volume fraction at the throat of the CMVM in vertical and horizontal stratified two phase flows.

The complete block diagram of the measurement electronics system is shown in Figure 4-15. It consists of seven stages; a pre-amplifier (see Figure 4-17), an amplifier stage, a half-wave rectifier, a low-pass filter, a non-inverting amplifier, buffer and zero offset adjustment and RC ripple filter.

To calibrate the conductance multiphase flow meter (i.e. CIVFM and CMVM) described in Sections 4.3.1 and 4.3.2, in simulated annular flow the zero offset stage (see Figure 4.16) was adjusted to give a zero output voltage when no water was present between the electrodes at the inlet and the throat of the Venturi (i.e. at the CIVFM and CMVM respectively). The amplifier stage (see Figure 4.16) was then adjusted to give a maximum output voltage when the area between the electrodes at the inlet and the throat of the Venturi was completely filled with water. After that, different diameters of nylon rods were inserted in the inlet and the throat of the Venturi to obtain the calibration curves for the CIVFM and the CMVM in which the water film thickness in annular flow (and hence the gas volume fraction at the inlet and the throat of the Venturi) can be related with the dc output voltages directly.

In a like manner, the conductance multiphase flow meter for use in simulated horizontal stratified flows was calibrated by adjusting a zero offset stage to give a zero output voltage when no water was present between the electrodes at the inlet and the throat of the Venturi. The area between the electrodes at the inlet and the throat of the Venturi was then completely filled with water and the amplifier stage was adjusted to give a maximum output voltage. Varying the water levels in simulated stratified flows and recording the dc output voltages enable the gas volume fraction at the inlet and the throat of the Venturi to be determined. The bench test on the conductance multiphase flow meter for simulated annular and simulated stratified flows is fully described in Chapter 5.

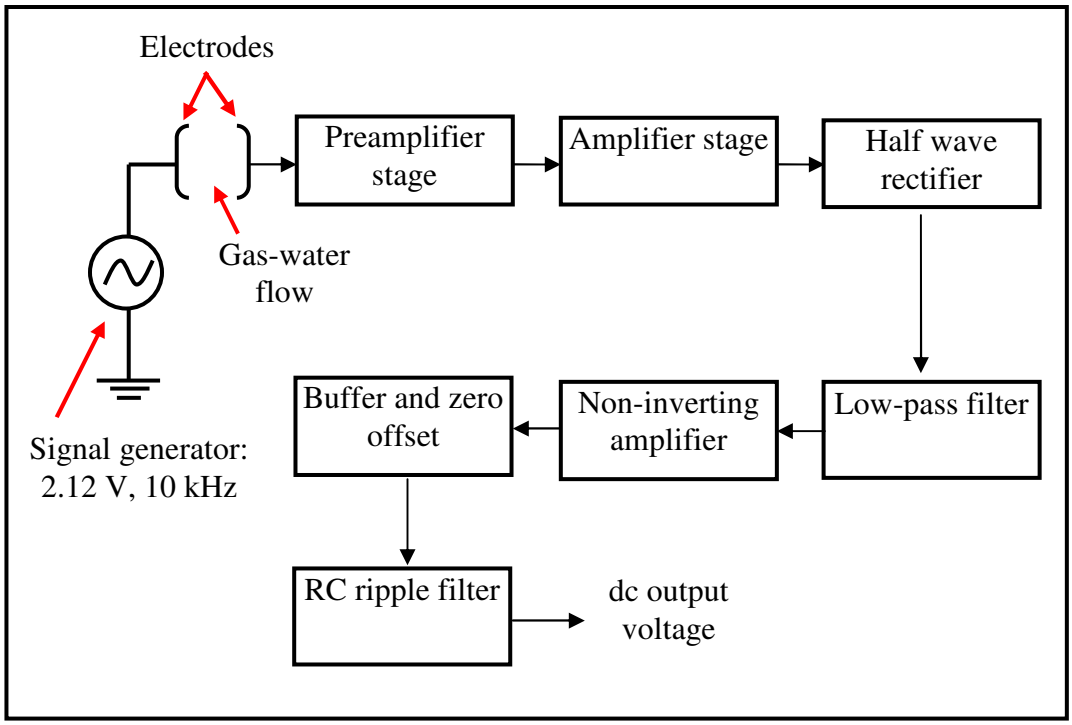

Figure 4-15: Block diagram of the measurement electronics

The circuit diagram of the conductance electronic circuit is shown in Figure 4-16. The excitation voltage and the wave frequency are 2.12 p-p volt and 10kHz respectively. The choice of the excitation frequency is very important since it would affect the operation of the probes. It has previously been mentioned [148] that, at low frequencies, a double layer effects might be appeared in which the conductance between the electrodes is affected by capacitance and resistive elements at the electrode-electrolyte interfaces.

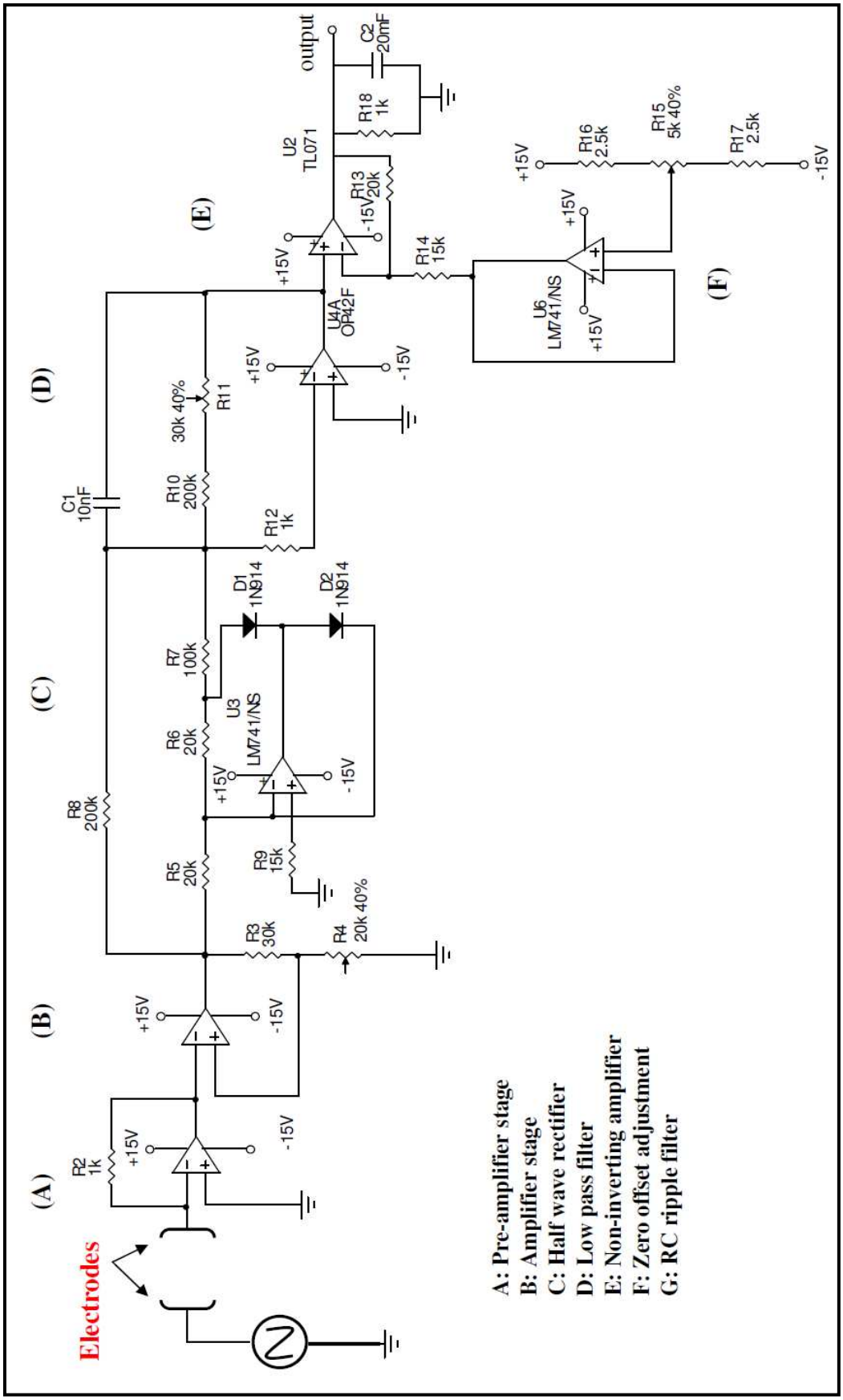

Figure 4-16: A schematic diagram of the conductance electronic circuit

Summary

A non-conductance UVT which can be used to measure phase flow rates in bubbly (approximately homogenous) gas-water two phase flows was designed. A combination of the UVT and FDM forms a two phase flow meter for homogenous flows.

The FDM was designed and constructed to measure the gas volume fraction at the inlet of the UVT in a homogenous gas-water two phase flow (see Section 4.1).

Separated flow in a Venturi meter is highly complex and the application of a homogenous flow model could not reasonably be expected to lead to accurate results. As a result, an advanced conductance multiphase flow meter was designed and constructed. One of the most advanced features of this design is that all parts can be assembled and disassembled easily. The conductance multiphase flow meter is also capable of measuring the gas volume fraction at the inlet and the throat of the Venturi.

The conductance multiphase flow meter consists of two parts (see Section 4.3);

(iii) the Conductance Inlet Void Fraction Meter (CIVFM) which is capable of measuring the gas volume fraction at the inlet of the Venturi.

(iv) the Conductance Multiphase Venturi Meter (CMVM) in which two ring electrodes are mounted at the throat to measure the gas volume fraction at the throat of the Venturi.

It should be noted that the advantage of designing and constructing the advanced conductance multiphase flow meter is that the gas volume fraction at the inlet and the throat of the Venturi can be obtained (instead of relying on prior knowledge of the mass flow quality, x) allowing the gas and the water mass flow rates in vertical annular and horizontal stratified flows to be measured using Equations (3.43), (3.59), (3.66) and (3.72). This makes the measurement technique described in this thesis

more practical in multiphase flow applications since the online measurement of x is difficult and not practical.

The design of WCSs was presented in Section 4.4. A WCS was used as an alternative method of measuring the water film flow rate in annular gas-water two phase flows (see also Sections 8.11 and 8.12).

The conductance electronic circuits were built and calibrated to give dc output voltages which are proportional to the conductance of the mixture which can then be related to the water film thicknesses in annular flow (and hence to the gas volume fraction at the inlet and the throat of the Venturi) and to the volume occupied by the liquid in a horizontal stratified flow (and hence, again, to the gas volume fraction at the inlet and the throat of the Venturi).

Chapter 5

Bench Tests on the Conductance Multiphase Flow Meter

Introduction

At the beginning of this chapter it should be reiterated that the Conductance Multiphase Flow Meter is a combination of the Conductance Inlet Void Fraction Meter (CIVFM) which is capable of measuring the gas volume fraction at the inlet of the Venturi in annular and stratified gas-water two phase flow and the Conductance Multiphase Venturi Meter (CMVM) one of the purposes of which is to measure the gas volume fraction at the throat of the Venturi in separated flows (i.e. annular and stratified gas-water two phase flows). The reason for measuring the gas volume fraction at the inlet and the throat of the Venturi is to determine the gas and the water mass flow rates in vertical annular and horizontal stratified flows using Equations (3.43), (3.59), (3.66) and (3.72). Relying on the measurement of the gas volume fraction at the inlet and the throat of the Venturi instead of prior knowledge of the mass flow quality x (as in the previous work described in Section 2.2) makes the measurement techniques described in this thesis more practical since the measurement of x is difficult in multiphase flow applications.

Before the CIVFM and the CMVM were used dynamically in the flow loop as a Conductance Multiphase Flow Meter, a number of experimental bench testing procedures were carried out. A bench test rig was designed and built in order to calibrate the conductance measurement systems of the conductance multiphase flow meter.

This chapter presents the static testing procedures carried out on the conductance multiphase flow meter to simulate annular and stratified flows. Section 5.1 describes the bench testing procedures for the conductance multiphase flow meter in simulated annular flow in which the calibration curve of the CIVFM that relates the gas volume fraction at the inlet of the Venturi with a dc output voltage can be obtained. The calibration of the CMVM in which the gas volume fraction at the throat of the Venturi can be found as a function of a second dc output voltage is also described in Section 5.1.

The experimental bench testing procedures carried out for the conductance multiphase flow meter (i.e. CIVFM and CMVM) in simulated stratified flow are described in Section 5.2.

5.1 Experimental procedure for the static testing of the conductance multiphase flow meter in simulated annular flow

A test rig was built to measure the simulated gas volume fraction at the inlet and the throat of the Venturi (i.e. at the CIVFM and the CMVM respectively) in simulated annular gas-water two phase flow. It should be noted that the static and dynamic measurements were taken at the laboratory conditions in which the temperature of the water was kept constant at 22.5^{o}C. Measurement of the water conductivity was taken using a conventional conductivity meter showed a value of 132.6μScm^{-1} for all of the experiments described in this thesis. [Note that for a device used in applications where the liquid conductivity is likely vary, the liquid conductivity should be measured on-line and the calibration curves should be compensated for such changes in conductivity, see further work in Chapter 11].

The simulation of the liquid film thickness and the gas volume fraction at the inlet of the Venturi (i.e. at the CIVFM) is described in Section 5.1.1. The experimental setup of simulated annular two phase flow through a CIVFM is presented in Section 5.1.2. The simulation of the liquid film thickness (and hence the gas volume fraction at the throat of the Venturi (i.e. at the CMVM)) and the experimental setup of simulated annular flow through a CMVM are described in Sections 5.1.3 and 5.1.4 respectively.

5.1.1 Simulation of the liquid film thickness and the gas volume fraction at the CIVFM in simulated annular flow

To simulate the film thickness in the vertical CIVFM, different diameters of nylon rods were inserted through the CIVFM [145,149]. The gap between the outer surface of the rod and the inner surface of the pipe wall was then filled with water, representing the water film that would occur in a real annular flow as shown in Figure 5-1. The nylon rod holder at the bottom of the system (see Figure 5-1) was used to hold different diameters of nylon rod in the static tests to ensure that the nylon rod was located at the precise centre of the system (i.e. the gap between the outer surface of the rod and the inner surface of the pipe wall was the same at any given axial location within the CIVFM).

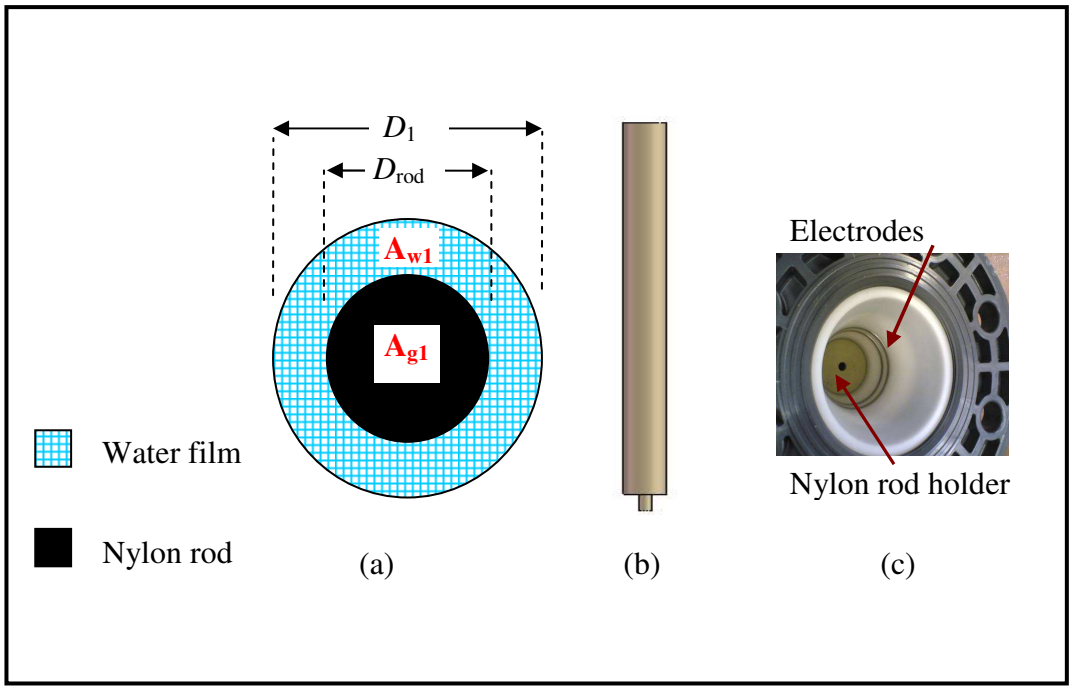

Figure 5-1: Configuration of the vertical simulated annular flow at the CIVFM; (a) film thickness in annular flow, (b) a picture of the nylon rod, (c) Nylon rod holder

From Figure 5-1, the water film thickness in simulated annular flow, $\delta_{1,sim,ann}$ at the inlet of the Venturi (i.e. at the CIVFM) is given by;

$$\delta_{1,sim,ann} = \frac{D_1 - D_{rod}}{2}$$

Equation (5.1)

where D_1 is the pipe diameter of the CIVFM (i.e. the same diameter as the inlet of the Venturi) and D_{rod} is the rod diameter.

The gas volume fraction at the inlet of the Venturi (i.e. at the CIVFM) is defined as the ratio of area occupied by the gas to the total flow area. Therefore, the gas volume fraction at the inlet of the Venturi in simulated annular flow $\alpha_{1,sim,ann}$ can be expressed as;

$$\alpha_{1,sim,ann} = \left(1 - \frac{2\delta_{1,sim,ann}}{D_1}\right)^2$$

Equation (5.2)

5.1.2 Experimental setup of simulated annular two phase flow through a CIVFM

Figure 5-2 shows the bench test experimental setup in vertical simulated annular flow through the CIVFM. One of the electrodes at the CIVFM was connected to the signal generator in which the excitation voltage and the sine-wave frequency were 2.12V p-p and 10kHz respectively. The other electrode (measurement electrode) was then connected to the conductance circuit (see Figure 4-16). The circuit was adjusted so that a zero output voltage was obtained when no water (only air) was present between the electrodes at the CIVFM. The area between the electrodes of the CIVFM was then completely filled with water and a maximum dc output voltage was obtained by adjusting the variable resistance in the amplifier stage (see Figure 4-16). Different diameters of nylon rod were then inserted through the CIVFM and the area between

the outer surface of the rod and the inner surface of the CIVFM was filled with water and the dc output voltages were recorded using the interfacing system (see Figure 5-2). The dc output voltage for each test was related to the water film thickness and hence the gas volume fraction at the inlet of the Venturi.

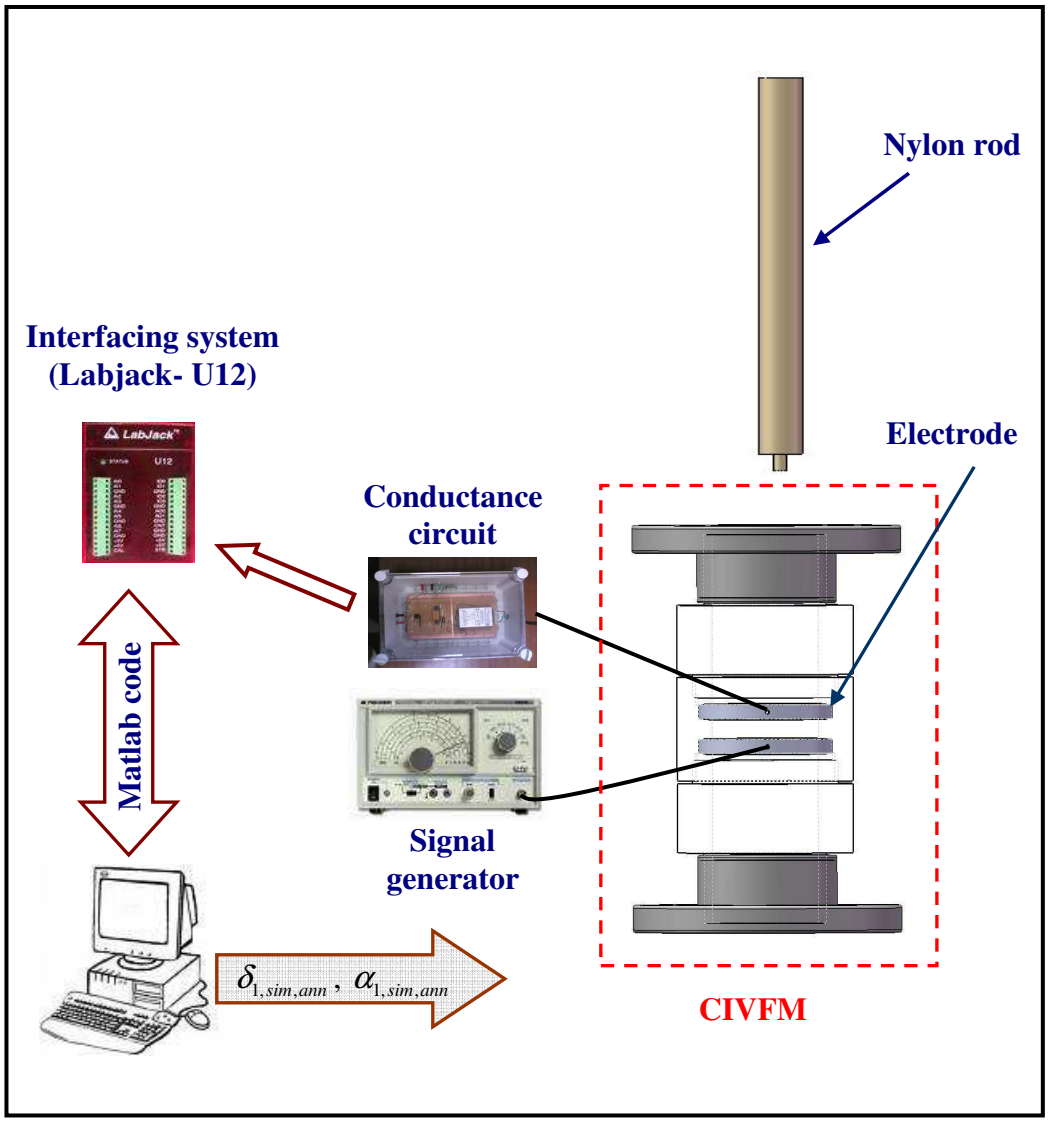

Figure 5-2: Bench test experimental setup of the simulated annular two phase flow through a CMVM

5.1.3 Simulation of the liquid film thickness and the gas volume fraction at the throat of the CMVM in simulated annular flow

Static tests on the throat section of the CMVM were performed in the same manner of the CIVFM (see Section 5.1.1) in which non-conducting nylon rods with different diameters were inserted in the throat section of the CMVM. The gap between the outer surface of the rod and the inner surface of the throat wall was then filled with water, representing the water film that would occur in a real annular gas-water two phase flow as shown in Figure 5-3.

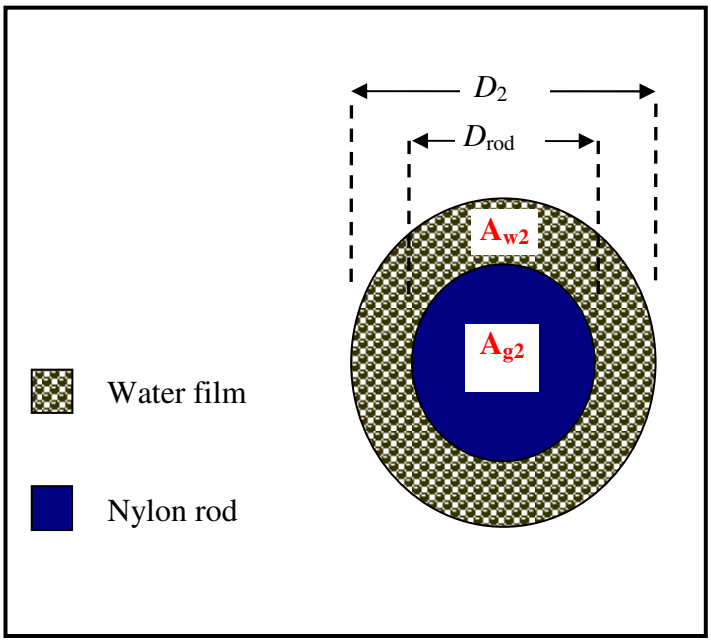

Figure 5-3: Configuration of the vertical simulated annular flow at throat section of the CMVM

From Figure 5-3, the water film thickness in simulated annular flow, $\delta_{2,sim,ann}$ at the throat section of the CMVM can be written as;

$$\delta_{2,sim,ann} = \frac{D_2 - D_{rod}}{2}$$

Equation (5.3)

The gas volume fraction at the throat of the CMVM in simulated annular flow $\alpha_{2,sim,ann}$ can be expressed as;

$$\alpha_{2,sim,ann} = \left(1 - \frac{2\delta_{2,sim,ann}}{D_2}\right)^2$$

Equation (5.4)

It should be noted that the water film thicknesses $\delta_{1,sim,ann}$ and $\delta_{2,sim,ann}$ in Equations (5.2) and (5.4) are measured from the CIVFM and the CMVM respectively.

Measurement of $\delta_{1,sim,ann}$ and $\delta_{2,sim,ann}$ enables the gas volume fractions $\alpha_{1,sim,ann}$ and $\alpha_{2,sim,ann}$ to be determined.

5.1.4 Experimental setup of simulated annular two phase flow through a CMVM

Figure 5-4 shows the bench test experimental setup for simulated annular flow through the CMVM. One of the electrodes at the throat of the CMVM was excited by a sine wave (2.12 V p-p and 10kHz) while the other electrode was connected to the conductance circuit (see Figure 4-16). A dc output voltage which is proportional to the water film thickness was recorded using the interfacing system (a Lab-jack U12) in which the relationship between the gas volume fraction $\alpha_{2,sim,ann}$ and the dc output voltage was obtained. It should be noted that before different diameters of nylon rod were inserted in the throat of CMVM, a zero output stage (see Figure 4-16) was adjusted to give a zero output voltage when no water was present between the electrodes and then a maximum dc output voltage was set when the throat of the CMVM was completely filled with water.

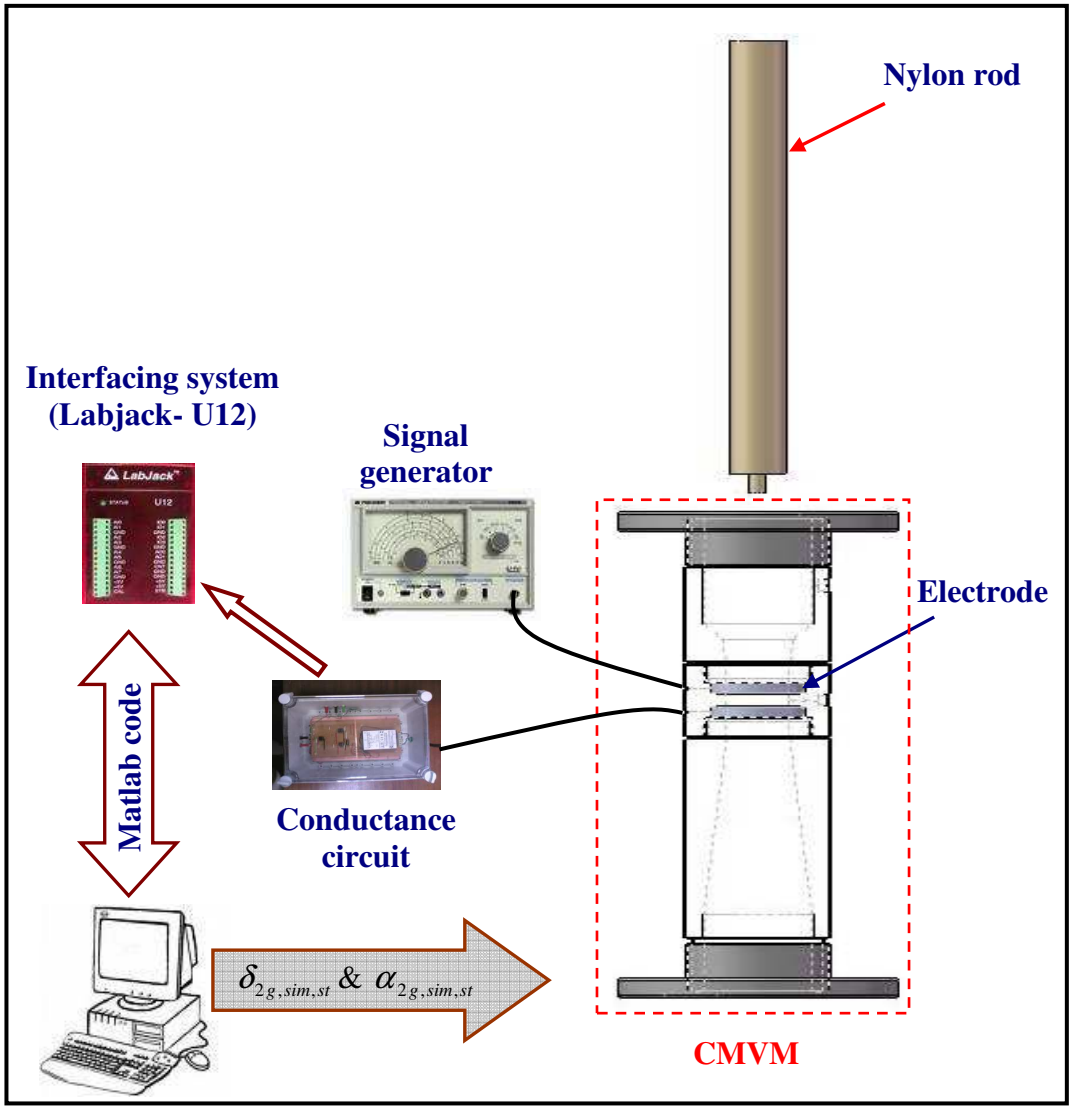

Figure 5-4: Bench test experimental setup of the simulated annular two phase flow through a CMVM

5.2 Experimental procedure for the static testing of the conductance multiphase flow meter in simulated stratified flow

For simulated horizontal stratified flow, the conductance multiphase flow meter was statically calibrated by varying the level of water at the inlet and the throat of the Venturi. The height of the water at the inlet of the Venturi (i.e. at the CIVFM) could then be related to the inlet gas volume fraction while the gas volume fraction at the throat of the CMVM could be obtained from the height of the water at the throat section (see also Section 5.2.2). The height of the water at the inlet and the throat of

the Venturi was measured by a ruler (see Figure 5-6). Figure 5-5 shows the configuration of the horizontal stratified gas-water two phase flow.

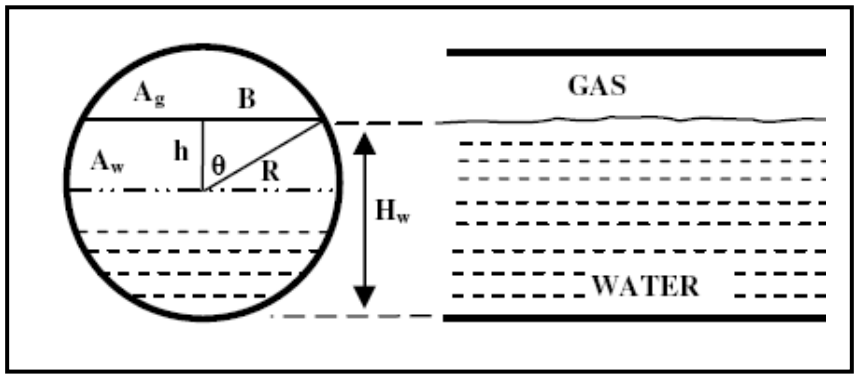

Figure 5-5: configuration of the horizontal stratified gas-water two phase flow.

From Figure 5-5, it is possible to write;

$$\theta = \cos^{-1}\frac{h}{R}$$

Equation (5.5)

where R is the radius of the pipe, θ and h are the angle and the height shown in Figure 5-5.

The area occupied by the gas A_g in Figure 5-5 can be written as;

$$A_g = \frac{2\theta}{360}\times\pi R^2 - Bh$$

Equation (5.6)

The parameter B in Equation (5.6) is given by;

$$B = \sqrt{R^2 - h^2}$$

Equation (5.7)

The general expression of the gas volume fraction α can then be expressed as;

$$\alpha = \frac{A_g}{A} = \left[\frac{2\theta}{360}\times\pi R^2 - h\sqrt{R^2 - h}\right]\cdot\frac{1}{\pi R^2}$$

Equation (5.8)

Equation (5-8) is a general form of the gas volume fraction. In other words, it can be used to calculate the gas volume fraction at the inlet and the throat of the Venturi.

5.2.1 Gas volume fraction at the inlet and the throat of the Venturi in simulated stratified gas-water two phase flow

The gas volume fraction at the inlet of the Venturi (i.e. at the CIVFM) and the gas volume fraction at the throat of the CMVM can both be determined with the aid of Equation (5.8) which is a general equation for the gas volume fraction and, by use of the appropriate variables, can be applied to either the CIVFM or the CMVM.

Therefore, the gas volume fraction at the inlet of the Venturi (i.e. CIVFM) in simulated horizontal stratified flow $\alpha_{1,sim,st}$ can be expressed as;

$$\alpha_{1,sim,st} = \frac{A_{g\,1,sim,st}}{A_{1.sim,st}} = \left[\frac{2\theta_{1,sim,st}}{360} \times \pi R_{1,sim,st}{}^{2} - h_{1,sim,st}\sqrt{R_{1,sim,st}^{2} - h_{1,sim,st}} \right] \cdot \frac{1}{\pi R_{1,sim,st}^{2}}$$

Equation (5.9)

where the subscript $1,sim,st$ refers to the inlet of the Venturi which is the CIVFM. For example, $R_{1,sim,st}$ is the radius of the pipe at the CIVFM (i.e. 40 mm).

In a like manner, the gas volume fraction at the throat section of the CMVM in simulated horizontal stratified flow $\alpha_{2,sim,st}$ can be expressed as;

$$\alpha_{2,sim,st} = \frac{A_{g\,2,sim,st}}{A_{1.sim,st}} = \left[\frac{2\theta_{2,sim,st}}{360} \times \pi R_{2,sim,st}{}^{2} - h_{2,sim,st}\sqrt{R_{2,sim,st}^{2} - h_{2,sim,st}} \right] \cdot \frac{1}{\pi R_{2,sim,st}^{2}}$$

Equation (5.10)

where the subscript $2,sim,st$ refers to the throat of the Venturi. For example, $R_{2,sim,st}$ is the radius of the pipe at the throat of the CMVM (i.e. 24 mm).

5.2.2 Bench test experimental setup for simulating stratified gas-water two phase flow through the conductance multiphase flow meter

This section describes the experimental setup for simulating stratified flow through the CIVFM and the CMVM. Figure 5-6 shows the bench experimental setup for simulated stratified two phase flow.

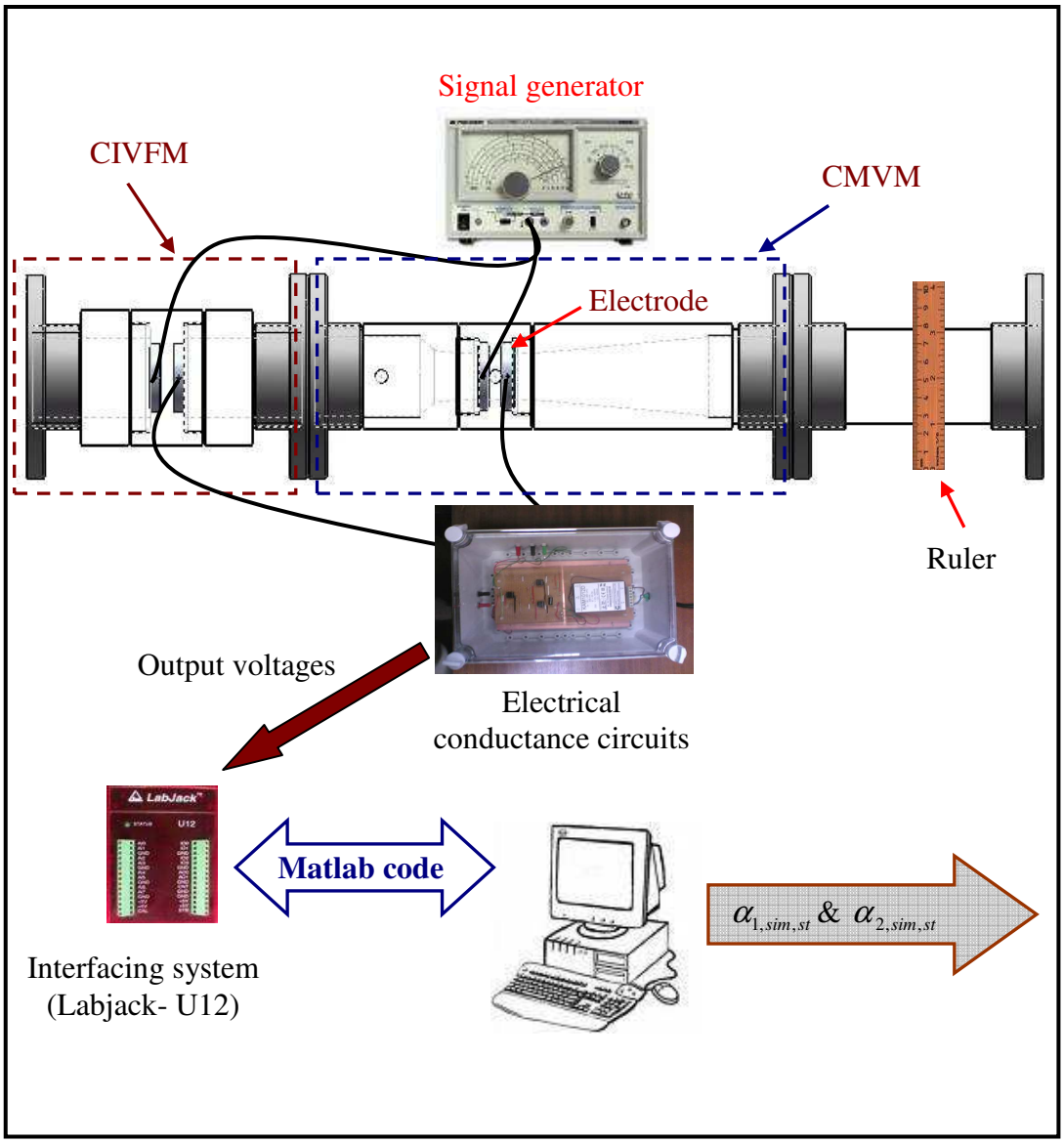

Figure 5-6: Bench test experimental setup of horizontal simulated stratified two phase flow through a CIVFM and CMVM

The zero offset stage (see Figure 4-16) was first adjusted to give a zero dc output voltage from the conductance circuits for both the CIVFM and CMVM when no water was present. The pipe section (i.e. CIVFM and CMVM) was then filled completely with water and maximum dc output voltages obtained from both circuits were set by adjusting the gain of the amplifier stage for each circuit (see Figure 4-16). The water level was then gradually varied and the dc output voltages from the two electrical conductance circuits (one connected to the electrodes of the CIVFM and the other connected to the electrodes at the throat section of the CMVM) which were related to the height of the water in the system, and hence to the gas volume fraction at the inlet and the throat, were recorded. The dc output voltages from two electrical conductance circuits (see Figure 4-16) were interfaced to the PC via a data acquisition unit, Labjack U-12. The operation of the Labjack U-12 was controlled using MATLAB software. The gas volume fractions $\alpha_{1,sim,st}$ and $\alpha_{2,sim,st}$ (see Equations (5.9) and (5.10)) in simulated stratified two phase flow could then be calculated as the water level in the horizontal CIVFM/CMVM system was altered.

It should be noted that cross-talk effects in simulated annular and stratified flows were examined and it was found that there were no effects on the conductance sensors of either CIVFM or CMVM. In simulated vertical annular flow, this was done as follows;

(i) 1st test: Cross-talk effect when the CIVFM was active;

1. The CIVFM and the CMVM were filled with water.
2. The excitation electrode at the CIVFM was then excited by the 10kHz 2.12V p-p signal.
3. The dc output voltages obtained from the measurement electrode at the throat section of the CMVM were recorded when different diameters of nylon rod were inserted at the CIVFM and the CMVM.

(ii) 2nd test: Cross-talk effect when the CMVM was active;

1. The CIVFM and the CMVM were filled with water.
2. The excitation electrode at the throat section of the CMVM were excited (i.e. active CMVM).
3. The dc output voltages were obtained from the measurement electrode at the CIVFM for different liquid film thicknesses (i.e. different diameters of nylon rod were used).

In a like manner, the cross-talk effect in simulated horizontal stratified flow (see Figure 5-6) was checked by exciting the excitation electrode at the CIVFM and recording the dc output voltages from the measurement electrode at the throat of the CMVM for different levels of water. The same test was performed in which the excitation electrode at the throat of the CMVM was activated and the dc output voltages were obtained from the measurement electrode at the CIVFM for different levels of water.

5.3 Experimental results from static testing of the conductance multiphase flow meter in simulated annular flow

As mentioned earlier, the conductance multiphase flow meter consists of two parts; (i) the conductance inlet void fraction meter (CIVFM) which is capable of measuring the water film thickness $\delta_{1,sim,ann}$ at the inlet of the Venturi in simulated annular flow and (ii) the Conductance Multiphase Venturi Meter (CMVM) which can be used to measure the water film thickness $\delta_{2,sim,ann}$ at the throat of the Venturi. Measurement of $\delta_{1,sim,ann}$ and $\delta_{2,sim,ann}$ enables the gas volume fractions $\alpha_{1,sim,ann}$ and $\alpha_{2,sim,ann}$ to be determined using Equations (5.2) and (5.4) respectively.

5.3.1 Experimental results from the conductance inlet void fraction meter (CIVFM) in simulated annular flow

Figure 5-7 shows the relationship between the dc output voltage $V_{1,sim,ann}$ from the CIVFM and the simulated water film thickness $\delta_{1,sim,ann}$ in the CIVFM obtained from the vertical simulated annular flow experiments. This relationship enables the actual water film thickness δ_1 to be determined in a real annular gas-water two phase flow (see Section 8.3).

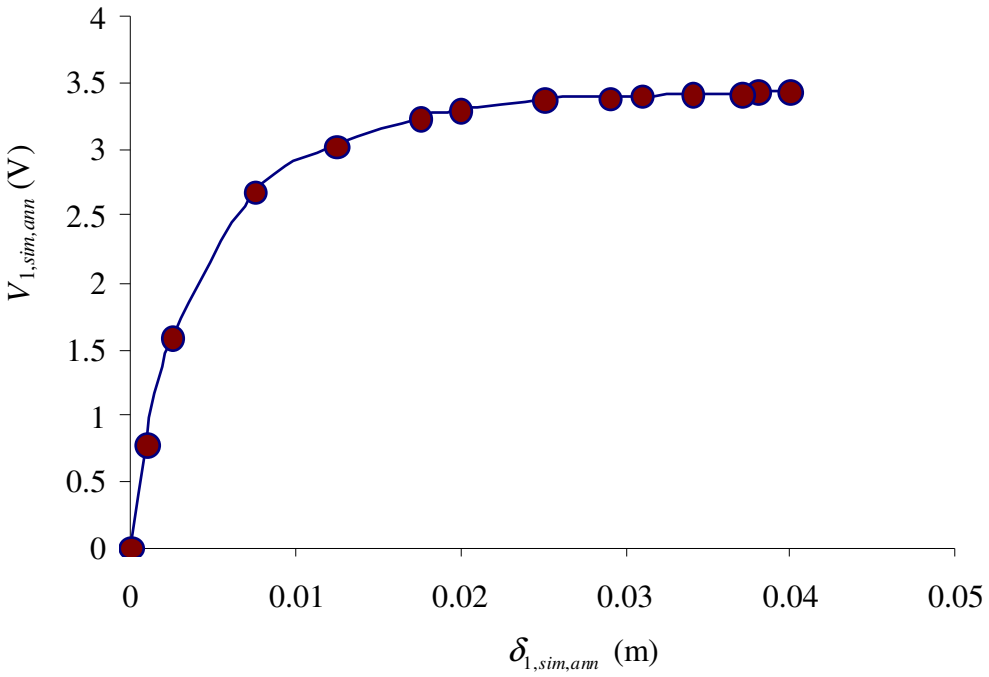

Figure 5-7: The relationship between the dc output voltage and the water film thickness at the Conductance Inlet Void Fraction Meter in a vertical simulated annular flow

Once the water film thickness $\delta_{1,sim,ann}$ at the CIVFM was obtained, the gas volume fraction $\alpha_{1.sim,ann}$ at the inlet of the Venturi (i.e. at the CIVFM) in simulated annular flow can then be easily determined from Equation (5.2). The gas volume fraction $\alpha_{1.sim,ann}$ can be plotted either as a function of the water film thickness $\delta_{1.sim,ann}$ or as a

function of the dc output voltage $V_{1,sim,ann}$ as shown in Figures 5-8 and 5-9 respectively.

It should be noted that the reason for plotting the independent variable (e.g. $\alpha_{1,sim,ann}$, $\alpha_{2,sim,ann}$, $\alpha_{1,sim,st}$ or $\alpha_{2,sim,st}$) on the vertical axis and the dependent variable (e.g. $V_{1,sim,ann}$, $V_{2,sim,ann}$, $V_{1,sim,st}$ or $V_{2,sim,st}$) on the horizontal axis, in some of the graphs in this chapter, is that the gas volume fractions $\alpha_{1,sim,ann}$, $\alpha_{2,sim,ann}$, $\alpha_{1,sim,st}$ and $\alpha_{2,sim,st}$ can be obtained from the corresponding dc output voltages $V_{1,sim,ann}$, $V_{2,sim,ann}$, $V_{1,sim,st}$ and $V_{2,sim,st}$. Therefore plotting gas volume fraction against dc output voltage enables a more convenient best fit polynomial equation to be obtained. This polynomial equation enables the gas volume fractions to be determined directly from the dc output voltages (obtained from the conductance circuits) in real annular and stratified flows.

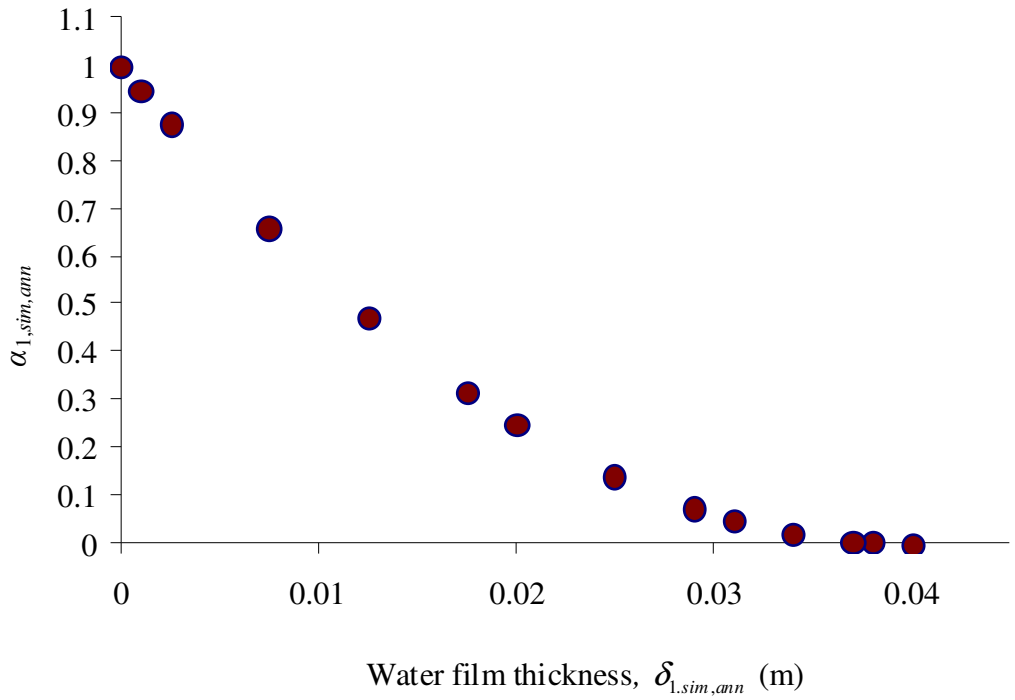

Figure 5-8: Variation of the gas volume fraction $\alpha_{1.sim,ann}$ at Conductance Inlet Void Fraction Meter with the water film thickness, $\delta_{1.sim,ann}$

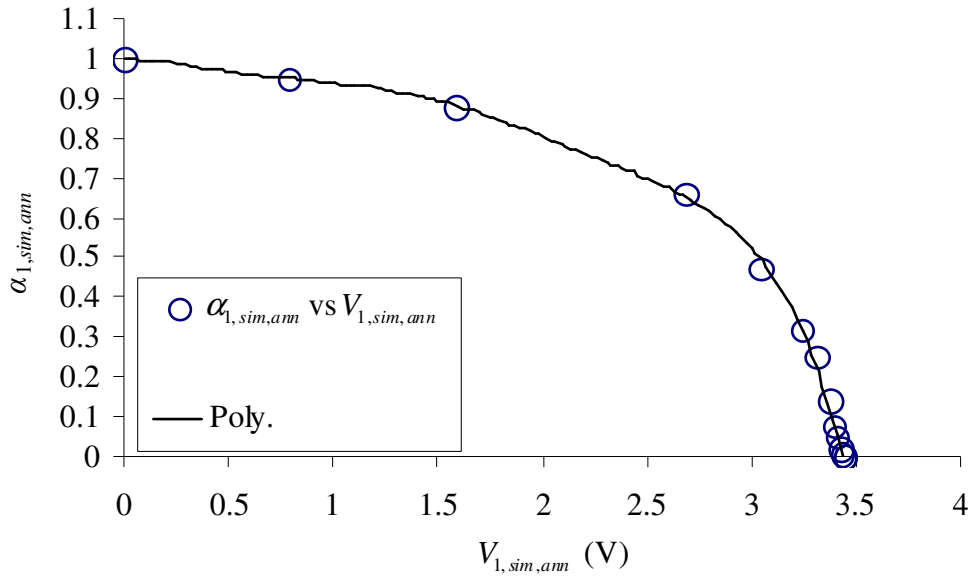

Figure 5-9: Variation of the gas volume fraction $\alpha_{1.sim,ann}$ with the dc output voltage $V_{1,sim,ann}$ from the Conductance Inlet Void Fraction Meter system

Equation (5.11) shows a good fit to the static experimental data of $\alpha_{1.sim,ann}$ over the full range of $V_{1,sim,ann}$.

$$\alpha_{1,sim,ann} = -0.0163V_{1,sim,ann}^{6} + 0.1378V_{1,sim,ann}^{5} - 0.429V_{1,sim,ann}^{4} + 0.5807V_{1,sim,ann}^{3} - 0.339V_{1,sim,ann}^{2} + 0.0062V_{1,sim,ann} + 0.9978$$

Equation (5.11)

5.3.2 Experimental results from the conductance multiphase Venturi meter (CMVM) in simulated annular flow

The two electrodes mounted at the throat of the CMVM were used to measure the film thickness $\delta_{2.sim,ann}$ at the throat of the Venturi. Measurement of $\delta_{2.sim,ann}$ enables the gas volume fraction $\alpha_{2.sim,ann}$ at the throat of the CMVM to be determined (see Equation (5.4)). Figure 5-10 shows the relationship between the dc output voltage $V_{2,sim,ann}$ obtained from the CMVM and the water film thickness $\delta_{2,sim,ann}$ in simulated annular flow.

The gas volume fraction $\alpha_{2.sim,ann}$ at the throat of the CMVM can then be determined from the water film thickness $\delta_{2,sim,ann}$ using Equation (5.4) as shown in Figure 5-11. The gas volume fraction $\alpha_{2.sim,ann}$ at the Venturi throat can be also related to the dc output voltage $V_{2,sim,ann}$ as shown in Figure 5-12.

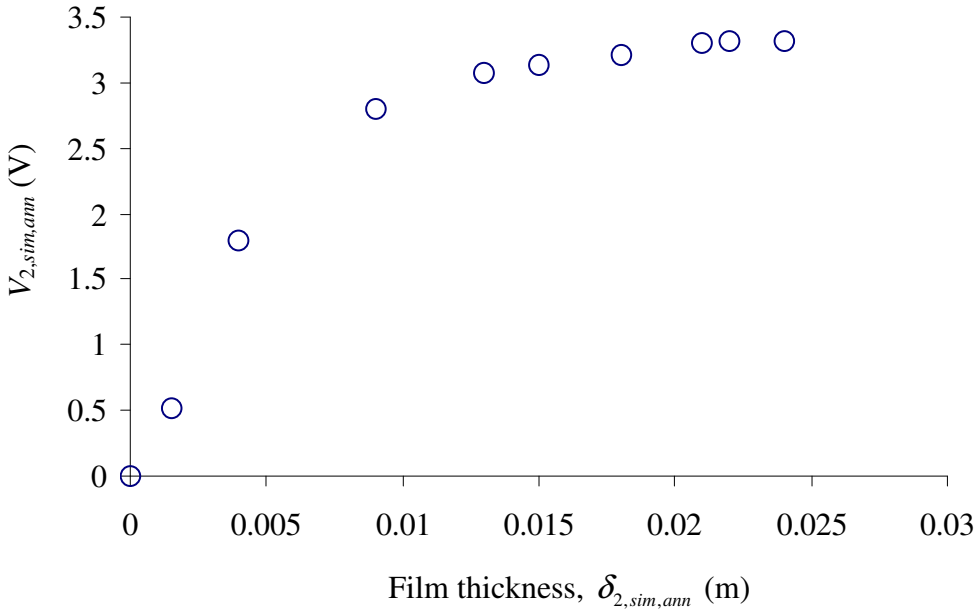

Figure 5-10: Relationship between $V_{2,sim,ann}$ and $\delta_{2,sim,ann}$ at throat of the Conductance Multiphase Venturi Meter in simulated annular flow

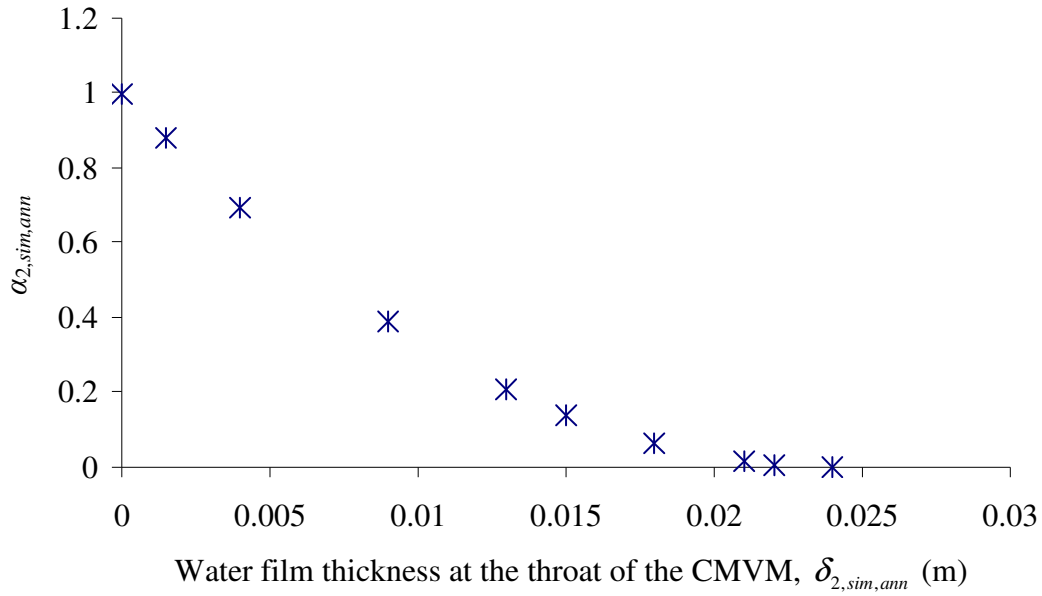

Figure 5-11 Variation of $\alpha_{2.sim,ann}$ with $\delta_{2,sim,ann}$ at the throat of the Conductance Multiphase Venturi Meter in simulated annular flow

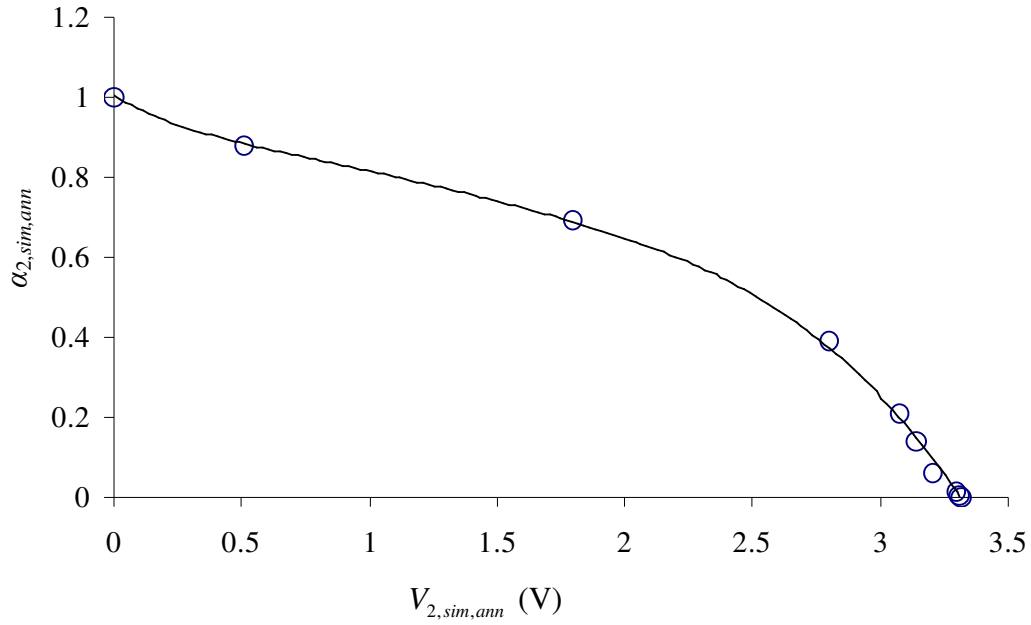

Figure 5-12: Relationship between the gas volume fraction $\alpha_{2.sim,ann}$ and the dc output voltage $V_{2,sim,ann}$ at the throat of the Conductance Multiphase Venturi Meter in simulated annular flow

A best fit to the static experimental data relating the gas volume fraction $\alpha_{2.sim,ann}$ at the throat of the CMVM to the dc output voltage $V_{2,sim,ann}$ (see Figure 5-12) is given by;

$$\alpha_{2,sim,ann} = 0.0038V_{2,sim,ann}^{6} - 0.0441V_{2,sim,ann}^{5} + 0.1873V_{2,sim,ann}^{4} - 0.4002V_{2,sim,ann}^{3} + 0.446V_{2,sim,ann}^{2} - 0.382V_{2,sim,ann} + 1.0044$$

Equation (5.12)

5.4 Experimental results from the static testing of the conductance multiphase flow meter in simulated stratified flow

In simulated horizontal stratified flow, the CIVFM was used to measure the gas volume fraction $\alpha_{1,sim,st}$ at the inlet of the Venturi. The gas volume fraction $\alpha_{2,sim,st}$ at the throat of the Venturi was measured by the two electrodes mounted at the throat of the CMVM (see Section 5.2.2). Reference measurements of $\alpha_{1,sim,st}$ and $\alpha_{2,sim,st}$ were obtained from the heights of the water at the CIVFM and the throat section of the

CMVM, $h_{1,sim,st}$ and $h_{2,sim,st}$ respectively using Equations (5.9) and (5.10). The water heights $h_{1,sim,st}$ and $h_{2,sim,st}$ were measured using a ruler as shown in Figure 5-6. The relationships between $V_{1,sim,st}$ and $h_{1,sim,st}$ and between $V_{2,sim,st}$ and $h_{2,sim,st}$ are described in detail below.

5.4.1 Bench results from the conductance inlet void fraction meter (CIVFM) in simulated stratified flow

Figure 5-13 shows the variation of the dc output voltage $V_{1.sim,st}$ with the water level $h_{1,sim,st}$ at the inlet of the Venturi in simulated stratified flow. Once the height $h_{1,sim,st}$ is obtained, the gas volume fraction $\alpha_{1,sim,st}$ can be easily determined from Equation (5.9). The calibration curve which relates the gas volume fraction $\alpha_{1,sim,st}$ and the dc output voltage $V_{1.sim,st}$ obtained from the CIVFM in simulated stratified flow is shown in Figure 5-14.

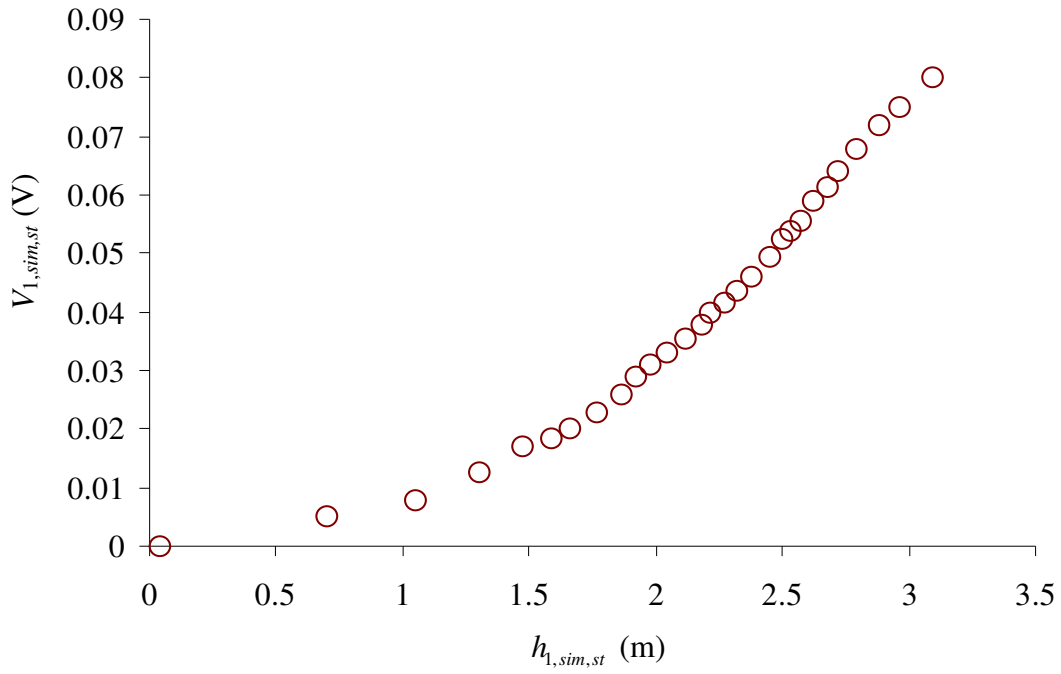

Figure 5-13: Variation of $V_{1.sim,st}$ with $h_{1,sim,st}$

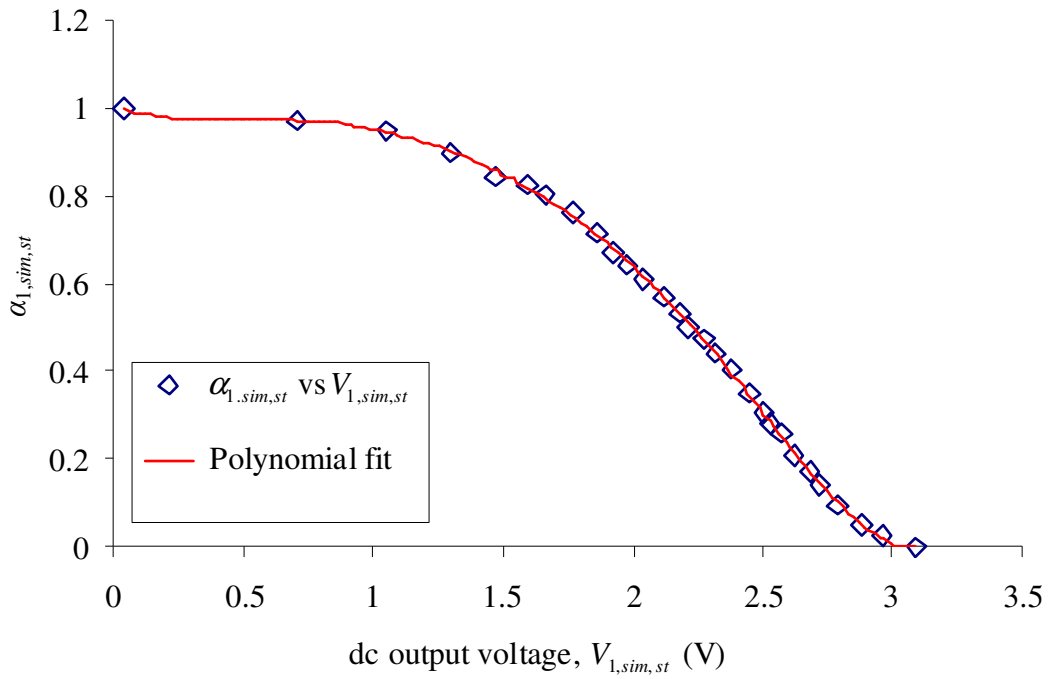

Figure 5-14: The relationship between the gas volume fraction, $\alpha_{1,sim,st}$ and the dc output voltage, $V_{1.sim,st}$

The red solid line in Figure 5-14 represents a best polynomial fit curve which relates the gas volume fraction, $\alpha_{1,sim,st}$ and the dc output voltage, $V_{1.sim,st}$. The best polynomial fit can be represented by the following equation;

$$\alpha_{1,sim,st} = 0.0209V_{1,sim,st}^{6} - 0.1726V_{1,sim,st}^{5} + 0.5677V_{1,sim,st}^{4} - 0.9809V_{1,sim,st}^{3} + 0.7827V_{1,sim,st}^{2} - 0.2752V_{1,sim,st} + 1.0098$$

Equation (5.13)

Equation (5.13) enables the gas volume fraction, $\alpha_{1,sim,st}$ to be determined from the dc output voltage, $V_{1.sim,st}$.

5.4.2 Bench results from the conductance multiphase Venturi meter (CMVM) in simulated stratified flow

The height of the water $h_{2,sim,st}$ at the throat of the Venturi in a simulated stratified flow was measured by a ruler (see Figure 5-6). The variations of the water level $h_{2,sim,st}$ with the dc output voltage $V_{2.sim,st}$ at the throat of the CMVM is shown in Figure 5-15.

Once $h_{2,sim,st}$ is measured, the gas volume fraction $\alpha_{2,sim,st}$ at the throat of the CMVM can be determined from Equation (5.10). Figure 5-16 shows the variation of the gas volume fraction $\alpha_{2,sim,st}$ with the dc output voltage $V_{2.sim,st}$ at the throat of the CMVM.

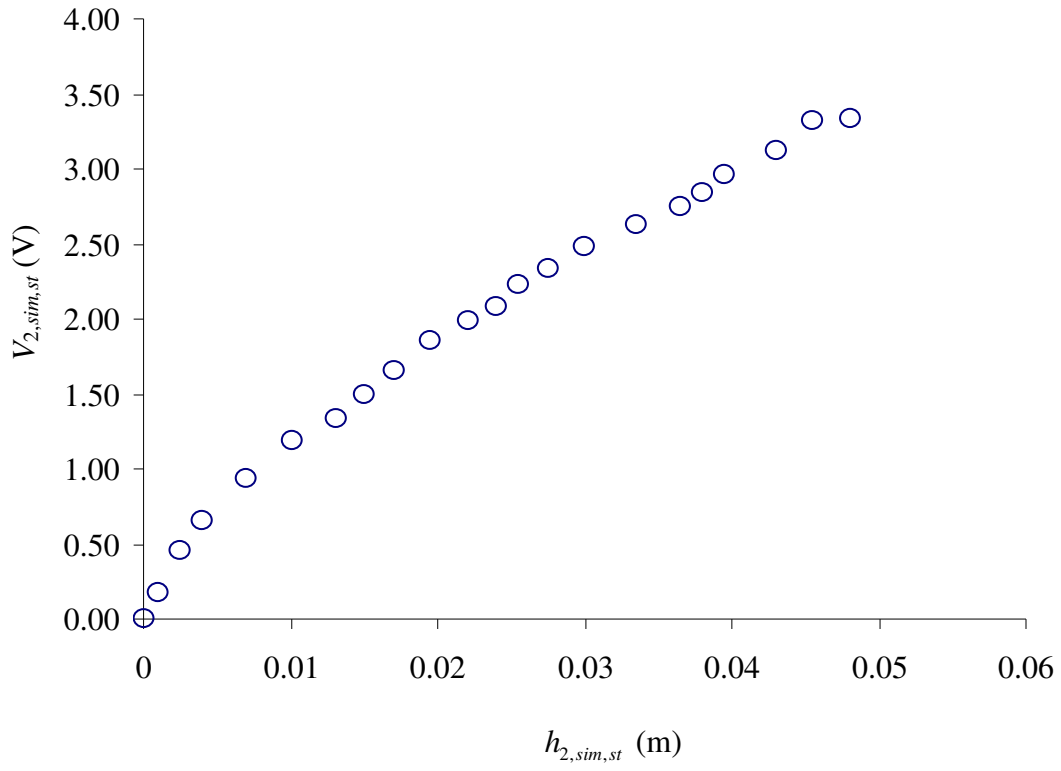

Figure 5-15: Variation of the dc output voltage, $V_{2,sim,st}$ with the water level, $h_{2,sim,st}$ at the throat of the Conductance Multiphase Venturi Meter in simulated stratified flow

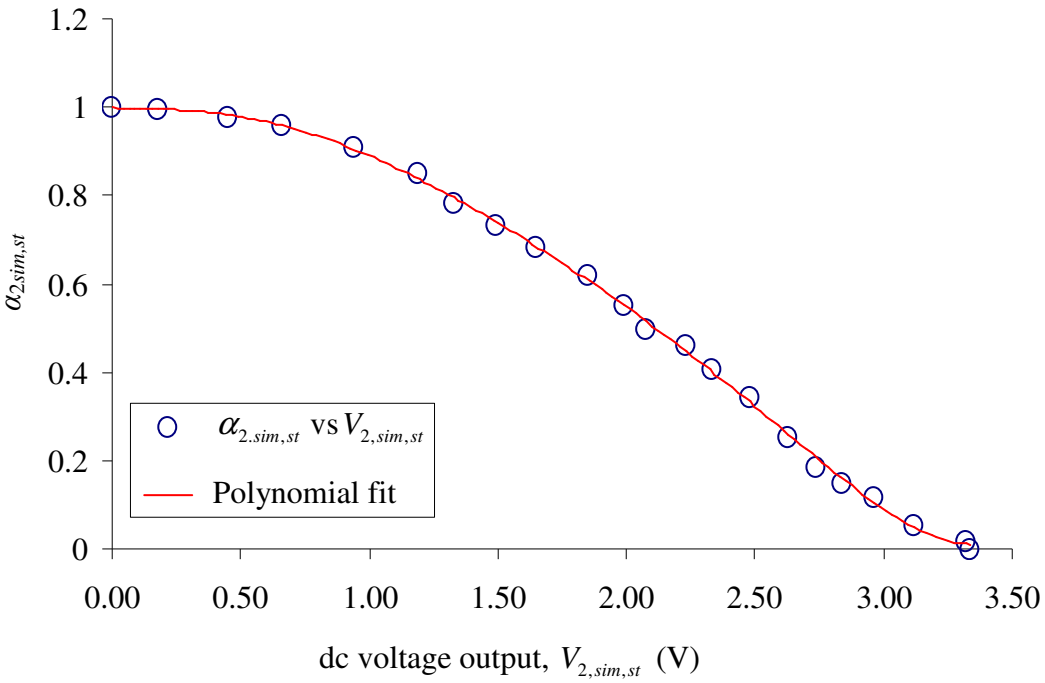

Figure 5-16: Calibration curve of the gas volume fraction $\alpha_{2,sim,st}$ at the throat of the Conductance Multiphase Venturi Meter in simulated stratified flow

The polynomial fit (red solid line in Figure 5-16) represents the calibration curve of the $\alpha_{2,sim,st}$ and can be expressed as;

$$\alpha_{2,sim,st} = 0.0075V^{6}_{2,sim,st} - 0.0668V^{5}_{2,sim,st} + 0.2235V^{4}_{2,sim,st} - 0.329V^{3}_{2,sim,st} + 0.0749V^{2}_{2,sim,st} - 0.0191V_{2,sim,st} + 0.9988$$

Equation (5.14)

In real stratified two phase flows, the measurement of the dc output voltage at the throat of the CMVM enables the actual gas volume fraction $\alpha_{2,st}$ (see Section 9.2) at the throat of the CMVM to be determined using Equation (5.14).

Summary

The reason for carrying out the static tests on the CIVFM and the CMVM was to find the relationships between the gas volume fractions and the dc output voltages (from the electrical conductance circuits) in both simulated annular flow and simulated stratified flow. These relationships enable the Conductance Multiphase Flow Meter to be used dynamically in real vertical annular and horizontal stratified gas-water two phase flows.

A number of bench experiments were performed to calibrate the Conductance Multiphase Flow Meter (which consists of the CIVFM and the CMVM) before it was used dynamically in a flow loop as a multiphase flow meter. The CIVFM is used to measure the gas volume fraction at the inlet of the Venturi while the CMVM is used to measure the gas volume fraction at the throat of the Venturi.

A bench test rig was designed and built in order to calibrate the Conductance Multiphase Flow Meter. Two different configurations of the bench test rig were used to calibrate the CIVFM and the throat section of the CMVM, respectively, in simulated annular and stratified flows (see Figures 5-2, 5-4 and 5-6).

The calibrations of the CIVFM and the CMVM enabled the gas volume fractions $\alpha_{1,sim,ann}$, $\alpha_{2,sim,ann}$, $\alpha_{1,sim,st}$ and $\alpha_{2,sim,st}$ to be dynamically determined in real vertical annular and horizontal stratified flows using Equations (5.11), (5.12), (5.13) and (5.14) respectively.

In simulated annular flow (see Section 5.1), the CIVFM and the CMVM were calibrated by inserting different diameters of nylon rod into the CIVFM and into the throat section of the CMVM and the gap between the outer surface of the rod and the inner surface of the pipe wall was filled with water, representing the water film that would occur in a real annular flow (see Figures 5-1, 5-2, 5-4 and 5-6). The dc output voltages $V_{1,sim,ann}$ and $V_{2,sim,ann}$ from the two electrical conductance circuits (see Figure 4-16), which were connected to the electrodes at the CIVFM and the CMVM

respectively, were recorded from which the gas volume fractions $\alpha_{1,sim,ann}$ and $\alpha_{2,sim,ann}$ could be determined from Equations (5.11) and (5.12).

In simulated stratified flow (see Figure 5-6), the heights of the water $h_{1,sim,st}$ (at CIVFM) and $h_{2,sim,st}$ (at the throat of the CMVM) were measured. $h_{1,sim,st}$ and $h_{2,sim,st}$ were then related to the dc output voltages $V_{1,sim,st}$ and $V_{2,sim,st}$ which were recorded from the electrical conductance circuits (see Figures 5-13 and 5-15). The gas volume fractions $\alpha_{1,sim,st}$ and $\alpha_{2,sim,st}$ could then be easily determined from $V_{1,sim,st}$ and $V_{2,sim,st}$ respectively using Equations (5.13) and (5.14).

It should be noted that the CIVFM and the CMVM were calibrated independently. Therefore, the electronics (see section 4.5) were setup differently in each experiment. In other words, the maximum dc output voltages (when the CIVFM and the CMVM were filled completely with water) were adjusted differently for each experiment.

Chapter 6

Experimental Apparatus and Procedures

Introduction

To carry out the measurements of two phase flows using the universal Venturi tube, UVT, (which was used for bubbly two phase flow, see Section 4.2) and the conductance multiphase flow meter (i.e. the conductance inlet void fraction meter, CIVFM and the conductance multiphase Venturi meter, CMVM, see Section 4.3) which was used to study the separated vertical annular and horizontal stratified flows, several items of equipment are needed. Note that, the UVT, the CIVFM and the CMVM represent the testing devices while other instruments in the flow loop (e.g. turbine flow meters, dp cells, etc) represent the reference and auxiliary devices. At the start of the current investigation the flow loop at the University of Huddersfield was capable of producing gas-liquid bubbly flows. This flow loop has an 80 mm internal diameter pipe and a 2.5 meter long test section and was used initially to study bubbly gas-water two phase flows using the UVT described in Chapter 4.

It should be noted that the bubbly gas-water two phase flow used in this thesis is approximately homogenous (i.e. its average properties on the scale of a few bubble diameters are approximately the same everywhere in the flow). Therefore, whenever the readers come across the term “homogenous flow” throughout this thesis, it refers to bubbly two phase flow, allowing the homogenous flow model described in Chapter 3 to be used. In effect, the flow is assumed to be homogenous and therefore assumed to behave as a single phase flow.

The flow loop was further developed as part of the current investigation to enable vertical annular gas-water flows and horizontal stratified gas-water flows to be established. An air blower was used to provide the necessary high gas flow rates and a variable area flow meter (VAF) was installed to measure these high gas flow rates.

This chapter describes the experimental setups used with bubbly gas-water two phase flows and with separated (annular and stratified) gas-water two phase flows. The flow loop used has three different configurations (i) vertical bubbly flow, (ii) vertical annular flow and (iii) horizontal stratified flow (see Section 6.1).

A description of the following instruments used on the flow loop, and the calibration of the reference measurement devices, is given in Section 6.2.

i) Turbine flow meters to provide a reference measurement of the water volumetric flow rates in bubbly and separated two phase flows respectively.
ii) Side channel blower (RT-1900) to provide the necessary high gas flow rates.
iii) Variable area flow meter to provide a reference measurement of the necessary high gas volumetric flow rates.
iv) Thermal mass flow meter to provide a reference measurement of the low gas flow rates.
v) Differential pressure devices.
vi) Temperature sensor, gauge pressure sensor and atmospheric pressure sensor.

The change over valve and flushing system and the calibration of the wall conductance sensor are described in Sections 6.3 and 6.4 respectively.

6.1 Multiphase flow loop capabilities

One of the multiphase phase flow loops available at the University of Huddersfield is capable of producing flows with water as the continuous phase. The gas phase is air with approximate density of 1.2 kgm^{-3}. For the current investigation the working section was constructed of an 80mm internal diameter pipe and was approximately 2.5m long. Photographs of the gas-water two phase flow loop used in the current research are shown in Figure 6-1. This flow loop has three configurations;

(i) vertical bubbly flow (see Section 6.1.1),
(ii) vertical annular flow (see Section 6.1.2), and
(iii) horizontal stratified flow (see Section 6.1.3).

These three configurations are described in detail below. Details of the reference measurement devices used in theses configurations are given in Section 6.2.

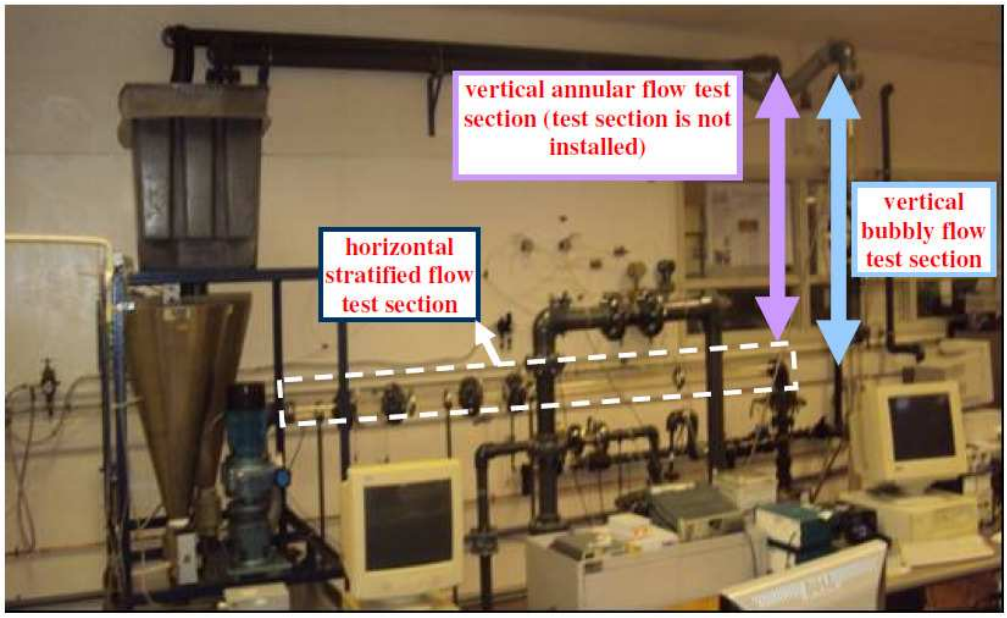

(a) Front view

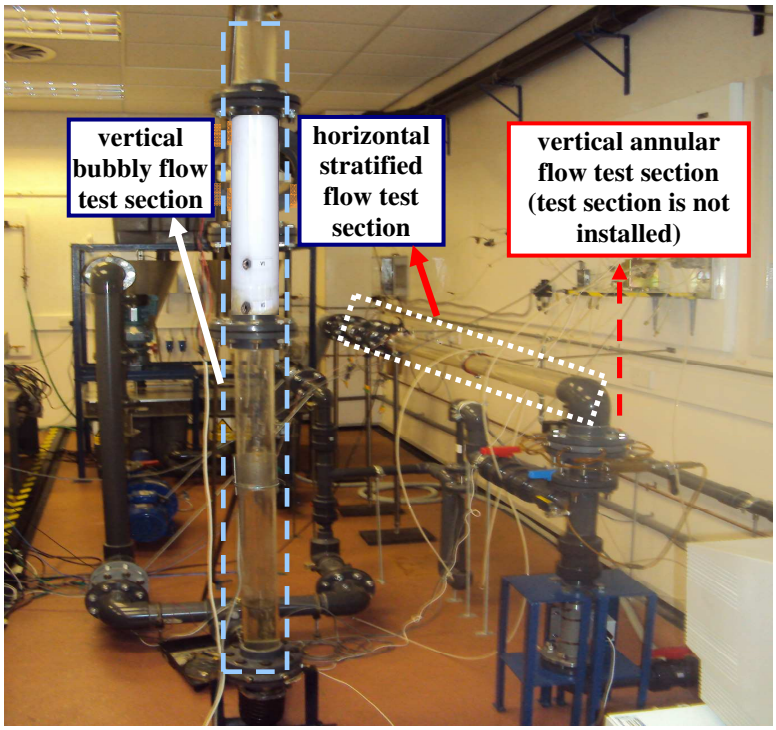

(b) Right view

Figure 6-1: Photographs of the gas-water two phase flow loop at the University of Huddersfield.

6.1.1 Vertical bubbly gas-water two phase flow configuration

The vertical bubbly gas-water two phase flow configuration is capable of providing flows with water as a continuous phase and air as a dispersed phase. A schematic diagram of the vertical bubbly gas-water flow configuration is shown in Figure 6-2 and this was used to conduct studies on the UVT in bubbly gas-water flows using the homogenous flow model described in Chapter 3. Combining the UVT and the flow density meter, FDM (which was used to measure the gas volume fraction $\alpha_{1,\mathrm{hom}}$ at the inlet of the Venturi for bubbly (approximately homogenous) two phase flows, see Sections 3.1.1 and 4.1) enables the mixture volumetric flow rate, $Q_{m,\mathrm{hom}}$ to be determined (see Equation (3.9)).

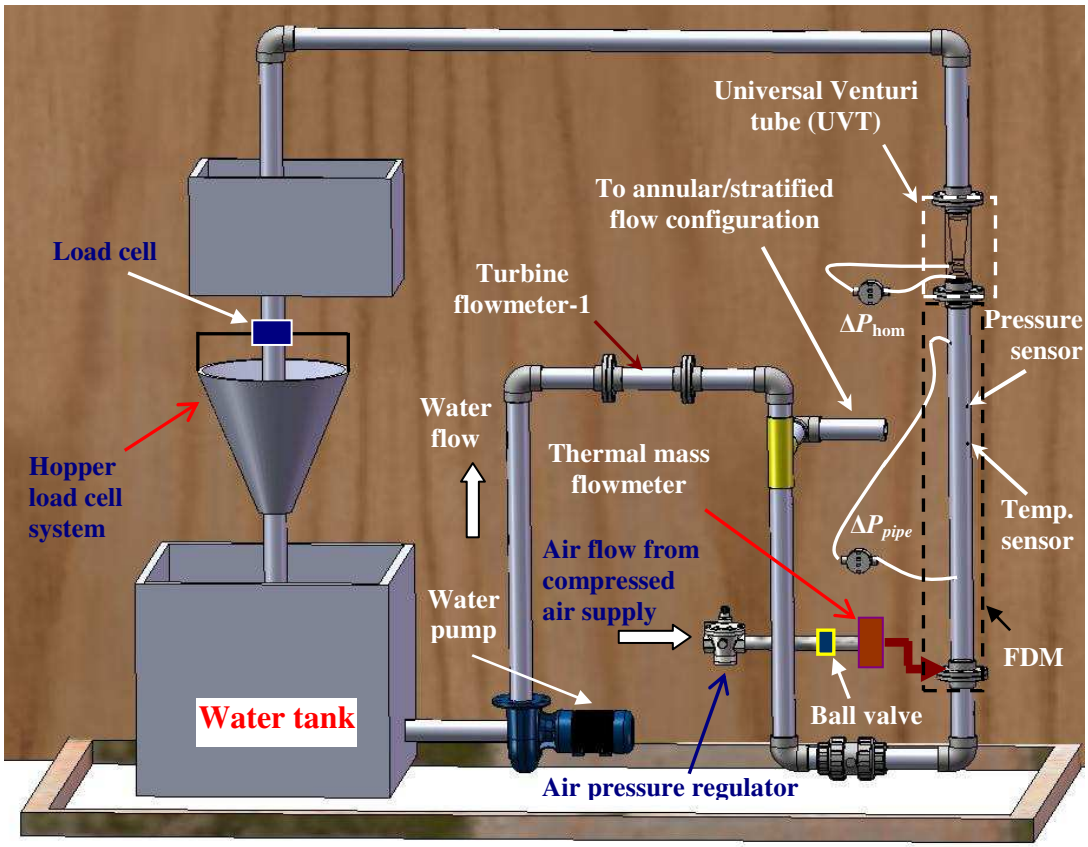

Figure 6-2: A schematic diagram of the vertical bubbly gas-water two phase flow configuration at the University of Huddersfield.

As shown in Figure 6-2, the water was pumped from the water tank into the test section (i.e. the vertical section which combines the FDM and the UVT, see also Figure 6-3) through turbine flow meter-1 using a multistage in-line centrifugal pump. The turbine flow meter-1 was used to provide a reference water volumetric flow rate, $Q_{w,ref}$. The calibration curve of this turbine flow meter is described in Section 6.2.2. It should be noted that two turbine flow meters were used in this study, one was used in the bubbly two phase flow configuration and was denoted "turbine flow meter-1", and the other was used in the separated (vertical annular and horizontal stratified) flow configurations and was denoted "turbine flow meter-2" (see Sections 6.1.2 and 6.1.3).

The air, from the laboratory compressed air supply, was injected into the base of the test section (via a plate with a series of equi-spaced 1mm diameter holes) and passed through an air regulator and manual ball valve which controlled the gas flow rate. The reference gas volumetric flow rate, $Q_{g,ref}$, was measured using the thermal mass flow meter installed on the air flow line. The thermal mass flow meter can be used over a range of 0-200 standard litres per minute (SLPM) (see Section 6.2.6). The measured gauge pressure in the test section was added to atmospheric pressure (measured using a barometer) to give the absolute pressure. The absolute pressure along with the measured temperature (from a thermocouple) in ^{o}K were used to correct the measured reference gas mass flow rate from the thermal mass flow meter to give the reference gas volumetric flow rate, $Q_{g,ref}$.

The sum of the reference gas and water volumetric flow rates gives the reference mixture volumetric flow rate, $Q_{m,ref}$. The predicted mixture volumetric flow rate, $Q_{m,\mathrm{hom}}$ (see Equation 3.9) obtained from the homogenous flow model (described in Chapter 3) using the FDM and UVT can be compared with the reference mixture volumetric flow rate, $Q_{m,ref}$ to analyse the error in the predicted measurement technique (see Chapter 7). In other words, the $Q_{m,ref}$ measured using turbine flow meter-1 and the thermal mass flow meter represents the reference measurement while $Q_{m,\mathrm{hom}}$ obtained from the FDM and the UVT in conjunction with the homogenous

flow model described in Section 3.1 represents the predicted (or estimated) measurement.

The hopper load cell system (see Figure 6-2) was used to calibrate turbine flow meter-1 used in the bubbly gas-water two phase flow configuration (see Section 6.2.1).

The test section of the bubbly gas-water two phase flow (including the FDM and the UVT) with interfacing system is shown in Figure 6-3. Measurement of the pressure drop, ΔP_{pipe}, across the FDM enables the gas volume fraction, $\alpha_{1,\text{hom}}$, to be determined using Equation (3.14). ΔP_{pipe} was measured using a Yokogawa DP cell, EJA 110A (see Section 6.2.3). The pressure drop ΔP_{hom} across the UVT was measured by the Honeywell DP cell, ST-3000 (see also Section 6.2.3). Once the gas volume fraction, $\alpha_{1,\text{hom}}$, and the pressure drop, ΔP_{hom}, are measured, the predicted mixture volumetric flow rate, $Q_{m,\text{hom}}$, in a bubbly two phase flow (assuming that the flow is homogenous) can then be estimated from Equation (3.9).

Six signals were interfaced with the PC via a data acquisition unit, Labjack U-12 (see Figure 6-3). The operation of the Labjack U-12 was controlled using MATLAB software. The six signals were the two dp signals (see Section 6.2.3), the reference gas volumetric flow rate from the thermal mass flow meter (see Section 6.2.6), the reference water volumetric flow rate from a turbine flow meter-1(see Section 6.2.2) which was interfaced via the CNT channel on the Labjack-U12, the gauge pressure signal and the temperature signal (see Section 6.2.7). Once all required signals were interfaced with the LabJack-U12, the MATLAB test program was run and the required flow parameters recorded. It should be noted that the signal conditioning unit (see Figure 6-3) was used to display the gas flow rate in SLPM, the temperature in ^{o}C and the gauge pressure in bar. The gas flow rate through the thermal gas mass flow meter which was monitored by the signal conditioning unit (in SLPM) can be manually controlled using the ball valve and the air regulator installed on the air flow line (see Figure 6-2).

Since the CNT channel (i.e. a counter) in a data acquisition unit (Labjack-U12) was a TTL square wave input and the output signal from the turbine flow meter-1 was a sine wave voltage, it was necessary to convert this sine wave voltage to a square wave voltage. The circuit shown in Figure 6-4 was designed to convert the output signal (sine wave) from the turbine flow meter-1 into a square wave signal.

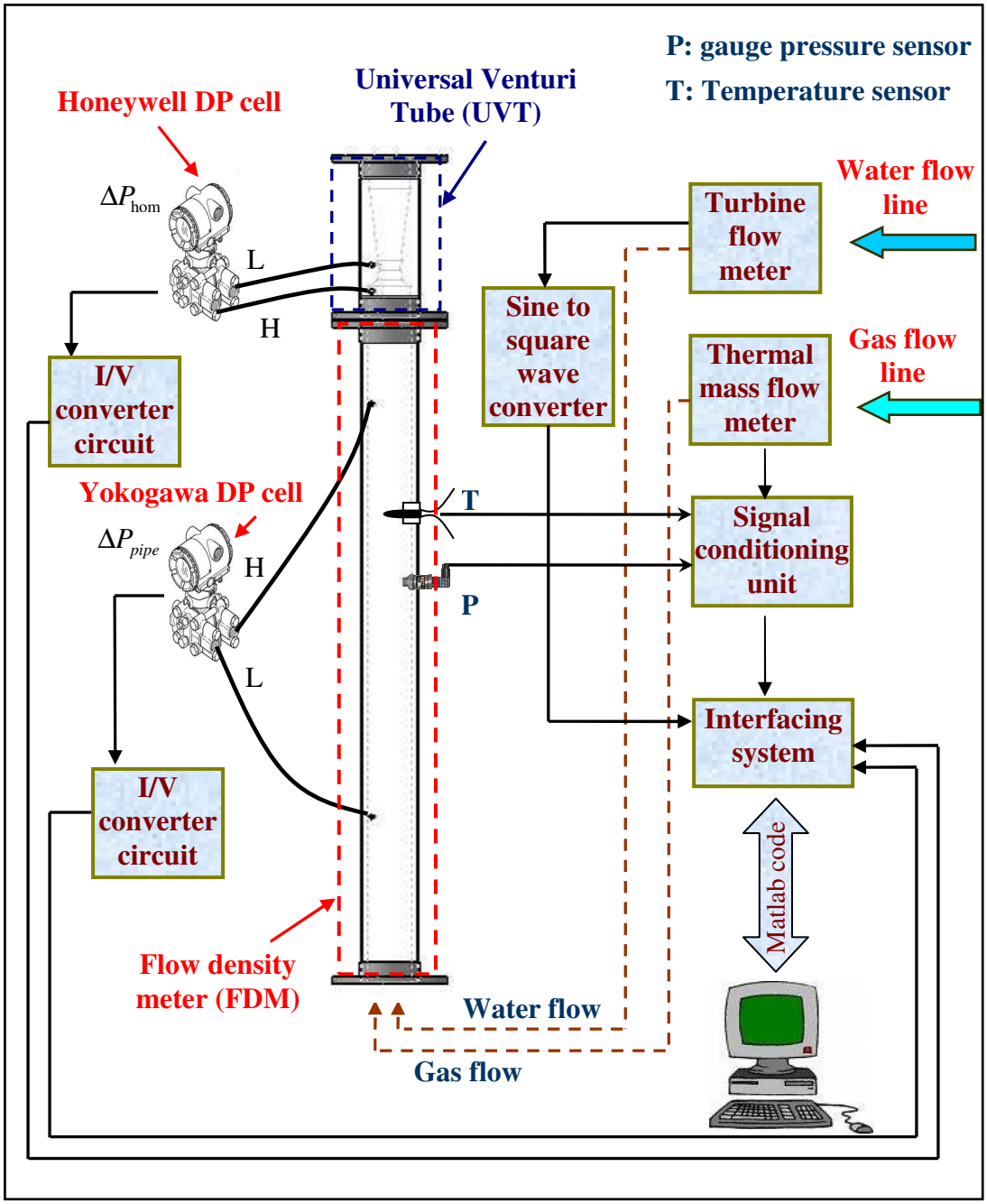

Figure 6-3: Flow test section of the bubbly gas-water two phase flow with interfacing system

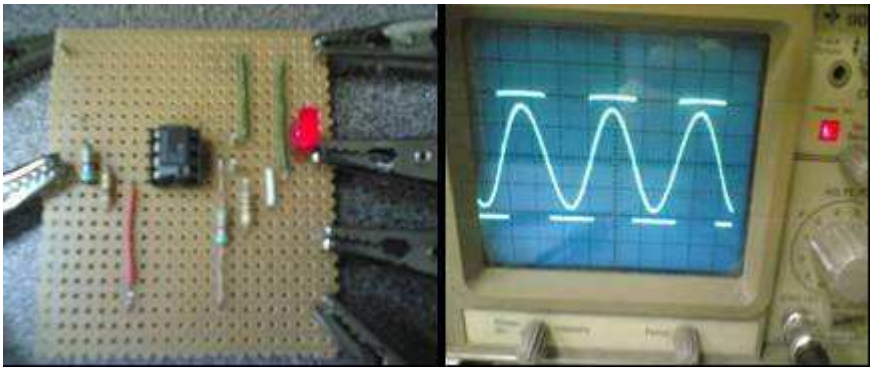

Figure 6-4: Sine-to-square wave converter (left), Test result of a sine-to-square wave converter (right)

The current outputs (4-20mA) from the two DP cells shown in Figure 6-3 were converted into voltage signals (1-5V) which could then be fed into the data acquisition unit (Labjack-U12). Figure 6-5 shows the current to voltage (I/V) converter circuit. It should be noted that two I/V converter circuits were built to convert the current outputs (4-20mA) from two dp cells into 1-5V signals simultaneously.

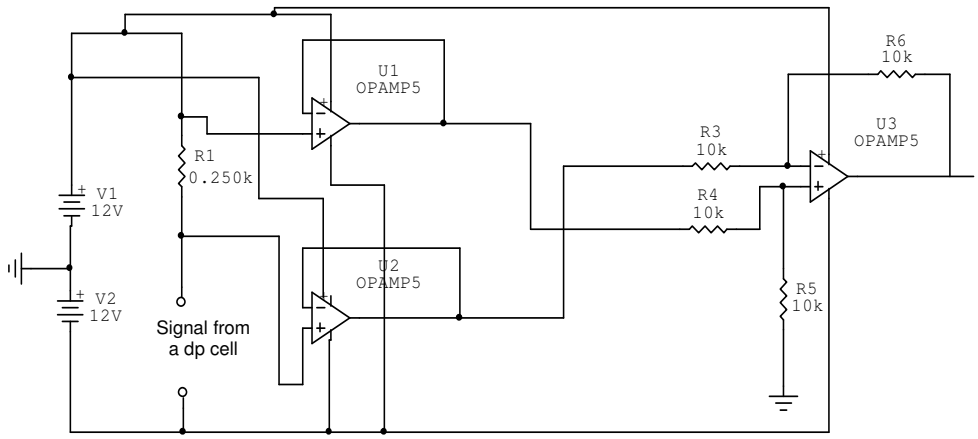

Figure 6-5: Schematic diagram of I/V converter circuit

6.1.2 Annular gas-water two phase flow configuration

In order to carry out the measurements using the conductance multiphase flow meter in annular (wet gas) flow, the vertical annular two phase flow configuration was developed. It should be noted that the conductance multiphase flow meter consists of; (i) the CIVFM, which is capable of measuring the gas volume fraction at the inlet of

the Venturi in vertical annular and horizontal stratified two phase flows (see Section 4.3.1) and (ii) the CMVM, which is capable of measuring the gas volume fraction at the throat of the Venturi in vertical annular and horizontal stratified two phase flows (see Section 4.3.2). A schematic diagram of the vertical annular two phase flow configuration is shown in Figure 6-6. This flow configuration also has an 80mm diameter, 2.5m long test section.

As shown in Figure 6-6, the water was pumped into the test section through turbine flow meter-2. It should be noted that this turbine flow meter is not the same as that used in the bubbly gas-water two phase flow configuration. Turbine flow meter-2 is brand new and was installed to provide a reference water volumetric flow rate in annular gas-water two phase flow (described in this section) and horizontal gas-water two phase flow (described in Section 6.1.3).

Pressurised air was pumped from the side channel blower, RT-1900 (see Section 6.2.5) into the test section through the VAF to provide the necessary high gas flow rates (up to 155 m^3hr^{-1}). A VAF was used to measure the reference gas volumetric flow rate supplied by the side channel blower (see Section 6.2.4). In order to measure the reference gas mass flow rate, $\dot{m}_{g,ref,wg}$, in annular (wet gas) flow, the absolute pressure P_1 and the absolute temperature T_1 were measured at the upstream section of the conductance multiphase flow meter. Measurements of P_1 (from a gauge pressure sensor, see Section 6.2.7) and T_1 (from a thermocouple) enabled the gas density ρ_{g1} at the inlet of the Venturi (i.e. at the CIVFM) to be determined using Equations (3.44) and (3.45). The reference gas volumetric flow rate, $Q_{g,ref,wg}$, in annular (wet gas) flow obtained from the VAF was then converted into the reference gas mass flow rate $\dot{m}_{g,ref,wg}$ using;

$$\dot{m}_{g,ref,wg} = \rho_{g1} Q_{g,ref,wg}$$

Equation (6.1)

The predicted gas mass flow rate, $\dot{m}_{g,wg}$, and the predicted water mass flow rate, $\dot{m}_{w,wg}$, obtained from the separated flow model described in Chapter 3 (Equations (3.66) and (3.72)) using the CIVFM and the CMVM can be compared with the

reference gas and water mass flow rates, $\dot{m}_{g,ref,wg}$ and $\dot{m}_{w,ref,wg}$, measured from the VAF and turbine flow meter-2 respectively, so that the error between the predicted measurements and the reference measurements in annular (wet gas) flow can be analysed (see Chapter 8).

A Honeywell dp cell, ST-3000 was used to measure the differential pressure, $\Delta P_{TP,wg}$, across the CMVM. A Yokogawa dp cell, EJA 110A, was used to measure the differential pressure, $\Delta P_{TP,pipe}$, across the vertical pipe. Although, $\Delta P_{TP,pipe}$ was not necessary to calculate the predicted gas and water mass flow rates, $\dot{m}_{g,wg}$ and $\dot{m}_{w,wg}$, it was recorded for use in possible further investigation that might be carried out in the future.

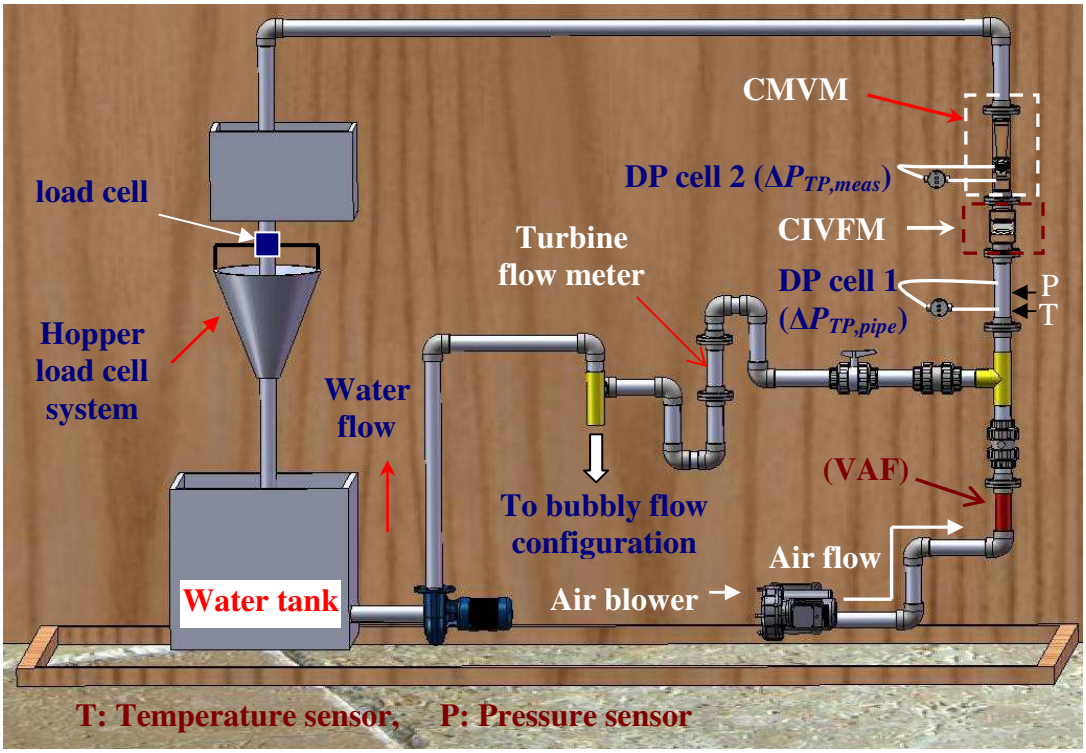

Figure 6-6: A schematic diagram of the vertical annular gas-water two phase flow loop at the University of Huddersfield.

A schematic diagram of the vertical annular (wet gas) flow test section (which includes the CIVFM and the CMVM) with the interfacing system is shown in Figure 6-7.

Two ring electrodes at the CIVFM and two ring electrodes at the throat section of the CMVM were used to measure the gas volume fractions $\alpha_{1.wg}$ and $\alpha_{2.wg}$ at the inlet and the throat of the Venturi respectively. The excitation voltage and the wave frequency of the excitation electrodes at the Venturi inlet (i.e. CIVFM) and the Venturi throat (i.e. throat section of the CMVM) were 2.12 p-p V and 10kHz respectively. The measurement electrodes were connected to the electrical conductance circuit (see Section 4.5) in which the gas volume fractions, $\alpha_{1.wg}$ and $\alpha_{2.wg}$, could be obtained from the dc output voltages using Equations (5.11) and (5.12) respectively. All measured signals were interfaced to the PC via a data acquisition unit, Labjack U-12. The operation of the Labjack U-12 was controlled using MATLAB software.

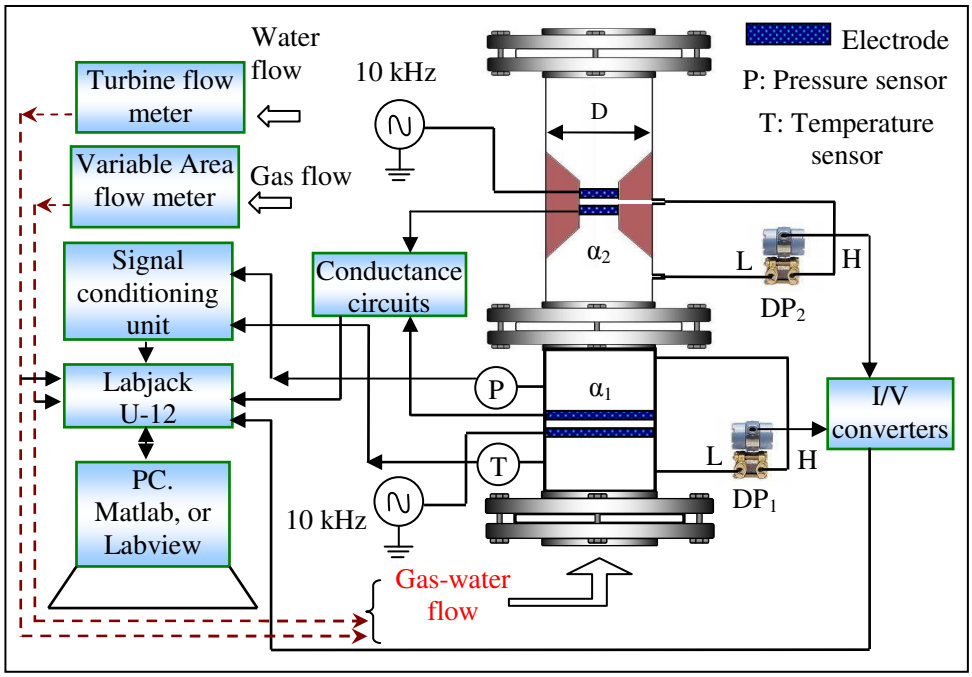

Figure 6-7: Schematic diagram of the vertical annular (wet gas) flow test section with interfacing system

6.1.3 Stratified gas-water two phase flow configuration

The two phase flow loop at the University of Huddersfield (see Figure 6-1) was further developed as part of the current investigation to enable horizontal stratified gas-water flows to be established. A schematic diagram of the horizontal stratified gas-water flow configuration is shown in Figure 6-8.

The horizontal stratified gas-water flow configuration is similar to the annular gas-water two phase flow configuration described in Section 6.1.2 except that in the horizontal stratified configuration, the test section which includes the CIVFM and the CMVM was mounted in a horizontal position (see Figures 6-8 and 6-9). In addition, the pressurised air was pumped into the test section using either;

(i) the laboratory air compressor (as used in bubbly flow configuration, see Section 6.1.1) to provide the necessary low gas flow rates allowing the thermal mass flow meter to be used to measure the reference gas mass flow rate or,

(ii) the side channel blower RT-1900 to provide a necessary high gas flow rates allowing the VAF to be used to measure the reference gas mass flow rate.

The range of the VAF (see Section 6.2.4) is $30m^3hr^{-1}$ to $200m^3hr^{-1}$. Therefore, any gas flow rate below $30m^3hr^{-1}$ could not be sensed by the VAF. This was the reason for using the laboratory air compressor line (as an alternative air supply) with the thermal mass flow meter to provide a reference gas mass flow rate for an air flow rate below $30m^3hr^{-1}$ (see the flow conditions of stratified gas-water two phase flows in Chapter 9, Table 9-1).

The same turbine flow meter used in annular two phase flow configuration (i.e. turbine flow meter-2) was used in the stratified two phase flow configuration to provide a reference water volumetric flow rate, $Q_{w,ref,st}$. The gas mass flow rate, $\dot{m}_{w,ref,st}$, in stratified two phase flows could be obtained by multiplying $Q_{g,ref,st}$ by the gas density, ρ_{g1}, obtained from Equations (3.44) and (3.45).

Since there was a substantial difference between the pressure drop in the gas phase at the top of the Venturi and the pressure drop in the water phase at the bottom of Venturi in stratified gas-water two phase flows, two differential pressure devices were used as shown in Figures 6-8 and 6-9. The inclined manometer (see Section 6.2.3) was used at the top of the Venturi to measure the pressure drop in the gas phase while the Honeywell dp (ST-3000) was used to measure the pressure drop in the water phase at the bottom of the Venturi (see the stratified flow model described in Section 3.2.1).

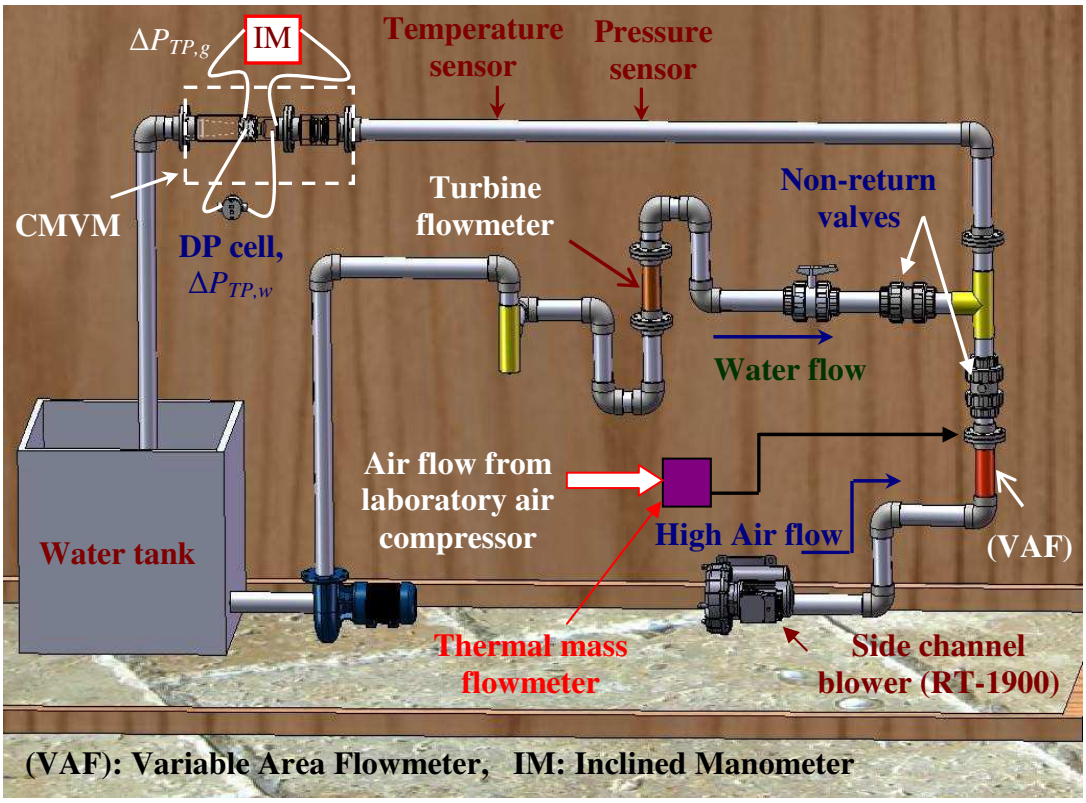

Figure 6-8: A schematic diagram of the horizontal (stratified) gas-water two phase flow loop at the University of Huddersfield.

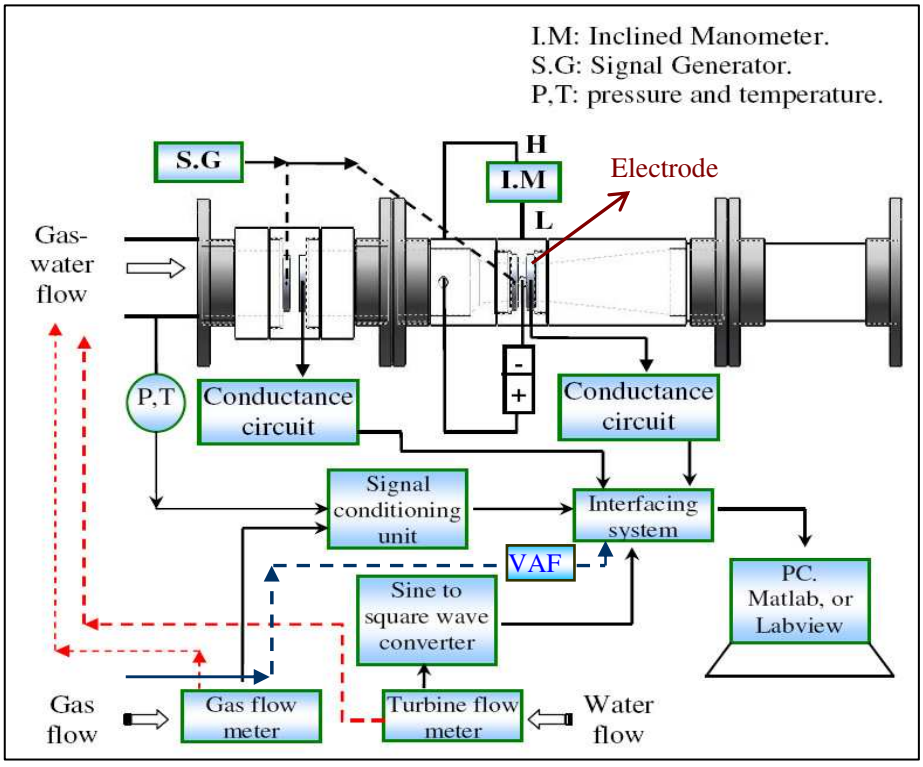

Figure 6-9: Schematic diagram of the horizontal stratified flow test section with interfacing system

6.2 Reference and auxiliary measurement devices used on the gas-water two phase flow loop

As mentioned earlier, the flow density meter, FDM (described in Section 4.1) and the UVT (described in Section 4.2) used in bubbly gas-water two phase flows and the conductance multiphase flow meters (CIVFM and CMVM) used in separated (vertical annular and horizontal stratified) two phase flows represent the testing devices. Other than the above devices, all other instruments on the flow loop are either reference measurement devices (e.g. hopper load cell system, turbine flow meters, thermal mass flow meter and VAF) or auxiliary devices (e.g. differential pressure transmitters, side channel blower RT-1900, temperature sensor, gauge pressure sensor and atmospheric pressure sensor). These devices are described below.

6.2.1 Hopper load cell system

The hopper load cell system with pneumatically actuated ball valve was used for calibrating water turbine flow meter-1 used in bubbly gas-water two phase flows (see Section 6.2.2). The hopper is suspended from a load cell as shown in Figure 6-10.

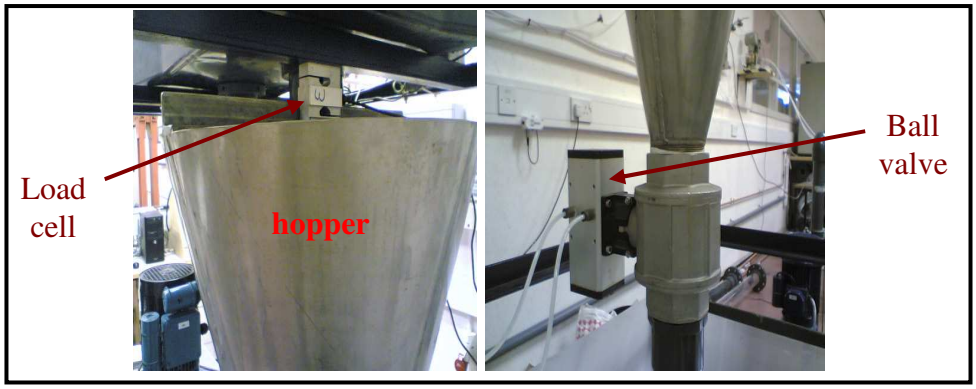

Figure 6-10: Photographs of the hopper load cell system

Before calibrating the turbine flow meter (see Section 6.2.2) using the hopper load cell system, the load cell was calibrated twice to ensure repeatability. Known volumes of the water were added to the water hopper. The full range of the load cell was 0 litre to 40 litre (i.e. 0kg to 40kg). The load cell and the valve (at the

base of the hopper) are connected to a PC. The resulting response (i.e. the output voltage) of the water hopper load cell V_w was recorded from the PC. The calibration curve of the water hopper load cell system is shown in Figure 6-11.

The principle of operation of the hopper load cell system is very simple. By closing the valve at the base of the hopper and recording the time taken for a known mass to be collected in the hopper, the mass flow rate $\dot{m}$ can be calculated. The volumetric flow rate Q can then be easily determined using;

$$Q = \frac{\dot{m}}{\rho_w}$$

Equation (6.2)

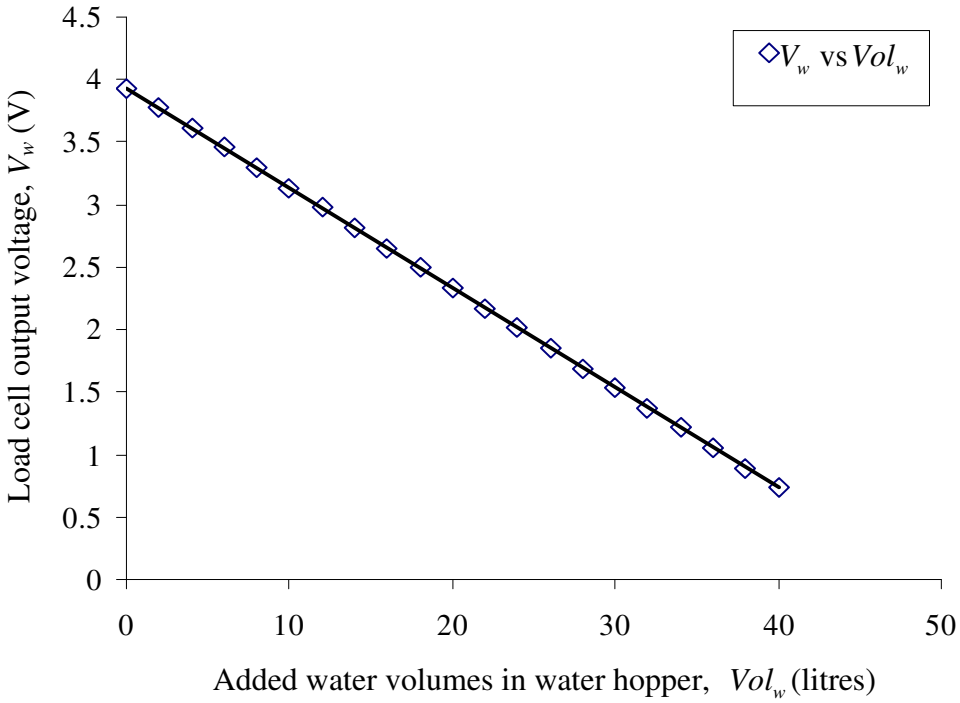

Figure 6-11: Calibration curve for water hopper load cell

The relationship between the output voltage V_w obtained form the water hopper load cell and the water volume added Vol_w (see Figure 6-11) can be expressed as;

$$V_w = -0.0801(Vol_w) + 3.935$$

Equation (6.3)

6.2.2 Turbine flow meters

A turbine flow meter is a device used to measure the fluid (normally water or gas) volume flow rate. It is designed so that the rotation frequency is directly proportional to the volumetric flow rate Q over the specified range of operation of the meter. A photograph of a turbine flow meter is shown in Figure 6-12. Two turbine flow meters were used in the current study. One was used to provide a reference water volumetric flow rate in bubbly two phase flows (i.e. turbine flow meter-1 which generated the output signal with frequency, fq_1) while the second turbine flow meter was used to provide a reference water volumetric flow rate in separated annular and horizontal stratified flows (i.e. the turbine flow meter-2 which generated the output signal with frequency, fq_2). The turbine flow meter-2 used in separated flows (see Figures 6-6 and 6-8) was relatively new and the calibration supplied by the manufacturer was assumed to be valid. The calibration data supplied by the manufacturer for this turbine flow meter gave the following relationship between the water volumetric flow rate Q_w and the measured frequency fq_2 of the output signal from the turbine flow meter-2.

$$Q_w = [9.2712432 \times 10^{-7} \times fq_2] \qquad (\mathrm{m^3 s^{-1}})$$

Equation (6.4)

where the constant 9.2712432×10^{-7} is called a meter factor.

The turbine flow meter-1 which was used in a bubbly gas-water two phase flow (see Figure 6-2) was installed more than five years ago and needed to be calibrated to check for any wear instead of just relying on the factory calibration data. The factory calibration for this meter was $0.0462\,\mathrm{m^3 hr^{-1} Hz^{-1}}$ over a design range of $3.41\,\mathrm{m^3 hr^{-1}}$ to $40.8\,\mathrm{m^3 hr^{-1}}$. For the current investigation, this meter was calibrated over a range of $3.947\,\mathrm{m^3 hr^{-1}}$ to $21.196\,\mathrm{m^3 hr^{-1}}$. The calibration of the turbine flow meter-1 was carried out by plotting the turbine meter frequency fq_1 against the water volumetric flow rate read from the water hopper load cell system described in Section 6.2.1. The data acquired from this calibration is shown in Figure 6-13.

Figure 6-12: A photograph of a turbine flow meter

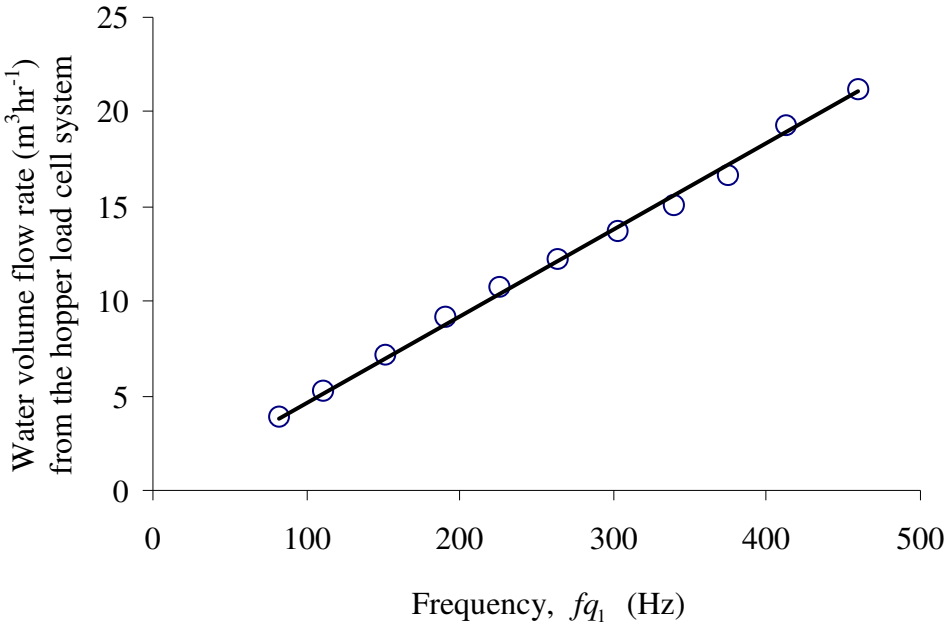

Figure 6-13: Calibration curve for turbine flow meter-1

Figure 6-13 shows that the turbine flow meter-1 has experienced little wear. The relationship between the water volumetric flow rate and the turbine meter frequency fq_1 of this meter is given by;

$$Q_w = 0.0460 \times fq_1 \qquad (\mathrm{m^3 hr^{-1}})$$

Equation (6.5)

where the constant 0.0460 is the meter factor obtained from the calibration.

6.2.3 Differential pressure devices

To estimate the mixture density (see Equations (3.8) and (3.14)) in a bubbly gas-water two phase flow using a FDM (see Sections 3.1.1 and 4.1) and to measure the differential pressure across the UVT (see Section 4.2) and the CMVM (see Section 4.3) accurately, it was necessary to calibrate the two differential pressure transmitters before running the air-water rig (see Figure 6-14). The two dp transmitters used were (i) Honeywell dp cell, ST-3000 and (ii) Yokogawa dp cell, EJA 110A [150]. A flushing system was installed to ensure that no air was trapped in either the transducer or the measurement lines. The flushing system is described in Section 6.3. The factory calibrations of these transmitters were performed in a range of 0 to 40 inches H_2O. For the current investigation the two dp cells were also re-calibrated with the pressure tapping separation of 1m.

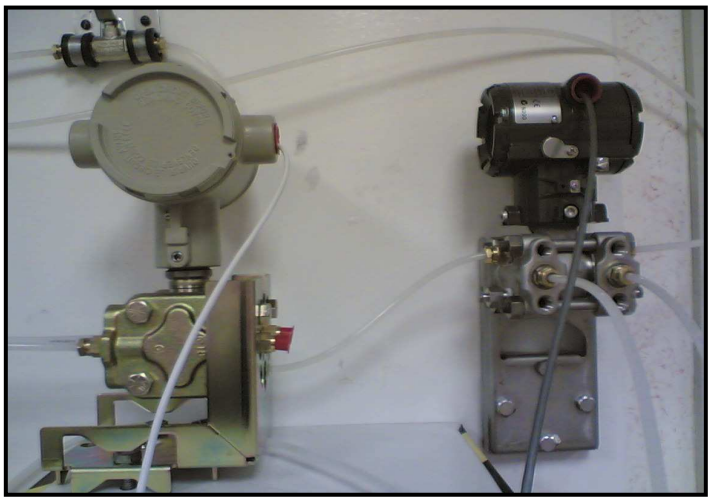

Figure 6-14: Photographs of Honeywell (left) and Yokogawa (right) dp cells

Since the output from the both dp cells was an electrical (4-20 mA) current, two current-to-voltage (I/V) converter circuits were designed and used to convert the current output signals from the dp cells (i.e. 4-20 mA) into the dc output voltages (1-5V) which can then be easily interfaced with a PC via a data acquisition unit, Labjack U-12. An I/V converter circuit was already described earlier in this chapter (see Section 6.1.1, Figure 6-5).

The calibration was carried out in different stages with increasing and decreasing water levels in the 1m long pipeline. The calibration curves for both dp cells are shown in Figures 6-15 and 6-16. It should be noted that the reason for plotting the differential pressure on the y-axis and the dc output voltage on the x-axis is that the best fit polynomial equation, which describes the differential pressure as a function of the dc output voltage, can be obtained directly from the graph.

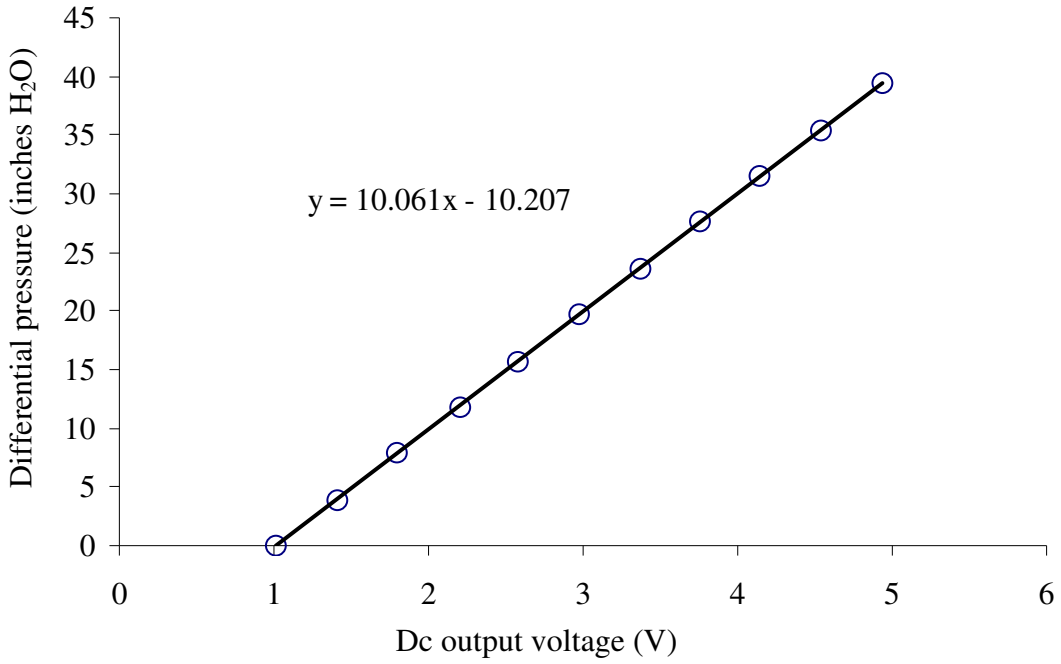

Figure 6-15: Calibration of the Yokogawa dP cell

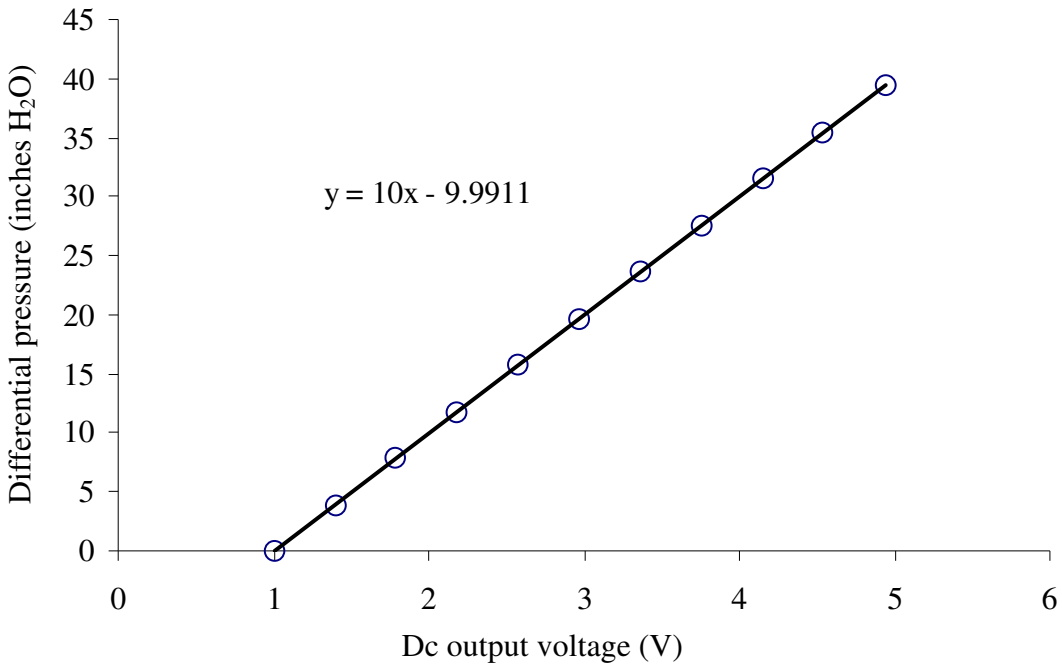

Figure 6-16: Calibration of the Honeywell dP cell

In horizontal stratified gas-water two phase flows, an inclined manometer was used to measure the gas pressure drop, $\Delta P_{TP,g}$ (see Equation (3.43) in Section 3.2.1) across the top side of the CMVM (see Figures 6-8 and 6-9 in Section 6.1.3). A photograph of an inclined manometer is shown in Figure 6-17. The manometer fluid is a red paraffin with a specific gravity S.G. of 0.784 at 20°C. This manometer has two inclined tubes; a long tube and a short tube as shown in Figure 6-17. Table 6-1 shows the pressure ranges for long and short tubes at different tube positions.

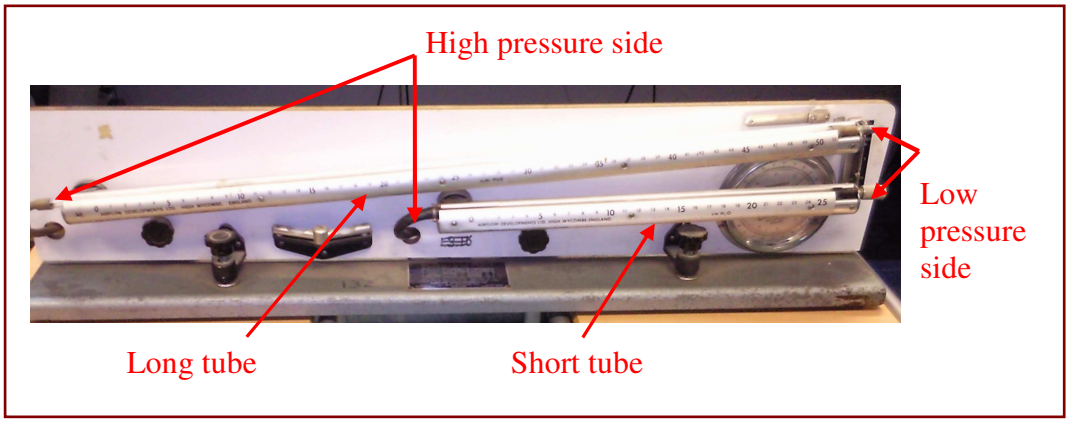

Figure 6-17: A photograph of an inclined manometer

Table 6-1: specifications of the inclined manometer

Tube position	Long tube		Short tube	
	Pressure range (cm WG)	Scale multiplier	Pressure range (cm WG)	Scale multiplier
Vertical	50	1.0	25	1
Top inclined	10	0.2	5	0.2
Middle inclined	NA	NA	2.5	0.1
Bottom inclined	5	0.1	1.25	0.05

6.2.4 The Variable Area Flowmeter (VAF)

A VAF meter was used to provide a reference measurement of the gas volumetric flow rate received from the side channel blower, RT-1900 (high air supply) that was used for annular and stratified gas-water two phase flows. A photograph of the VAF is shown in Figure 6-18. The output from the VAF can be analogue and/or dc voltage signals. The analogue signal can be directly read from the analogue gauge which was calibrated by the manufacturer to give the gas volumetric flow rate in a range of $30m^3hr^{-1}$ to $200m^3hr^{-1}$. The dc output voltages from the VAF were related to the readings obtained from the analogue gauge for different values of the gas volumetric flow rate. In other words, the dc output voltage from the VAF was checked against the analogue signal read from the gauge meter on the front of the VAF for different values of the gas volumetric flow rates. The relationship between the dc output voltage V_{VAF} and the gas volumetric flow rate Q_g (read from the gauge meter) is shown in Figure 6-19.

Figure 6-18: A photograph of the VAF

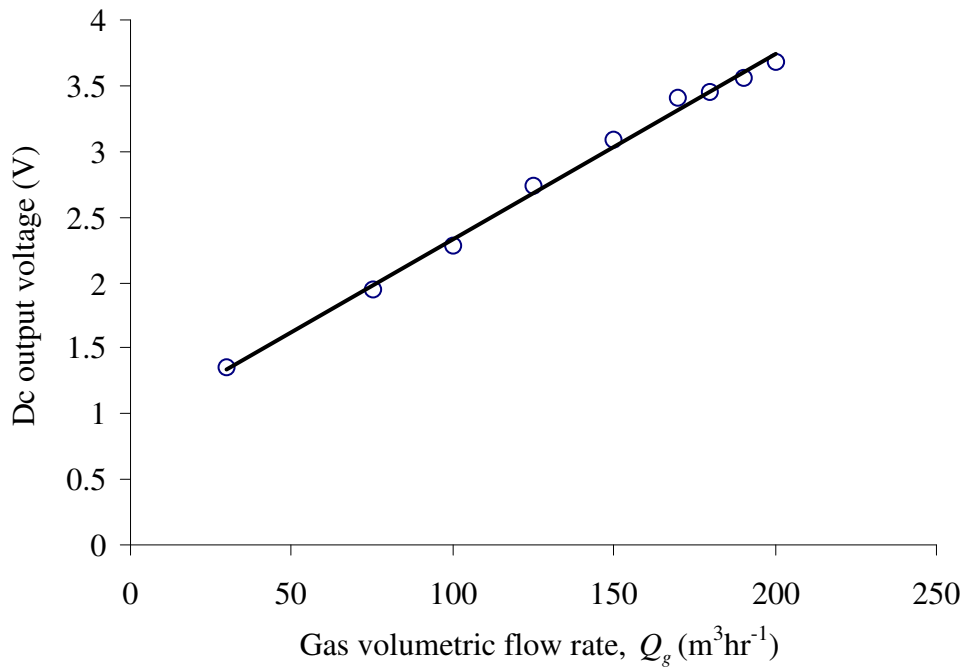

Figure 6-19: The relationship between the dc output voltage and the gas volumetric flow rate in a VAF

The relationship between the dc output voltage, V_{VAF}, and the gas volumetric flow rate, Q_g in a VAF (see Figure 6-19) can be expressed as;

$$Q_g = \frac{V_{VAF} - 0.9168}{0.0141} \qquad (m^3hr^{-1})$$

Equation (6.6)

Note that, the gas volumetric flow rate Q_g can be converted into the gas mass flow rate, $\dot{m}_g$, using;

$$\dot{m}_g = \rho_g Q_g$$

Equation (6.7)

The gas density, ρ_g, in Equation (6.7) can be calculated using Equations (3.44) and (3.45), see also Section 6.2.7.

6.2.5 Side channel blower (RT-1900)

The side channel blower (RT-1900, 60Hz) was installed on the flow loop to provide the necessary high gas flow rates in separated vertical annular and horizontal stratified flows (see Sections 6.1.2 and 6.1.3). A photograph of the side channel blower (RT-1900) and its specification are shown in Figure 6-20. It is clear from Figure 6-20 that the gas volumetric flow rate Q_g supplied by the side channel blower depends on the differential pressure ΔP.

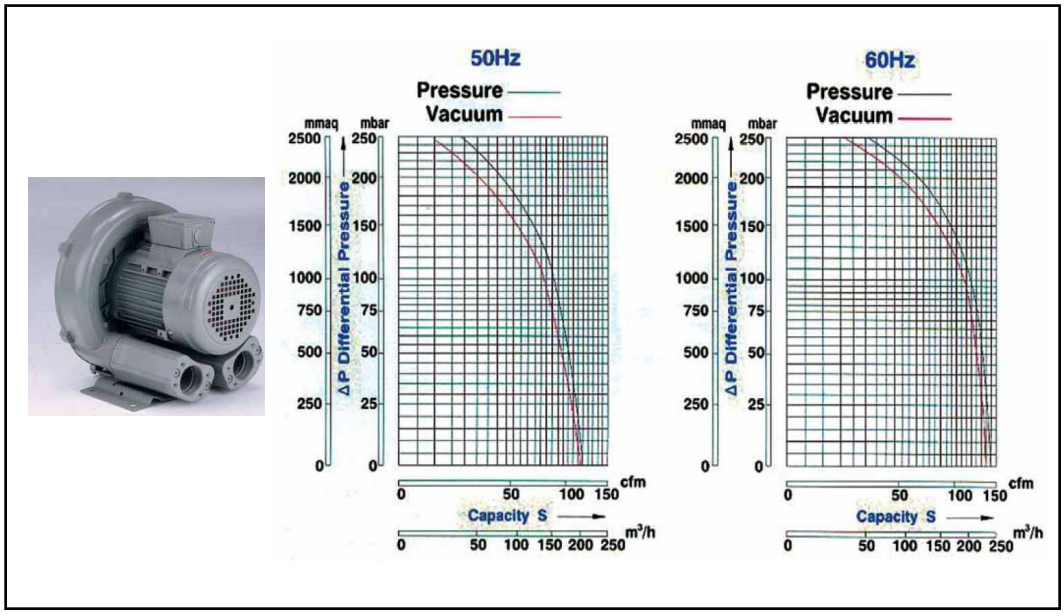

Figure 6-20: A photograph of the side channel blower (RT-1900) and its specification

One of the challenges encountered in this study was that the side channel blower (RT-1900) could not provide enough gas flow rate to support a smooth liquid film flow rate in vertical annular gas-water two phase flows. This in turn, produced pulsations in the liquid film and led to significant error in the water mass flow rate calculated from Equation (3.72). Therefore, an alternative technique was used to measure the water mass flow rate in annular two phase flows. This alternative technique was based on the wall conductance sensor (see Sections 4.4 and 6.3).

6.2.6 The thermal mass flow meter

The thermal mass flow meter was used to provide a reference measurement of the gas volumetric flow rate supplied by the laboratory air compressor (low air supply). The thermal mass flow meter (Hasting Model HFM, HFM 200 series) can be used in a range of 0-200 SLPM with accuracy of ±1% F.S and repeatability of ±0.1% F.S. The measured gauge pressure (obtained from the pressure transducer, PDCR 810-0799, see Section 6.2.7) in the test section was added to atmospheric pressure (from a barometer) to give the absolute pressure. The absolute pressure along with the measured temperature (from a thermocouple) in ^{o}K are used to correct the measured reference gas mass flow rate from the thermal mass flow meter to give the reference gas volumetric flow rate, $Q_{g,ref}$. A photograph of the thermal mass flow meter is shown in Figure 6-21.

Figure 6-21: Thermal mass flowmeter

The thermal mass flow meter was calibrated using the gas meter G10. The calibration curve is shown in Figure 6-22. The solid line in Figure 6-22 shows the reference line (i.e. 45^o line).

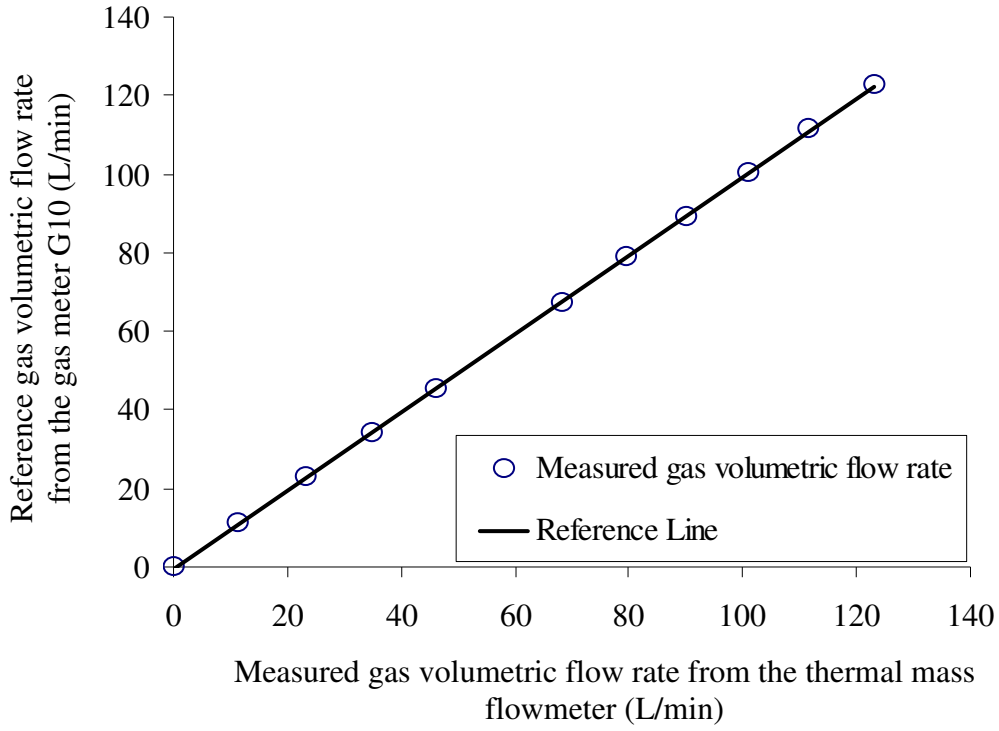

Figure 6-22: calibration of the thermal mass flowmeter

6.2.7 Temperature sensor, gauge pressure sensor and atmospheric pressure sensor

Measurement of the absolute pressure P_1 and the absolute temperature T_1 (from the thermocouple) at the upstream section of the Venturi meter enabled the gas density to be determined (see Chapter 3, Equations (3.44) and (3.44)). Measured gauge pressure was added to atmospheric pressure (from a barometer) to give absolute pressure.

Once the gas density at the upstream section of the Venturi was obtained, the gas mass flow rate can be easily converted into the gas volumetric flow rate or vice-versa. This was applied in the bubbly, vertical annular and horizontal stratified flows.

The gauge pressure sensor used was silicon-diaphragm type, PDCR 810 series manufactured by RS Components LTD. The data sheet of the PDCR 810-0799 pressure transducer claims a combined non-linearity, hysteresis and repeatability of ±0.1% B.S.L (best straight line). The pressure range is 0-2 bar with temperature effect of ± 0.5% within 0 to 50^{o}C. As mentioned earlier, adding the gauge pressure, from the pressure transducer PDCR 810-0799, and the atmospheric pressure, from a barometer, enabled the absolute pressure to be determined. The barometer used in this study was the electronic barometer BA888. The temperature was measured using a thermocouple (J-type).

6.3 The change over valve and flushing system

As mentioned in Chapter 3, many differential pressure transmitters can not read a differential pressure if the pressure at the 'high' input is less than the pressure at the 'low' input. In a bubbly two phase flow through a Venturi, in which the inlet and the throat are connected to the dp cell via water filled lines, the two phase air-water pressure drop across a Venturi meter may change its sign from positive to negative. This situation can never arise in a single phase flow (see Section 3.1.2). A change-over valve system was used to overcome this problem (see Figure 6-23).

It should be noted that the change-over valve system was only used in a bubbly gas-water two phase flow through a UVT in which the pressure drop across the Venturi may change its sign. The flushing system was used to remove any air bubble in the transducer diaphragms and the water filled lines connected to '+' and '-' inputs of the dp cells.

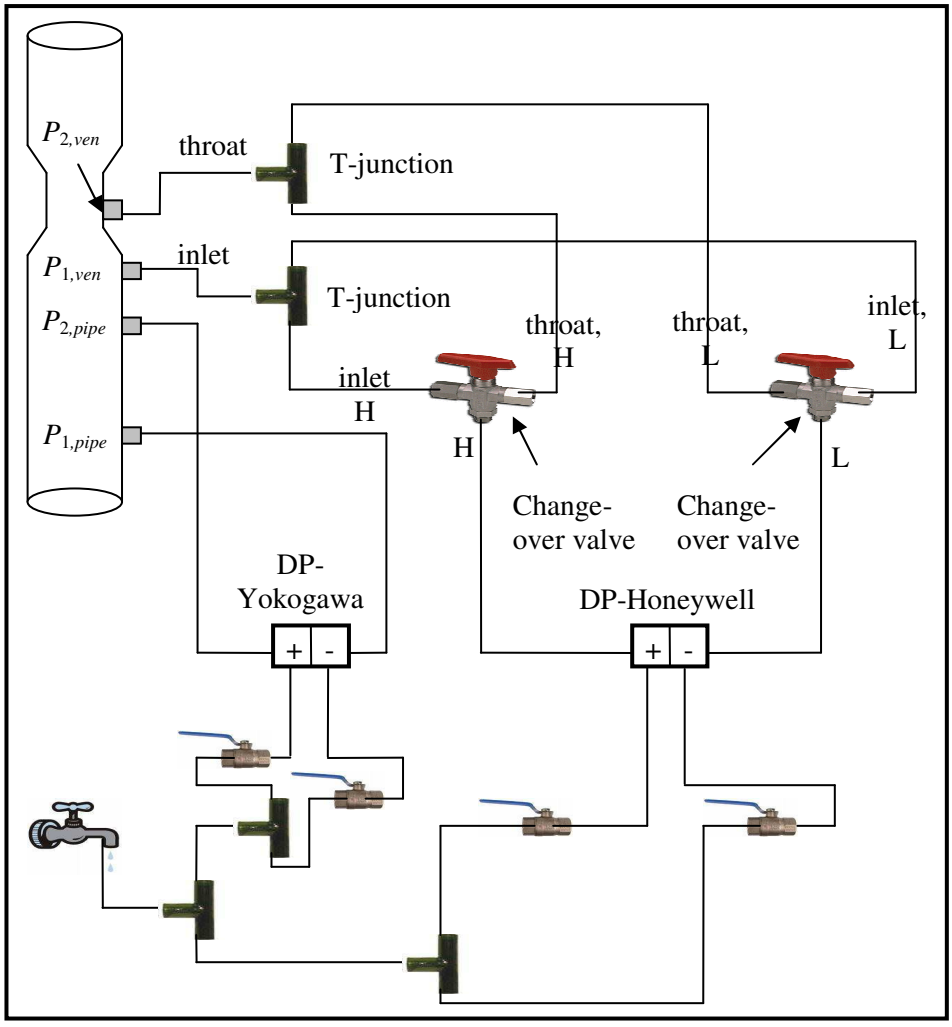

Figure 6-23: Change-over valve and flushing system

6.4 Calibration of the wall conductance sensor

As mentioned earlier, the side channel blower could not provide a smooth liquid film flow rate for all flow conditions causing the error in the water mass flow rate to be greater than the expected error. As a result, the wall conductance sensors were used (in parallel with the current research) as an alternative method for measuring the liquid flow rate in annular gas-water two phase flows (see Sections 4.4 and 8.7). It should be noted that the wall conductance sensors were investigated by Al-Yarubi (2010) [147]. The data provided from the wall conductance sensors (i.e. the relationship between the entrainment fraction in the gas core with the gas superficial velocity, see Section 8.7) was used in conjunction with the conductance multiphase

flow meter to measure the total water mass flow rate in annular two phase flows (see Chapter 8).

Since the data obtained from the wall conductance sensors was used to modify the water mass flow rate using the conductance multiphase flow meter, it is necessary to give a brief description about the calibration of the wall conductance sensor carried out by Al-Yarubi (2010) [147]. This calibration was accomplished by placing different sizes of solid cylindrical non-conducting plugs concentrically in the main body of the flow meter. The gap between the outer diameter of a particular solid core and the inner surface of the pipe wall was then filled with water, representing the water film that would occur in a real annular flow as shown in Figure 6-24. The calibration procedure of the wall conductance sensors was similar to the calibration procedure for CIVFM and CMVM described in Section 4.5 and Chapter 5. Al-Yarubi (2010) [147] gives a full detail on the calibration of the wall conductance sensors (see Figure 6-25).

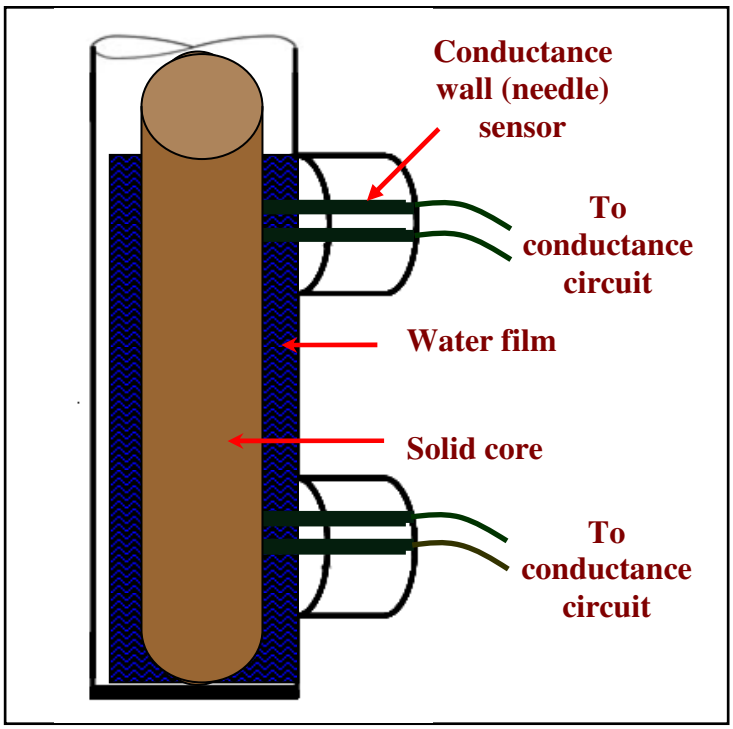

Figure 6-24: Calibration setup of the wall conductance sensors

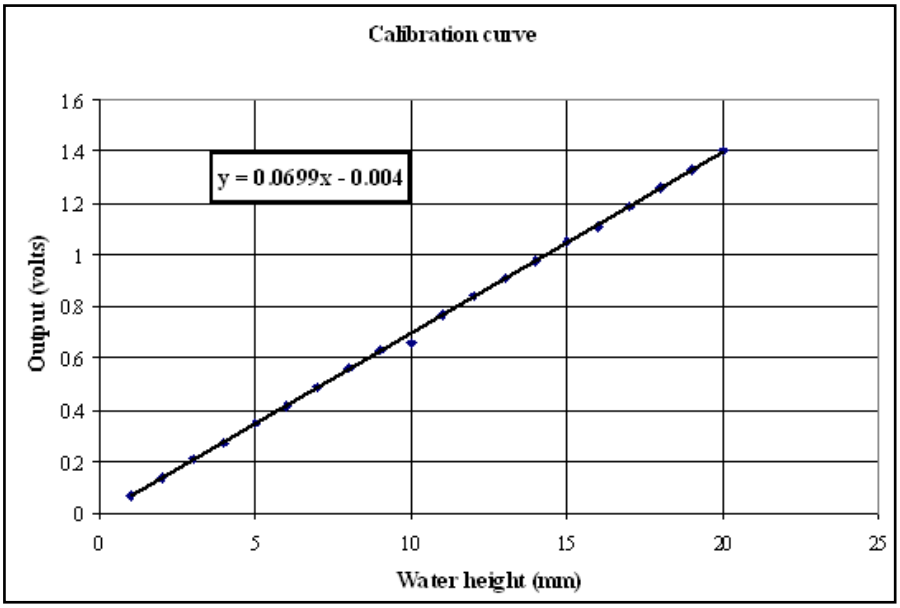

Figure 6-25: Calibration curve of the wall conductance sensor

Summary

To carry out the measurements of two phase flows using a UVT and the conductance multiphase flow meter (i.e. CIVFM and CMVM) in different flow regimes, several items of equipment are needed. The experiments were carried out using the resources already available at the University of Huddersfield. The two phase flow loop was initially used to study the bubbly gas-water two phase flows. This flow loop was further developed as part of the current investigation to enable vertical annular gas-water flows and horizontal stratified gas-water flows to be established. The flow loop used has three different configurations (i) vertical bubbly flow, (ii) vertical annular flow, and (iii) horizontal stratified flow (see Section 6.1).

The FDM (see Section 4.1), the UVT (see Section 4.2), the CIVFM (see Section 4.3.1) and the CMVM (see Section 4.3.2) represented the testing devices while all other devices on the flow loop were reference and auxiliary devices (e.g. turbine flow meter, dp cells, etc). A description of the reference and auxiliary devices was presented in Section 6.2.

In bubbly gas-water two phase flows, the reference water volumetric flow rate was obtained from the turbine flow meter-1 while the reference gas volumetric flow rate was obtained from the thermal mass flow meter. In vertical annular two phase flows, the reference water volumetric flow rate and the reference gas volumetric flow rate were obtained from the turbine flow meter-2 (see Section 6.2.2) and the VAF respectively (see Section 6.2.4). In horizontal stratified flows, the reference water volumetric flow rate was also obtained from the turbine flow meter-2. Two reference gas flow meters were used in a horizontal stratified flow; (i) the thermal mass flow meter to provide a reference measurement for low gas flow rates, and (ii) the VAF to provide a reference measurement for high gas flow rates.

Chapter 7

Experimental Results for Bubbly Gas-Water Two Phase Flows through a Universal Venturi Tube (UVT)

Introduction

At the beginning of this chapter it should be restated that the bubbly gas-water two phase flow considered in this thesis is approximately homogenous (i.e. its average properties on the scale of a few bubble diameters are approximately the same everywhere in the flow). Therefore, whenever the readers come across the term "homogenous flow" throughout this thesis, it refers to bubbly two phase flow, allowing the homogenous flow model described in Chapter 3 to be used. In effect, the flow is assumed to be homogenous and therefore assumed to behave as a single phase flow.

The UVT (see Section 4.2) was used to study a bubbly (or approximately homogenous) gas-water two phase flow in which it was used in conjunction with the FDM (see Section 4.1) to measure the gas volume fraction $\alpha_{l,hom}$ at the inlet of the Venturi (see Equation (3.14)). The gas volume fraction $\alpha_{l,hom}$ measured by the FDM at the inlet of the Venturi in a homogenous flow is assumed to be constant throughout the UVT. Once the mixture density was obtained, the mathematical model described

in Section 3.1 can be used to determine the mixture volumetric flow rate $Q_{m,\text{hom}}$ (see Equation 3.9).

This chapter presents and discusses the experimental results obtained for homogenous gas-water two phase flow using a UVT. The slip ratio *S* in a homogenous gas-water two phase flow can be assumed unity since both phases are assumed to travel with the same velocity.

The mathematical model of a homogenous gas-water two phase flow through the UVT described in Section 3.1 was applied to study the bubbly gas-water two phase flows in which the gas present within the liquid was in the form of many bubbles of a small size (approximately 5-8 mm diameter). It has been found that this model works well for $\alpha_{1,\text{hom}} \leq 17.48\%$. Beyond this limit the mathematical model of a homogenous gas-water two phase flow through the UVT starts to break down. This is due to the onset of slug flow where individual gas bubbles merge to form a large gas mass or slug that is often cylindrical (bullet) in shape.

7.1 Bubbly air-water flow conditions through the Universal Venturi Tube

Experiments were carried out in vertical upward gas-water flows using a UVT (non-conductance Venturi meter, without electrodes). 92 different flow conditions were tested with the water reference volumetric flow rate, $Q_{w,ref,\text{hom}}$ in the range of 1.057×10^{-3} $m^3s^{-1}$to 4.152×10^{-3} m^3s^{-1} (3.81 m^3hr^{-1} to 14.9 m^3hr^{-1}). For the gas reference volumetric flow rate, $Q_{g,ref,\text{hom}}$ the range was 2.648×10^{-5} m^3s^{-1} to 1.264×10^{-3} m^3s^{-1} (0.095 m^3hr^{-1} to 4.551 m^3hr^{-1}). The homogenous velocity (or mixture superficial velocity) U_h was in the range of 0.237 to 1.055 ms^{-1}.

Three different sets of data were tested. The water flow rate in the first and second sets of data was kept constant while in the third set of data both the water and the gas flow rates were varied. The summary of the flow conditions of all three sets of data is given in Table 7-1.

Table 7-1: Flow conditions of all three sets of data in a homogenous flow

Flow conditions	Set #1	Set #2	Set #3
$Q_{w,ref,\hom}$ (m^3s^{-1})	1.339×10^{-3}	1.937×10^{-3}	1.057×10^{-3} to 4.152×10^{-3}
$Q_{g,ref,\hom}$ (m^3s^{-1})	3.329×10^{-5} to 1.264×10^{-3}	1.178×10^{-4} to 1.015×10^{-3}	2.648×10^{-5} to 1.181×10^{-3}
U_h (ms^{-1})	0.309 to 0.574	0.448 to 0.651	0.237 to 1.055

7.2 Flow loop friction factor

In fluid dynamics, the friction factor is the term which relates the pressure loss due to friction along a given length of pipe to the average velocity of the fluid flow (see Equation (3.27)). The value of the friction factor, f depends primarily on the relative roughness of the pipe surface. Benedict (1980) [151] and Massey (1989) [152] gave a full review of the frictional pressure loss in single liquid phase flows.

Measurement of the differential pressures across a 1 meter long pipe at different values of the single phase (water) volumetric flow rate obtained from the turbine flow meter-1 described in Section 6.2.2 (and hence at different values of the water velocity) enabled the friction factor f to be determined using Equation (3.27). The experimental data in Figure 7-1 shows a classic increase in f as the flow (water) velocity decreases. A good fit equation to the experimental data over the full range of flow velocities is also shown in Figure 7-1.

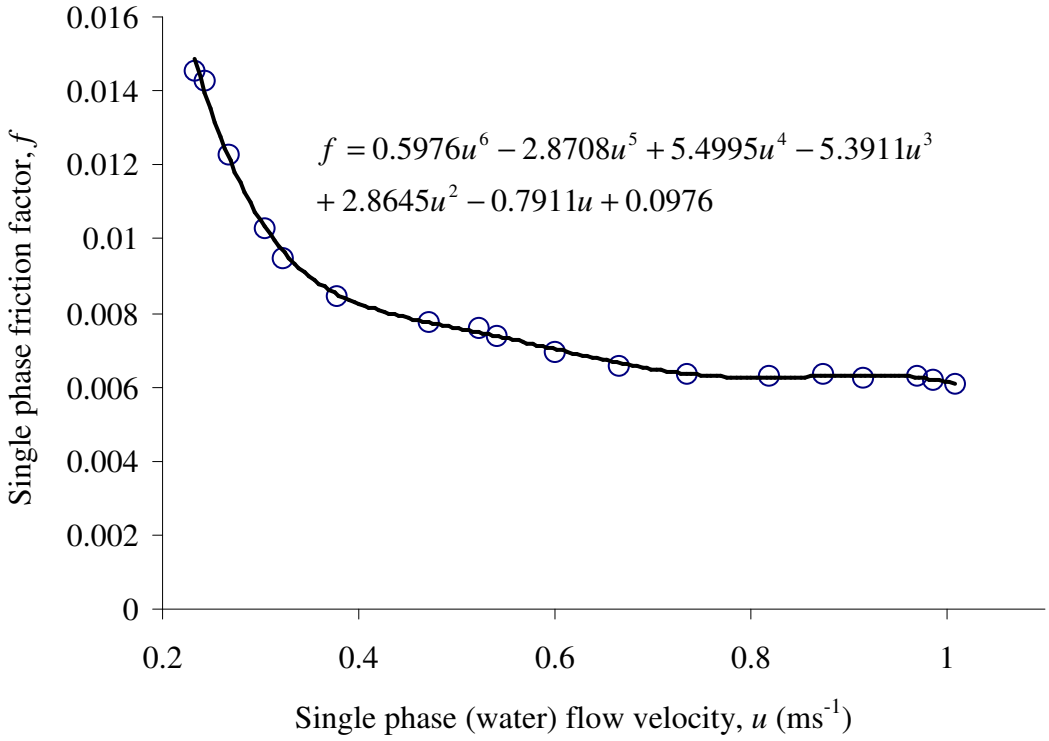

Figure 7-1: Friction factor variation with single phase flow velocity

In order to estimate the friction factor f for the two phase flows, it was necessary to determine the mixture superficial velocity (or homogenous velocity) U_h using the following equation;

$$U_h = \frac{Q_{w,ref,\hom} + Q_{g,ref,\hom}}{A}$$

(Equation 7.1)

where $Q_{w,ref,\hom}$ is the reference water volumetric flow rate in bubbly (homogenous) gas-water two phase flow obtained from the turbine flow meter-1 described in Section 6.2.2, $Q_{g,ref,\hom}$ is the reference gas volumetric flow rate in bubbly two phase

flow obtained from the thermal mass flow meter described in Section 6.2.6 and A is the cross-sectional area of the pipe (ID = 80 mm).

Combining the homogenous velocity U_h, defined by Equation (7.1), and the single phase friction factor calibration data shown in Figure 7-1 enables the frictional pressure loss term $F_{m,pipe}$ (which was defined by Equation 3.13) to be determined. The frictional pressure loss term $F_{m,pipe}$ (see Equation 3.13) together with the measured differential pressure across a 1m length of pipe (using a Yokogawa dp cell, EJA 110A) were used to give a measure of the gas volume fraction, $\alpha_{1,\text{hom}}$, in the FDM (see Equation (3.14) and Sections 4.1 and 6.1.1).

7.3 Analysis of the pressure drop across the Universal Venturi Tube in bubbly gas-water two phase flows

In multiphase flow measurements, the relationship between the overall mass or volume flow rate and the pressure drop across the Venturi is not unique and includes also the flow quality or holdup. Figure 7-2 shows the relationship between the pressure drop across the UVT, ΔP_{hom} and the homogenous velocity (mixture superficial velocity), U_h. It is seen that for $\alpha_{1,\text{hom}} \leq 17.48\%$, the trend can be approximated by a square root relationship. For $\alpha_{1,\text{hom}} > 17.48\%$ (i.e. the onset of slug flow), the points start to move away from the approximated trend.

It should be mentioned that the homogenous flow model, described in Chapter 3, starts to break down when the gas volume fraction $\alpha_{1,\text{hom}}$ increases above 17.48% (see Section 7.5).

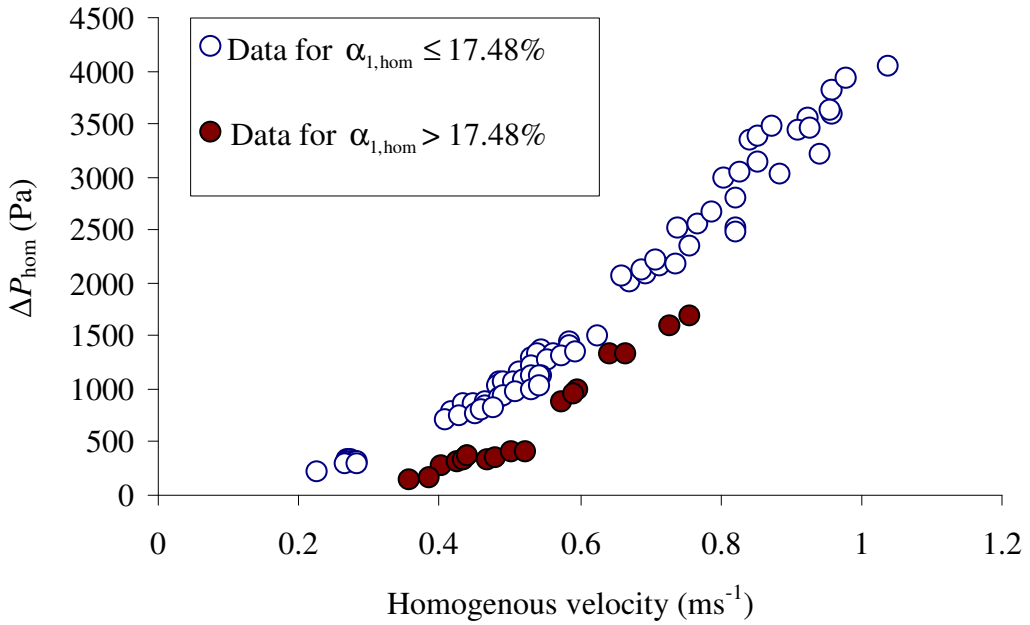

Figure 7-2: Differential pressure drop across the Universal Venturi Tube, ΔP_{hom} in bubbly gas-water two phase flows for all sets of data

7.4 Variation of the discharge coefficient in a homogenous gas-water two phase flow through a Venturi meter

To account for the frictional and turbulence losses in the UVT a discharge coefficient was introduced (see Equation (3.9)). It is defined as the ratio between the actual to theoretical flow rates. The homogenous discharge coefficient $C_{d,\text{hom}}$ in Equation (3.9) is given by;

$$C_{d,\text{hom}} = \frac{Q_{m,ref,\text{hom}}}{Q_{m,\text{hom}}}$$

Equation (7.2)

where $Q_{m,ref,\text{hom}}$ is the reference mixture volumetric flow rate obtained from adding the reference water volumetric flow rate $Q_{w,ref,\text{hom}}$ (obtained from the turbine flow meter-1 described in Section 6.2.2) and the reference gas volumetric flow rate $Q_{g,ref,\text{hom}}$ (obtained from the thermal mass flow meter described in Section 6.2.6). $Q_{m,\text{hom}}$ in Equation (7.2) is the predicted mixture volumetric flow rate which was defined by Equation (3.9).

The data of the discharge coefficient for Venturi meters in single phase flows is well established in the literature. In contrast, existing literature on discharge coefficients in two phase flows is very limited. Most of the research conducted on Venturi meters defined the discharge coefficient similar to that in incompressible single phase flow (e.g. Murdock (1962) [47], Chisholm (1967, 1977) [48,49] and Lin (1982) [51]).

Moissis and Radovcich (1963) [104] defined the discharge coefficient similar to that in single phase flow. They showed that at low values of the gas volume fraction (< 0.5), where the homogenous flow model was valid, the discharge coefficient was independent of the gas volume fraction. When the gas volume fraction was higher than about 0.5, the gas discharge coefficient increased with increasing the gas volume fraction. The authors concluded that, the reason of this was due to the effect of the slip velocity.

Figure 7-3 shows the variations of the homogenous discharge coefficient $C_{d,\mathrm{hom}}$ with the gas volume fraction $\alpha_{1,\mathrm{hom}}$ for all three sets of data (i.e. sets #1, 2 and 3, (see Table 7-1)). It is seen that for $\alpha_{1,\mathrm{hom}} \leq 17.48\%$ the variations in the homogenous discharge coefficient $C_{d,\mathrm{hom}}$ shows that $C_{d,\mathrm{hom}}$ can be treated as independent of the gas volume fraction $\alpha_{1,\mathrm{hom}}$. For $\alpha_{1,\mathrm{hom}} \leq 17.48\%$, $C_{d,\mathrm{hom}}$ has an average value of 0.948. For $\alpha_{1,\mathrm{hom}} > 17.48\%$ the calculated values of the homogenous discharge coefficient $C_{d,\mathrm{hom}}$ increased above 1 and the value of $C_{d,\mathrm{hom}}$ is now seen to be dependent upon the gas volume fraction $\alpha_{1,\mathrm{hom}}$.

It should be noted that the gas volume fraction $\alpha_{1,\mathrm{hom}}$ at the inlet of the UVT, described in Section 4.2, was measured using the FDM described in Sections 3.1.1 and 4.1. The gas volume fraction $\alpha_{1,\mathrm{hom}}$ (see Equation (3.14)) obtained from the FDM was assumed to be constant throughout the UVT since the bubbly gas-water two phase flow used in the current research was approximately homogenous.

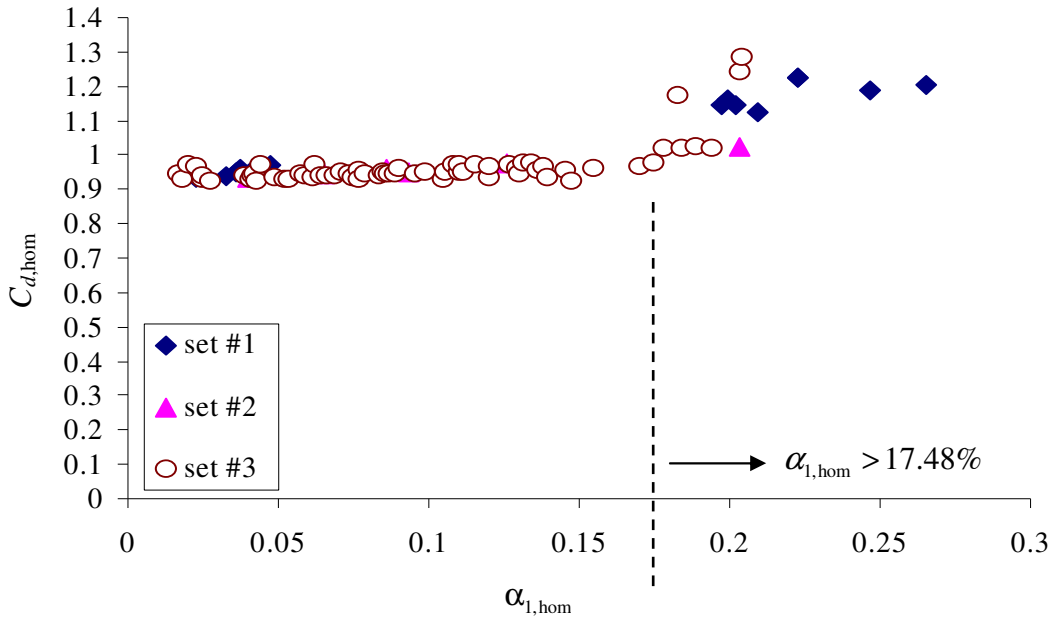

Figure 7-3: Variations of the homogenous discharge coefficient $C_{d,\text{hom}}$ with the inlet gas volume fraction $\alpha_{l,\text{hom}}$

Figure 7-4 shows the variation of $C_{d,\text{hom}}$ with the gas or water superficial velocity. It is clear from Figure 7-4 that, in general, at higher gas superficial velocity ($U_{gs} > 0.199$ ms^{-1}) and lower water superficial velocity ($U_{ws} < 0.297$ ms^{-1}), the discharge coefficient $C_{d,\text{hom}}$ increased above 1 and the value of $C_{d,\text{hom}}$ is seen to be dependent upon the gas or water superficial velocity.

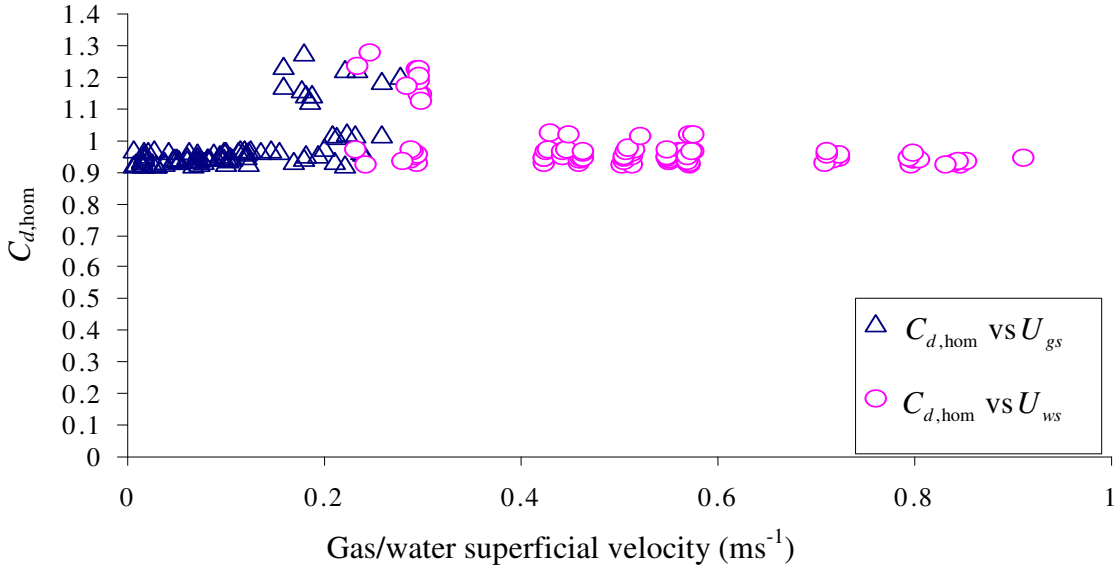

Figure 7-4: Variation of the homogenous discharge coefficient, $C_{d,\text{hom}}$ with the gas/water superficial velocity

7.5 Analysis of the percentage error between the reference and the predicted mixture volumetric flow rates in homogenous gas-water two phase flows

Once the appropriate signals from the UVT and the FDM have been measured (see Section 6.1.1), the predicted mixture volumetric flow rate $Q_{m,\text{hom}}$ can be determined using Equation (3.9). The percentage error, $\varepsilon_{Q_{m,\text{hom}}}$ in the predicted mixture volumetric flow rate can be expressed as;

$$\varepsilon_{Q_{m,\text{hom}}} = \left(\frac{Q_{m,\text{hom}} - Q_{m,ref,\text{hom}}}{Q_{m,ref,\text{hom}}} \right) \times 100\%$$

Equation (7.3)

Figures 7-5 to 7-7 show the percentage error $\varepsilon_{Q_{m,\text{hom}}}$ in the predicted mixture volumetric flow rate for all sets of data (see Table-7-1) using different values of homogenous discharge coefficients (i.e. $C_{d,\text{hom}}$=0.940, 0.948 and 0.950 respectively). It should be noted that the reason of using the two different values of $C_{d,\text{hom}}$ (i.e. $C_{d,\text{hom}}$=0.940 and 0.950) other than the mean value of the homogenous discharge coefficient (i.e. $C_{d,\text{hom}}$=0.940) was to compare the mean value error $\bar{\varepsilon}_{Q_{m,\text{hom}}}$ at different values of $C_{d,\text{hom}}$.

It is again clear from Figures 7-5 to 7-7 that the homogenous model starts to break down when $\alpha_{1,\text{hom}} > 17.48\%$. This is due to the onset of the slug flow regime. It is also seen that the minimum mean value error $\bar{\varepsilon}_{Q_{m,\text{hom}}}$ (i.e. minimum average value of $\varepsilon_{Q_{m,\text{hom}}}$) for $\alpha_{1,\text{hom}} \leq 17.48\%$ can be achieved at $C_{d,\text{hom}-optimum} = 0.948$ (see Figure 7-6). Table 7-2 summarises the mean value error $\bar{\varepsilon}_{Q_{m,\text{hom}}}$ for different values of the discharge coefficient $C_{d,\text{hom}}$. The homogenous flow model described in Section 3.1 works well for $\alpha_{1,\text{hom}} \leq 17.48\%$. Beyond that, the transition between bubbly and slug flow regimes occurs and the use of the homogenous flow model is not expected to achieve accurate results.

Table 7- 2: Mean values of $\bar{\varepsilon}_{Q_{m,\text{hom}}}$ for different values of $C_{d,\text{hom}}$

$C_{d,\text{hom}}$	$\bar{\varepsilon}_{Q_{m,\text{hom}}}$ (%)
0.940	-0.858
0.948	-0.015
0.950	0.196

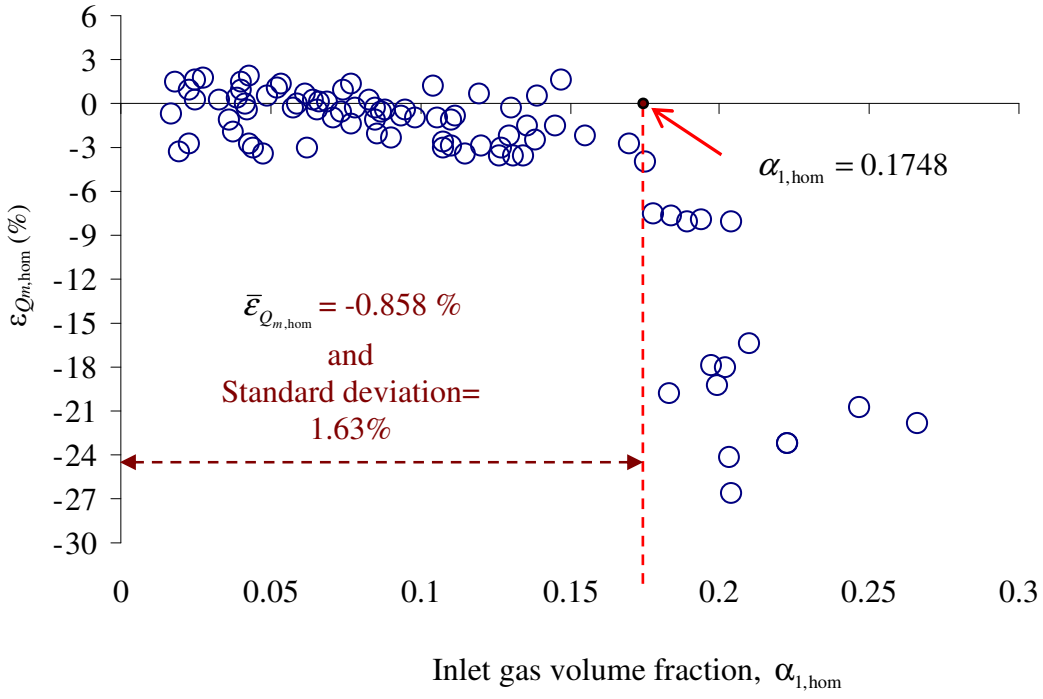

Figure 7-5: Percentage error $\varepsilon_{Q_{m,\text{hom}}}$ in the predicted mixture volumetric flow rate $Q_{m,\text{hom}}$ at $C_{d,\text{hom}} = 0.940$

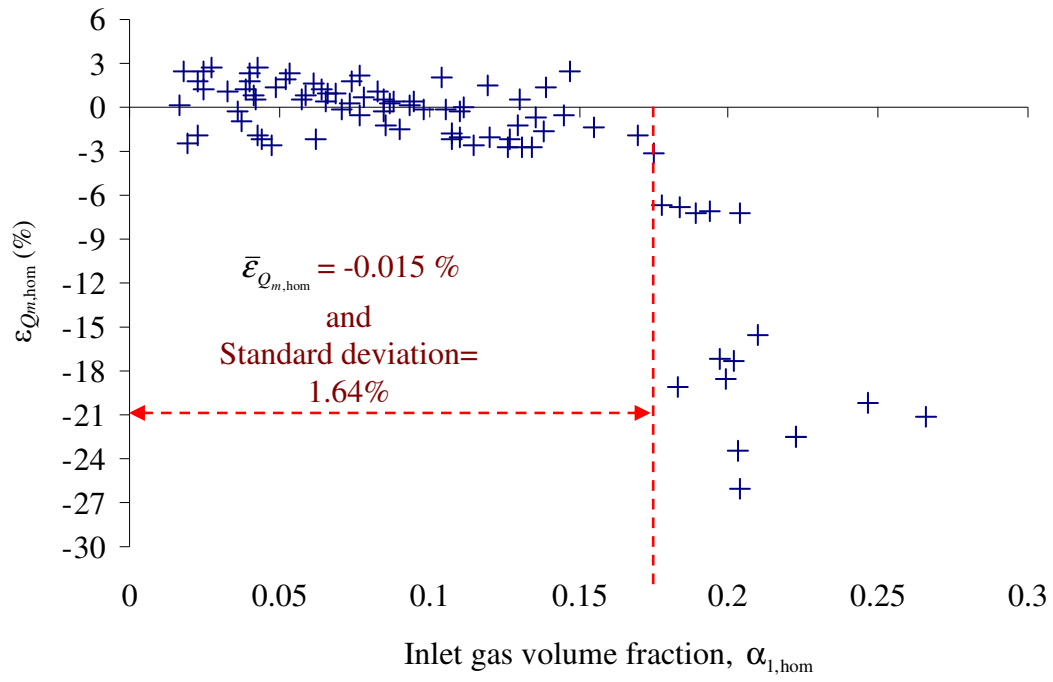

Figure 7-6: Percentage error $\varepsilon_{Q_{m,\mathrm{hom}}}$ in the predicted mixture volumetric flow rate $Q_{m,\mathrm{hom}}$ at at $C_{d,\mathrm{hom}-optimum} = 0.948$

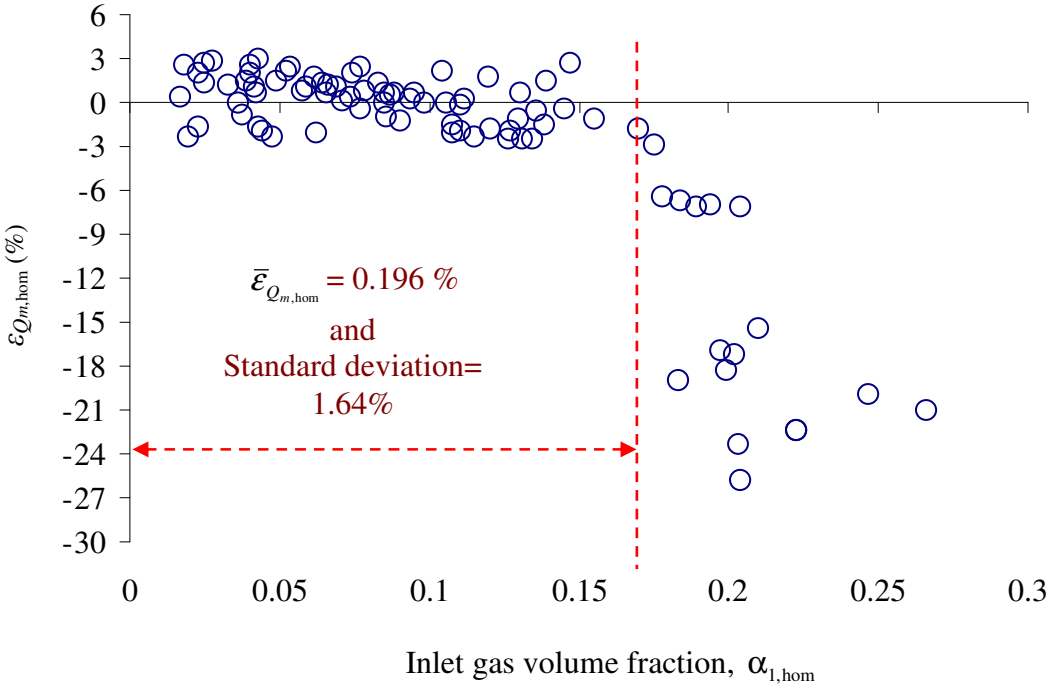

Figure 7-7: Percentage error $\varepsilon_{Q_{m,\mathrm{hom}}}$ in the predicted mixture volumetric flow rate $Q_{m,\mathrm{hom}}$ at at $C_{d,\mathrm{hom}} = 0.950$

7.6 A prediction of two phase pressure drop sign change through a vertical pipe and a Venturi meter in homogenous gas-water two phase flows

Most of the experimental data in bubbly (homogenous) two phase flow described in this thesis were taken with '+' input of the dp cell connected to the inlet of the Venturi and the '-' input of the dp cell connected to the throat of the Venturi. However, the two phase gas-water pressure drop across the UVT in a homogenous flow could sometimes change its sign and the pressure at the '+' input of the dp cell could be less than the pressure at the '-' input of the dp cell. This is because the mixture density is lower than the density of water. The prediction of the pressure drop sign change in two phase flow allows the differential pressure cell to be correctly installed. For correct operation of the dp cell, the pressure at the '+' input of the dp cell must be greater than the pressure at the '-' input of the dp cell. Therefore, the change-over valves can be used to ensure that the high pressure tap was always connected to '+' input and the low pressure tap was always connected to '-' input of the dp cell (see Section 6.3).

A new series of experiments were carried out in vertical upward gas-water flows to predict the two phase pressure drop sign change through a vertical pipe and the Venturi meter in a homogenous gas-water two phase flow. A new model was developed (see Section 3.1.2) to predict the sign change of the two phase pressure drop across the Venturi, and checked against data recently obtained from the bubbly gas-water flow rig (see Figure 6-2) at the University of Huddersfield. The prediction of the two phase pressure drop through a vertical pipe was also investigated (see Section 3.1.3) and compared with experimental data. Four sets of data with different flow conditions were tested for the reference water volumetric flow rate $Q_{w,ref,\mathrm{hom}}$ in the range of $3.08\times10^{-4}\,\mathrm{m^{-3}s^{-1}}$ to $5.03\times10^{-3}\,\mathrm{m^{-3}s^{-1}}$ and for values of the reference gas volumetric flow rate $Q_{g,ref,\mathrm{hom}}$ in the range of $2.92\times10^{-6}\,\mathrm{m^{-3}s^{-1}}$ to$1.2\times10^{-3}\,\mathrm{m^{-3}s^{-1}}$. At each set of data $Q_{w,ref,\mathrm{hom}}$ was fixed while $Q_{g,ref,\mathrm{hom}}$ was varied. The homogenous velocity U_h was in the range of 0.075 to $1.174\,\mathrm{ms^{-1}}$. The gas volume

fraction was in the range of 0.025 to 0.260. The flow conditions of all four sets of data are summarized in Table 7-3.

Table 7-3: Flow conditions of two phase pressure drop sign change for all four sets of data in a homogenous gas-water two phase flow

Flow conditions	Set #I	Set #II	Set #III	Set #IV
$Q_{w,ref,\text{hom}}$ (m^3s^{-1})	3.08×10^{-4}	1.22×10^{-3}	3.27×10^{-3}	5.03×10^{-3}
$Q_{g,ref,\text{hom}}$ (m^3s^{-1})	6.44×10^{-5} to 4.71×10^{-4}	4.89×10^{-5} to 1.20×10^{-3}	2.92×10^{-6} to 1.08×10^{-3}	2.99×10^{-6} to 8.68×10^{-4}
$\alpha_{1,\text{hom}}$	0.046 to 0.184	0.025 to 0.260	0.050 to 0.165	0.050 to 0.110
U_h (ms^{-1})	0.075 to 0.156	0.254 to 0.485	0.651 to 0.866	1.002 to 1.174

7.6.1 Experimental results of the predicted two phase pressure drop sign change through the Universal Venturi Tube

From the dimensions of the UVT , described in Section 4.2, it is possible to calculate K_1 and K_2 in Equations (3.22) and (3.23). Therefore;

$$K_1 = 3358.1 \text{ and } K_2 = 588.6$$

Equation (7.4)

Substituting Equation (7.4) into Equations (3.25) and (3.26) would respectively give;

$$C_1 = 588.6\alpha_{1,\text{hom}}$$

Equation (7.5)

and;

$$C_2 = 3358.1(1-\alpha_{1,\text{hom}})U_h^2 + F_{mv}$$

Equation (7.6)

where F_{mv} is the frictional pressure loss (from the inlet to the throat of the Venturi) and is defined by Equation (3.17).

It was demonstrated (in Section 3.1.2) that the measured differential pressure across the dp cell is negative when $C_1 > C_2$ and positive when $C_1 < C_2$.

Figure 7-8 shows the variation of the differential pressure drop across the Venturi meter ΔP_{hom} with the reference gas volumetric flow rate $Q_{g,ref,\text{hom}}$ (obtained from the thermal mass flow meter, see Section 6.2.6) for all sets of data. It is clear that at set-I, (in which $Q_{w,ref,\text{hom}}$ was small and $C_1 > C_2$), ΔP_{hom} was negative for different values of $Q_{g,ref,\text{hom}}$. When $Q_{w,ref,\text{hom}}$ increased, ΔP_{hom} was always positive. It is seen from Figure 7-8 that at lower water and gas flow rates, the coefficient C_1 becomes greater than C_2 which leads to negative differential pressure across the dp cell.

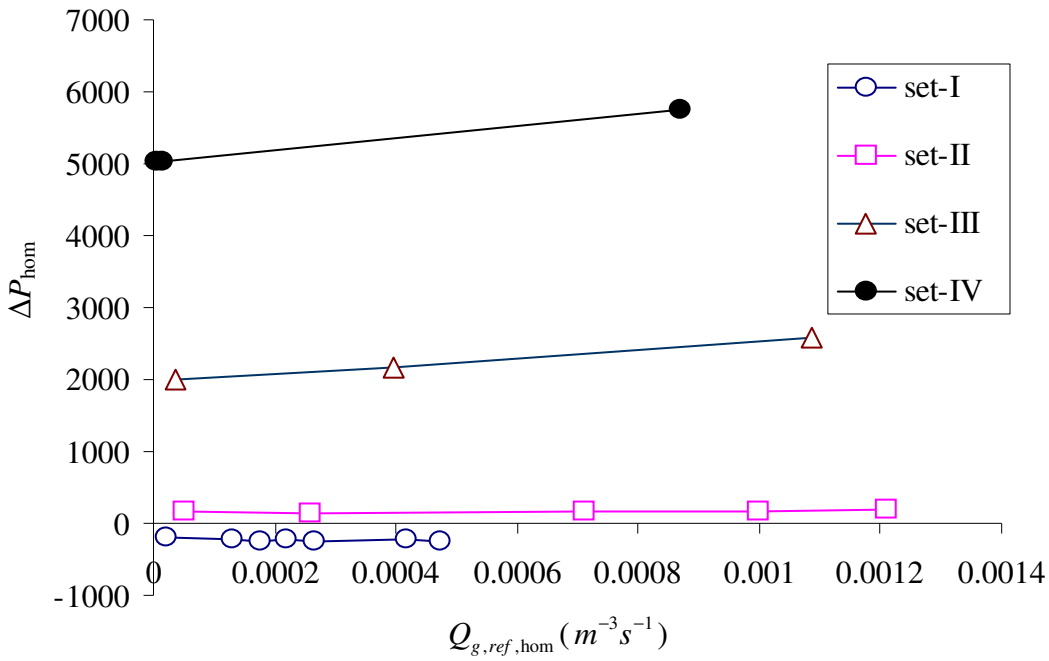

Figure 7-8: Pressure drop sign change in a homogenous two phase flow through the Venturi meter

Since set-I demonstrates negative values of ΔP_{hom}, it is meaningful to represent the data as a clustered column chart as shown in Figure 7-9. This makes the comparison between the coefficients C_1 and C_2 more visible. It should be noted that the values of the negative differential pressure were incorrect. Therefore the change over-valve system (see Section 6.3) could be used in set-I to correct the differential pressure drop and to ensure that the high pressure tap was connected to the '+' input of the dp cell and the low pressure tap was connected to the '-' input of the dp cell.

The differential pressure drop across the Venturi meter, ΔP_{hom} for sets of data II,III and IV are always positive since $C_1 < C_2$ (see Figures 7-10 to 7-12).

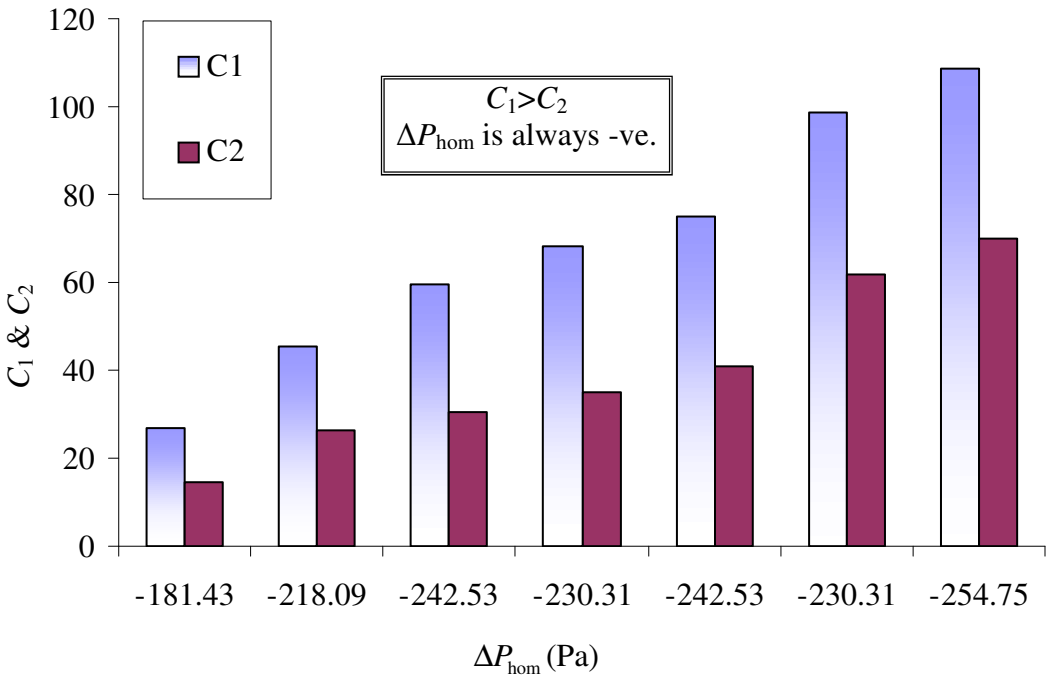

Figure 7-9: Comparison between C_1 and C_2 for set-I through the UVT

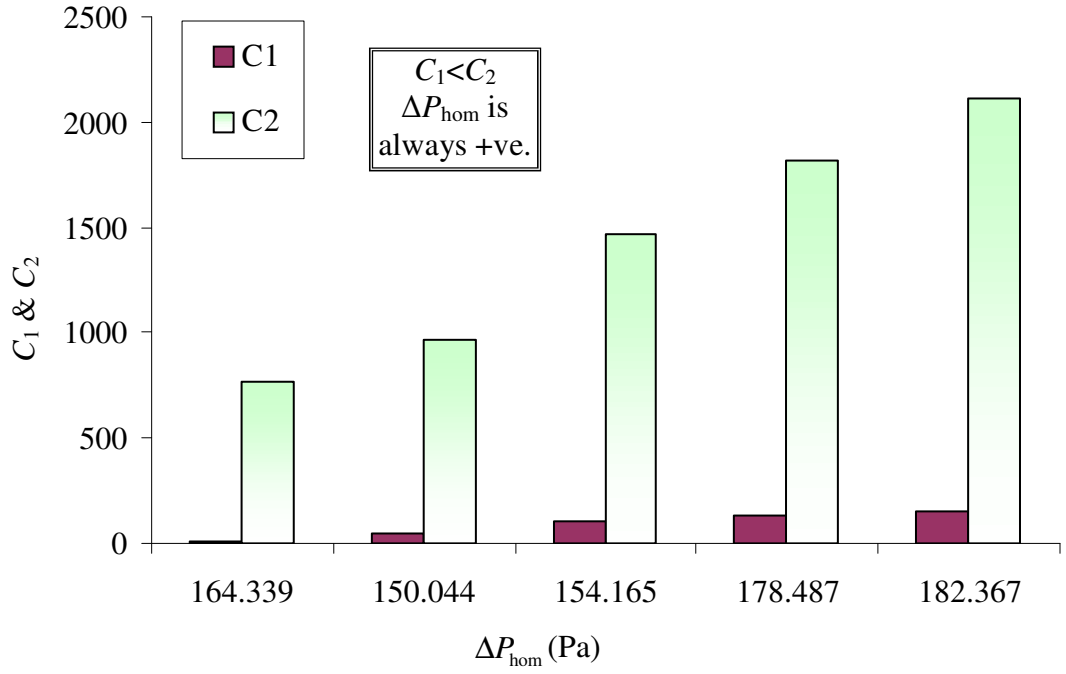

Figure 7-10: Comparison between C_1 and C_2 for set-II through the UVT

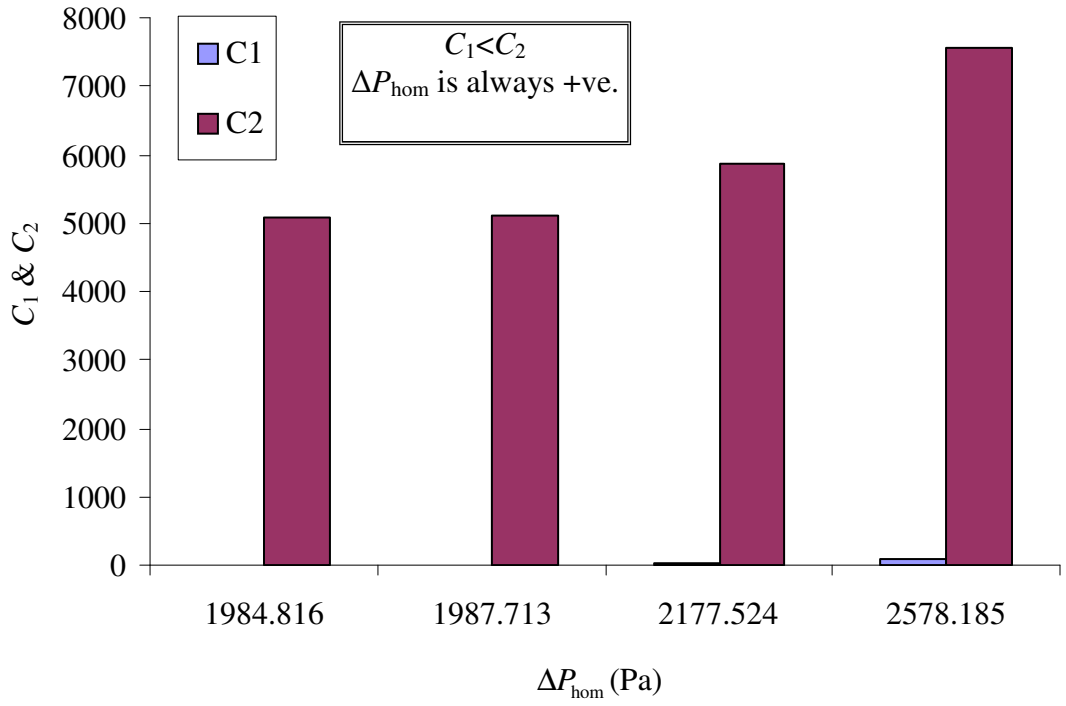

Figure 7-11: Comparison between C_1 and C_2 for set-III through the UVT

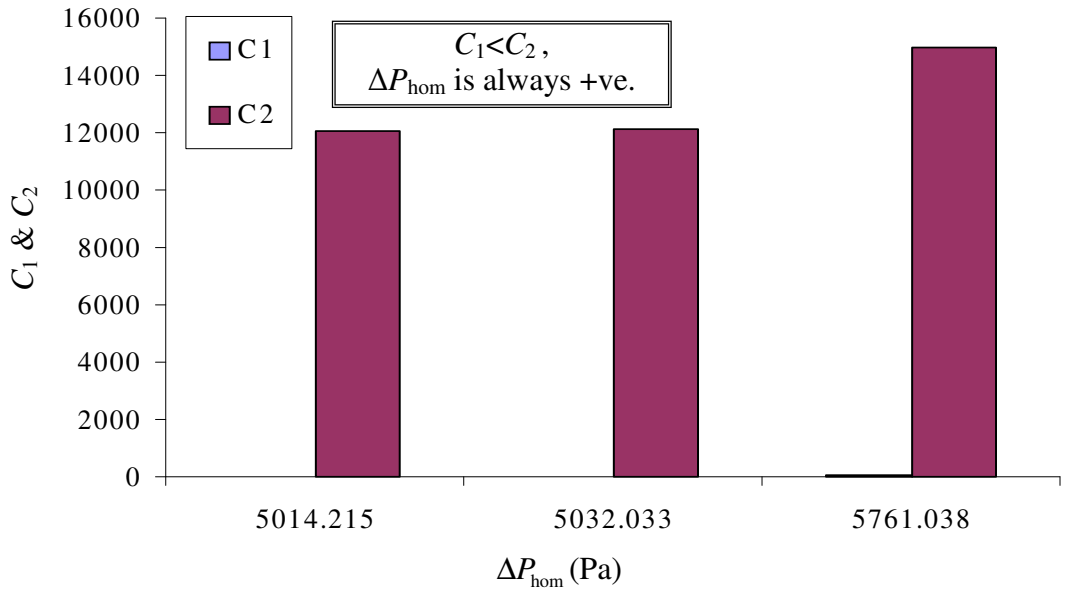

Figure 7-12: Comparison between C_1 and C_2 for set-IV through the UVT

7.6.2 Experimental results of the predicted two phase pressure drop sign change across the vertical pipe

It was demonstrated in Section 3.1.3 that the pressure drop across the dp cell in the two phase flow ΔP_{pipe} becomes negative if;

$$U_h^2 > \hat{K}$$

Equation (7.7)

where;

$$\hat{K} = k^* \frac{\alpha_{1,\text{hom}}}{f}$$

Equation (7.8)

and;

$$k^* = \frac{g\cos\theta(\rho_w - \rho_g)D}{2\rho_w} = 0.392$$

Equation (7.9)

It should be noted that the constant, k^* depends on the flow and experimental conditions. Substituting Equation (7.9) into (7.8) gives;

$$\hat{K} = 0.392\frac{\alpha_{1,\text{hom}}}{f}$$

Equation (7.10)

Therefore, ΔP_{pipe} is negative when;

$$U_h^2 > 0.392\frac{\alpha_{1,\text{hom}}}{f}$$

Equation (7.11)

Figure 7-13 shows the relationship between the differential pressure drop across a vertical pipe ΔP_{pipe} (i.e. across the flow density meter, FDM, see Section 4.1) and the gas superficial velocity U_{gs} for all four sets of data. It is seen that the values of ΔP_{pipe} are always positive in sets I and II where U_h^2 is always less than $\hat{K}$. In set-III, one value of ΔP_{pipe} was negative while in set-IV two values were negative. A negative value of the differential pressure drop ΔP_{pipe} indicates that, Equation (7.11) is satisfied.

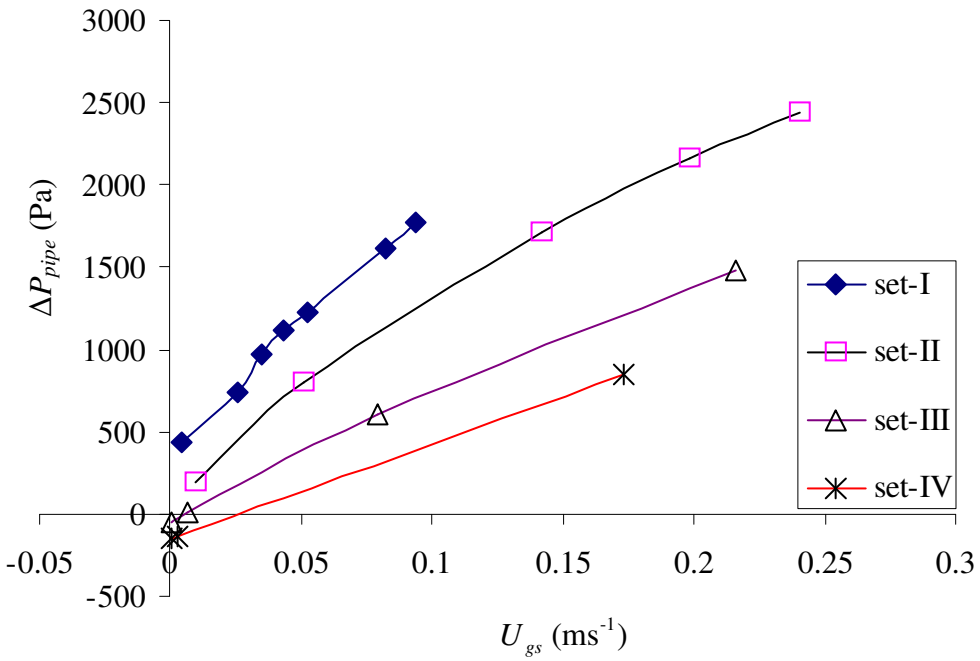

Figure 7-13: Variation of ΔP_{pipe} with U_{gs} for all sets of data in a homogenous vertical pipe flow

Figures 7-14 and 7-15 show the comparison between the homogenous velocity U_h and the coefficient $\hat{K}$ with differential pressure drop ΔP_{pipe} across the vertical pipe for sets III and IV. It is clear from these figures that some values of differential pressure drop become negative when $U_h^2 > \hat{K}$.

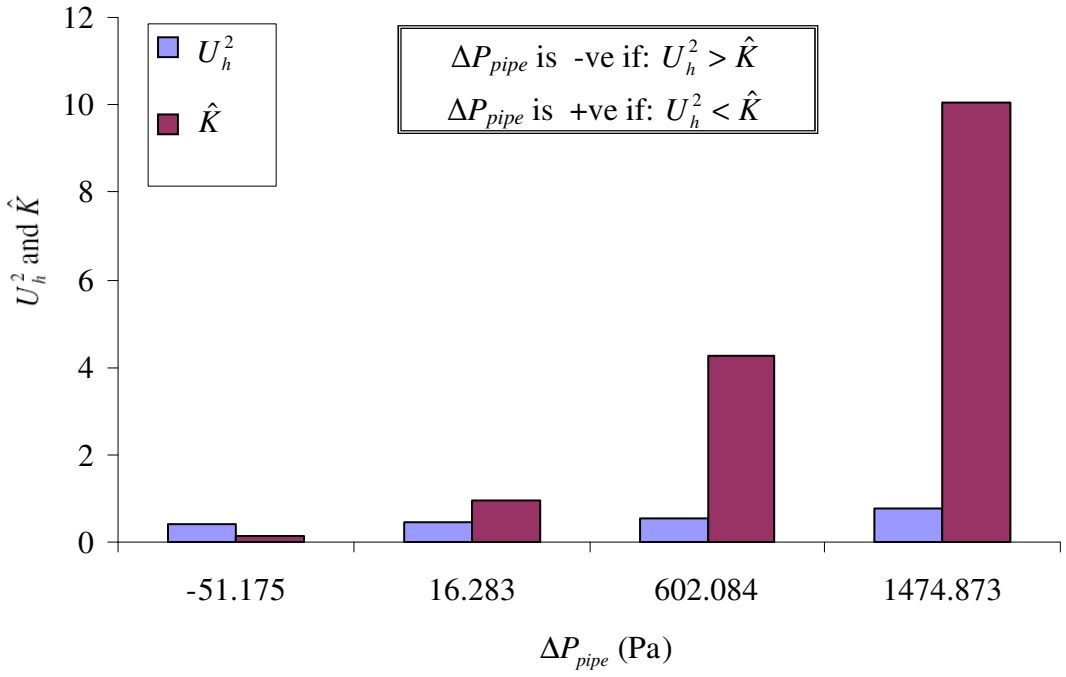

Figure 7-14: Comparison between U_h^2 and $\hat{K}$ for set-III in a vertical pipe

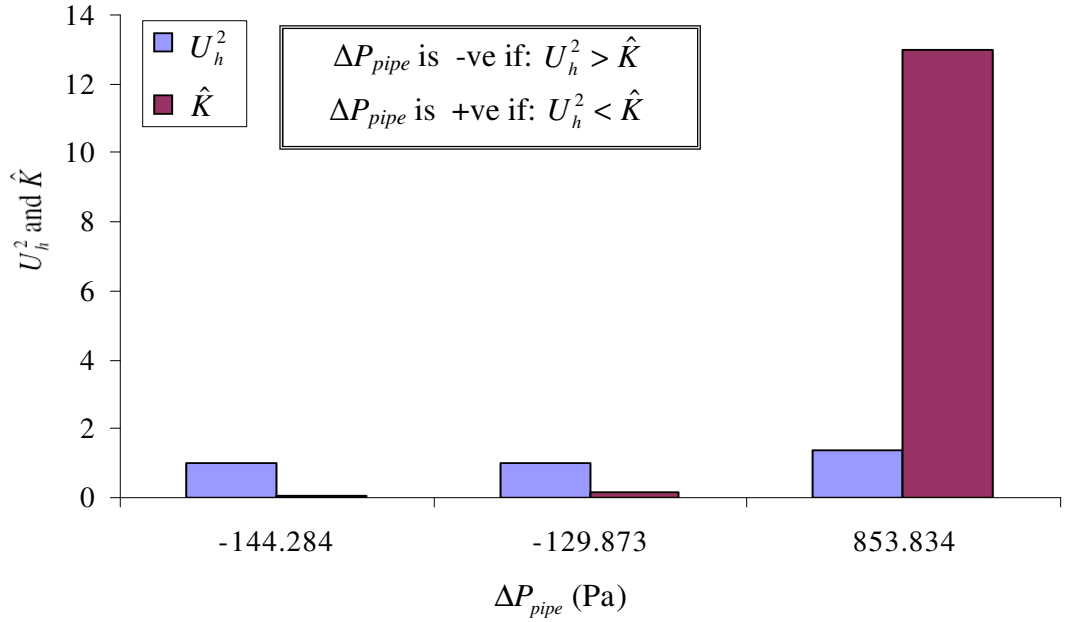

Figure 7- 15: Comparison between U_h^2 and $\hat{K}$ for set-IV in a vertical pipe

7.7 A map of the two phase pressure drop sign change across the Venturi meter and the vertical pipe

At this stage, it is possible to develop a map of the two phase pressure drop sign change across the UVT and the vertical pipe (i.e. FDM). In other words, two theoretical lines can be plotted which represent margins or limits of the pressure drop sign change across the Venturi and the vertical pipe respectively.

The theoretical line of the two phase pressure drop sign change across the Venturi can be determined by making ΔP_{hom} in Equation (3.24) equals to zero. Therefore;

$$C_1 = C_2$$

Equation (7.12)

Combining Equations (7.5), (7.6), (7.12) and (3.17) and solving for $\alpha_{1,\text{hom}}$ gives;

$$\alpha_{1,\text{hom}}\Big|_{\Delta P_{\text{hom}}=0} = \frac{\left(\frac{2\rho_w h_t}{D^*}\right) f\, U_h^{2*} + 3358.1 U_h^2}{588.6 + 3358.1 U_h^2}$$

Equation (7.13)

where $\alpha_{1,\text{hom}}\Big|_{\Delta P_{\text{hom}}=0}$ is the inlet gas volume fraction in a homogenous two phase flow when $\Delta P_{\text{hom}} = 0$, f is the single phase friction factor (see Section 7.2 and Equation (3.27)), U_h^* is the average homogenous velocity between the inlet and the throat of the Venturi (see Equation (3.19), D^* is the average diameter between the inlet and the throat of the Venturi (i.e. (inlet diameter + throat diameter)/2) and U_h is the homogenous velocity (see Equation (7.1)).

The constants (3358.1 and 588.6) in Equation (7.13) depend on the flow and experimental conditions.

The theoretical line of the two phase pressure drop sign change across the vertical pipe can now be obtained by setting ΔP_{pipe} in Equation (3.28) equals to zero. Therefore;

$$\alpha_{1,\hom}\Big|_{\Delta P_{pipe}=0} gh_p \cos\theta(\rho_w - \rho_g) = \frac{2\rho_w h_p f U_h^2}{D}$$

Equation (7.14)

Since $\rho_w >> \rho_g$, then $\rho_w - \rho_g \approx \rho_w$. In a vertical pipe, $\cos\theta = 1$. Therefore, Equation (7.14) becomes;

$$\alpha_{1,\hom}\Big|_{\Delta P_{pipe}=0} = \left(\frac{2f}{D\,g}\right) U_h^2$$

Equation (7.15)

Now, plotting $\alpha_{1,\hom}\Big|_{\Delta P_{\hom}=0}$ vs U_h and $\alpha\Big|_{\Delta P_{pipe}=0}$ vs U_h in Equations (7.13) and (7.15) respectively, represents the theoretical lines of the two phase pressure drop sign change across the Venturi and the vertical pipe respectively.

Figure 7-16 shows the map of the homogenous gas-water two phase pressure drop sign change across the UVT and the vertical pipe for all data sets. The limit between negative and positive values of $\Delta P_{\hom}$ is indicated by Line-A in which $\Delta P_{\hom} = 0$ (see Equation (7.13)). The theoretical line denoted as Line-B which represents the limit between positive and negative values of the homogenous two phase pressure drop sign change across the vertical pipe is also shown in Figure 7-16.

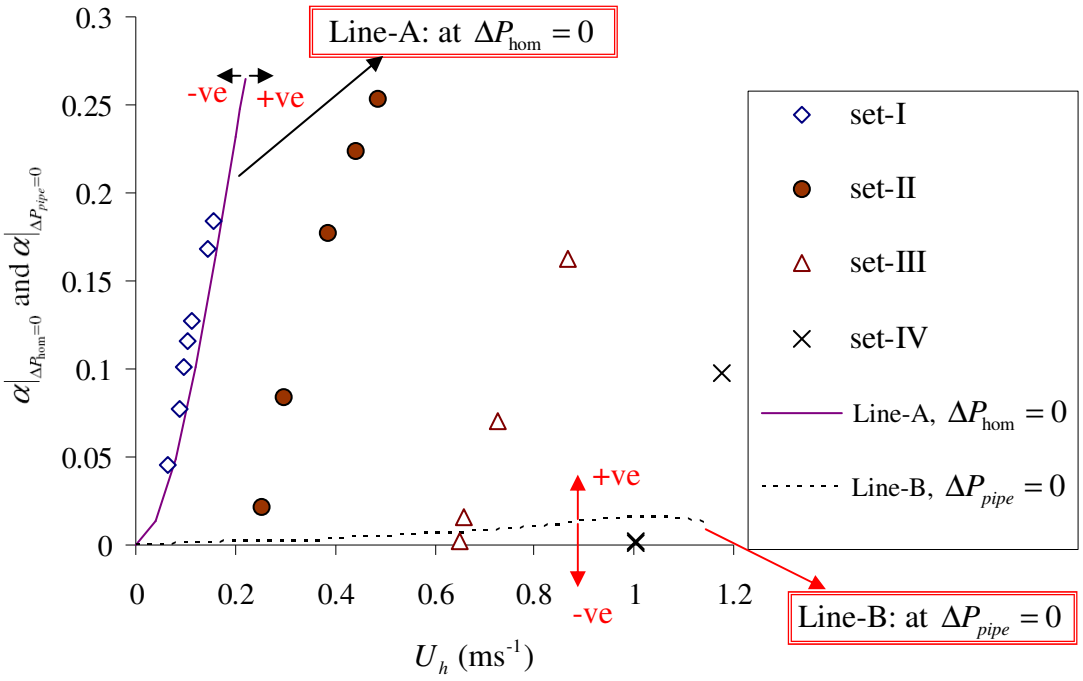

Figure 7-16: Map of the homogenous two phase pressure drop sign change across the Venturi and the vertical pipe for all sets of data

Summary

Experiments were carried out in homogenous gas-water two phase flows through the UVT in which different flow conditions were tested. The gas volume fraction at the inlet of the Venturi $\alpha_{1,\text{hom}}$ was measured using the FDM. $\alpha_{1,\text{hom}}$ was assumed to be constant throughout the UVT since the bubbly two phase flow was approximately homogenous.

The homogenous discharge coefficient $C_{d,\text{hom}}$ (see Equation (7.2)) was investigated in Section 7.4. It was found that the average homogenous discharge coefficient $C_{d,\text{hom}}$ was 0.948, which represented the optimum value at which the minimum average error was obtained in the predicted homogenous volumetric flow rate (see Section 7.5).

The percentage error in the predicted mixture volumetric flow rate $\varepsilon_{Q_{m,\text{hom}}}$ in homogenous two phase flows through the UVT was plotted for different values of homogenous discharge coefficients (see Figure 7-5 to 7-7). It was observed that the homogenous flow model starts to break down when the gas volume fraction $\alpha_{1,\text{hom}}$ increased above 17.48% (the onset of the slug flow regime). It was also inferred from Figures 7-5 to 7-7 that the optimum value of the mixture discharge coefficient $C_{d,\text{hom}}$ which gives the minimum mean value error $\bar{\varepsilon}_{Q_{m,\text{hom}}}$ (for $\alpha_{1,\text{hom}} \le 17.48\%$) was 0.948.

A new model to predict the two phase pressure drop sign change across the Venturi meter and the vertical pipe was investigated (see Section 7.6). It was observed that for ΔP_{hom} to be negative, C_1 must be greater than C_2 and for ΔP_{pipe} to be negative, U_h^2 must be greater than $\hat{K}$ (see Equations (7.4) to (7.11)). A map was developed which showed the pressure drop sign change across the Venturi meter and the vertical pipe for homogenous two phase flow (see Figure 7.16). Two theoretical lines were plotted which represent limits of the pressure drop sign change across the Venturi and the vertical pipe in a homogenous gas-water two phase flow (see Equations (7.13) and (7.15)).

Chapter 8

Experimental Results for Annular (wet gas) Flow through a Conductance Multiphase Flow Meter

Introduction

Separated flow in a Venturi meter is highly complex and the application of the homogenous flow model described in Section 3.1 could not be expected to lead to highly accurate results. If this is the case, the gas volume fraction measurement technique at the throat of the Venturi must also be introduced instead of just relying on the gas volume fraction measurement at the inlet of the Venturi as in homogenous flows [153]. The conductance multiphase flow Meter which consists of the Conductance Inlet Void Fraction Meter (CIVFM, see Section 4.3.1), and the Conductance Multiphase Venturi Meter (CMVM, see Section 4.3.2) was designed to measure the gas volume fraction at the inlet and the throat of the Venturi.

Previous models described in Section 2.2 depend on prior knowledge of the mass flow quality x. Online measurement of x is difficult and not practical in multiphase flow applications. The new model described in this thesis (see Section 3.2) depends on measurement of the gas volume fraction at the inlet and the throat of the Venturi rather than prior knowledge of the mass flow quality x which makes the measurement technique more reliable and practical.

This chapter discusses the experimental results of vertical annular (wet gas) flow through a conductance multiphase flow meter. The error in the predicted water mass flow rate, using the conductance multiphase flow meter, in annular (wet gas) flows was larger than expected. This was due to (a) the limitation in the side channel blower which could not provide sufficient gas under all flow conditions causing a pulsation in the liquid film flow, and (b) the fact that the effect of the liquid droplets in the gas core was not considered in the vertical annular (wet gas) flow model described in Section 3.2.2. Therefore, an alternative approach which was based on the wall conductance sensor (WCS, see Sections 4.4 and 6.4) was used to measure the total water mass flow rate in annular flow. It should be noted that the work performed on the WCSs was investigated by Al-Yarubi (2010) [147]. The data (i.e. the relationship between the entrainment fraction and the gas superficial velocity) obtained from the WCSs was used to modify the equation for the water mass flow rate (Equation (3.72)) using the conductance multiphase flow meter, so that the total water mass flow rate can be predicted instead of just relying on the water mass flow rate in the liquid film. The results of the alternative method are presented and discussed in Section 8.7.

8.1 Flow conditions of vertical annular (wet gas) flows

Experiments were carried out in a vertical upward annular gas-water two phase flow (wet gas flow) using the conductance multiphase flow meter. Eighty five different flow conditions were tested. The summary of the flow conditions is given in Table 8-1. Four different sets of data were investigated in which the water flow rates were kept constant while the gas flow rates were varied. The reason for fixing the water flow rate and varying the gas flow rate is that with varying water flow rate it was difficult to maintain the gas flow rate at a constant value for all flow conditions. This was due to the limitation in the air blower (see Sections 6.2.5 and 8.6).

Table 8-1: Flow conditions of all four sets of data in annular (wet gas) flow

Data set no.	*Gas superficial velocity* $U_{gs,wg}$ (ms^{-1})	*Water superficial velocity* $U_{ws,wg}$ (ms^{-1})
wg-1	6.919 to 8.566	0.0104
wg-2	6.350 to 8.259	0.0163
wg-3	6.837 to 8.323	0.0153
wg-4	6.451 to 7.903	0.0123

8.2 Study of the gas volume fraction at the inlet and the throat of the Venturi in annular (wet gas) flows

To determine the gas and the water mass flow rates using Equations (3.66) and (3.72) respectively, measurements of the gas volume fractions $\alpha_{1,wg}$ and $\alpha_{2,wg}$ (see Equations (5.11) and (5.12)) at the inlet and the throat of the Venturi in annular (wet gas) flow must be obtained. To do this, a novel conductance multiphase flow meter was designed and constructed (see Section 4.3). The two ring electrodes at the CIVFM and the two ring electrodes at the throat section of the CMVM were used to measure the gas volume fractions $\alpha_{1,wg}$ and $\alpha_{2,wg}$ at the inlet and the throat of the Venturi (see Chapters 4 and 5).

Figures 8-1 to 8-4 show the variations of the gas volume fractions $\alpha_{1,wg}$ and $\alpha_{2,wg}$ at the inlet and the throat of the Venturi with the gas and water superficial velocities $U_{gs,wg}$ and $U_{ws,wg}$ respectively in vertical annular (wet gas) flows. It can be seen from these figures that, in general, the gas volume fraction $\alpha_{1,wg}$ at the inlet of the Venturi (obtained from the CIVFM) was greater than the gas volume fraction $\alpha_{2,wg}$ at the

throat of the Venturi (obtained from the two electrodes at the throat section of the CMVM). This difference becomes more visible at lower water flow rates (data set# wg1). It should be noted that, although, considerable theoretical and experimental studies have been published to describe the performance of the Venturi meters in annular flow, there is very limited, if any, data in the literature with which the current results can be compared. Most of the data available in the literature depends on prior knowledge of the mass flow quality *x* and the over-reading factor [154] and not the actual measurements of the gas volume fractions $\alpha_{1.wg}$ and $\alpha_{2.wg}$ at the inlet and the throat of the Venturi as in the current study. Online measurement of *x* is difficult and not practical in multiphase flow applications. However, the difference between the gas volume fraction at the inlet and the throat of the Venturi was investigated by Malayeri et al. (2001) [155] who studied the behaviour of gas-liquid bubbly flow through a vertical Venturi using a gamma-ray densitometer and found that the gas void fraction at the throat was always less than that at the inlet of the Venturi at fixed water flow rate over a range of gas flow rates. Although their results were obtained in bubbly gas-liquid flows, the results reported in Figures 8-1 to 8-4, which was obtained from separated vertical annular (wet gas) flows, agree with the results obtained by Malayeri et al. (2001).

A plot of $\alpha_{2,wg}$ vs $\alpha_{1,wg}$ is shown in Figure 8-5. Unlike homogenous flow, the gas volume fraction at the inlet and the throat of the Venturi in annular flow cannot be assumed to be equal. The data presented in Figures 8.1 to 8-5 proves that, measuring of the gas volume fraction $\alpha_{2,wg}$ at the throat of the Venturi is necessary in separated flows (since $\alpha_{1,wg}$ is not equal $\alpha_{2,wg}$), instead of just relying on the measurement of the inlet gas volume fraction as in homogenous flows described in Chapter 7, where the gas volume fraction at the inlet of the UVT was assumed to be constant throughout the UVT.

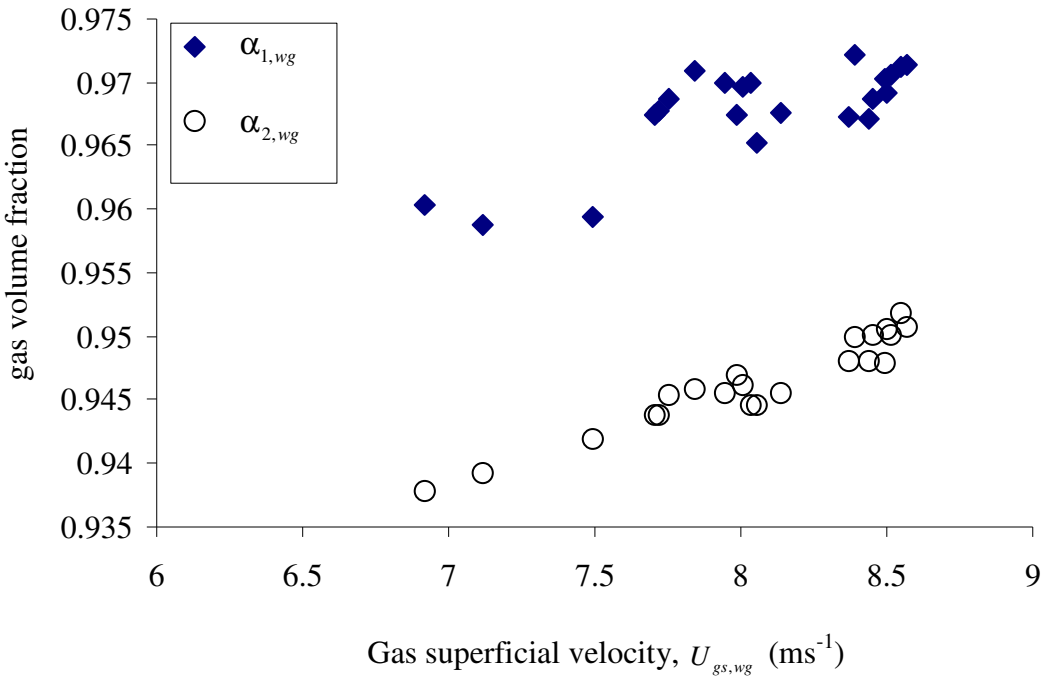

Figure 8-1: Variations of $\alpha_{1,wg}$ and $\alpha_{2,wg}$ (at $U_{ws,wg} = 0.0104$ ms^{-1}) in vertical annular (wet gas) flows, set# wg-1

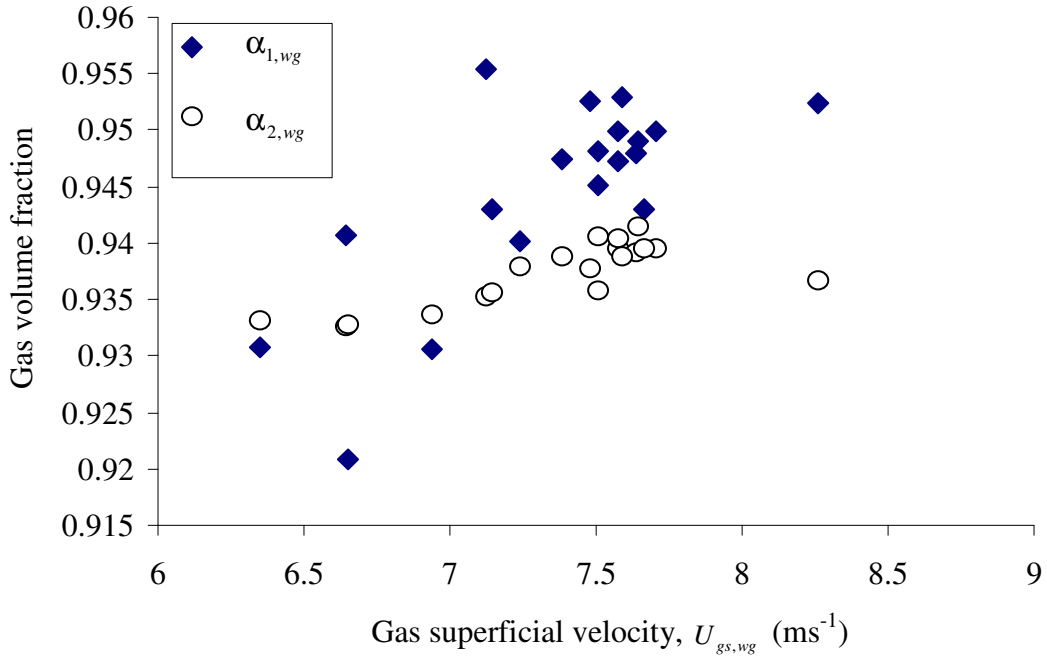

Figure 8-2: Variations of $\alpha_{1,wg}$ and $\alpha_{2,wg}$ (at $U_{ws,wg} = 0.0163$ ms^{-1}) in vertical annular (wet gas) flows, set# wg-2

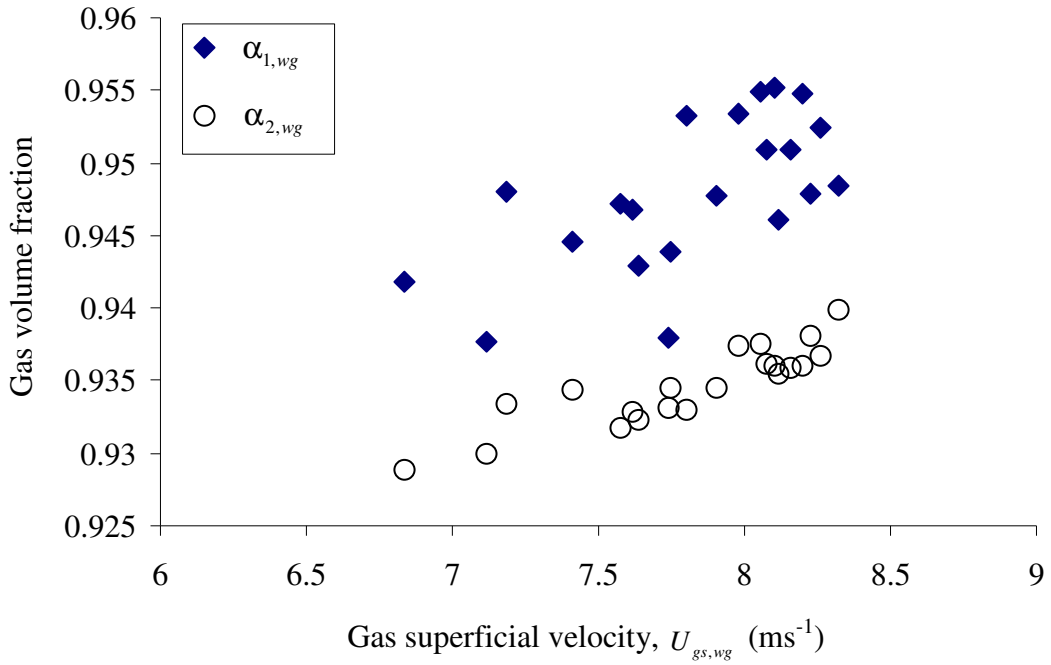

Figure 8-3: Variations of $\alpha_{1,wg}$ and $\alpha_{2,wg}$ (at $U_{ws,wg} = 0.0153$ ms^{-1}) in vertical annular (wet gas) flows, set# wg-3

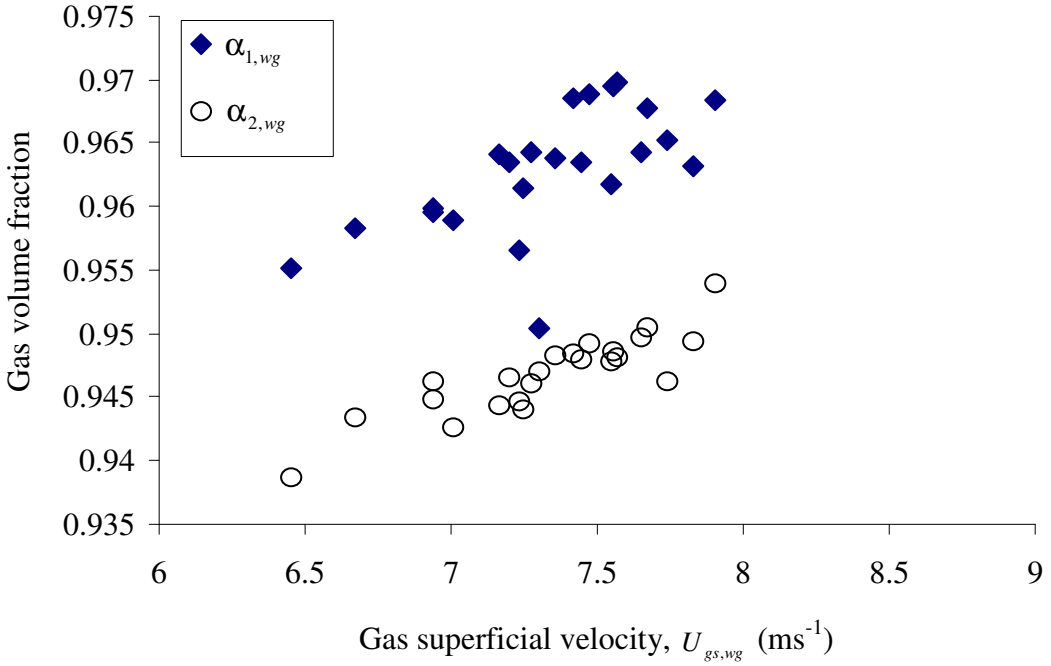

Figure 8-4: Variations of $\alpha_{1,wg}$ and $\alpha_{2,wg}$ (at $U_{ws,wg} = 0.0123$ ms^{-1}) in vertical annular (wet gas) flows, set# wg-4

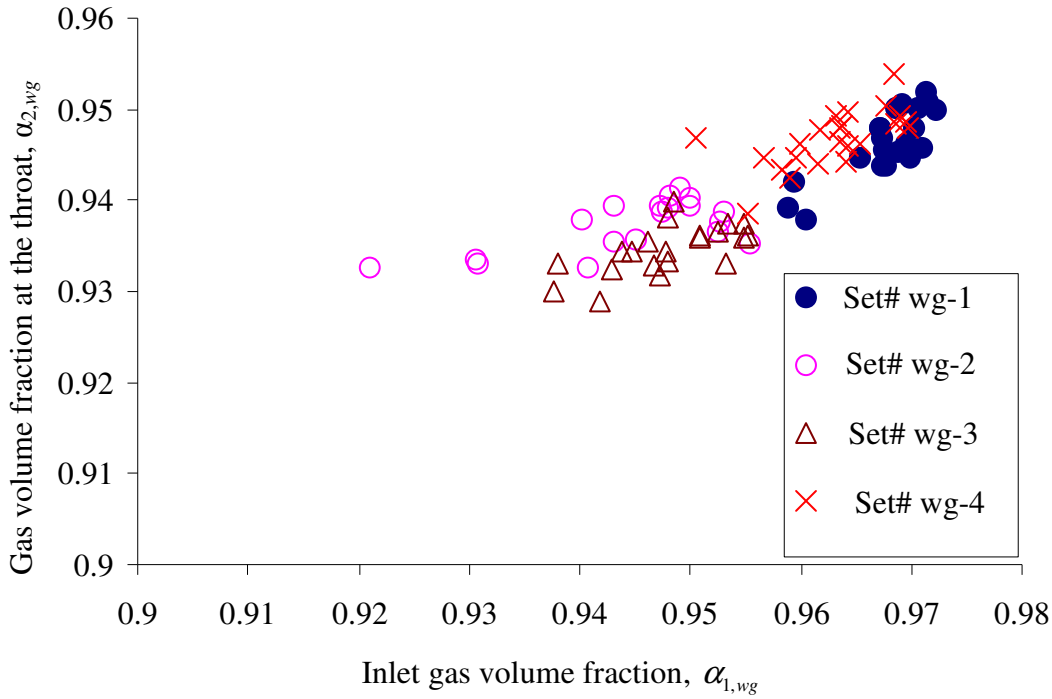

Figure 8-5: The relationship between $\alpha_{1,wg}$ and $\alpha_{2,wg}$

8.3 The liquid film at the inlet and the throat of the Venturi meter

As mentioned in Chapter 4, two ring electrodes flush mounted with the inner surface of the CIVFM and two ring electrodes flush mounted with the inner surface of the throat section in the CMVM were used to measure the film thickness at the inlet and the throat of the Venturi (see Section 5.3) . Figure 8-6 shows the variation of the film thickness at the inlet and the throat of the Venturi for all sets of data. It can be seen that, in general, the film thickness at the inlet was greater than the film thickness at the throat of the Venturi. For set# wg-1 (i.e. at lower fixed water superficial velocity, see Table 8-1), the film thicknesses δ_1 and δ_2 were close to each other. As the water superficial velocity increased (i.e. sets# wg-2, wg-3 and wg-4), the difference between δ_1 and δ_2 increased.

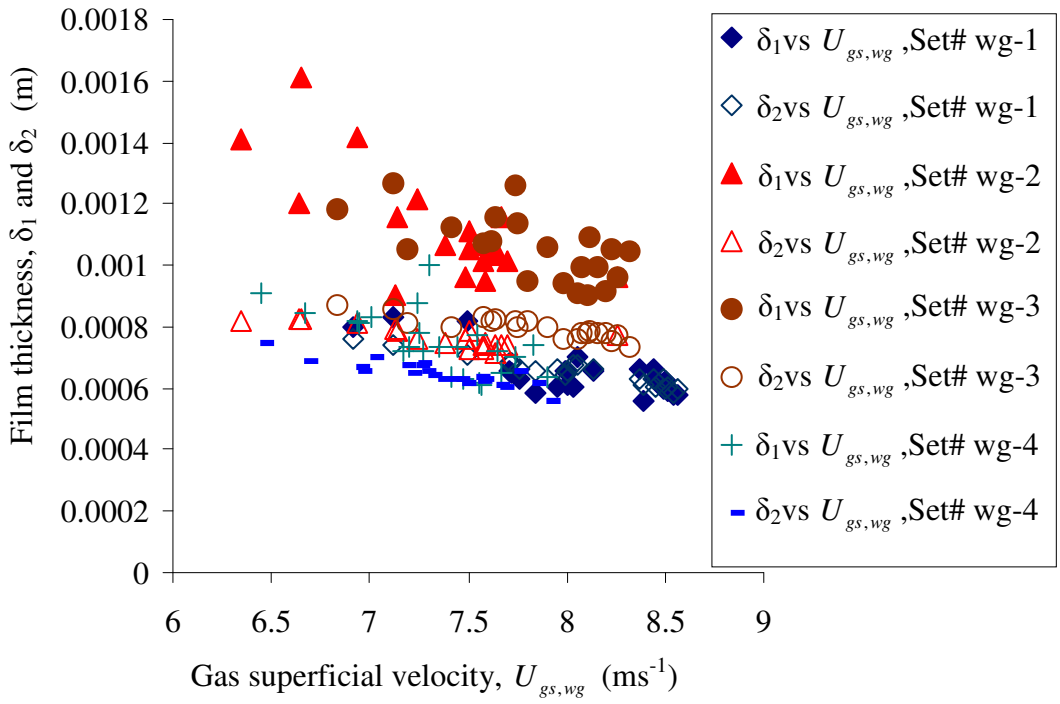

Figure 8-6: The relationship between the film thickness at the inlet and the throat of the Venturi

Comparing the results for the liquid film thickness shown in Figure 8-6 with the results for inlet/throat gas volume fractions discussed in the previous section (Section 8.2), one can observe that although the gas volume fraction at the inlet of the Venturi was greater than that at the throat, the liquid film thickness at the inlet is still greater than that at the throat. The physical interpretation of this is given below.

It is well known that the gas volume fraction in annular flow is given by;

$$\alpha = \frac{A_g}{A} = \frac{\pi(R-\delta)^2}{\pi R^2}$$

Equation (8.1)

where A_g is the area of the gas core, A is the cross-sectional area of the pipe, R is the internal radius of the pipe and δ is the film thickness.

Re-arranging Equation (8.1) gives;

$$\alpha = 1 - \frac{2\delta}{R} + \frac{\delta^2}{R^2}$$

Equation (8.2)

Since $\delta << R$, Equation (8.2) can be written as;

$$\alpha = 1 - \frac{2\delta}{R}$$

Equation (8.3)

Differentiating Equation (8.2) gives;

$$d\alpha = \left[\frac{-2}{R}\right] d\delta + \left[\frac{2\delta}{R^2}\right] dR$$

Equation (8.4)

In Equation (8.4), if dR is negative then $d\alpha$ is negative. If $d\delta$ is negative then $d\alpha$ is positive. However, if $\frac{2\delta}{R^2} dR - \frac{2d\delta}{R} < 0$ then $d\alpha$ is negative even if $d\delta$ is negative.

8.4 Study of the gas discharge coefficient in vertical annular (wet gas) flows

The discharge coefficient is well defined in a single-phase flow. In multiphase flows, the discharge coefficient is still elusive in that it depends on the modelling approach adopted. The gas discharge coefficient $C_{dg,wg}$ in a vertical annular (wet gas) flow through the Venturi meter is given by Equation (3.70) which can be expressed as;

$$C_{dg,wg} = \frac{\dot{m}_{g,ref,wg}}{\dot{m}_{g,wg}}$$

Equation (8.5)

where $\dot{m}_{g,ref,wg}$ is the reference gas mass flow rate obtained from the variable area flowmeter, VAF in annular wet gas flow (see Sections 6.1.2 and 6.2.4) and $\dot{m}_{g,wg}$ is the predicted gas mass flow rate obtained from the conductance multiphase flow meter and the separated vertical annular flow model described in Chapter 3 (see Equation (3.66)).

In order to measure $\dot{m}_{g,ref,wg}$ in Equation (8.5), the absolute pressure P_1 (from the gauge pressure sensor and the barometer, see Section 6.2.7) and the absolute

temperature T_1 (from the thermocouple, see also Section 6.2.7) were measured at the upstream section of the Venturi. Measurement of P_1 and T_1 enabled the gas density ρ_{g1} at the inlet of the Venturi to be determined (see Equations (3.44) and (3.45)). The reference gas volumetric flow rate $Q_{g,ref,wg}$ obtained from the variable area flow meter, VAF (see Section 6.2.4) could then be converted into the reference gas mass flow rate $\dot{m}_{g,ref,wg}$ using;

$$\dot{m}_{g,ref,wg} = \rho_{g1} Q_{g,ref,wg}$$

Equation (8.6)

Figures 8-7 to 8-10 show the variations of the gas discharge coefficient $C_{dg,wg}$ with the gas superficial velocity $U_{gs,wg}$ for different, constant values of the water superficial velocity $U_{ws,wg}$ in vertical annular (wet gas) flows through the Venturi.

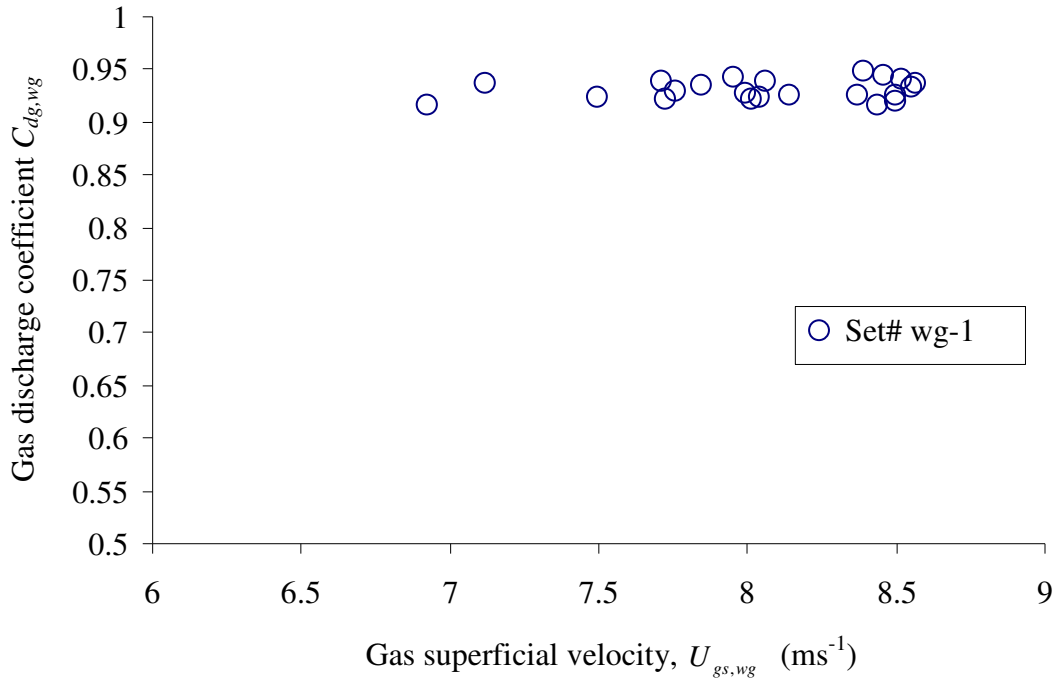

Figure 8-7: Variation of $C_{dg,wg}$ with $U_{gs,wg}$ (at $U_{ws,wg} = 0.0104$ ms^{-1}) in vertical annular (wet gas) flows through the Venturi

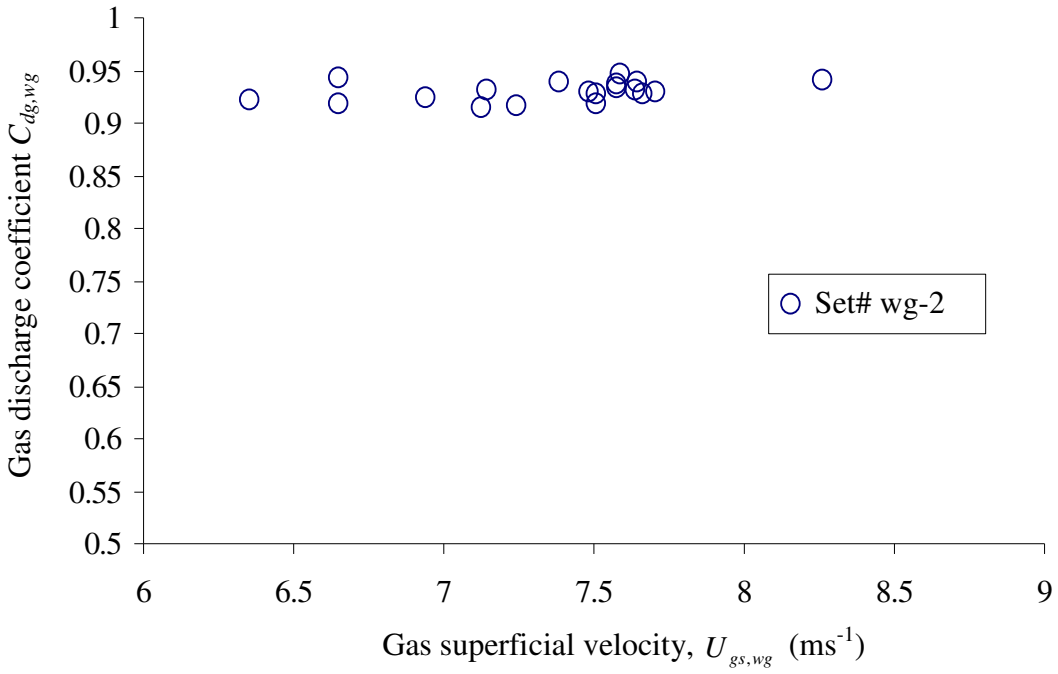

Figure 8-8: Variation of $C_{dg,wg}$ with $U_{gs,wg}$ (at $U_{ws,wg} = 0.0163\,\mathbf{ms^{-1}}$) in vertical annular (wet gas) flows through the Venturi

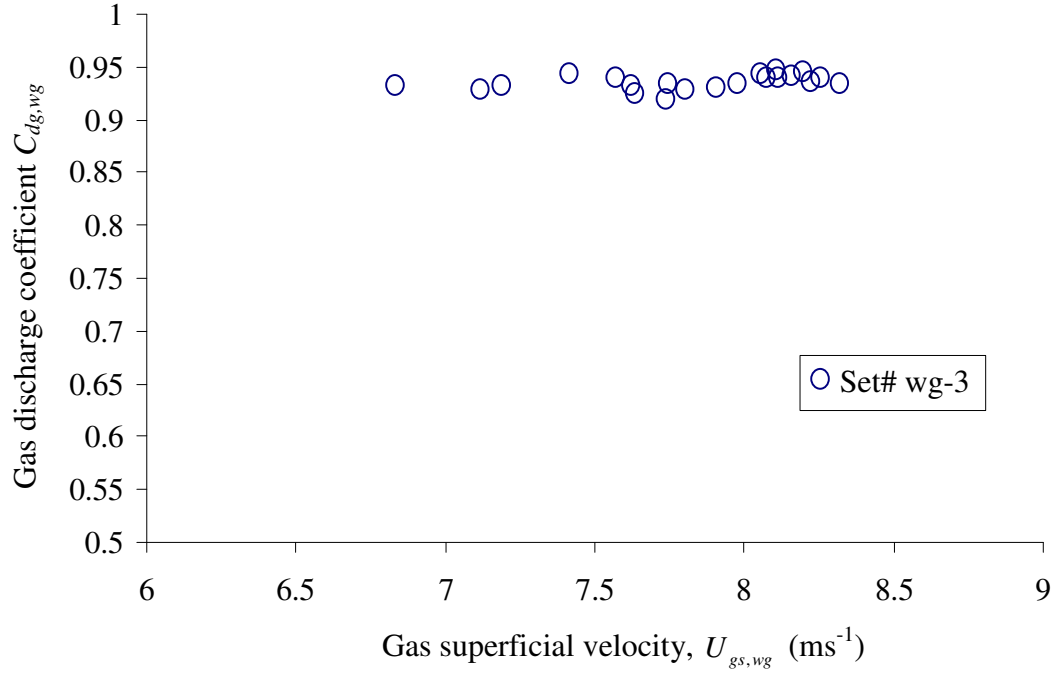

Figure 8-9: Variation of $C_{dg,wg}$ with $U_{gs,wg}$ (at $U_{ws,wg} = 0.0153\,\mathbf{ms^{-1}}$) in vertical annular (wet gas) flows through the Venturi

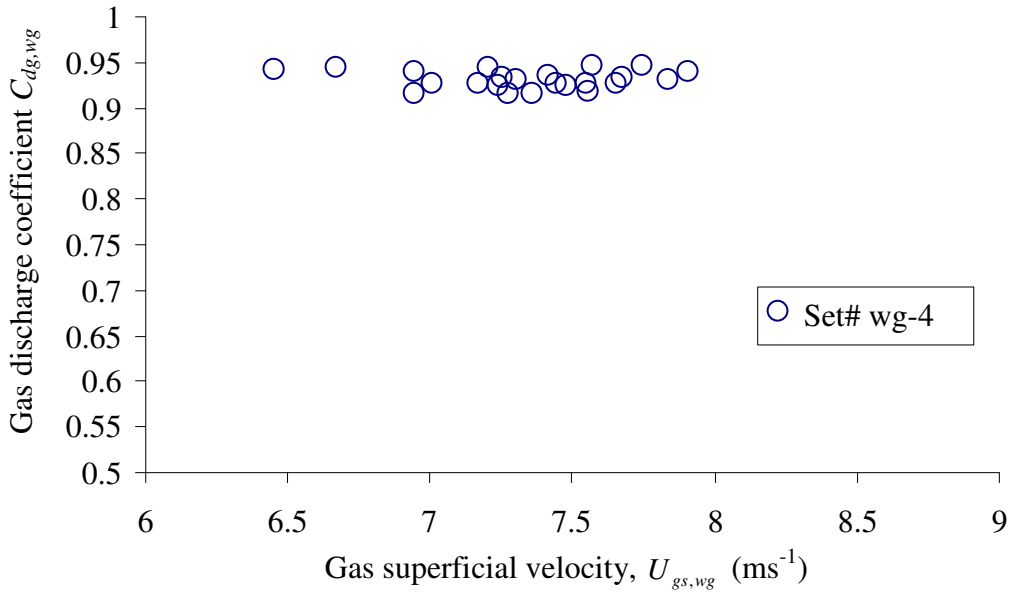

Figure 8-10: Variation of $C_{dg,wg}$ with $U_{gs,wg}$ (at $U_{ws,wg} = 0.0123\,\mathbf{ms^{-1}}$) in vertical annular (wet gas) flows through the Venturi

From Figures 8-7 to 8-10, the mean value for the discharge coefficient $C_{dg,wg}$ for all of the flow conditions is given by $C_{dg,wg} = 0.932$. This value of the $C_{dg,wg}$ represents the optimum value where the minimum average percentage error in the predicted gas mass flow rate is obtained (see Section 8.5).

8.5 Discussion of the percentage error in the predicted gas mass flow rate in vertical annular (wet gas) flows through the Venturi meter

The percentage error $\varepsilon_{\dot{m}_{g,wg}}$ in the predicted gas mass flow rate can be expressed as;

$$\varepsilon_{\dot{m}_{g,wg}} = \left(\frac{\dot{m}_{g,wg} - \dot{m}_{g,ref,wg}}{\dot{m}_{g,ref,wg}} \right) \times 100\%$$

Equation (8.7)

Figures 8-11 to 8-13 show the percentage error $\varepsilon_{\dot{m}_{g,wg}}$ in the predicted gas mass flow rate for $C_{dg,wg}$ = 0.920, 0.932 and 0.933. The reason of choosing different values of $C_{dg,wg}$ was to show the sensitivity of the errors in the predicted gas mass flow rate to

selected values of the gas discharge coefficient. The mean value of the percentage error (red solid line) in the predicted gas mass flow rate $\bar{\varepsilon}_{\dot{m}_{g,wg}}$ and the standard deviations *STD* of the percentage error in the predicted gas mass flow rate for different values of $C_{dg,wg}$ are shown in Figures 8-11 to 8-13 and Table 8-2.

Table 8-2: summary of $\bar{\varepsilon}_{\dot{m}_{g,wg}}$ and *STD* with different values of $C_{dg,wg}$ in annular (wet gas) flows

$C_{dg,wg}$	$\bar{\varepsilon}_{\dot{m}_{g,wg}}$ (%)	*STD(%)*
0.920	-1.330	0.97
0.932	-0.043	0.98
0.933	0.064	0.98

The standard deviation *STD* shown in Figures 8-11 to 8-13 (and also in Table 8-2), which represents an indication of the scattered of the data about $\bar{\varepsilon}_{\dot{m}_{g,wg}}$, is given by;

$$STD = \sqrt{\frac{\sum (y - \bar{y})^2}{N}}$$

Equation (8.8)

Where y, $\bar{y}$ and *N* are the sample, the sample mean (average) and the sample size respectively.

It is clear from Figures 8-11 to 8-13 (and also from Table 8-2) that the minimum value of $\bar{\varepsilon}_{\dot{m}_{g,wg}}$ (i.e. -0.043%) is obtained at $C_{dg,wg}$=0.932 (see Figure 8-12). This value of the gas discharge coefficient represents the optimum value in which the minimum value of $\bar{\varepsilon}_{\dot{m}_{g,wg}}$ is attained. An estimated error $\varepsilon_{\dot{m}_{g,wg}}$ in the predicted gas mass flow rate for $C_{dg,wg} = 0.932$ was scattered randomly between a maximum positive value of +1.79% and a maximum negative value of -1.69%.

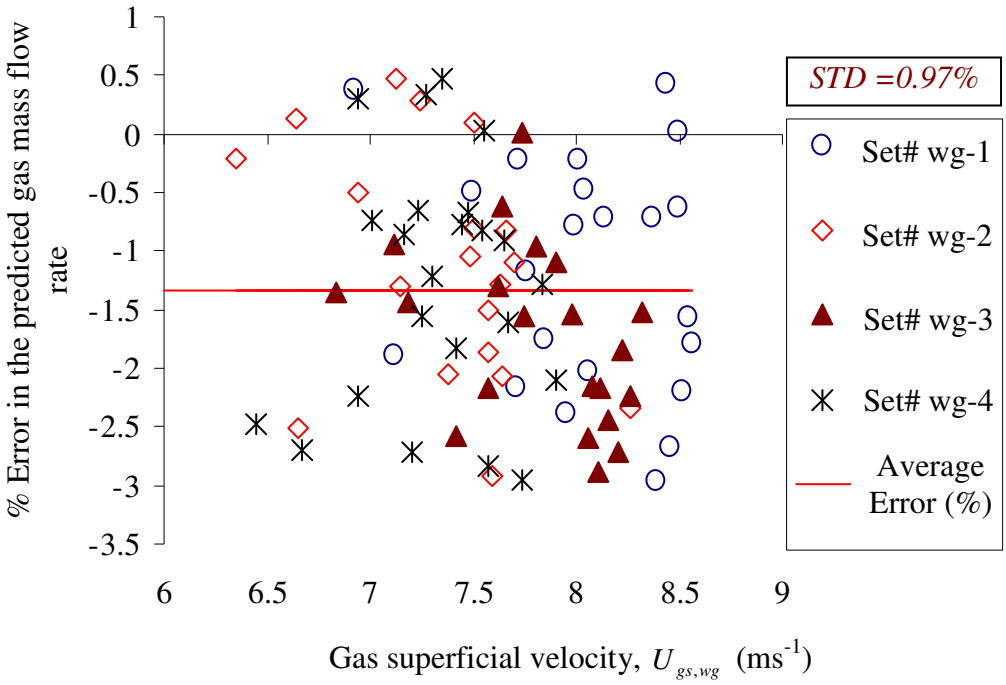

Figure 8-11: The percentage error in the predicted gas mass flow rate for all sets of data, $C_{dg,wg} = 0.920$

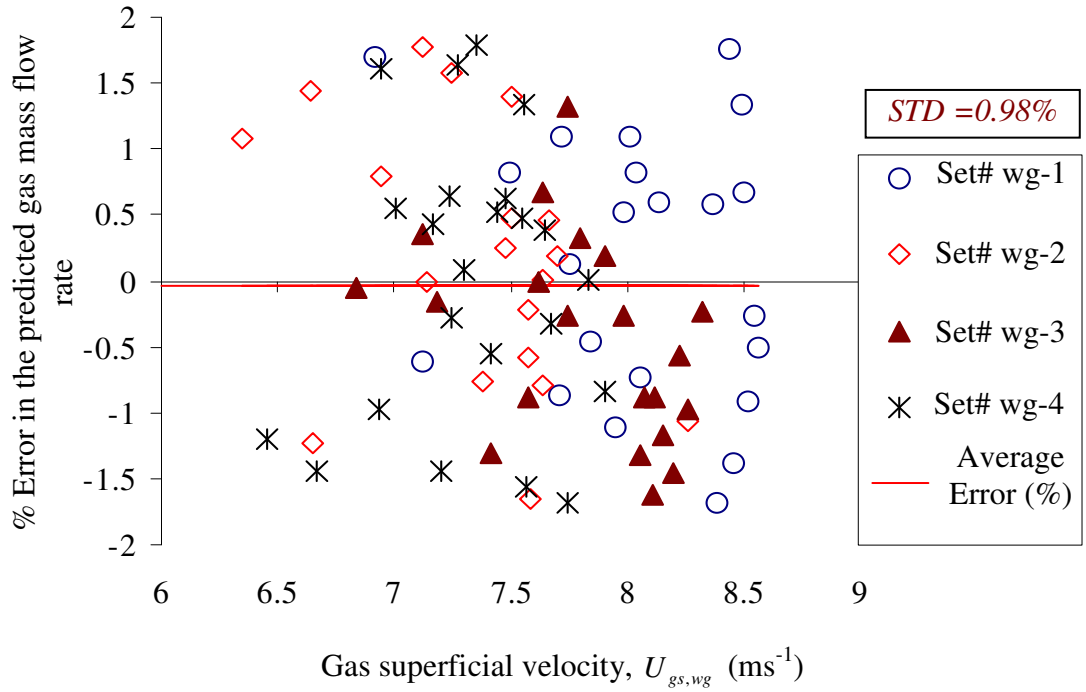

Figure 8-12: The percentage error in the predicted gas mass flow rate for all sets of data, $C_{dg,wg} = 0.932$

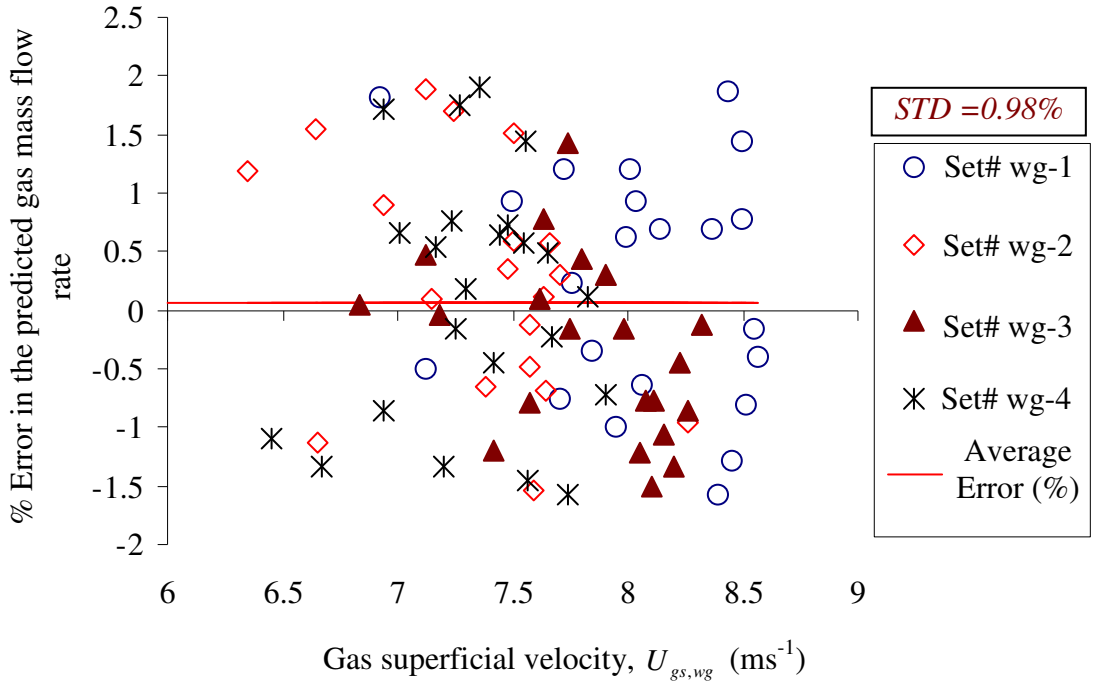

Figure 8-13: The percentage error in the predicted gas mass flow rate for all sets of data, $C_{dg,wg} = 0.933$

8.6 The percentage error in the predicted water mass flow rate in vertical annular (wet gas) flows through the Venturi meter

One of the major difficulties in measuring the water flow rate using the conductance multiphase flow meter with an 80mm ID pipe was that the outlet gas flow rate from the side channel blower (RT-1900) could not always be maintained at a constant value when the water flow rate was varied. In other words, with increasing water flow rate in the test section (i.e. increasing the system resistance by exerting more pressure on the outlet of the fan blower, see Section 6.1.2) it was very difficult to maintain constant gas flow rate using an 80 mm ID pipe since the gas flow rate from the outlet of the side channel blower decreases as the water flow rate (and hence ΔP in Figure 8-14) increases. This is why the water flow rate was kept constant while the gas flow rate was varied in each set of data (see Table 8-1).

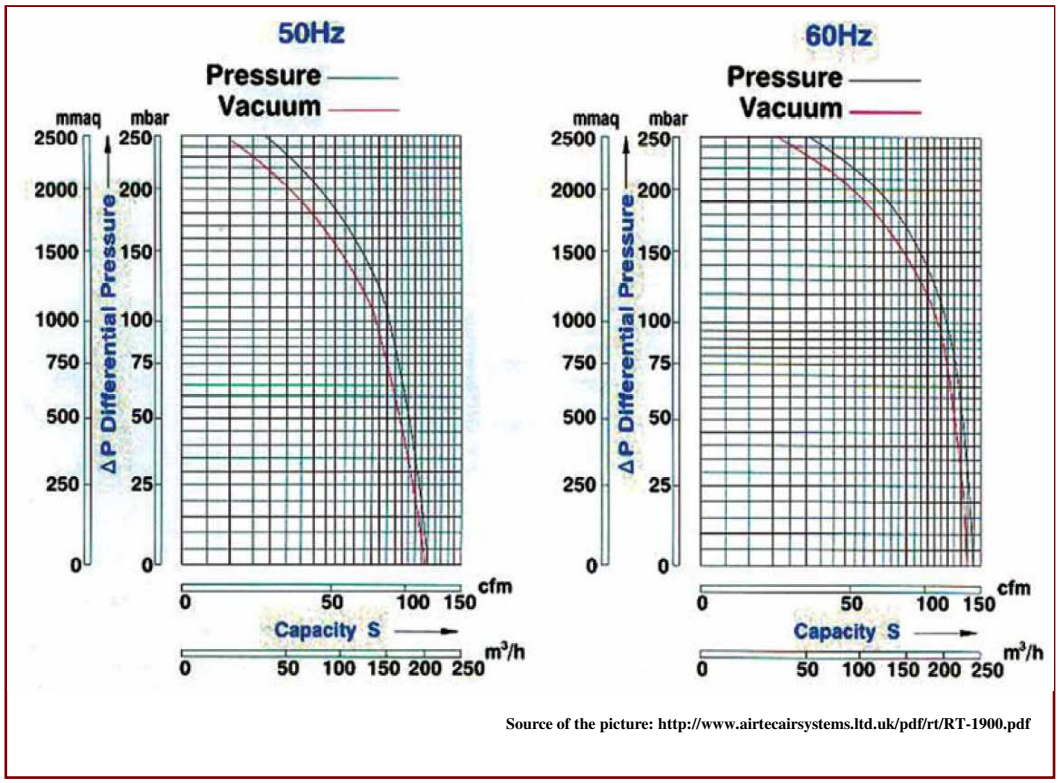

Figure 8-14: The specifications of the side channel blower (RT-1900)

Another challenge was that due to the limitation in the air fan (side channel blower (RT-1900)), the side channel blower could not achieve a stable liquid film flow rate at all flow conditions. In other words, pulsations occurred in the liquid film.

A new set of data was analysed in which the gas flow rate was kept constant while the water flow rate was varied. The values of the water flow rates (and also the fixed value of the gas flow rate) in this set of data were chosen in a way so that the possible stable liquid film flow could be established. The gas superficial velocity was kept constant at an average value of 7.57 ms^{-1}. The reference water volumetric flow rate was in the range of 5.026×10^{-5} m^3s^{-1} to 6.378×10^{-5} m^3s^{-1}. This range of the water flow rate was quite narrow because as mentioned above, increasing the water flow rate increases the differential pressure in the side channel blower and hence decreases the outlet gas flow rate (see Figure 8-14) which produces pulsations in the water flow rate and leads to unstable liquid film flow.

The water discharge coefficient $C_{dw,wg}$ in annular two phase flows can be expressed as;

$$C_{dw,wg} = \frac{\dot{m}_{w,ref,wg}}{\dot{m}_{w,wg}}$$

Equation (8.9)

The variation of the water discharge coefficient $C_{dw,wg}$ in vertical annular (wet gas) flows with the reference water mass flow rate $\dot{m}_{w,ref,wg}$ for the new set of data is shown in Figure 8-15. It is clear that the water discharge coefficient $C_{dw,wg}$ was above unity. This was due to the unsteady liquid film flow rate (caused by the limitation in the side channel blower) and also due to the assumption that there were no liquid droplets in the gas core.

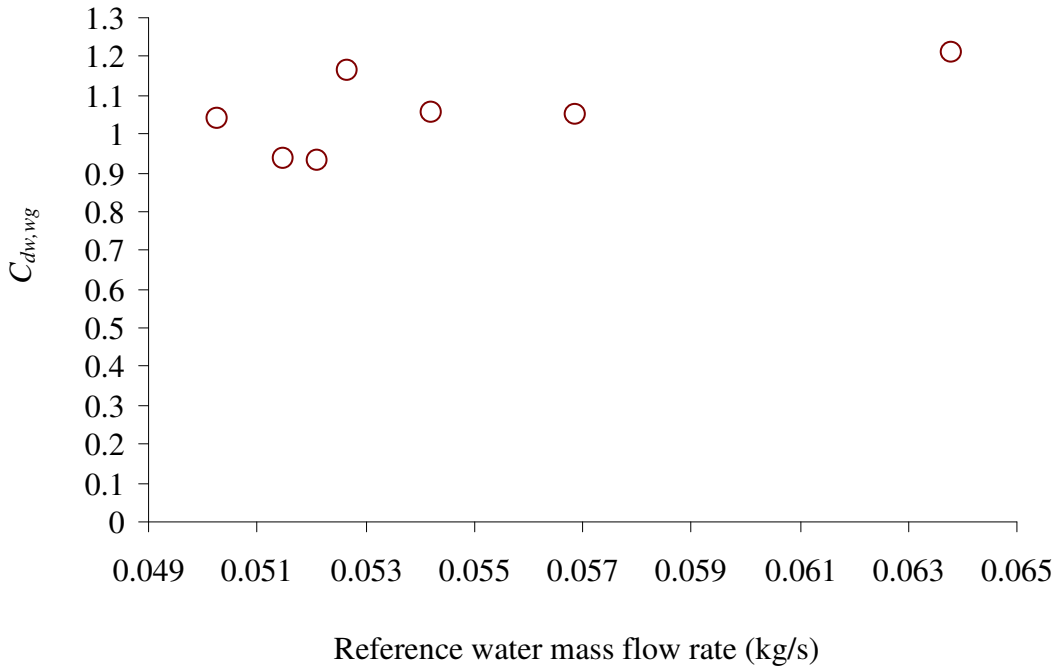

Figure 8-15: Variations of the water discharge coefficient

The percentage error in the predicted water mass flow rate $\varepsilon_{\dot{m}_{w,wg}}$ is given by;

$$\varepsilon_{\dot{m}_{w,wg}} = \frac{\dot{m}_{w,wg} - \dot{m}_{w,ref,wg}}{\dot{m}_{w,ref,wg}} \times 100\%$$

Equation (8.10)

where $\dot{m}_{w,ref,wg}$ is the reference water mass flow rate obtained from the turbine flow meter-2 (see Section 6.2.2). The reference water mass flow rate can be obtained from multiplying the reference water volumetric flow rate, measured directly from the turbine flow meter-2, by the water density. The predicted water mass flow rate, $\dot{m}_{w,wg}$, is obtained from Equation (3.72). It should be noted that $\dot{m}_{w,wg}$ in Equation (3.72) and also in Equation (8.10) does not account for any water droplets in the gas core.

It should be also noted that the water discharge coefficient $C_{dw,wg}$ shown in Figure 8-15 (and also given by Equation (8.9)) is defined based on the predicted water mass flow rate $\dot{m}_{w,wg}$ (see Equation (3.72)). The reasons for getting a relatively large error ($> \pm 10\%$) in the water mass flow rate were due to; (i) the assumption that the entire water flow existed in the liquid film (i.e. the water droplet flow rate was not included in the $\dot{m}_{w,wg}$ (Equation (3.72)), and (ii) the pulsations in the water film flow which caused an unsteady water film flow rate.

Experiments were carried out in annular gas-water two phase flows in parallel with the current research at the University of Huddersfield to measure the water film flow rate (Al-Yarubi (2010) [147]). Section 8.7 discusses an alternative method of measuring the water film flow rate. This alternative method is based on the wall conductance sensor (WCS) which was described in Sections 4.4 and 6.4.

8.7 Alternative approach of measuring the water mass flow rate in annular gas-water two phase flows

It should be noted that the work done on the WCS by Al-Yarubi (2010) [147] was done using the flow loop described in Section 6.1.2. The purpose of presenting the work done on the WCSs was to show how this method could be used to give information about the variation of the entrainment fraction, *E* with the gas superficial velocity. The data on the entrainment fraction, *E,* obtained from the WCSs was then

used to estimate the total water mass flow rate using the conductance multiphase flow meter (see Equations (8.16) and (8.17)). In other words, the purpose of using the WCS was to find the entrainment fraction, *E,* reported in Figure 8-17.

As stated above, the modulus of the error in the predicted water mass flow rate using Equation (3.72) was greater than expected (>10%). As a result, a new approach for measuring the water flow rate was adopted [147]. The new approach is based on WCSs (see Sections 4.4 and 6.4). Experiments with different flow conditions were carried out at the University of Huddersfield in parallel with the current research to measure the water flow rate in annular gas-water two phase flows in a 50mm ID pipe using the WCSs [147]. Carrying out the experiments in a 50mm ID pipe instead of an 80mm ID pipe enables the side channel blower to achieve a stable water film flow. Different flow conditions were tested with the gas superficial velocity in the range of 10.61 to 24.76 ms^{-1} and for values of the water superficial velocity in the range of 0.047 to 0.260 ms^{-1}.

The water film thickness δ in annular gas-water two phase flows using the WCSs could be determined from the data reported in Figure 6-25 (see the calibration of the WCS in Section 6.4, for more information, refer to [147]). Once the film thickness δ was obtained the cross-sectional area of the liquid film A_f can be determined using;

$$A_f = \pi\left\{R_{wcs}^2 - (R_{wcs} - \delta)^2\right\}$$

Equation (8.11)

where R_{wcs} is the pipe internal radius (the radius of the wall conductance meter, see Section 4.4) and δ is the film thickness.

Al-Yarubi used two WCSs to measure the liquid film velocity $U_{f,corr}$ using a cross correlation technique described in Section 2.1.2.6. Figure 8-16 shows the process of the cross-correlation that was applied to one of the flow conditions in annular gas-water two phase flows using the WCSs in which the water film velocity $U_{f,corr}$ can be determined [147].

Once the area of the water film A_f and the water film velocity $U_{f,corr}$ were obtained, the water film volumetric flow rate Q_{wf} can be determined using;

$$Q_{wf} = A_f U_{f,corr}$$

Equation (8.12)

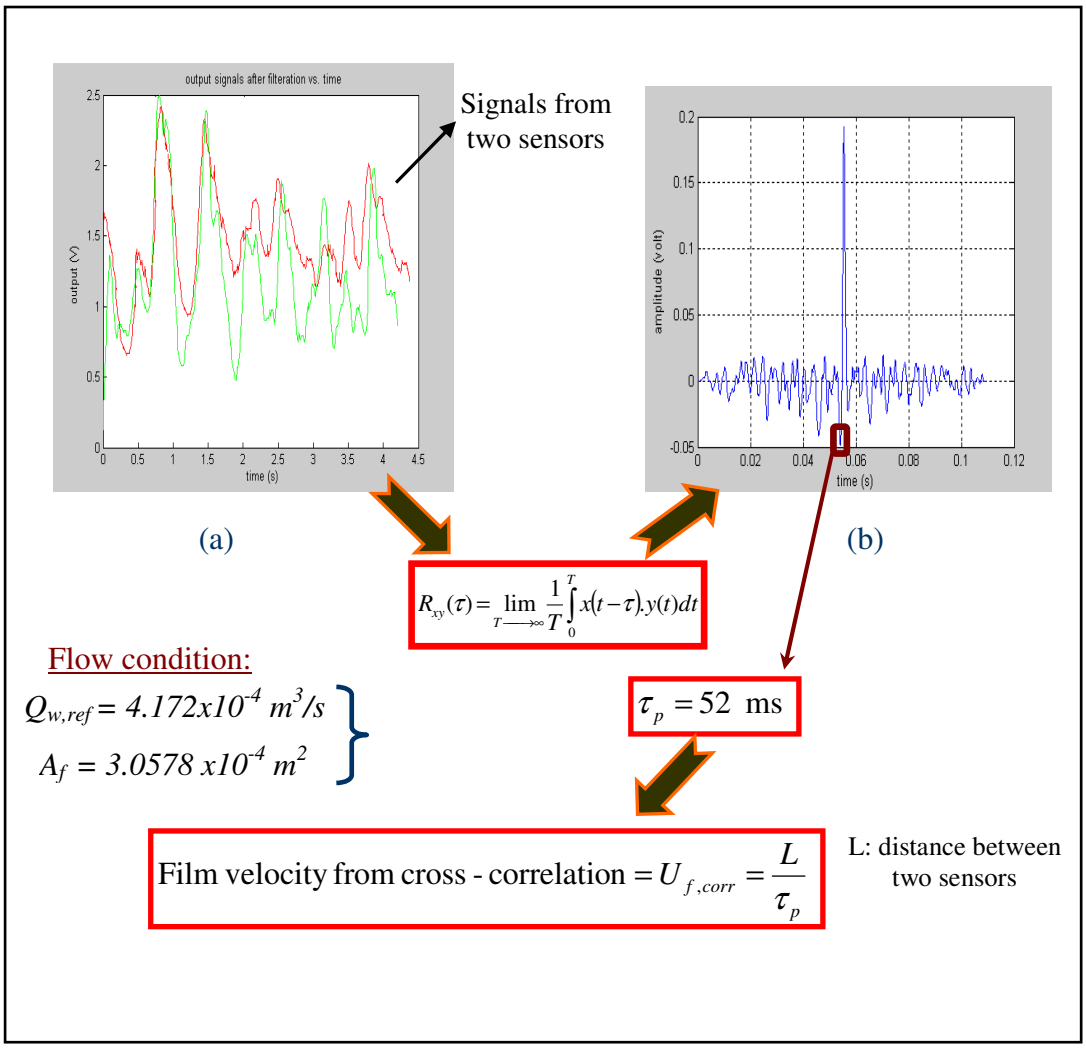

Figure 8-16: Cross correlation technique using the wall conductance sensors

The reference water volumetric flow rate $Q_{w,ref,wg}$ (measured from the turbine flow meter-2, see Section 6.2.2) is the sum of the water film volumetric flow rate Q_{wf} and the water droplet volumetric flow rate Q_{wc} in the gas core. Therefore;

$$Q_{w,ref,wg} = Q_{wf} + Q_{wc}$$

Equation (8.13)

The water droplet volumetric flow rate at the gas core, Q_{wc} can be related to the entrainment fraction, E, using [147];

$$Q_{wc} = \frac{EQ_{wf}}{(1-E)}$$

Equation (8.14)

Combining Equations (8.12), (8.13) and (8.14) gives;

$$E = 1 - \frac{A_f U_{f,corr}}{Q_{w,ref,wg}}$$

Equation (8.15)

Figure 8-17, from Al-Yarubi (2010) [147], shows the relationship between the entrainment fraction, E, and the gas superficial velocity for different values of the water superficial velocity. A best fit equation of the average entrainment fraction over the full range of the gas superficial velocities for different values of the water superficial velocity is also shown in Figure 8-17.

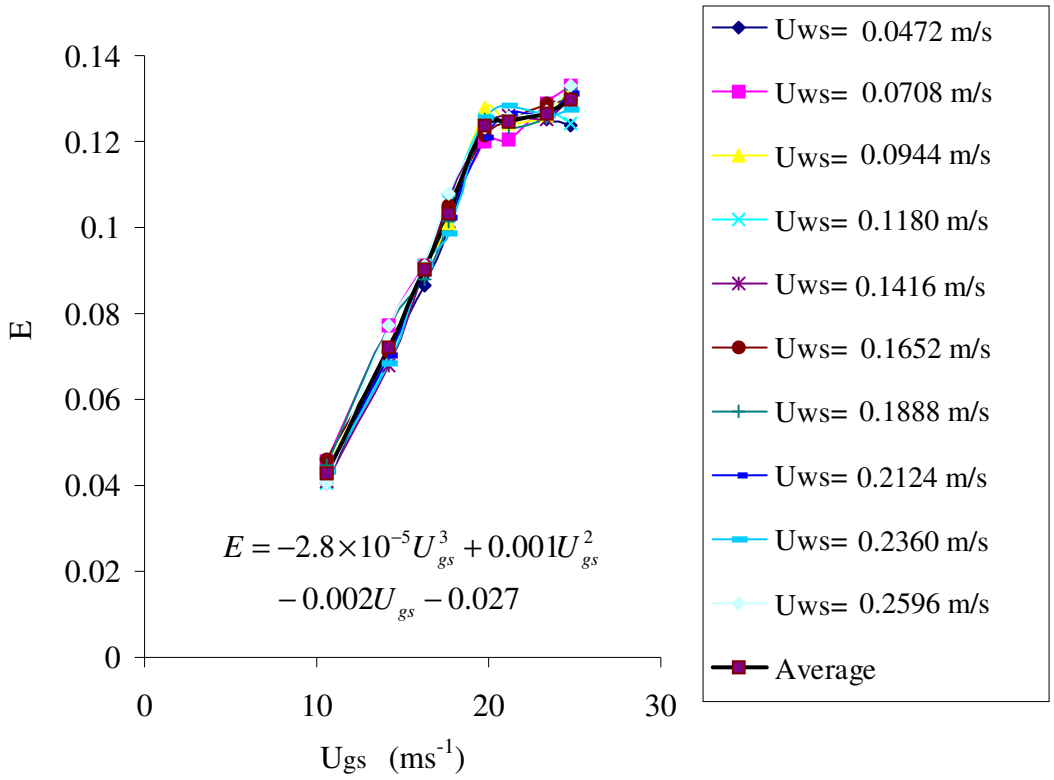

Figure 8-17: Variations of the entrainment fraction *E* with the gas superficial velocity for different values of the water superficial velocity

Up to this point, the required data has been obtained from the work done by Al-Yarubi (2010) [147] (i.e. Figure 8-17). To benefit from his work, the data in Figure 8-17 can now be used to estimate the entrainment fraction *E*. As mentioned in Section 8.6, a new set of data was analysed in which the gas flow rate was kept constant while the water flow rate was varied. The values of the water flow rates and the fixed value of the gas flow rate in this set of data were chosen in a way so that the possible stable liquid film flow could be established. Since the value of the gas superficial velocity, in this set of data, was kept constant at an average value of 7.57 ms^{-1}, the approximate value of the entrainment fraction *E* corresponding to this value of the gas superficial velocity was 0.0405 (i.e. the minimum value of the entrainment fraction *E* shown in Figure 8-17). It should be noted that this value of *E* could be assumed to be constant since the range of the water volumetric flow rate used for the new set of data was quite small (i.e. 5.026×10^{-5} m^3s^{-1} to 6.378×10^{-5} m^3s^{-1}, see Section 8.6).

Equation (8-14) can be rewritten as;

$$\dot{m}_{w,gc,wg} = \frac{E\,\dot{m}_{w,wg}}{(1-E)}$$

Equation (8.16)

where $\dot{m}_{w,gc,wg}$ is the mass flow rate of the entrained liquid droplets in the gas core and $\dot{m}_{w,wg}$ is the water mass flow rate in the liquid film (i.e. Equation (3.72)).

It is now possible to estimate the total water mass flow rate $\dot{m}_{w,total,wg}$ in annular (wet gas) flow using;

$$\dot{m}_{w,total,wg} = \dot{m}_{w,gc,wg} + \dot{m}_{w,wg}$$

Equation (8.17)

$\dot{m}_{w,wg}$ in Equation (8.17) is the water mass flow rate assuming that the entire liquid existed in the liquid film (i.e. the mass flow rate of the liquid film, see Equation (3.72)).

The percentage error in the predicted total water mass flow rate can be then expressed as;

$$\varepsilon_{\dot{m}_{total,wg}} = \frac{\dot{m}_{w,total,wg} - \dot{m}_{w,ref,wg}}{\dot{m}_{w,ref,wg}} \times 100\%$$

Equation (8.18)

where $\dot{m}_{w,ref,wg}$ is the reference water mass flow rate in annular (wet gas) flow obtained from multiplying the reference water volumetric flow rate $Q_{w,ref,wg}$ (obtained directly from the turbine flow meter-2, see Section 6.2.2) by the water density.

Figure 8-18 shows the percentage error $\varepsilon_{\dot{m}_{total,wg}}$ in the predicted total water mass flow rate. It should be noted that the average value of the water discharge coefficient $C_{dw,wg}$ for all of the flow conditions was 1.057 (see Figure 8-15). Whenever the selected values of $C_{dw,wg}$ were close to 1.057, the error in the total water mass flow rate $\varepsilon_{\dot{m}_{total,wg}}$ becomes less. Therefore, the selected value of the $C_{dw,wg}$ (which was used

in calculating $\dot{m}_{w,wg}$, see Equation (3.72)) was chosen to be 0.995. The mean percentage error in the predicted total water mass flow rate $\bar{\varepsilon}_{\dot{m}_{total,wg}}$ and the standard deviation were 0.550% and 6.495% respectively.

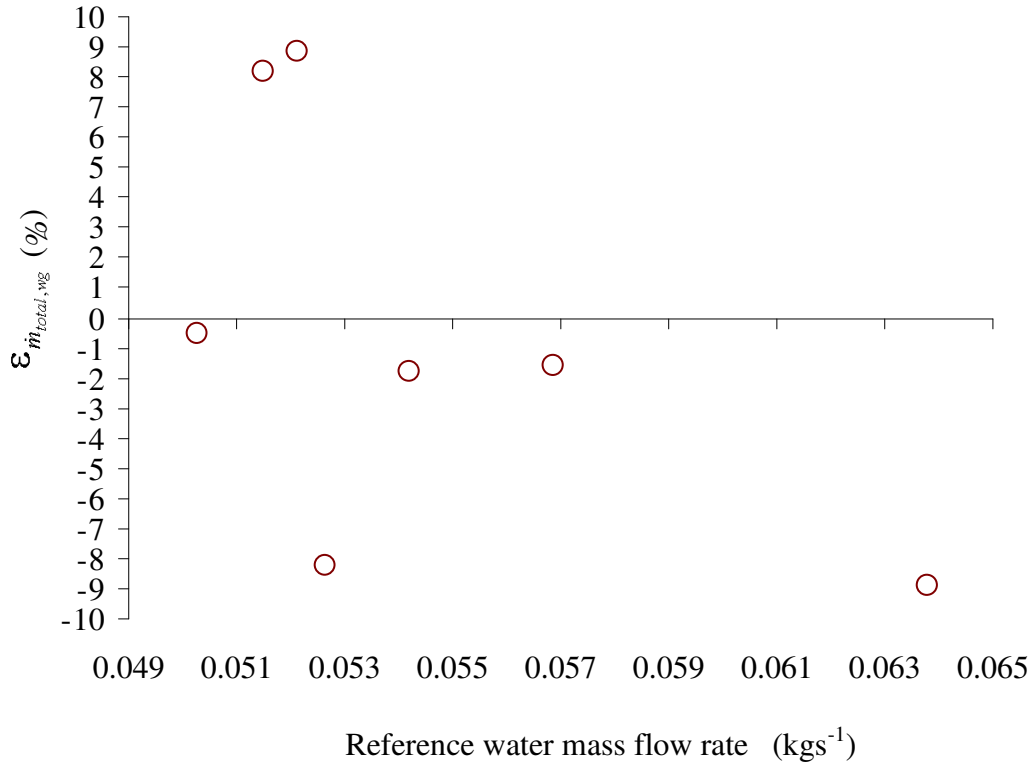

Figure 8-18: Percentage error in the predicted total water mass flow rate

The new proposed technique to measure the total water mass flow rate and the gas mass flow rate in annular (wet gas) flows using a Conductance Cross Correlation Meter (CCCM) in conjunction with the Conductance Multiphase Venturi Meter (CMVM) is described, in detail, as possible further work in Chapter 11.

Summary

A novel conductance multiphase flow meter (i.e. CIVFM and CMVM) in conjunction with the separated vertical annular flow model described in Section 3.2.2 was used to study annular gas-water two phase flows. Four sets of data were investigated in which the water flow rate was kept constant while the gas flow rate was varied (see Table 8-1). An additional new set of data was also investigated in this study in which the gas flow rate was kept constant while the water flow rate was varied.

One of the major difficulties encountered in this investigation was that the side channel blower could not achieve a stable liquid film flow rate in all flow conditions and pulsations occurred in the liquid film. An alternative method for measuring the water flow rate was discussed. This method was based on wall conductance sensors (see Sections 4.4 and 8.7).

The gas volume fraction at the inlet and the throat of the Venturi was measured using two ring electrodes at the inlet (i.e. at the CIVFM) and two ring electrodes at the throat of the CMVM respectively. It was found that in general, the gas volume fraction $\alpha_{1,wg}$ at the inlet of the Venturi was greater than the gas volume fraction $\alpha_{2,wg}$ at the throat of the Venturi. At a lower water flow rate (data set# wg1), this difference becomes more visible.

The gas discharge coefficient $C_{dg,wg}$ (Equation (8.5)) was investigated. The optimum value of the gas discharge coefficient which gives a minimum average value of the percentage error in the predicted gas mass flow rate (i.e. $\bar{\varepsilon}_{\dot{m}_{g,wg}} = -0.043\%$) was found to be 0.932 (see Section 8.5).

The percentage error in the predicted water mass flow rate using Equation (3.72) was larger than expected. This was because; (i) the $\dot{m}_{w,wg}$ in Equation (3.72) assumed that the entire water flow rate was represented by the liquid film flow rate. In other words, the flow rate of the water droplets is not included in $\dot{m}_{w,wg}$ and, (ii) the pulsations

occurred in the water film which caused unsteady water film flow rate. An alternative technique (based on the wall conductance sensors, see Sections 4.4 and 6.4) was used so that the total water mass flow rate using the conductance multiphase flow meter (CIVFM and CMVM) was estimated.

Chapter 9

Experimental Results for Stratified Gas-Water Two Phase Flows through a Conductance Multiphase Flow Meter

Introduction

Stratified flow is one of the most common flow regimes encountered in horizontal gas-liquid two phase flows. In a horizontal stratified gas-water two phase flow, the water flows at the bottom of the pipe while the gas phase flows along the top of the pipeline. Since a stratified flow is one of the separated flow regimes the velocity ratio (i.e. slip ratio *S*, see Equations (3.60) and (3.61)) is not unity. Therefore, relying only on the measurement of the gas volume fraction at the inlet of the Venturi (as in homogenous flow model) would not be expected to give accurate results.

A new mathematical model for horizontal stratified gas-water two phase flows through a Venturi meter was investigated (see Section 3.2.2). Unlike the previous models described in Section 2.2, this model does not require prior knowledge of the mass flow quality *x* but it depends on the measurement of the gas volume fractions $\alpha_{1,st}$ (measured from the two ring electrodes at the inlet of the Venturi (i.e. at the CIVFM, see Section 4.3.1)) and $\alpha_{2,st}$ (measured from the two ring electrodes at the throat of the CMVM, see Section 4.3.2). Measurement of $\alpha_{1,st}$ (see Equation (5.13)) and $\alpha_{2,st}$ (see Equation (5.14)) enables the gas and the water mass flow rates $\dot{m}_{g,st}$ and $\dot{m}_{w,st}$ to be determined (see Equations (3.43) and (3.59)). Due to the substantial difference between the water and the gas differential pressures across the CMVM in a stratified two phase flow (i.e. the maximum pressure drops in the gas and the water phases across the Venturi were 232.7 Pa and 100.0 Pa respectively), two differential

pressure measurement devices were used (see Section 6.2.3). A Honeywell dp cell (ST-3000) was used to measure the pressure drop in the water phase while an inclined manometer was used to measure the pressure drop in the gas phase (see Section 6.3.2).

This chapter presents and discusses the experimental results obtained in horizontal stratified gas-water two phase flows through a conductance multiphase flow meter, and in which the predicted gas and water mass flow rates, $\dot{m}_{g,st}$ and $\dot{m}_{w,st}$ were measured and compared with the reference gas and water mass flow rates. Following the convention in the literature, the gas and the water flow rates discussed in this chapter are presented in terms of the mass flow rates.

9.1 Flow conditions of horizontal stratified gas-water two phase flows

A series of experiments were carried out in horizontal stratified gas-water two phase flows using the conductance multiphase flow meter (i.e. CIVFM and CMVM, see Section 4.3). The experiments were conducted using one of the multiphase flow loops at the University of Huddersfield which was capable of providing stratified gas-water two phase flows (see the stratified flow configuration in Section 6.1.3). Five different sets of data were used to study horizontal stratified two phase flows. In the first three sets, the water flow rate was kept constant while the gas flow rate was varied. The gas flow rates were kept constant and the water flow rates were varied in the remaining two sets of data (see Table 9-1).

It should be noted that the values of the low gas superficial velocity $U_{gs,st}$ in data sets; 'st-1', 'st-2', 'st-4' and 'st-5' (see Table 9-1) were obtained from dividing the reference gas volumetric flow rate (measured from the thermal mass flow meter which was installed on the low gas flow line, see Section 6.2.6) by the cross-sectional area of the pipe. The high values of the gas superficial velocity in the set of data 'st-3' were obtained from dividing the reference gas volumetric flow rate (measured from the Variable Area Flowmeter, VAF which was installed on the high gas flow line in which the side channel blower was used to provide high gas flows, see Sections 6.1.3

and 6.2.4) by the cross-sectional area of the pipe. The values of the water superficial velocity were obtained from dividing the reference water volumetric flow rate measured from the turbine flow meter-2 (see Section 6.2.2) by the cross-sectional area of the pipe.

Table 9-1: Flow conditions in stratified gas-water two phase flow

Data set no.	water superficial velocity in stratified flows, $U_{ws,st}$ (ms^{-1})	Gas superficial velocity in stratified flows, $U_{gs,st}$ (ms^{-1})
st-1	0.013	0.171 to 0.595
st-2	0.017	0.278 to 0.568
st-3	0.019	1.467 to 4.444
st-4	0.025 to 0.057	0.361
st-5	0.037 to 0.070	0.321

9.2 Variations in the gas volume fraction at the inlet and the throat of the Venturi in a stratified gas-water two phase flow

The conductance multiphase flow meter, which consists of the CIVFM and the CMVM, was designed to measure the gas volume fraction at the inlet and the throat of the Venturi in separated horizontal stratified gas-water two phase flows. The CIVFM was used to measure the gas volume fraction $\alpha_{1,st}$ at the inlet of the Venturi (see Equation (5.13)) while the CMVM was used to measure the gas volume fraction $\alpha_{2,st}$ at the throat of the Venturi (see Equation (5.14)).

Figure 9-1 shows the variation of the gas volume fractions $\alpha_{1,st}$ and $\alpha_{2,st}$ at the inlet and the throat of the Venturi respectively with the gas superficial velocity $U_{gs,st}$ for data set ‘st-1’ and data set ‘st-2’ (i.e. at low gas flow rates and fixed values of the

water flow rate, see Table 9-1). It is clear from Figure 9-1 that the gas volume fraction $\alpha_{2,st}$ (at the throat of the Venturi) is greater than the gas volume fraction $\alpha_{1,st}$ (at the inlet of the Venturi). In addition, the variation in the gas volume fraction $\alpha_{1,st}$, from one flow condition to another, was greater than that which occurred in the gas volume fraction $\alpha_{2,st}$ at the throat of the Venturi. It should be mentioned that, although, considerable theoretical and experimental studies have been published to describe the performance of the Venturi meters in stratified flows, there is very limited, if any, data in the literature with which the current results can be compared. Most of the data available in the literature depends on prior knowledge of the mass flow quality x and the over-reading factor [154] and not the actual measurements of the gas volume fractions $\alpha_{1.st}$ and $\alpha_{2.st}$ at the inlet and the throat of the Venturi as in the current study.

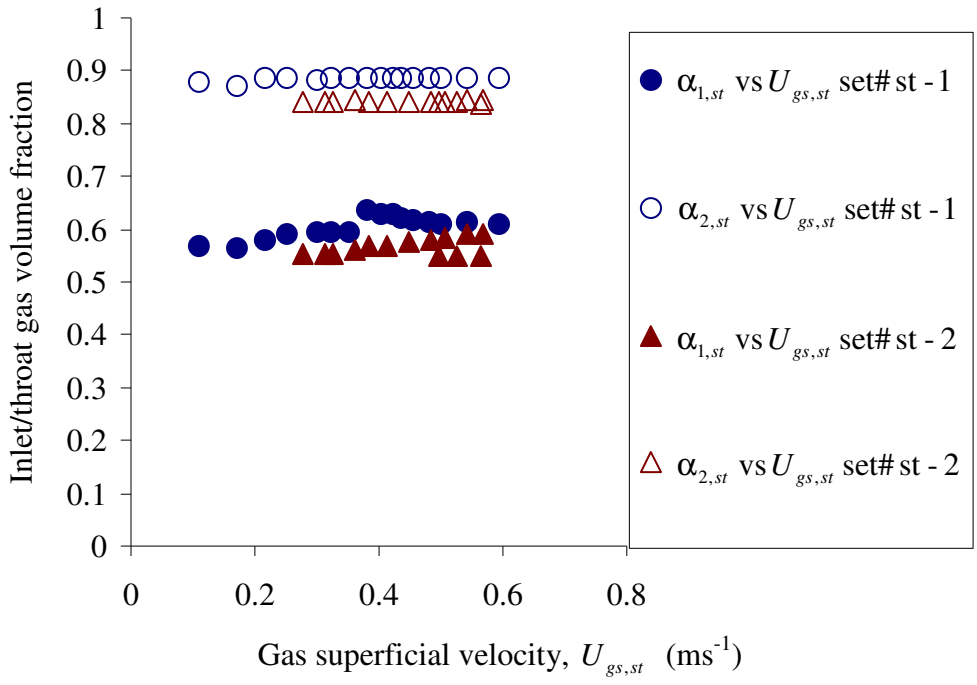

Figure 9-1: Variations of $\alpha_{1,st}$ and $\alpha_{2,st}$ with $U_{gs,st}$ at low gas flow rates and fixed water flow rates (sets of data: 'st-1' and 'st-2')

Figure 9-2 shows the variation of $\alpha_{1,st}$ and $\alpha_{2,st}$ with $U_{gs,st}$ for set of data 'st-3' (i.e. at high gas flow rates and fixed water flow rate, see Table 9-1). It can be seen from Figures 9-1 and 9-2 that at fixed values of the water flow rate and varying gas flow rates, the gas volume fraction $\alpha_{2,st}$ at the throat of the Venturi was greater than the gas volume fraction $\alpha_{1,st}$ at the inlet of the Venturi. It can be also seen from Figure 9-2 that, as the gas superficial velocity increased the difference between $\alpha_{1,st}$ and $\alpha_{2,st}$ decreased.

The variations of the gas volume fractions $\alpha_{1,st}$ and $\alpha_{2,st}$ at varying water flow rates and fixed values of the gas flow rate (i.e. sets of data: 'st-4' and 'st-5') are shown in Figure 9-3. It can be seen from Figure 9-3 that the gas volume fraction decreases as the water flow rate increases. The gas volume fraction $\alpha_{2,st}$ is always greater than $\alpha_{1,st}$. This is because the gas-water boundary undergoes a step change in height from the inlet to the throat of the Venturi (see Figure 3-4 in Section 3.2.1).

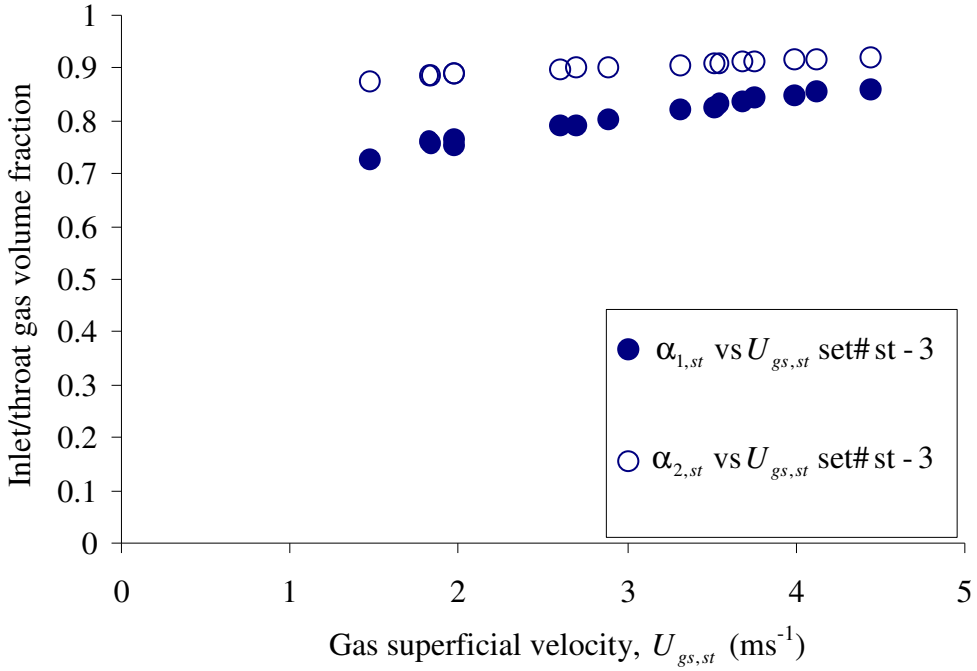

Figure 9-2: Variations of $\alpha_{1,st}$ and $\alpha_{2,st}$ with $U_{gs,st}$ at high gas flow rates and fixed water flow rate (data set: 'st-3')

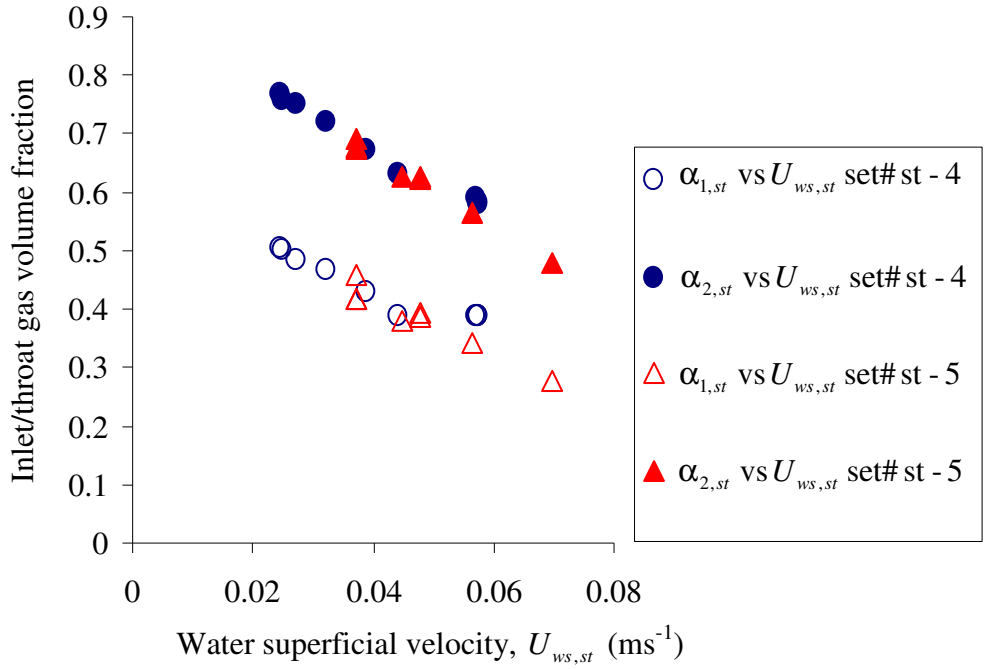

Figure 9-3: Variations of $\alpha_{1,st}$ and $\alpha_{2,st}$ with $U_{ws,st}$ at fixed gas flow rates and varying water flow rates (sets of data: 'st-4' and 'st-5')

9.3 Variations of the water height at the inlet and the throat of the Venturi

The height of the water $h_{1,st}$ and $h_{2,st}$ at the inlet and the throat of the Venturi (i.e. at the CIVFM and the throat section of the CMVM) in a stratified gas-water two phase flow can be measured using the conductance technique described in Chapters 4 and 5. The relationship between the heights of the water $h_{1,st}$ and $h_{2,st}$ at the inlet and the throat of the Venturi and the water superficial velocity $U_{ws,st}$ when the gas flow rates were fixed (i.e. sets of data: 'st-4' and 'st-5', see Table 9-1) is shown in Figure 9-4. The height of the water $h_{1,st}$ at the inlet of the Venturi measured from the two ring electrodes flush mounted with the inner surface of the CIVFM (see Section 4.3.1) was always greater than the water height $h_{2,st}$ at the throat of the Venturi which was measured from the two electrodes at the throat section of the CMVM. Visual observation of the flow was also indicated that the gas-water boundary undergoes a reduction in height from the inlet to the throat of the Venturi (see Section 3.2.1).

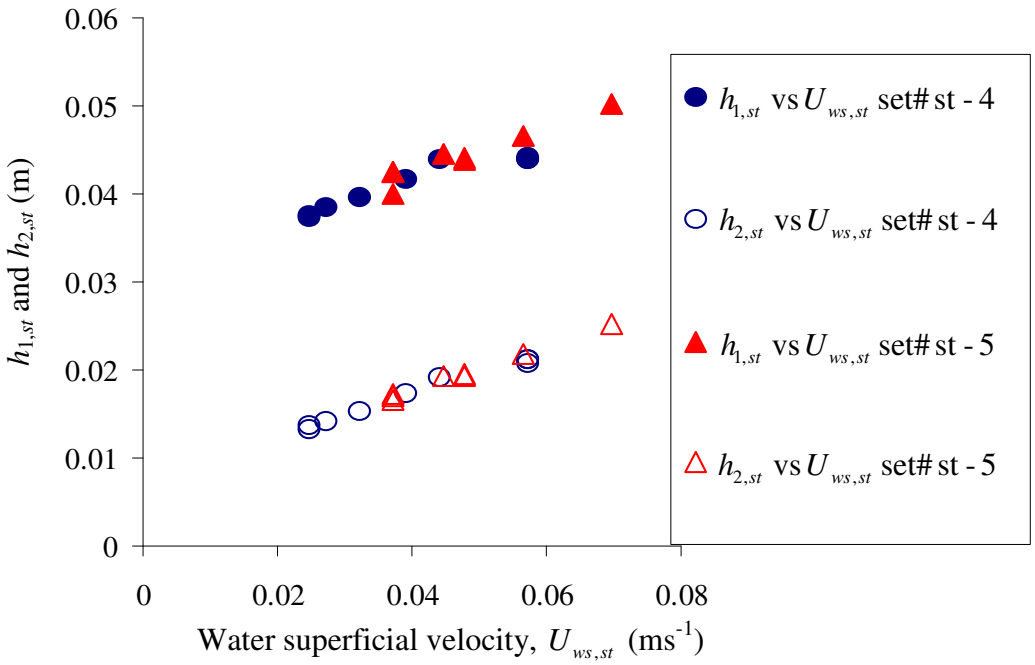

Figure 9-4: The relationship between $U_{ws,st}$ and ($h_{1,st}$ and $h_{2,st}$) at fixed gas flow rates and varying water flow rates (sets of data: 'st-4' and 'st-5')

Figure 9-5 shows the relationship between the relative heights of the water at the inlet and the throat of the Venturi, $\frac{h_{1,st}}{D_1}$ and $\frac{h_{2,st}}{D_2}$ respectively for fixed values of the gas flow rate and varying water flow rates (i.e. sets of data: 'st-4' and 'st-5'). Note that D_1 is the internal diameter of the Venturi inlet and is equal to 80mm and D_2 is the internal diameter of the Venturi throat and is equal to 48mm (see Section 4.3.2). The solid lines (i.e. blue and red lines) in Figure 9-5 represent the linear regression lines for the relative heights of the water at the inlet and the throat of the Venturi respectively. It is seen that as the water superficial velocity increased the difference between the relative heights of the water at the inlet and the throat of the Venturi decreased. In other words, as the water superficial velocity $U_{ws,st}$ increased, the difference between the two blue solid lines and the difference between the two red solid lines become less (see Figure 9-5).

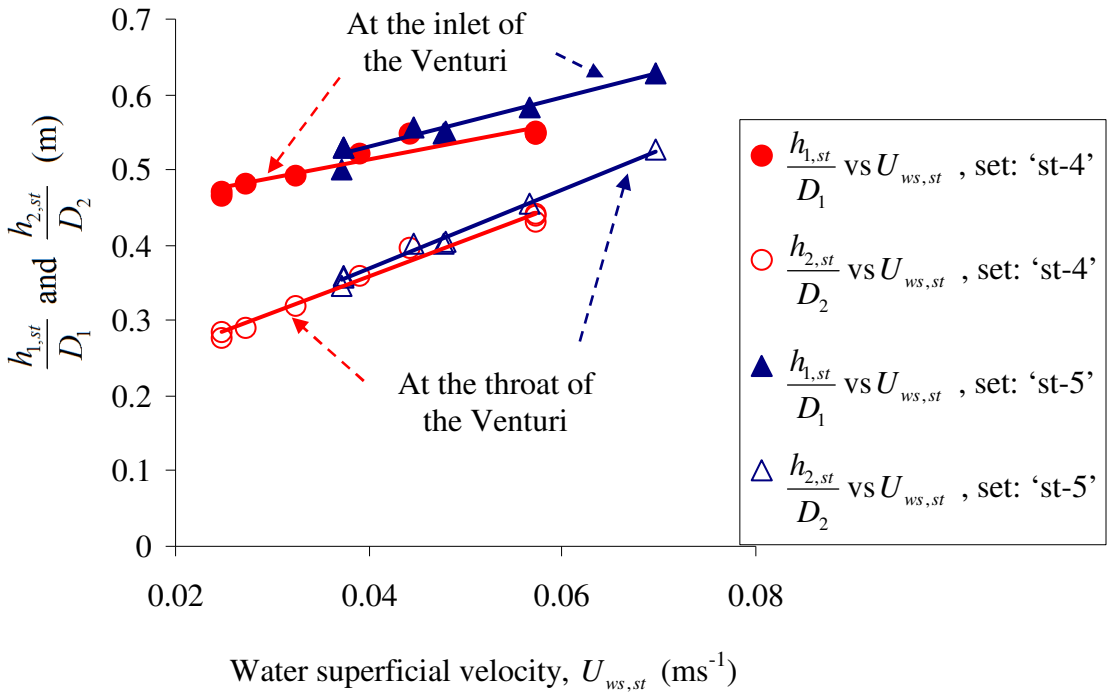

Figure 9-5: The relationship between the relative heights of the water at the inlet and the throat of the Venturi for sets of data: 'st-4' and 'st-5'

9.4 Study of the discharge coefficient in a stratified gas-water two phase flow

The discharge coefficients in single phase flows are well established and the practical data of the single phase discharge coefficient is readily available in the literature. Little is known about the discharge coefficients in separated two phase flows and the data available in the literature is very limited. Most of the research conducted in two phase flows defined the discharge coefficient similar to that in single phase flows (refer for example to; Murdock (1962) [47], Chisholm (1967, 1977) [48,49] and Lin (1982) [51]).

Zanker (1966) [156] showed that in a horizontal Venturi and Venturi nozzles, the discharge coefficient decreased slightly with the gas volume fraction. The author concluded that, the reason of this was due to the effect of mixture compressibility.

The gas and the water discharge coefficients in a stratified gas-water two phase flow through a Venturi meter are respectively given by;

$$C_{dg,st} = \frac{\dot{m}_{g,ref,st}}{\dot{m}_{g,st}}$$

Equation (9.1)

and;

$$C_{dw,st} = \frac{\dot{m}_{w,ref,st}}{\dot{m}_{w,st}}$$

Equation (9.2)

where $\dot{m}_{g,st}$ and $\dot{m}_{w,st}$ are the predicted gas and water mass flow rates (see Equations (3.43) and (3.59)). $\dot{m}_{g,ref,st}$ and $\dot{m}_{w,ref,st}$ are the reference gas and water mass flow rates. $\dot{m}_{g,ref,st}$ was obtained from multiplying the reference gas volumetric flow rate from either the variable area flow meter (VAF) or the thermal mass flowmeter by the gas density ρ_{g1} obtained from Equations (3.44) and (3.45), while $\dot{m}_{w,ref,st}$ was obtained from multiplying the reference water volumetric flow rate from the turbine flow meter-2 (see Section 6.2.2) by the water density.

Figure 9-6 shows the variation of the gas discharge coefficient $C_{dg,st}$ for data set 'st-1' and data set 'st-2' (i.e. at fixed values of the water flow rate and varying low gas flow rates). The variation of the $C_{dg,st}$ at fixed water flow rate and varying high gas flow rates (data set 'st-3') is shown in Figure 9-7.

From Figures 9-6 and 9-7, a mean value for the gas discharge coefficient $C_{dg,st}$ is given by $C_{dg,st} = 0.965$. This value of the $C_{dg,st}$ represents the optimum value where the minimum average percentage error in the predicted gas mass flow rate can be obtained (see Section 9.5). It should be noted that the mean value of the gas discharge coefficient was obtained by averaging the overall data reported in Figures 9-6 and 9-7.

Figure 9-8 shows the variation of the water discharge coefficient $C_{dw,st}$ in a stratified gas water two phase flow at fixed values of the gas flow rate and varying water flow rates (i.e. sets of data: 'st-4' and 'st-5').

From Figure 9-8, the water discharge coefficient $C_{dw,st}$ can be averaged to 0.935. This value of the $C_{dw,st}$ gives a minimum mean value error in the predicted water mass flow rate (see Section 9.5).

The percentage error in the predicted gas and water mass flow rates for different values of the gas and water discharge coefficients, $C_{dg,st}$ and $C_{dw,st}$ are analysed in Section 9.5. Three different values of $C_{dg,st}$ and three different values of $C_{dw,st}$ (including optimum (mean) values of the $C_{dg,st}$ and $C_{dw,st}$ given above) were chosen in which the percentage error in the predicted gas and water mass flow rates were compared for selected values of the $C_{dg,st}$ and $C_{dw,st}$ (see Section 9.5).

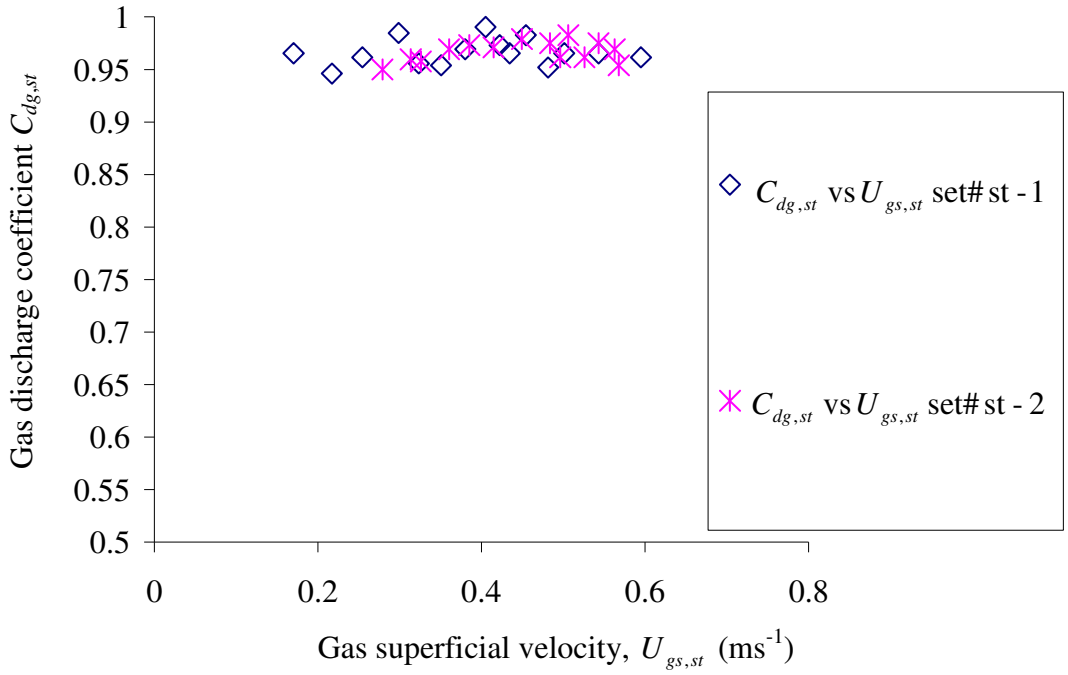

Figure 9-6: Variation $C_{dg,st}$ at fixed values of the water flow rate and varying low gas flow rates (sets of data: 'st-1' and 'st-2', Average value of $C_{dg,st}$ =0.967)

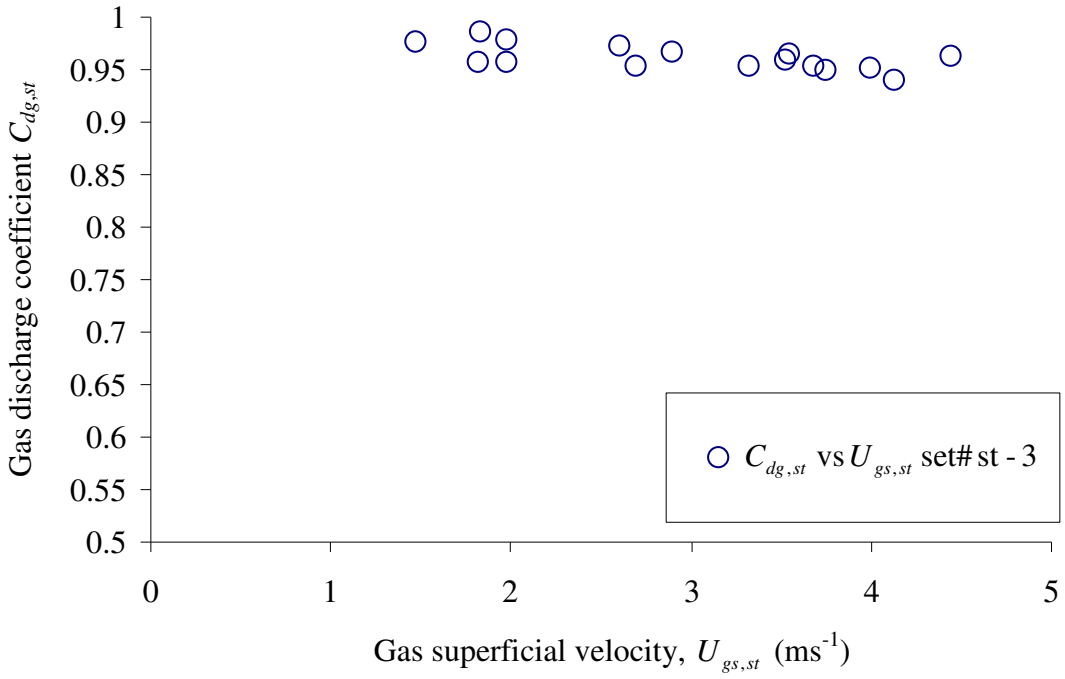

Figure 9-7: Variation of $C_{dg,st}$ at fixed water flow rate and varying high gas flow rates (data set 'st-3', Average value of $C_{dg,st}$ = 0.963)

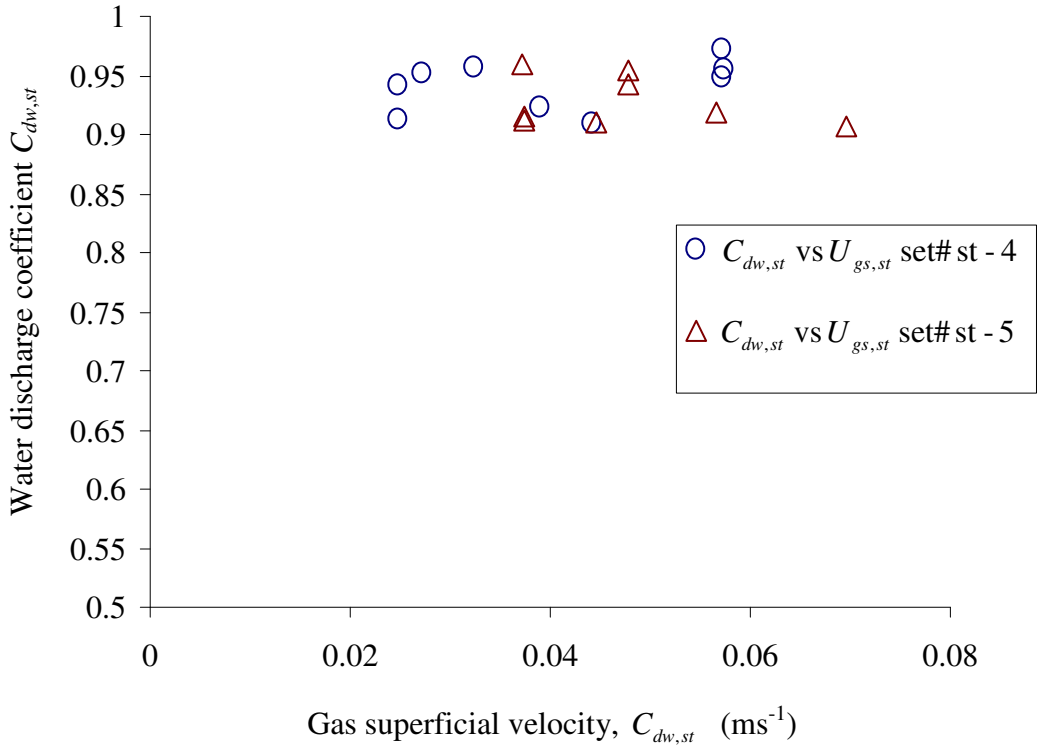

Figure 9-8: Variation of the water discharge coefficient, $C_{dw,st}$ at fixed values of the gas flow rate and varying water flow rates (sets of data: 'st-4' and 'st-5')

9.5 The percentage error in the predicted gas and water mass flow rates in stratified gas-water two phase flows

This section discusses the percentage error in the predicted gas and water mass flow rates for different values of the discharge coefficients. Three different values of $C_{dg,st}$ (i.e. $C_{dg,st} = 0.960, 0.965 \text{ and } 0.970$) and three different values of $C_{dw,st}$ (i.e. $C_{dw,st} = 0.930, 0.935 \text{ and } 0.940$) were chosen. It should be reiterated that the average values (i.e. optimum values) of the $C_{dg,st}$ and $C_{dw,st}$ were 0.965 and 0.935 respectively (see Section 9.4). The reason of choosing different values of $C_{dg,st}$ and $C_{dw,st}$ was to show the sensitivity of errors in the predicted gas and water mass flow rates to selected values of the discharge coefficient. The percentage error in the predicted gas and water mass flow rates, $\varepsilon_{\dot{m}_{g,st}}$ and $\varepsilon_{\dot{m}_{w,st}}$ are given respectively by;

$$\varepsilon_{\dot{m}_{g,st}} = \frac{\dot{m}_{g,st} - \dot{m}_{g,ref,st}}{\dot{m}_{g,ref,st}} \times 100\%$$

Equation (9.3)

and;

$$\varepsilon_{\dot{m}_{w,st}} = \frac{\dot{m}_{w,st} - \dot{m}_{w,ref,st}}{\dot{m}_{w,ref,st}} \times 100\%$$

Equation (9.4)

Figure 9-9 shows the percentage error $\varepsilon_{\dot{m}_{g,st}}$ in the predicted gas mass flow rate (see Equation (9.3)) at fixed values of the water flow rate and varying low gas flow rates (i.e. sets of data: 'st-1' and 'st-2') for $C_{dg,st}$ = 0.960, 0.965, and 0.970.

Figure 9-10 shows the percentage error in the predicted gas mass flow rate $\varepsilon_{\dot{m}_{g,st}}$ at fixed water flow rate and varying high gas flow rates (i.e. data set: 'st-3') for $C_{dg,st}$=0.960, 0.965 and 0.970. The summary of the mean value error in the predicted gas mass flow rate, $\bar{\varepsilon}_{\dot{m}_{g,st}}$ and the standard deviation (*STD*) at different values of the gas discharge coefficient which was obtained from the data reported in Figures 9-9 and 9-10 is given in Table 9-2.

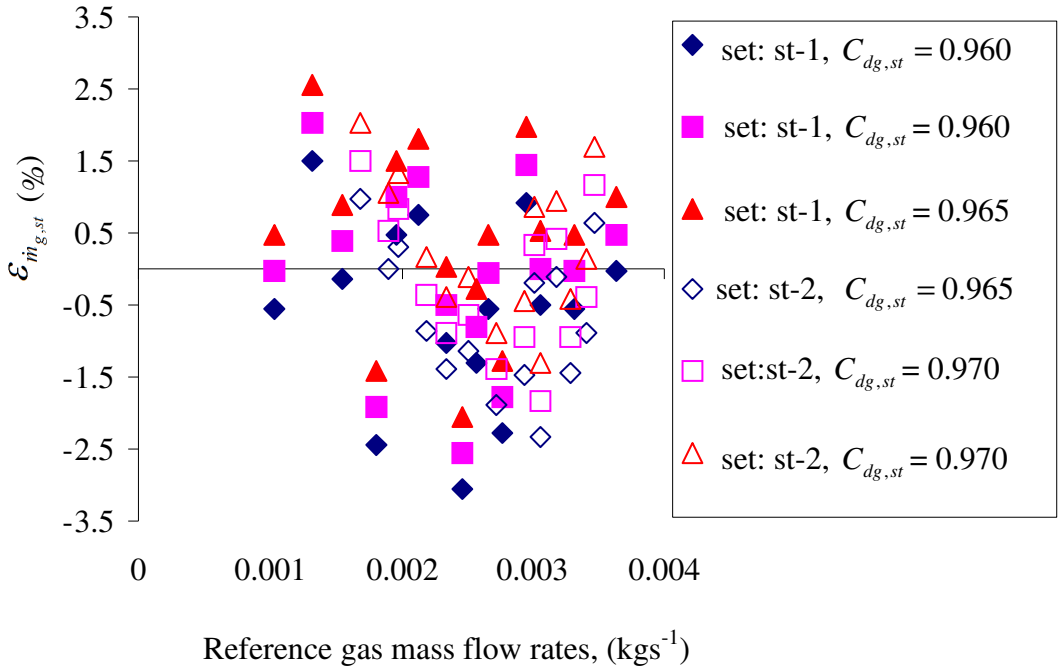

Figure 9-9: The percentage error in the predicted gas mass flow rate at fixed water flow rates and varying low gas flow rates (sets of data: 'st1' and 'st2')

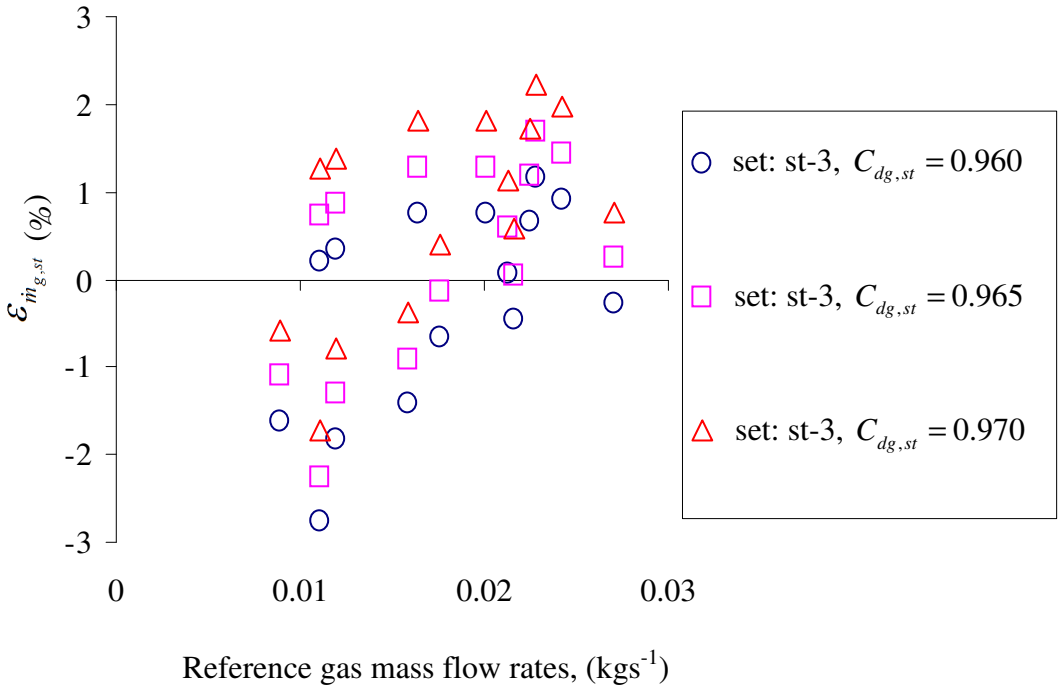

Figure 9-10: The percentage error in the predicted gas mass flow rate at fixed water flow rate and varying high gas flow rates (data set: 'st-3')

Table 9-2: Mean value of percentage error $\bar{\varepsilon}_{\dot{m}_{g,st}}$ and the *STD* of percentage error in the predicted gas mass flow rate for $C_{dg,st}$ = 0.960, 0.965 and 0.970 (at sets of data: 'st-1', 'st-2' and 'st-3')

$C_{dg,st}$	$\bar{\varepsilon}_{\dot{m}_{g,st}}$ (%)	*STD(%)*
0.960	-0.515	1.134
0.965	0.003	1.140
0.970	0.521	1.146

It is clear from Figures 9-9 and 9-10 and also from Table 9-2 that the optimum value of the gas discharge coefficient $C_{dg,st,optimum}$ which gives a minimum value of the $\bar{\varepsilon}_{\dot{m}_{g,st}}$ is 0.965, even with small variations in the standard deviations.

Figure 9-11 shows the percentage error in the predicted water mass flow rate $\varepsilon_{\dot{m}_{w,st}}$ (see Equation (9.4)) at fixed values of the gas flow rate and varying water flow rates (i.e. sets of data: 'st-4' and 'st-5', see Table 9-1) for $C_{dw,st}$ = 0.930, 0.935 and 0.940. Table 9-3 summarises the mean value of the percentage error $\bar{\varepsilon}_{\dot{m}_{w,st}}$ and the standard deviation *STD* of the percentage error in the predicted water mass flow rate that could be obtained from the data reported in Figure 9-11.

Figure 9-11 and Table 9-3 show that a water discharge coefficient $C_{dw,st,optimum}$ = 0.935 gives a minimum value for $\bar{\varepsilon}_{\dot{m}_{w,st}}$ (i.e. the average value of the water discharge coefficient, see Figure 9-8). It should be noted that the value of the water discharge coefficient was affected by the substantial change in the position of the gas-water boundary (interface) from the inlet to the throat of the Venturi (see Section 3.2.1 and Figure 3-4).

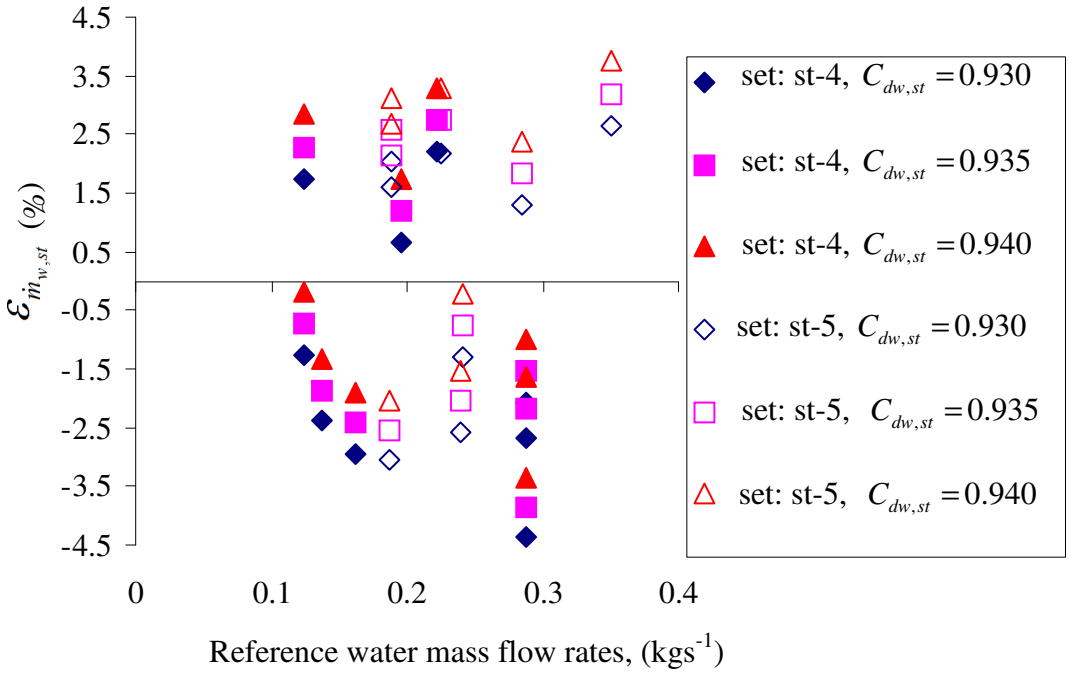

Figure 9-11: The percentage error in the predicted water mass flow rate at fixed values of the gas flow rate (sets of data: 'st-4' and 'st-5')

Table 9-3: Mean value of the percentage error $\bar{\varepsilon}_{\dot{m}_{w,st}}$ and the *STD* of percentage error in the predicted water mass flow rate for $C_{dw,st}$ = 0.930, 0.935, and 0.940 (at sets of data: 'st-4' and 'st-5')

$C_{dwg,st}$	$\bar{\varepsilon}_{\dot{m}_{w,st}}$ (%)	*STD(%)*
0.930	-0.486	2.281
0.935	0.049	2.294
0.940	0.584	2.306

At the end of this section, it can be concluded that, based on the results described in this section, the performance of the novel conductance multiphase flow meter, was very good and can be relied upon in stratified two phase flow applications. Although, the conductance multiphase flow meter was tested under a maximum absolute pressure of about 103 KPa (measured at the inlet of the Venturi using the gauge

pressure sensor and the barometer, see Section 6.2.7), the conductance multiphase flow meter in conjunction with the horizontal stratified flow model described in Section 3.2.1 can still be used under very high pressure conditions.

Unlike the previous correlations described in Section 2.2, the new stratified flow model (see Section 3.2.1) does not require prior knowledge of the mass flow quality *x* but depends on the measurement of the gas volume fraction at the inlet and the throat of the Venturi which makes the measurement technique described in this thesis more practical.

9.6 Analysis of the actual velocity at the inlet and the throat of the Venturi in stratified gas-water two phase flows

Once the gas and the water mass flow rates were determined using Equations (3.43) and (3.59) the actual gas and water velocities $U_{g1,st}$, $U_{g2,st}$, $U_{w1,st}$ and $U_{w2,st}$ at the inlet and the throat of the Venturi can be determined. The actual gas and water velocities $U_{g1,st}$, $U_{g2,st}$, $U_{w1,st}$ and $U_{w2,st}$ at the inlet and the throat of the Venturi can be respectively expressed as;

$$U_{g1,st} = \frac{\dot{m}_{g,st}}{A_1 \alpha_{1,st} \rho_{g1}}$$

Equation (9.5)

and [by combining Equations (3.34) and (3.36)];

$$U_{g2,st} = \frac{\dot{m}_{g,st}}{A_2 \alpha_{2,st} \rho_{g2}} = \frac{\dot{m}_{g,st}}{A_2 \alpha_{2,st} \rho_{g1} (\hat{P})^{1/\gamma}}$$

Equation (9.6)

and;

$$U_{w1,st} = \frac{\dot{m}_{w,st}}{(1-\alpha_{1,st}) A_1 \rho_w}$$

Equation (9.7)

and;

$$U_{w2,st} = \frac{\dot{m}_{w,st}}{(1-\alpha_{2,st})A_2\rho_w}$$

Equation (9.8)

The subscript '*st*' is added to distinguish between stratified flows and other flow regimes.

It should be noted that $\dot{m}_{g,st}$ and $\dot{m}_{w,st}$ in Equations (9.5) to (9.8) are determined using the optimum (mean) values of the gas and the water discharge coefficients (i.e. $C_{dg,st} = 0.965$ and $C_{wg,st} = 0.935$ respectively).

Figure 9-12 shows the variation of the actual gas and water velocities at fixed values of the water flow rate and varying low gas flow rates (sets of data: 'st-1' and 'st-2'). Figure 9-13 shows the variations of $U_{g1,st}$, $U_{g2,st}$, $U_{w1,st}$ and $U_{w2,st}$ with the $U_{gs,st}$ at fixed water flow rate and varying high gas flow rates (i.e. data set: 'st-3'). It can be seen from Figures 9-12 and 9-13 that the velocity at the throat is greater than the velocity at the inlet. This is because the fluid entering the Venturi is accelerated to a higher velocity as the flow area is decreased. In other words, at the throat, the pressure decreases to a minimum where the velocity increases to a maximum. (i.e. Bernoulli equation). It is also clear from Figures 9-12 and 9-13 that the variations in the actual water velocities at the inlet and the throat of the Venturi were smaller than the variations in the actual gas velocities (note that, data set 'st-1' and data set 'st-2' were taken under constant values of the water superficial velocity). Therefore, at fixed values of the water flow rate and varying low and high gas flow rates (i.e. sets of data: 'st-1', 'st-2' and 'st-3'), the effect of increasing the gas superficial velocity $U_{gs,st}$ on the water velocity was very small. In other words, the values of $U_{w1,st}$ and $U_{w2,st}$ seem to be independent of $U_{gs,st}$.

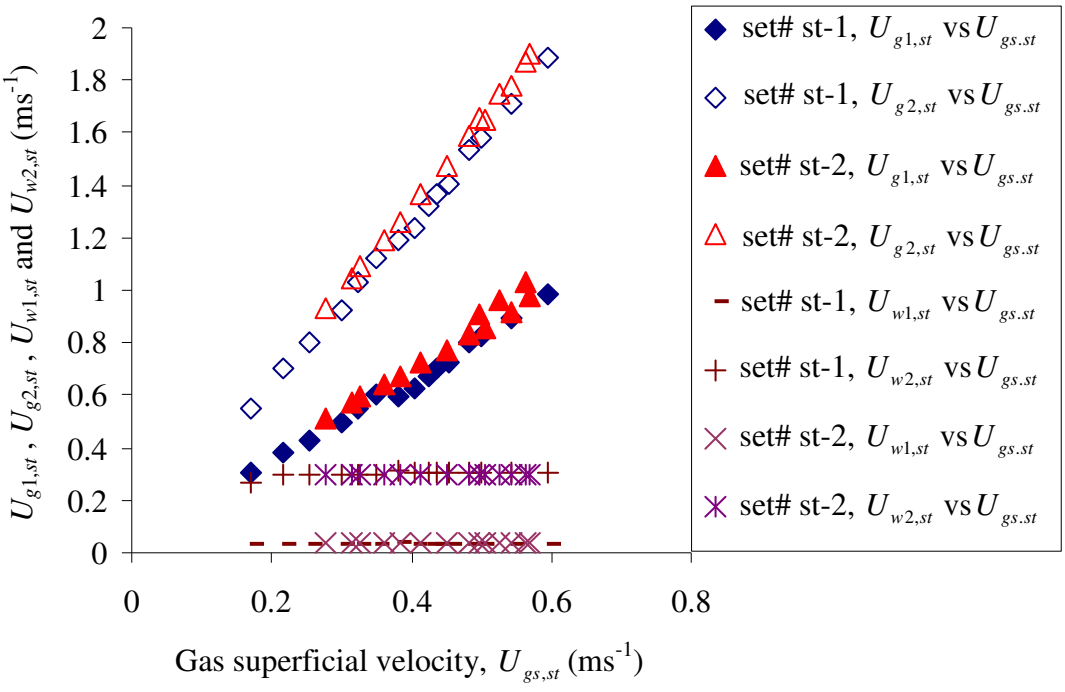

Figure 9-12: Actual gas and water velocities at fixed values of the water flow rate and varying low gas flow rates (sets of data: 'st-1' and 'st-2')

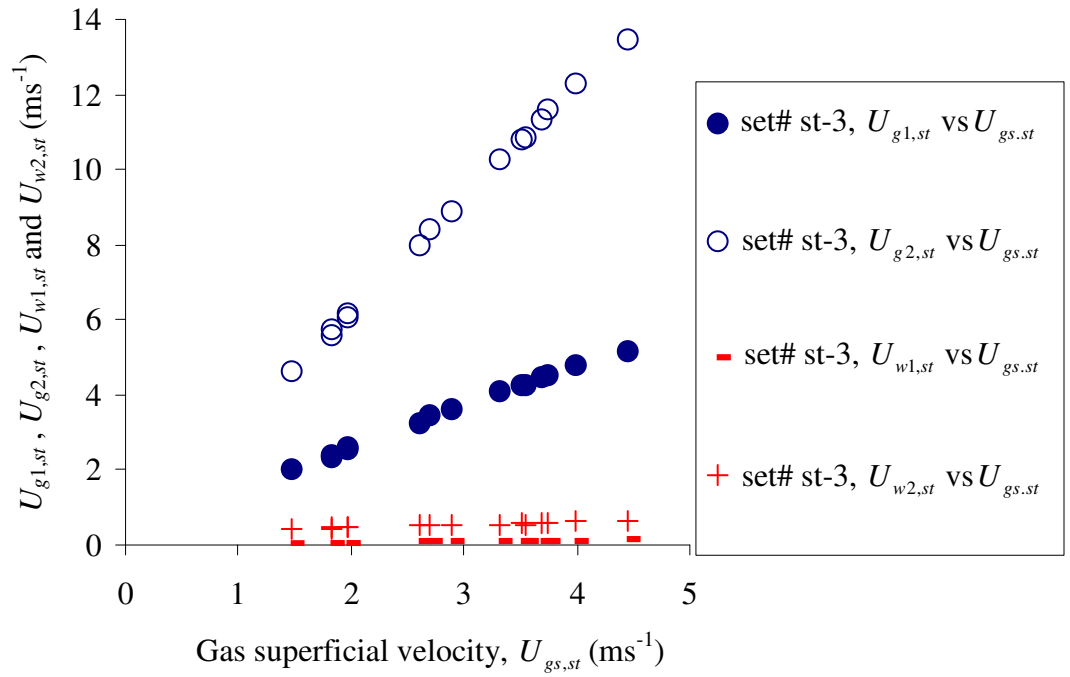

Figure 9-13: Actual gas and water velocities at fixed water flow rate and varying high gas flow rates (data set: 'st-3')

Figure 9-14 shows the variations of $U_{g1,st}$, $U_{g2,st}$, $U_{w1,st}$ and $U_{w2,st}$ with the water superficial velocity, $U_{ws,st}$ at fixed values of the gas flow rate and varying water flow rates (i.e. sets of data: 'st-4' and 'st-5', see Table 9-1). It is seen that $U_{g1,st}$ and $U_{g2,st}$ are strongly dependent on $U_{ws,st}$. In other words, the effect of increasing $U_{ws,st}$ on $U_{g1,st}$ and $U_{g2,st}$ was very obvious. The reason of this might come from the fact that the water is an incompressible phase while the gas phase is compressible. Due to the difference in densities between the water and the gas phases in stratified flows, the gas phase is likely to move faster than the water phase. In addition, the effect of substantial change in the position of the gas-water boundary from the inlet to the throat of the Venturi (see Section 3.2.1 and Figure 3-4) on the gas phase (i.e. on the gas velocity) would be expected to be greater than that would occur for the water phase.

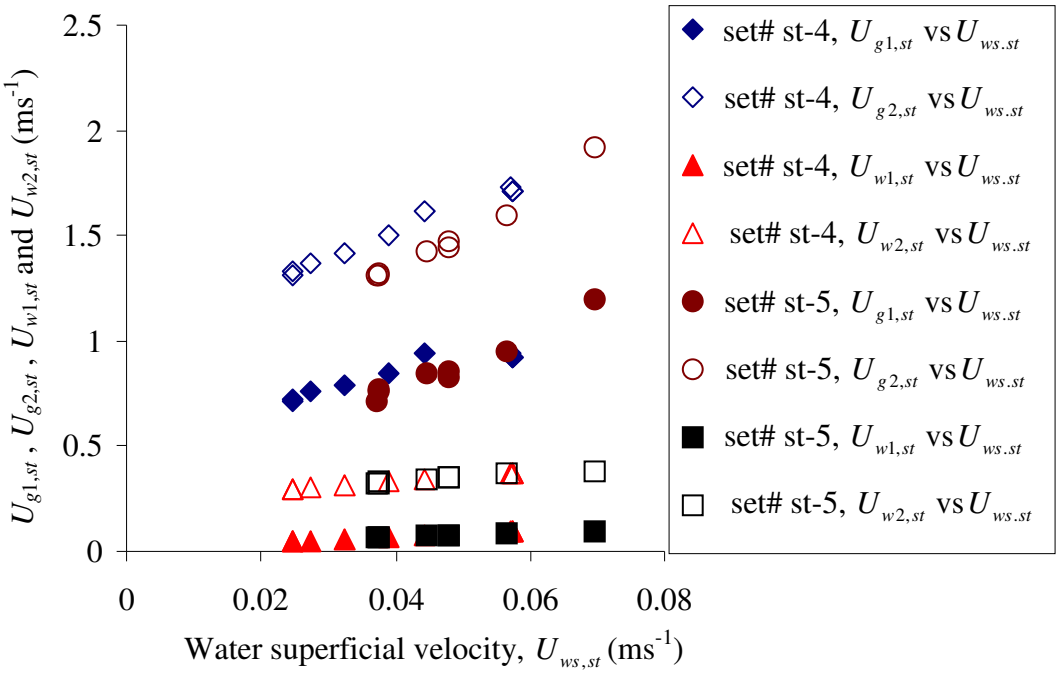

Figure 9-14: Actual gas and water velocities at fixed values of the gas flow rate and varying water flow rates (sets of data: 'st-4' and 'st-5')

9.7 Slip ratio (velocity ratio) at the inlet and the throat of the Venturi

Slip ratio in two phase flow, which is defined as the ratio of the gas velocity to the water velocity, is an important parameter affecting the stability of the flow system. Bankoff (1960) [157] and Thang (1976) [33] proposed that the phase slip in bubbly two phase flow was entirely a result of the non-uniform distribution of both phases and the effect of the local relative velocity between the gas and the liquid phases that may be caused by buoyancy and flow acceleration.

As mentioned earlier, most of the studies conducted in stratified two phase flows using Venturi meters depend on prior knowledge of the mass flow quality x and the over-reading factor $O.R$ (see Chapter 2). Unlike the previous work, the new measurement technique (and also the novel separated flow model, see Chapter 3) described in this thesis depends on the measurement of the gas volume fraction at the inlet and the throat of the Venturi. Therefore, very limited, if any, data is available in the literature with which the current results can be compared.

The slip ratio at the inlet and the throat of the Venturi were mathematically defined by Equations (3.60) and (3.61) as;

$$S_{1,st} = \frac{U_{g1,st}}{U_{w1,st}}$$

Equation (9.9)

and;

$$S_{2,st} = \frac{U_{g2,st}}{U_{w2,st}}$$

Equation (9.10)

where the subscript '*st*' refers to the stratified gas-water two phase flow through a Venturi meter.

Figure 9-15 shows the relationship between the slip ratio ($S_{1,st}$ and $S_{2,st}$) and the gas superficial velocity $U_{gs,st}$ at fixed values of the water flow rate and varying low gas flow rates (i.e. sets of data: 'st-1' and 'st-2'). Figure 9-16 shows the variation of the slip ratio (velocity ratio) $S_{1,st}$ and $S_{2,st}$ with the gas superficial velocity at fixed water flow rate and varying high gas flow rates (data set: 'st-3'). The slip ratio $S_{1,st}$ and $S_{2,st}$ at the inlet and the throat of the Venturi at fixed values of the gas flow rate and varying water flow rates (i.e. sets of data: 'st-4' and 'st-5') is shown in Figure 9-17.

It was inferred from Figures 9-15 to 9-17 that the slip ratio $S_{1,st}$ at the inlet is greater than the slip ratio $S_{2,st}$ at the throat of the Venturi. The effect of the substantial change in the position of the gas-water boundary from the inlet to the throat of the Venturi (see Section 3.2.1 and Figure 3-4) might contribute in this reduction of the slip ratios between the inlet and the throat of the Venturi.

Thang (1976) [33] who studied the Venturi in bubbly two phase flows concluded that, at higher void fraction, the slip ratios were found to decrease between the inlet and the throat of the Venturi. He justified this by the effect of gas expansion at the throat of the Venturi which accelerated the liquid phase and thus reduced the relative velocity with an increasing turbulent mixing. He stated that a clear reduction of slip ratio between the inlet and the throat of the Venturi might also be due to the length of the converging channel which prompted more mixing in the flow. He also showed that at lower void fraction, the trend in the slip ratio was reversed between the throat and the inlet (i.e. $S_{2,st} > S_{1,st}$).

Due to the lack of adequate information in the literature on slip ratios between the inlet and the throat of the Venturi in stratified two phase flows, the effect of the slip ratios in separated two phase flows using Venturi meters needs further study and research.

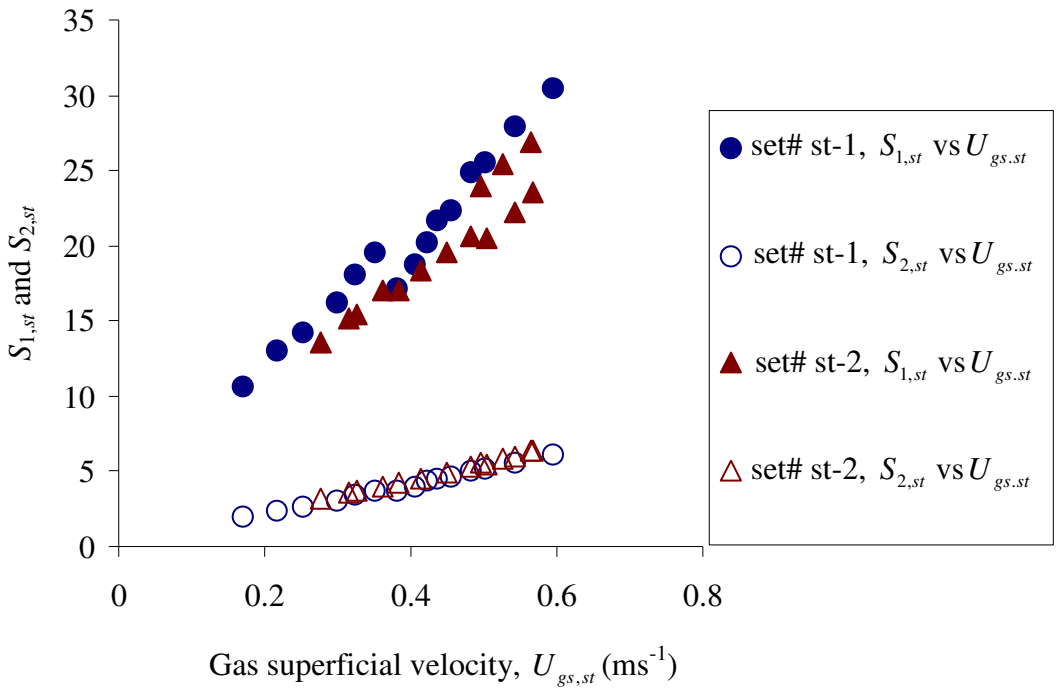

Figure 9-15: Variation of $S_{1,st}$ and $S_{2,st}$ with the gas superficial velocity at fixed values of the water flow rate and varying low gas flow rates (sets: st-1 and st-2)

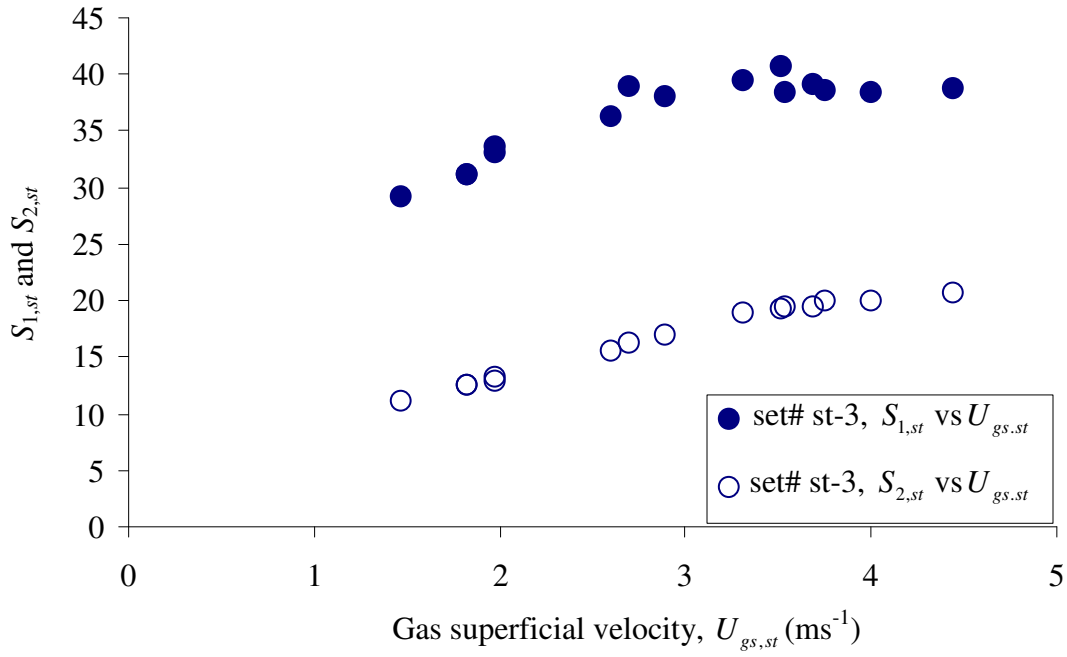

Figure 9-16: Variation of $S_{1,st}$ and $S_{2,st}$ with the gas superficial velocity at fixed water flow rate and varying high gas flow rates (data set: 'st-3')

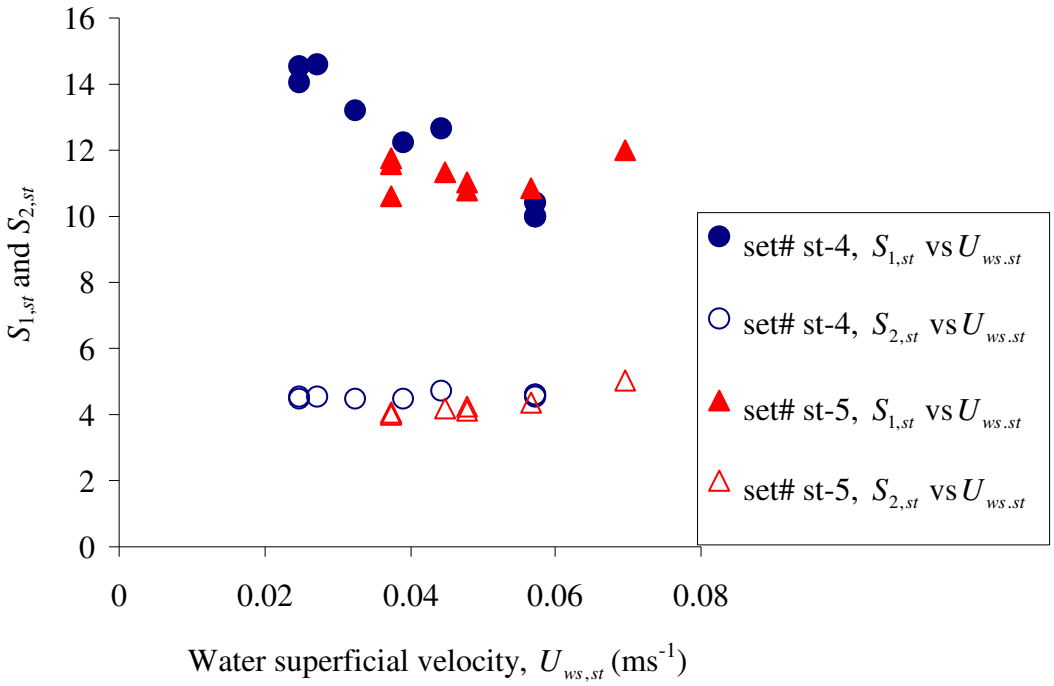

Figure 9-17: Variation of $S_{1,st}$ and $S_{2,st}$ with the water superficial velocity at fixed values of the gas flow rates and varying water flow rates (sets: 'st-4' and s't-5')

Summary

The experimental results for stratified gas-water two phase flows through a conductance multiphase flow meter were discussed in this chapter. Five sets of data were tested (see Table 9-1). It was observed from the analysis of the gas volume fraction at the inlet and the throat of the Venturi that the gas volume fraction $\alpha_{2,st}$ (obtained from the two electrodes at the throat section of the CMVM) was higher than the inlet gas volume fraction $\alpha_{1,st}$ (obtained from the two electrodes at the CIVFM).

The gas and the water discharge coefficients $C_{dg,st}$ and $C_{wg,st}$ were discussed in Section 9.4. It was inferred from the analysis of the gas and water discharge coefficients in stratified gas-water two phase flows that the gas discharge coefficient $C_{dg,st}$ can be averaged to 0.965 while the average value of the $C_{wg,st}$ was 0.935. These are the optimum values of the gas and water discharge coefficient in which the minimum mean value error in the predicted gas and water mass flow rates $\bar{\varepsilon}_{\dot{m}_{g,st}}$ and $\bar{\varepsilon}_{\dot{m}_{w,st}}$ was obtained.

The percentage error in the predicted gas and water mass flow rates, $\varepsilon_{\dot{m}_{g,st}}$ and $\varepsilon_{\dot{m}_{w,st}}$ (see Equations (9.3) and (9.4)) for different values of $C_{dg,st}$ and $C_{wg,st}$ were obtained and tabulated in Tables 9-2 and 9-3. It was found that the minimum value of the $\bar{\varepsilon}_{\dot{m}_{g,st}}$ and $\bar{\varepsilon}_{\dot{m}_{w,st}}$ were achieved for $C_{dg,st} = 0.965$ and $C_{wg,st} = 0.935$ respectively.

The slip ratio (velocity ratio) at the inlet and the throat of the Venturi was analysed in Section 9.7. It was seen that the slip ratio $S_{1,st}$ at the inlet of the Venturi was always greater than the slip ratio $S_{2,st}$ at the throat of the Venturi meter.

The major advantage of the new model described in this research over the previous correlations (see Chapter 2) is that the new model does not require prior knowledge of the mass flow quality, x which makes the measurements more practical since an

online measurement of the mass flow quality is difficult and not practical in nearly all multiphase flow applications. The novel model is based on the measurement of the gas volume fractions at the inlet and the throat of the Venturi (see Section 3.2).

Chapter 10

Conclusions

10.1 Conclusions

The work in this thesis has been focused on the development of new solutions for non-invasive multiphase flow rate measurement by developing a novel conductance multiphase flow meter which is capable of measuring the gas and the water flow rates in vertical annular (wet gas) and horizontal stratified gas-water two phase flows. The conductance multiphase flow meter consists of the Conductance Inlet Void Fraction Meter (CIVFM), with two ring electrodes flush mounted with the inner surface of the pipe, which is capable of measuring the gas volume fraction at the inlet of the Venturi and the Conductance Multiphase Venturi Meter (CMVM), with two ring electrodes flush mounted with the inner surface of the throat section, which is capable of measuring the gas volume fraction at the throat of the Venturi meter.

In bubbly gas-water two phase flows, the Universal Venturi Tube, UVT (i.e. non conductance Venturi meter, see Section 4.2) was used in conjunction with the flow density meter (which was used to measure the gas volume fraction $\alpha_{1,\text{hom}}$ at the inlet of the UVT, see Section 4.1) to study the bubbly (approximately homogenous) gas-water two phase flows. Measurement of $\alpha_{1,\text{hom}}$ enabled the mixture volumetric flow rate $Q_{m,\text{hom}}$ to be determined (see Equation (3.9)).

It was inferred from the experimental results obtained for bubbly gas-water two phase flows that the minimum mean value error in the predicted mixture volumetric flow rate could be achieved when the mixture discharge coefficient $C_{d,\text{hom}}$ was 0.948 (see Section 7.5). The mean value of the percentage error in the predicted mixture

volumetric flow rate, $\bar{\varepsilon}_{Q_{m,\text{hom}}}$ at $C_{d,\text{hom}} = 0.948$ was -0.015%. Three different values of $C_{d,\text{hom}}$ were chosen in order to show the sensitivity of errors in the predicted mixture volumetric flow rate to selected values of the discharge coefficient $C_{d,\text{hom}}$. This is reported in Table 10-1 below (see also Section 7.5).

Table 10-1: Summary of the $\bar{\varepsilon}_{Q_{m,\text{hom}}}$ for different values of $C_{d,\text{hom}}$

$C_{d,\text{hom}}$	$\bar{\varepsilon}_{Q_{m,\text{hom}}}$ (%)
0.940	-0.858
0.948	-0.015
0.950	0.196

It is clear from Table 10-1 that the minimum value of $\bar{\varepsilon}_{Q_{m,\text{hom}}}$ can be achieved at $C_{d,\text{hom}} = 0.948$. Note that, this value of $C_{d,\text{hom}}$ represents the average value for all flow conditions.

It was also inferred from the experimental results obtained in bubbly (approximately homogenous) gas-water two phase flows, see Chapter 7, that the homogenous flow model described in Chapter 3 started to break down when the gas volume fraction $\alpha_{1,\text{hom}}$ at the inlet of the Venturi (obtained from the flow density meter, see Section 4.1) increased above 17.48%. This was due to the onset of the slug regime where the transition from bubbly-to-slug flow regime occurred. It should be reiterated that the gas volume fraction $\alpha_{1,\text{hom}}$ in bubbly (approximately homogenous) gas-water two phase flows was assumed to be constant throughout the universal Venturi tube.

Separated flow in a Venturi meter is highly complex (where the velocity ratio, S≠1) and the application of a homogenous flow model could not reasonably be expected to lead to highly accurate results. In other words, the gas volume fraction at the inlet is

not the same as that at the throat of the Venturi. Therefore, the gas volume fraction measurement technique at the throat must also be introduced instead of just relying on the gas volume fraction measurement at the inlet of the Venturi. As a result, a novel conductance multiphase flow meter was designed and manufactured (see Chapter 4). A new separated (vertical annular and horizontal stratified) gas-water two phase flow model was also investigated (see Chapter 3). Unlike the previous models available in the literature, the new model depends on the measurement of the gas volume fraction at the inlet and the throat of the Venturi instead of prior knowledge of the mass flow quality as in the previous models. This makes the measurement techniques (including the new model) more practical since the online measurement of the mass flow quality is difficult and not practical in nearly all multiphase flow applications.

The experimental results for the vertical annular (wet gas) flows (see Chapter 8) showed that the minimum average percentage error $\bar{\varepsilon}_{\dot{m}_{g,wg}}$ in the predicted gas mass flow rate, which was -0.043%, could be obtained at the gas discharge coefficient $C_{dg,wg} = 0.932$ (see Table 10-2). This value of the gas discharge coefficient, which represents the optimum value, was the average value of $C_{dg,wg}$ for all flow conditions in vertical annular flow.

Table 10-2: Summary of $\bar{\varepsilon}_{\dot{m}_{g,wg}}$ with different values of $C_{dg,wg}$ in annular (wet gas) flows

$C_{dg,wg}$	$\bar{\varepsilon}_{\dot{m}_{g,wg}}$ (%)
0.920	-1.330
0.932	-0.043
0.933	0.064

The percentage error in the predicted water mass flow rate in annular (wet gas) flows was larger than expected (>±10%). This was due to the pulsation that was occurred in the liquid film and also due to the fact that the water droplets mass flow rate at the gas core was not considered in the separated flow model described in Section 3.2.

Therefore, an alternative method was used to measure the water mass flow rate in vertical annular two phase flows using the wall conductance sensors described in Chapter 4. The data obtained from the wall conductance sensors (i.e. the volume fraction of the liquid droplets in the gas core) was used in conjunction with the data obtained from the conductance multiphase flow meter to modify the predicted water mass flow rate $\dot{m}_{w,wg}$. The mean percentage error $\bar{\varepsilon}_{\dot{m}_{total,wg}}$ in the predicted total water mass flow rate, which was determined using $C_{dw,wg}$ =0.995, was 0.550%.

The experimental results for horizontal stratified gas-water two phase flows (see Chapter 9) showed that the minimum mean percentage error $\bar{\varepsilon}_{\dot{m}_{g,st}}$ in the predicted gas mass flow rate can be attained when the gas discharge coefficient, $C_{dg,st} = 0.965$. Again, this value of the gas discharge coefficient represents the average value for all flow conditions. The summary of $\bar{\varepsilon}_{\dot{m}_{g,st}}$ at different values of $C_{dg,st}$ is given in table 10-3 (see Section 9.5).

Table 10-3: Summary of the $\bar{\varepsilon}_{\dot{m}_{g,st}}$ for different values of $C_{dg,st}$

$C_{dg,st}$	$\bar{\varepsilon}_{\dot{m}_{g,st}}$ (%)
0.960	-0.515
0.965	0.003
0.970	0.521

The mean percentage error in the predicted water mass flow rate in horizontal stratified gas-water two phase flows is summarised in Table 10-4.

Table 10-4: Summary of the $\bar{\varepsilon}_{\dot{m}_{g,st}}$ for different values of $C_{dg,st}$

$C_{dwg,st}$	$\bar{\varepsilon}_{\dot{m}_{w,st}}$ (%)
0.930	-0.486
0.935	0.049
0.940	0.584

It is clear from Table 10-4 that the minimum average value of $\bar{\varepsilon}_{\dot{m}_{g,st}}$ is achieved at $C_{dwg,st} = 0.935$ (optimum value of the water discharge coefficient which was calculated from averaging the values of the water discharge coefficient for all flow conditions). An estimated error in the predicted water mass flow rate for horizontal stratified two phase flows at an optimum value of the water discharge coefficient (i.e. $C_{dwg,st} = 0.935$) was found to be scattered randomly between +3.19% and - 3.86%.

10.2 Present contribution

The contribution made to knowledge by this thesis includes:

- A separated flow model to measure the gas and the water mass flow rates in horizontal stratified gas-water two phase flows.

- A separated flow model to measure the gas and the water flow rates in vertical annular (wet gas) flows.

- Designing a novel conductance inlet void fraction meter (CIVFM) which is capable of measuring the gas volume fraction at the inlet of the Venturi (or at any other straight pipe section).

- Designing a novel conductance multiphase Venturi meter (CMVM) which is capable of measuring the gas volume fraction at the throat of the Venturi.

- The work has resulted in a novel combination of online measurement techniques (i.e. CIVFM and CMVM) to measure the gas and liquid flow rates in annular (wet gas) flows and horizontal stratified gas-water two phase flows.

Chapter 11

Further work

In this chapter, suggestions and recommendations are given for further work on measuring gas-water two phase flows using the conductance multiphase flow meter which consists of the Conductance Inlet Void Fraction Meter (CIVFM) and the Conductance Multiphase Venturi Meter (CMVM). The recommendations and suggestions for further work are divided into sections and sub-sections as follows;

11.1 Water-gas-oil three phase flow meter

The experimental work described in this thesis has focused on gas-water two phase flows. Further work would be required to develop a three phase flow meter (i.e. oil-water-gas). A sensor tube is proposed (see Section 11.1.1).

11.1.1 A bleed sensor tube

The conductance techniques described in this thesis could also be applied to water-gas-oil 3 phase flows, provided that water forms the continuous phase in the liquid film. This can be done using an on-line sampling system (a sensor tube) whereby part of the liquid film (oil and water) is periodically extracted into a vertical tube (see Figure 11-1). A density meter, based on the differential pressure measurement technique (see Sections 2.1.1.1 and 3.1), is then used to measure the liquid density, prior to the liquid being released back in to the main flow line. The liquid density measurement enables the oil and water volume fractions in the liquid to be measured. This sampling technique is only applicable to annular oil-water-gas three phase flows.

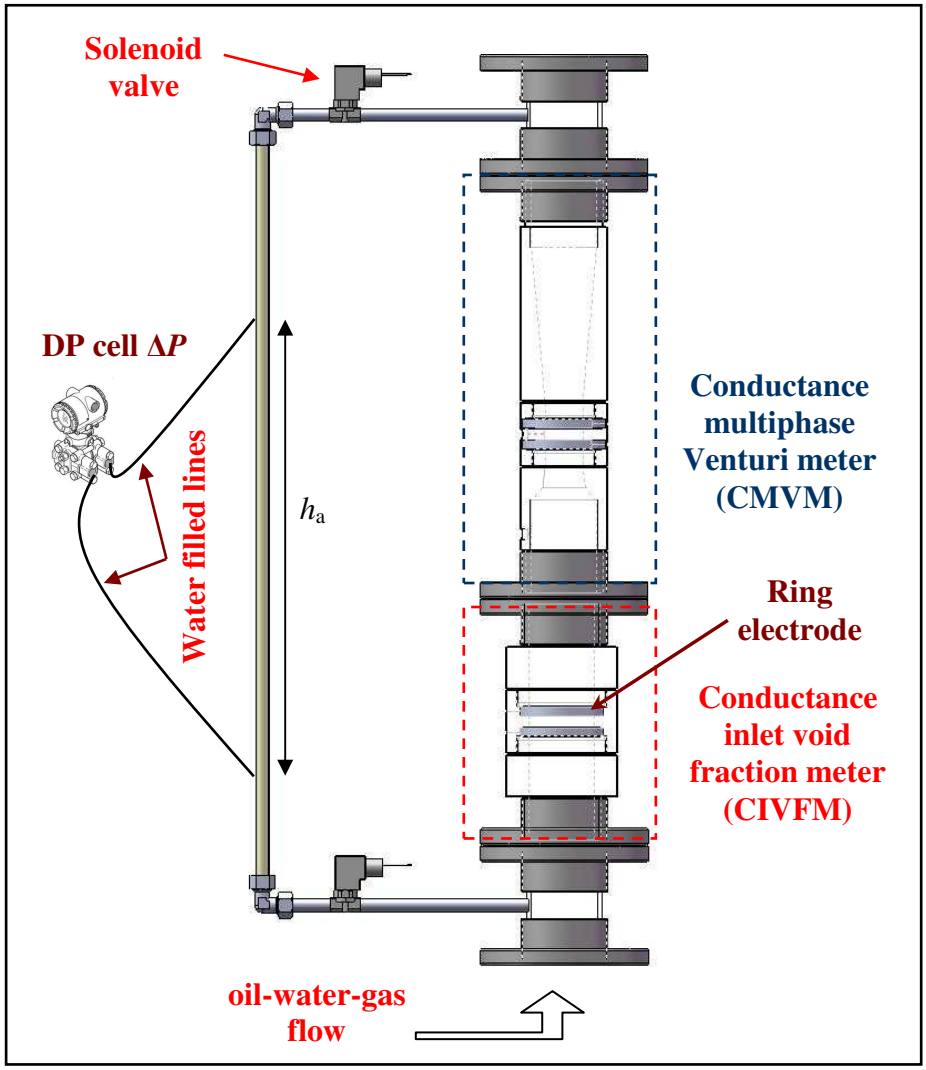

Figure 11-1: An on-line sampling system (bleeding sensor tube)

With reference to Figure 11-1 (assuming *that the differential pressure sensor is connected to the tappings via water filled lines*), the density $\rho_{o,w}$ of the oil and water mixture can be calculated using;

$$\Delta P = \rho_w \, g \, h_a \, - \rho_{o,w} \, g \, h_a$$

Equation (11.1)

where ΔP is the pressure drop across the vertical sensor tube, $\rho_{o,w}$ is the mixture (oil and water) density, ρ_w is the water density, g is the acceleration of the gravity and h_a is the pressure tapping separation.

Re-arranging Equation (11.1) gives;

$$\rho_{o,w} = \rho_w - \left\{ \frac{\Delta P}{g h_a} \right\}$$

Equation (11.2)

It is well known that;

$$\rho_{o,w} = \alpha_{o,f} \rho_o + \alpha_{w,f} \rho_w$$

Equation (11.3)

where $\alpha_{o,f}$ and $\alpha_{w,f}$ are the volume fractions of the oil and water in the liquid film respectively and ρ_o is the oil density.

It is also known that;

$$\alpha_{o,f} + \alpha_{w,f} = \alpha_f = 1$$

Equation (11.4)

where α_f is the liquid (oil and water) volume fraction in the film.

Combining Equations (11.2) to (11.4) enables the oil and the water volume fractions $\alpha_{o,f}$ and $\alpha_{w,f}$ in the liquid film to be determined. It should be noted that the values of $\alpha_{o,f}$ and $\alpha_{w,f}$ are also likely to be the correct values for the oil and water volume fractions in the gas core.

The overall oil, gas and water volume fractions in a pipe can be expressed as;

$$\alpha_o + \alpha_w + \alpha_g = 1$$

Equation (11.5)

where α_g is the gas volume fraction.

The overall oil and water volume fractions in Equation (11.5) are respectively given by;

$$\alpha_o = \alpha_{o,f}\ \alpha_f$$

Equation (11.6)

and;

$$\alpha_w = \alpha_{w,f}\ \alpha_f$$

Equation (11.7)

Once the gas volume fraction α_f of the oil-water mixture in the liquid film is obtained from a sensor tube, the mixture (liquid film) conductivity σ_m can be easily determined using the Maxwell equation. Therefore;

$$\sigma_m = \sigma_w \frac{2 - 2\alpha_f}{2 + \alpha_f}$$

Equation (11.8)

where σ_w is the water conductivity.

Once the conductivity σ_m of the oil-water mixture in the liquid film is obtained, the calibration curves of the CIVFM and the CMVM (which relates the gas volume fractions to the output voltages obtained from the conductance electronic circuit, see Chapter 5) can then be modified to account for the actual liquid mixture conductivity, calculated from the sensor tube and the water conductivity which is also measured on-line. This can be done as follow,

It is well known that the conductance of the mixture S_m is given by;

$$S_m = K\sigma_m$$

Equation (11.9)

where K is the cell constant and σ_m is conductivity of the mixture in the liquid film (**Note that**, if the water is only present in the liquid film then the conductivity of the mixture σ_m in Equation (11.9) is equal to the conductivity of the water, σ_w).

If the water is only present in the liquid film then, the output voltage V_w from the conductance electronic circuit described in Section 4.5 is given by;

$$V_w = K_a S_m$$

Equation (11.10)

where K_a is the conductance circuit gain.

Substituting Equations (11.9) into (11.10) gives;

$$V_w = K_a K(\alpha_g)\sigma_w$$

Equation (11.11)

The term (α_g) is added in Equation (11.11) just to show that K is a function of the gas volume fraction α_g.

Equation (11.11) is used when the liquid film contains water only. Equation (11.11) can be re-written as;

$$K(\alpha_g) = \frac{V_m}{\sigma_w K_a}$$

Equation (11.12)

where σ_w is the water conductivity.

From equation (11.12), it is possible to plot $K(\alpha_g)$ vs α_g and obtain a relationship between α_g and $K(\alpha_g)$.

If the, water continuous, oil-water mixture presents in the liquid film, the output voltage V_m from the conductance circuit is given by;

$$V_m = K_a K(\alpha_g)\sigma_m$$

Equation (11.13)

Re-arranging Equation (11.3) gives;

$$K(\alpha_g) = \frac{V_m}{K_a \sigma_m}$$

Equation (11.14)

Since the relationship between $K(\alpha_g)$ and α_g when only water is present in the liquid film is known, the gas volume fraction, when the oil-water mixture is present in the liquid film, can be obtained using Equation (11.14).

11.2 Segmental conductive ring electrodes

In order to make the conductance multiphase flow meter (CIVFM and CMVM) independent of the probe calibration in stratified gas-water two phase flows, the ring electrodes at the inlet and the throat of the Venturi (see Figures 4-7 and 4-9) can be replaced by segmental conductive ring electrodes, SCREs (see Figure11-2). The segmental electrodes act as on-off switches and they are independent on temperature and salinity of the water. Each electrode is connected to an electronic circuit. When the water flows through the SCREs, the electrodes that are in contact with the water will be active in which the output voltage from the corresponding electronic circuits can be recorded. This enables the water level to be measured. Measurement of the water level in stratified gas-water two phase flows enables the gas volume fraction to be determined using Equation (5.8). The advantage of using SCREs over the conductance ring electrodes described in Section 4.3, is that the SCREs do not need a calibration. Further work should be continued using this type of electrodes.

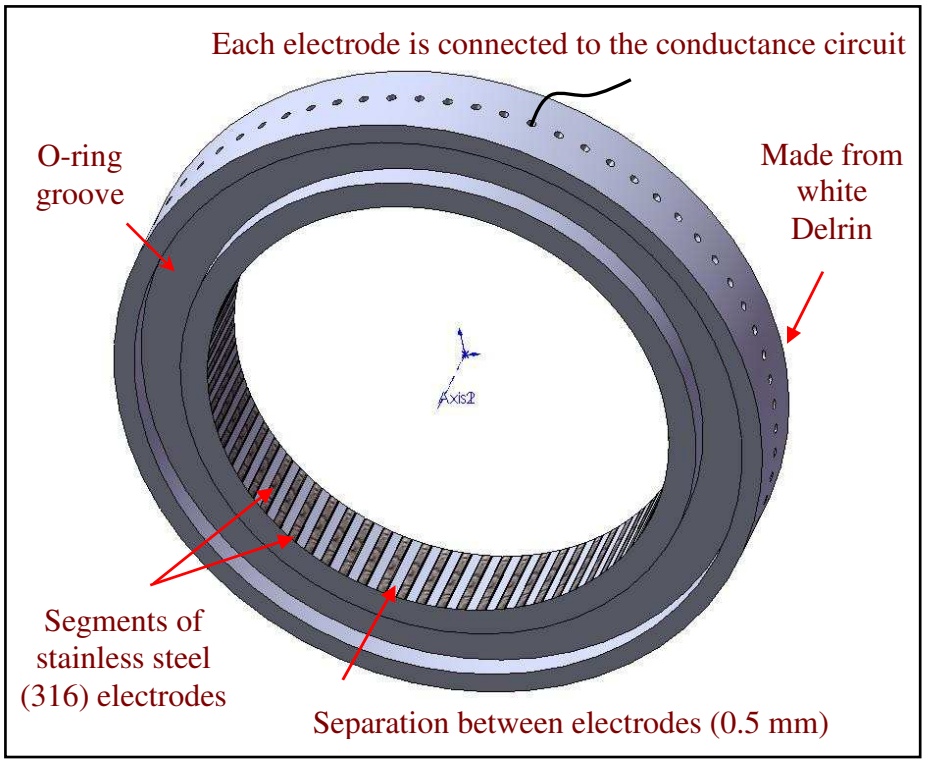

Figure 11-2: Segmental conductive ring electrode

11.3 Digital liquid film level sensor

In annular gas-water two phase flows, a digital liquid film level sensor (DLFLS) could be designed to measure the liquid film thickness and hence the gas volume fraction at the inlet and the throat of the Venturi. The DLFLS consists of sensitive and insensitive regions as shown in Figure 11-3. Each probe is connected to an electronic circuit via insulating wire in insensitive region as shown in Figure (11-4). The separation between each probe could be less than 1 mm (or could need to be less than 0.5 mm). The basic principle of the DLFLS is that the probes which are in contact with the liquid (providing that the water is a continuous phase in the liquid film) will be 'ON' while other probes will be 'OFF'. Therefore the probes in the DLFLS act as on-off switches and the output voltages from the corresponding circuits are proportional to the liquid film thickness in annular two phase or even three phase flows (providing that the water is the continuous phase in the liquid film).

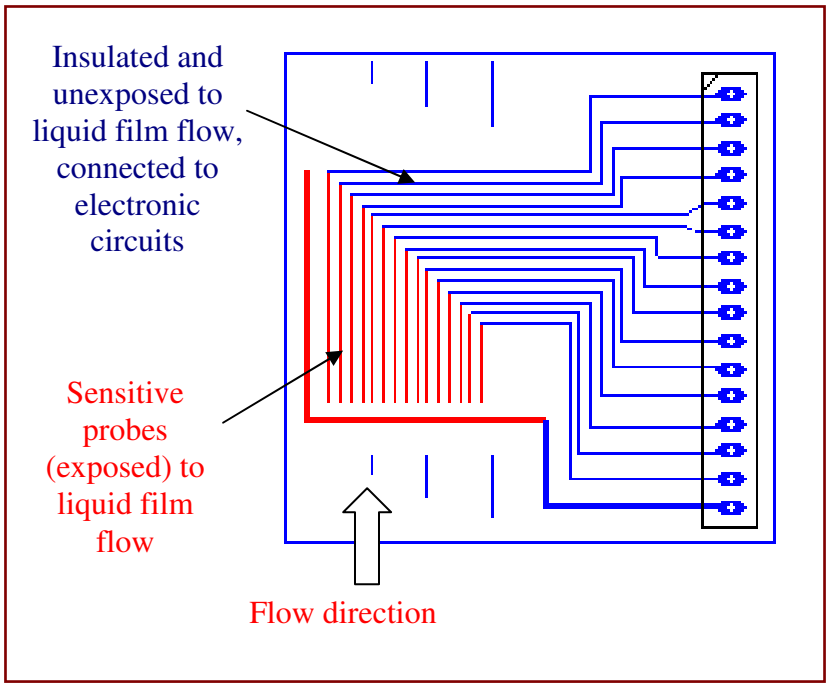

Figure 11-3: PCB layout of the Digital Liquid Film Level sensor (DLFLS)

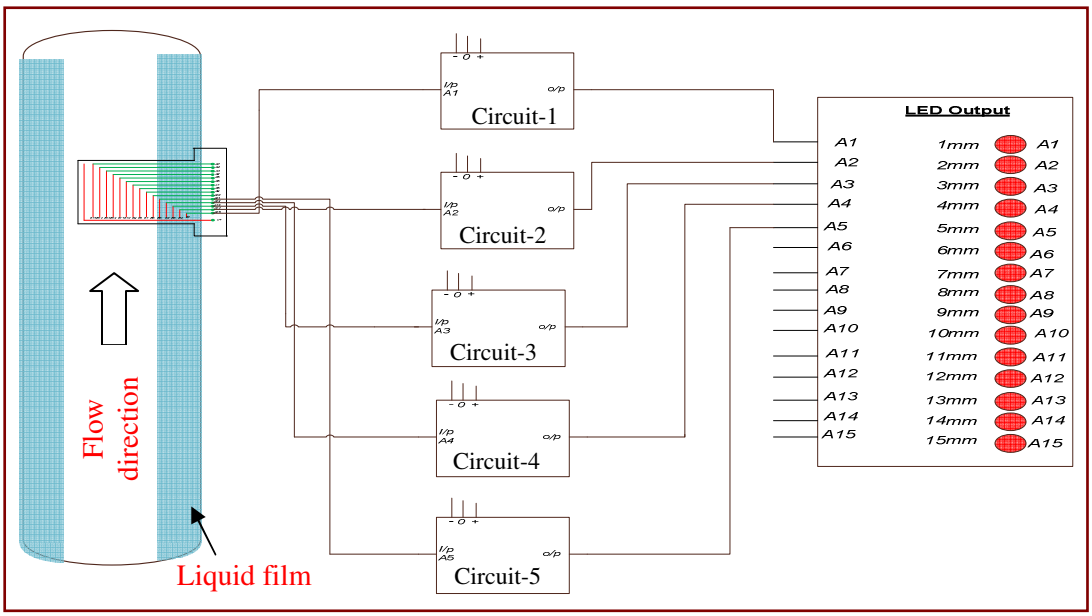

Figure 11-4: A schematic diagram of the DLFLS setup

11.4 An intermittent model for the slug flow regime

The separated flow model (i.e. vertical annular and horizontal stratified gas-water flows) was already investigated in Chapter 3. Slug flow models for horizontal and vertical flows through a Venturi are still elusive and have to be investigated. A possible model for slug flow could combine the homogenous flow model (described in Section 3.1) and the separated flow model (described in Section 3.2). If the intermittent model is used, instantaneous measurements of the differential pressure and the conductance impedance through the Venturi are required. The intermittent flow model (see Figure 11-4) can be treated as a combination of;

- Homogenous and separated flows or,
- Homogenous and single phase (gas) flows, especially, when the gas phase in slug flow is assumed to occupy the total area of the pipe.

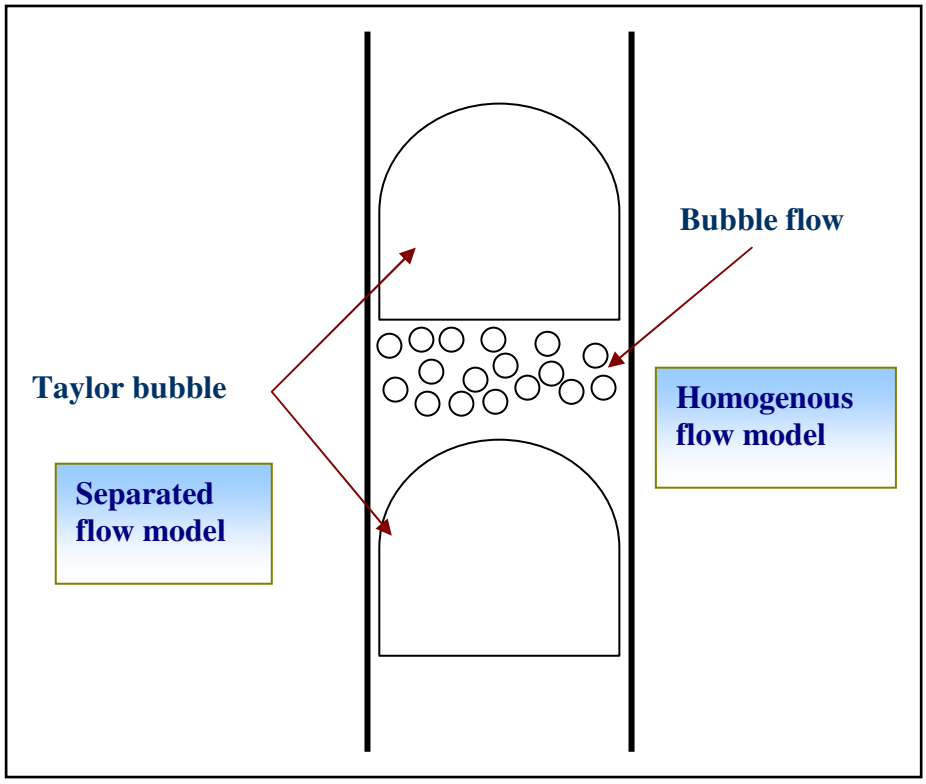

Figure 11-5: The intermittent flow model (a combination of the homogenous and separated flow model)

11.5 The proposed method of measuring the water mass flow rate in annular gas-water two phase flows

As mentioned earlier in Chapter 8, the modulus of the error in the predicted water mass flow rate using Equation (3.72) was greater than expected (>10%). The reasons of getting a quite big error in the water mass flow rate were due to;

- the assumption that the entire liquid flow existed in the liquid film (i.e. the water droplet flow rate was not included in the $\dot{m}_{w,wg}$ (Equation (3.72)).
- the pulsations in the water film flow (due to the limitation in the side channel blower RT-1900, see Section 6.2.5) which caused unsteady water film flow rate.

As a result of the above limitations, an alternative technique for measuring the total water mass flow rate in annular two phase flows is proposed. The proposed technique of measuring the total water mass flow rate in annular two phase flows is based on the Conductance Cross-Correlation Meter (CCCM) as shown in Figure 11-6. In other words, the inlet section of the Venturi meter (i.e. CIVFM, see Section 4.3)) could be replaced by the CCCM. Carrying out the experiments in a 50 mm internal diameter pipe instead of an 80 mm internal diameter pipe enables the side channel blower (RT-1900) to establish a stable water film flow. The new approach of measuring the total water mass flow rate in annular gas-water two phase flows is described below.

The water film thickness δ in annular gas-water two phase flows can be measured using the upstream conductance electrodes (or the downstream conductance electrodes) flush mounted with inner surface of the Conductance Cross-Correlation Meter, CCCM (see Figure 11-6). It should be noted that the calibration of the CCCM, the electronic circuits and the measurement technique used to measure the film thickness at the inlet of the Venturi are similar to that used for the conductance inlet void fraction meter, CIVFM described in Section 4.5 and Chapter 5. Once the film thickness δ is obtained the cross sectional area of the liquid film A_f can be determined using;

$$A_f = \pi\left\{R_{cccm}^2 - (R_{cccm} - \delta)^2\right\}$$

Equation (11.15)

where R_{cccm} is the pipe internal radius (the radius of the conductance cross-correlation meter, CCCM, see Figure 11-6) and δ is the film thickness.

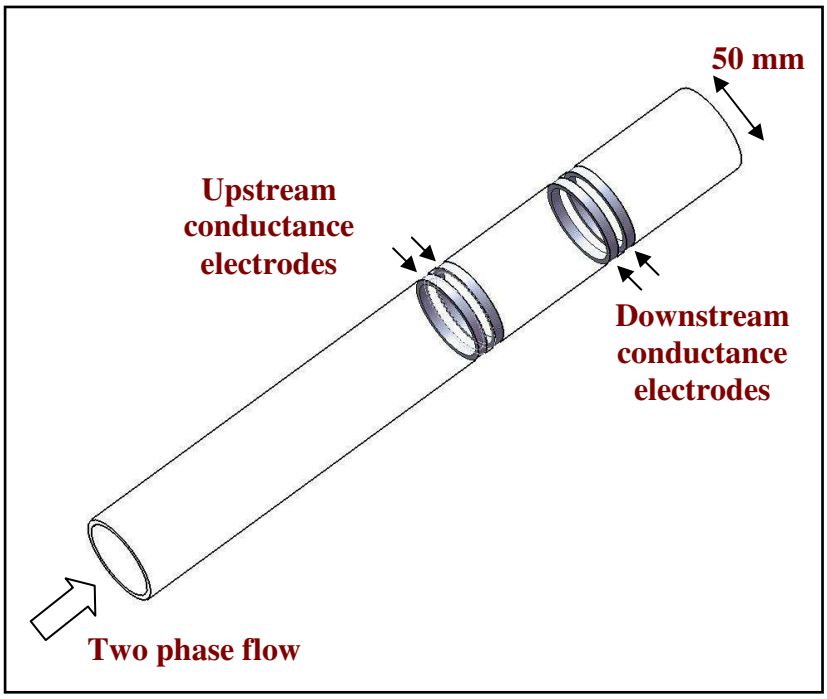

Figure 11-6: A conductance cross-correlation meter

The liquid film velocity $U_{f,corr}$ in annular flow can be determined by the conductance cross-correlation meter, CCCM using the conductance electronic circuit described in Section 4.5 (see also Section 2.1.2.6). Once the area of the water film A_f and the water film velocity $U_{f,corr}$ is obtained, the water film volumetric flow rate Q_{wf} can be determined using;

$$Q_{wf} = A_f U_{f,corr}$$

Equation (11.16)

It is well know that the reference water volumetric flow rate $Q_{w,ref,wg}$ (measured from the turbine flow meter-2, see Section 6.2.2) is the sum of the water film volumetric flow rate Q_{wf} and the water droplet volumetric flow rate Q_{wc} in the gas core. Therefore;

$$Q_{w,ref,wg} = Q_{wf} + Q_{wc}$$

Equation (11.17)

The water droplet volumetric flow rate in the gas core, Q_{wc} can be related to the "entrainment fraction" E using;

$$Q_{wc} = \frac{EQ_{wf}}{(1-E)}$$

Equation (11.18)

Combining Equations (11.16), (11.17) and (11.18) gives;

$$E = 1 - \frac{A_f U_{f,corr}}{Q_{w,ref,wg}}$$

Equation (11.19)

It is now possible to estimate the total water mass flow rate $\dot{m}_{total}$ in annular two phase flow using;

$$\dot{m}_{total} = \dot{m}_{wc} + \dot{m}_{wf}$$

Equation (11.20)

where $\dot{m}_{wc}$ is the water mass flow rate of the entrained water droplets and $\dot{m}_{wf}$ is the mass flow rate of the liquid film.

$\dot{m}_{wc}$ and $\dot{m}_{wf}$ in Equation (11.20) can be respectively given by;

$$\dot{m}_{wc} = \rho_w Q_{wc}$$

Equation (11.21)

and;

$$\dot{m}_{wf} = \rho_w Q_{wf}$$

Equation (11.22)

where ρ_w is the water density.

The percentage error in the predicted total water mass flow rate can be then expressed as;

$$\varepsilon_{\dot{m}_{total,wg}} = \frac{\dot{m}_{total,wg} - \dot{m}_{w,ref,wg}}{\dot{m}_{w,ref,wg}} \times 100\%$$

Equation (11.23)

where $\dot{m}_{w,ref,wg}$ is the reference water mass flow rate in annular (wet gas) flow obtained from multiplying the reference water volumetric flow rate $Q_{w,ref,wg}$ (obtained directly from the turbine flow meter-2, see Section 6.2.2) by the water density.

Combining the conductance cross-correlation meter (which is capable of measuring the gas volume fraction and the liquid film velocity at the inlet of the Venturi) with the conductance multiphase Venturi meter, CMVM described in Section 4.3 (which is capable of measuring the gas volume fraction at the throat of the Venturi) enables the gas and the water flow rate to be determined. In other words, the liquid flow rate could be measured from the conductance cross correlation meter while the CMVM in conjunction with the inlet gas volume fraction data provided by the cross-correlation meter could be used to measure the gas flow rate using the vertical annular flow model described in Section 3.2.2.

References

[1] Scott Bufton and Gene Thomas, "Calibration Requirements for Multiphase Meters," *3rd International Conference on Multiphase Metering Conference*, Aberdeen, Scotland: IBC UK Conference Limited, 1997.

[2] Nederveen, N., et al., "Wet Gas Flow Measurement," Paper Number 19077-MS , SPE Gas Technology Symposium. Dallas, Texas, 1989.

[3] A.D. Hall, "State-of-the art and the future of multiphase flowmeters," *The Future of Multiphase Metering*, London, UK: IBC UK Conference Limited, 1998.

[4] P. Mehdizadeh, *2006 Worldwide Multiphase and Wet Gas Metering Installations'*, 2007.

[5] K. Kelly, "Operating Experiences for the World's First Commercial Installed Multi-Phased Meters in the Liverpool Bay Field," *5th International Conference -Field Application & New Technologies for Multiphase Metering*, Aberdeen: IBC UK Conference Limited, 1999.

[6] E.F. Caetano, R.T.H. Machado, C.B. Kuchpil, Costa e Silva, and Borges Filho, "Multiphase Metering Qualification Process at PETROBRAS-field application stage," *5th International Conference -Field Application & New Technologies for Multiphase Metering*, Aberdeen: IBC UK Conference Limited, 1999.

[7] A. Humphrey, "Criteria For Selection of the Multiphase Meter for BP ETAP," *3rd International Conference on Multiphase Metering Conference*, Aberdeen, Scotland: IBC UK Conference Limited, 1997.

[8] P. Mehdizadeh, "Multiphase Measuring Advances Continue'," *Oil & Gas Journal*, vol. July 9, 2001.

[9] G.F. Hewitt, *Measurement of the two phase flow parameters*, London: Academic Press, 1978.

[10] G.W. Govier and K. Aziz, *The Flow of Complex Mixtures in Pipes*, Litton Educational, Inc. van Nostrand Ltd., 1972.

[11] Afshin J. Ghajar and Clement C. Tang, "Chapter 1: Advances in Void Fraction, Flow Pattern Maps and Non-Boiling Heat Transfer Two-Phase Flow in Pipes with Various Inclinations," *Advances in Multiphase Flow and Heat Transfer*, Advances in Multiphase Flow and Heat Transfer. eISBN: 978-1-60805-080-2, 2009.

[12] P. Spedding and D. Spence, "Flow regimes in two-phase gas-liquid flow," *International Journal of Multiphase Flow*, vol. 19, Apr. 1993, pp. 245-280.

[13] J.M. Mandhane, G.A. Gregory, and K. Aziz, "A flow pattern map for gas--liquid flow in horizontal pipes," *International Journal of Multiphase Flow*, vol. 1, Oct. 1974, pp. 537-553.

[14] D. Barnea, O. Shoham, Y. Taitel, and A. Dukler, "Flow pattern transition for gas-liquid flow in horizontal and inclined pipes. Comparison of experimental data with theory," *International Journal of Multiphase Flow*, vol. 6, Jun. 1980, pp. 217-225.

[15] R.N. Steven, "Wet gas metering with a horizontally mounted Venturi meter," *Journal of Flow Measurement and Inst.*, vol. 361-372, 2002, pp. 361-372.

[16] A.W. Jamieson, *Wet gas metering – The unexpected challenge status and trends on
technology and applications*, 2001.
[17] Department of Trade and Industry DTI, *Guidance Notes for Petroleum Measurement Under the Petroleum (Production) Regulations*, Licensing and Consents Unit, Issue 7: 2003.
[18] P. Mehdizadeh and J. Williamson, *Principles of Multiphase Measurements*, State of Alaska: Alaska Oil and Gas Conservation Commission, 2004.
[19] Dykesteen, Eivind, et al, *Handbook of Multiphase Metering*, Norwegian Society for Oil and Gas Measurement, published by NFOGM, 2005.
[20] R.W. Lockhart and R.C. Martinelli, "Proposed correlation of data for isothermal two-phase, two-component flow in pipes," *Chem. Eng. Prog.*, vol. 45, 1949, pp. 39–48.
[21] J. Couput, P. Gajan, V. de Laharpe, and A. Strzelecki, "Wet gas metering in the upstream area: needs, applications & developments.," Scotland: 18th North Sea Flow Measurement Workshop, 2000.
[22] P. Mehdizadeh and J. Marrelli, "Wet gas metering: trends in applications and technical developments," San Antonio, TX: SPE 77351, 2002 SPE Annual Technical Conference and Exhibition, 2002.
[23] NEL, *The Evaluation of Wet Gas Metering Technologies for Offshore Application: Part1 – Differential Pressure Meters, Flow Measurement Guidance Note*, no. 40, London, UK: 2003.
[24] Y. GENG, J. ZHENG, T. SHI, and G. SHI, "Wet Gas Meter Development Based on Slotted Orifice Couple and Neural Network Techniques," *Chinese Journal of Chemical Engineering*, vol. 15, Mar. 2007, pp. 281-285.
[25] ASME, The American Society of Mechanical Engineers, *Wet Gas Flowmetering Guideline*, Technical Report, ASME MFC-19G-2008: 2008.
[26] Y. Li, J. Wang, and Y. Geng, "Study on wet gas online flow rate measurement based on dual slotted orifice plate," *Flow Measurement and Instrumentation*, vol. 20, Aug. , pp. 168-173.
[27] J. Coad, *Finding and Using Oil*, Oxford: Heineman Library, 2009.
[28] Royal Dutch/Shell Group of Companies, *The Petroleum handbook*, Amsterdam; Oxford: Elsevier, 1966.
[29] W.-. Deckwer and A. Schumpe, "Improved tools for bubble column reactor design and scale-up," *Chemical Engineering Science*, vol. 48, 1993, pp. 889-911.
[30] J. Steinemann and R. Buchholz, "Application of an Electrical Conductivity Microprobe for the Characterization of bubble behavior in gas-liquid bubble flow," *Particle and Particle Systems Characterization*, vol. 1, 1984, pp. 102-107.
[31] M.P. Dudukovic, Y. Pan, and S. Degaleesan, "Experimental study of gas-induced liquid-flow structures in bubble columns," *AIChE Journal*, vol. 47, pp. 1913-1931.
[32] R. Lau, R. Mo, and W.S. Beverly Sim, "Bubble characteristics in shallow bubble column reactors," *Chemical Engineering Research and Design*, vol. 88, Feb. 2010, pp. 197-203.
[33] N.T. Thang, "A study of two-phase flow through Venturis," PhD, University of New South Wales, 1976.
[34] A. Prakash, A. Margaritis, H. Li, and M.A. Bergougnou, "Hydrodynamics and

local heat transfer measurements in a bubble column with suspension of yeast," *Biochemical Engineering Journal*, vol. 9, Dec. 2001, pp. 155-163.

[35] C. Tang and T.J. Heindel, "Estimating gas holdup via pressure difference measurements in a cocurrent bubble column," *International Journal of Multiphase Flow*, vol. 32, Jul. 2006, pp. 850-863.

[36] K. Tsuchiya and O. Nakanishi, "Gas holdup behavior in a tall bubble column with perforated plate distributors," *Chemical Engineering Science*, vol. 47, Sep. , pp. 3347-3354.

[37] S. Saxena and N. Rao, "Heat transfer and gas holdup in a two-phase bubble column: Air-water system -- Review and new data," *Experimental Thermal and Fluid Science*, vol. 4, Mar. 1991, pp. 139-151.

[38] H. Jin, S. Yang, M. Wang, and R. Williams, "Measurement of gas holdup profiles in a gas liquid cocurrent bubble column using electrical resistance tomography," *Flow Measurement and Instrumentation*, vol. 18, Oct. , pp. 191-196.

[39] H. Cui, J. Chaouki, and Mostoufi, "A Comparison of Two- and Single-Phase Models for Fluidized-Bed Reactors," vol. 40, pp. 119-127.

[40] J.A.M. Kuipers, W.P.M. van Swaaij, and P.J.G. Huttenhuis, "The effect of gas-phase density on bubble formation at a single orifice in a two-dimensional gas-fluidized bed," *Chemical Engineering Science*, vol. 51, pp. 5273-5288.

[41] J. Werther, "Measurement techniques in fluidized beds," *Powder Technology*, vol. 102, Apr. 1999, pp. 15-36.

[42] M. Asif, "Volume contraction behaviour of binary solid-liquid fluidized beds," *Powder Technology*, vol. 145, Jul. 2004, pp. 113-122.

[43] B.G. Ravelli S Perichizzi A, "Description, applications and numerical modelling of bubbling fluidized bed combustion," *Progress in Energy and Combustion Science*, vol. 34, pp. 224-253.

[44] Q. Zhang, C. Huang, D. Jiang, X. Wei, Z. Qian, and F. Wei, "Particle Measurement Sensor for in situ determination of phase structure of fluidized bed," *Particuology*, vol. 7, Jun. 2009, pp. 175-182.

[45] H. Piepers, H. Piepers, and Song, "Investigation on bubble characteristics in a gas fluidized bed," *Chemical Engineering Science*, vol. 52, pp. 829-841.

[46] S.D. Kim and Y. Kang, "Heat and mass transfer in three-phase fluidized-bed reactors--an overview," *Chemical Engineering Science*, vol. 52, Nov. 1997, pp. 3639-3660.

[47] J.W. Murdock, "Two-phase flow measurements with orifices," *Journal of Basic Engineering*, vol. 84, 1962, pp. 419-433.

[48] D. Chisholm, "Flow of Incompressible Two-Phase Mixtures Through Sharp-Edged Orifices," *Journal of Mechanical Engineering Science*, vol. 9, 1967, pp. 72-78.

[49] D. Chisholm, "Research note: Two-Phase Flow Through Sharp-Edged Orifices," *Journal of Mechanical Engineering Science*, vol. 19, 1977, pp. 128-130.

[50] R.V. Smith and J.T. Leang, "Evaluations of Correction For Two-Phase Flowmeter Three Current-One New," *Journal of Engineering for Power*, vol. 97, 1975, pp. 589-594.

[51] Z.H. Lin, "Two-phase flow measurements with sharp-edged orifices," *International Journal of Multiphase Flow*, vol. 8, 1982, pp. 683-693.

[52] de Leeuw, "Wet Gas Flow Measurement by Means of a Venturi Meter and a

Tracer Technique," *North Sea Flow Measurement Workshop, Norway, Shell Expro.*, Scotland: 1994.

[53] de Leeuw, "Liquid correction of Venturi meter readings in wet gas flow," *North Sea Flow Measurement Workshop, Norway, Shell Expro.*, The Netherlands: 1997.

[54] Abbas H. A. M. Hasan, "An Investigation of Homogenous and Non-Homogenous Two Phase Flow Model by Means of Venturi Meter," University of Huddersfield, 2005.

[55] A.J. Holt, B.J. Azzopardi, and Biddulph, "Calculation of two-phase pressure drop for vertical upflow in narrow passages by means of a flow pattern specific model," *Trans IChemE*, vol. 77, 1999, pp. 7-15.

[56] Chistophe Boyer, Anne-Marie Dquenne, and Gabriel Wild, "Measuring techniques
in gas-liquid and gas-liquid-solid reactors," *Chemical engineering Science*, vol. 57, 2002, pp. 3185-3215.

[57] Li-qiu Ping, Zhi-ming Wang, and Jian-guang Wei, "Pressure drop models for gas-liquid two-phase flow and its application in underbalanced drilling," *Journal of Hydrodynamics, Ser. B*, vol. 18, 2006, pp. 405-411.

[58] G. Matsui, "Identification of flow regimes in vertical gas-liquid two-phase flow using differential pressure fluctuations," *International journal of multiphase flow*, vol. 10, 1984, pp. 711-720.

[59] L.A. Glasqow, L.E. Erickson, C.H. Lee, and S.A. Patel, "Wall pressure fluctuations and bubble size distributions at several positions in an airlift fermentor," *Chemical engineering communications*, vol. 29, 1984, pp. 311-336.

[60] J. Drahos and J. Cermak, "Diagnostics of gas-liquid flow patterns in chemical engineering systems," *Chemical engineering and processing*, vol. 26, 1992, pp. 4069-4075.

[61] F. Jonhsson, R.C. Zijerveld, J.C. Schouten, C.M. van den Bleek, and B. Leckner, "Characterization of fluidization regimes by time-series analysis of pressure fluctuations," *International journal of multiphase flow*, vol. 26, 2000, pp. 663- 715.

[62] C.L. Spigt, *On the hydraulic characteristics of a boiling water channel with natural circulation*, University of Eindhoven: 1966.

[63] H.O. Olsen, *Theoretical and experimental investigation of impedance void meters*, Norway,: 1967.

[64] N.A. Tsochatzidis, T.D. Karapantsios, M.V. Kostoglou, and A.J. Karabelas, "A conductance probe for measuring liquid fraction in pipes and packed beds," *International Journal of Multiphase Flow*, vol. 18, 1992, pp. 653-667.

[65] Gui-Bo Zheng, Ning-De Jin, Xiao-Hui Jia, Peng-Ju Lv, and Xing-Bin Liu, "Gas–liquid two phase flow measurement method based on combination instrument of turbine flowmeter and conductance sensor," *International Journal of Multiphase Flow*, vol. 34, 1992, pp. 1031-1047.

[66] M. Fossa, "Design and performance of a conductance probe for measuring the liquid fraction in two-phase gas-liquid flows," *International Journal of Multiphase Flow*, vol. 9, 1998, pp. 387-397.

[67] E.A. Hammer and G.A. Johansen, "Measurement Principles in Multiphase Metering- Their Benefits and Limitations," *The Future of Multiphase Metering*, London, UK: IBC UK Conference Limited, 1998.

[68] James Cory, "The Measurement of Volume Fraction and Velocity Profiles in Vertical and Inclined Multiphase Flows," University of Huddersfield, 1999.
[69] Nickolaos Panagiotopoulos, "Measurement of the Local Properties of Multiphase Flows," University of Huddersfield, 2009.
[70] M. Abouelwafa, A. Sami, E. Kendall, and M. John, "The Use of Capacitance Sensors for Phase Percentage Determination in Multiphase Pipelines," *IEEE Instrumentation and Measurement Society*, vol. 29, 1980, pp. 24 - 27.
[71] M.H. Chun and C.K. Sung, "Parametric effects on the void fraction measurement
by capacitance transducers," *International Journal of Multiphase Flow*, vol. 12, 1986, pp. 627–640.
[72] J. Maxwell, *A Treatise on Electricity and Magnetism*, Clarendon Press, Oxford, 1881.
[73] K.H. Albusaidi, "An investigation of multiphase flow metering techniques.," PhD Thesis, University of Huddersfield, 1997.
[74] V. Beek, "Dielectric behavior of heterogeneous system," Progr. Dielec., 1967, pp. 76-77 and 92-101.
[75] T.S. Ramu and Y. Rao, "On the Evaluation of Conductivity of Mixtures of Liquid Dielectrics," *IEEE Transactions on Electrical Insulation*, vol. EI-8, 1973, pp. 55-60.
[76] M.T. Shu, C.B. Weinberger, and Y.H. Lee, "A simple capacitance sensor for void fraction measurement in two-phase flow," *Ind. Eng. Chem. Fundam*, vol. 21, 1982, pp. 175–181.
[77] E.F. May, B.F. Graham, A.S. Chauhan, and R.D. Trengove, "Shear and electrical property measurements of water-in-oil emulsions and implications for multiphase flow meters," *Energy Fuels*, vol. 22, 2008, pp. 3308–3316.
[78] P.B. Whalley, "Handbook of Multiphase Systems. Edited by G. HETSRONI. Hemisphere/McGraw Hill, 1982. 1492 Pp. US $64.50," *Journal of Fluid Mechanics*, vol. 129, 1983, pp. 500-502.
[79] M.S.A. Abouelwafa and E. Kendall, "The measurement of component ratios in multiphase systems using alpha -ray attenuation," *Journal of Physics E: Scientific Instruments*, vol. 13, 1980, pp. 341-345.
[80] M. Petrick and B.S. Swanson, "Radiation attenuation method of measuring density of a two-phase fluid," *The Review of Scientific Instruments*, vol. 29, 1958, pp. 1079-1085.
[81] G.P. Lucas, "The Measurement of Two-Phase Flow Parameters in Vertical and Deviated Flows," PhD, University of Manchester Institute of Science and Technology, 1987.
[82] A.V. Smith, "Fast response multi-beam X-ray absorption technique for identifying phase distributions during steam–water blowdowns," *Journal of the British Nuclear Energy Society*, vol. 14, 1975, pp. 227–235.
[83] R.D. Wesley, "Performance of drag-disc turbine and gamma densitometer in LOFT," USNRC, Proceedings of Meeting of Review Group on Two-Phase Flow Instrumentation, NUREG-0375 (Paper No. 15), 1977.
[84] A. Chan and S. Banerjee, "Design aspects of gamma densitometers for void fraction measurements in small scale two-phase flows," *Nuclear Instruments and Methods in Physics Research*, vol. 190, Nov. 1981, pp. 135-148.
[85] G. Sonneck, *On the computation of the density of a two-phase mixture using data from a three-beam gamma densitometer*, Osterreichisches

Forschungszentrum Seibersdrof, Austria, Report OEFZS-4206: 1983.
[86] C. Bishop and G. James, "Analysis of multiphase flows using dual-energy gamma densitometry and neural networks," *Nuclear Instruments and Methods in Physics Research Section A: Accelerators, Spectrometers, Detectors and Associated Equipment*, vol. 327, Apr. 1993, pp. 580-593.
[87] E. Åbro and G.A. Johansen, "Improved void fraction determination by means of multibeam gamma-ray attenuation measurements," *Flow Measurement and Instrumentation*, vol. 10, Jun. 1999, pp. 99-108.
[88] H.A. Johnson and A. Abou-Sabe, "Heat transfer and pressure drop for turbulent flow of air-water mixtures in a horizontal pipe," *Transactions of the ASME*, vol. August, 1952, pp. 77-985.
[89] E.A. Hammer, "Three component flow measurement in oil/gas/water mixtures using capacitance transducers," Ph.D. thesis, University of Manchester, 1983.
[90] K. Cho, S. Kim, and Y. Lee, "A fast EIT image reconstruction method for the two-phase flow visualization," *International Communications in Heat and Mass Transfer*, vol. 26, Jul. 1999, pp. 637-646.
[91] D. Schmitz and D. Mewes, "Tomographic imaging of transient multiphase flow in bubble columns," *Chemical Engineering Journal*, vol. 77, Apr. 2000, pp. 99-104.
[92] T. Dyakowski, "Process tomography applied to multi-phase flow measurement," *Measurement Science and Technology*, vol. 7, 1996, p. 343.
[93] D.L. George, J.R. Torczynski, K.A. Shollenberger, T.J. O'Hern, and S.L. Ceccio, "Validation of electrical-impedance tomography for measurements of material distribution in two-phase flows," *International Journal of Multiphase Flow*, vol. 26, Apr. 2000, pp. 549-581.
[94] M. Byars, "Developments in electrical capacitance tomography," Hannover, Germany: Keynote Review Paper presented at the Second World Congress on Industrial Process Tomography, 2001.
[95] S. Liu, H. Wang, F. Jiang, R. Yan, X. Dong, and W.Q. Yang, "ECT Visualization of Two Phase Flows," *Volume 1*, Manchester, England: 2004, pp. 443-449.
[96] M. Soleimani, "A Shape Reconstruction Method for Two Phase Materials Using Resistance Tomography Data," *Fluids Engineering*, Orlando, Florida, USA: 2005, pp. 771-774.
[97] I. Ismail, J. Gamio, S. Bukhari, and W. Yang, "Tomography for multi-phase flow measurement in the oil industry," *Flow Measurement and Instrumentation*, vol. 16, 2005, pp. 145-155.
[98] N.W. King and G.L. Purfit, "Design and operation of a test facility for evaluating
water-in-oil samples," London: BHRA 2nd International Conference on Multi-Phase Flow (Paper J3), 1985.
[99] G. Falcone, G.F. Hewitt, and C. Alimonti, *Multiphase Flow Metering: Principles and Applications: 54*, Elsevier Science, 2009.
[100] N. Adorni, F. Casagrande, and L. Cravorolo, *Experimental data on two-phase adiabatic flow; liquid film thickness, phase and velocity distributions, pressure drops in vertical gas-liquid flow*, CISE Report R35 (EUREAC 150): 1961.
[101] F.A. Schraub, "Isokinetic Sampling Probe Techniques Applied to Two Component, Two-Phase Flow," *ASME*, vol. Paper No. 67-WA/FE-28, 1966.
[102] G.F. Hewitt and L.G. Gill, "Sampling probe studies of gas core in annular two-

phase flow -- 3," *Chemical Engineering Science*, vol. 23, 1968, pp. 677-686.
[103] G.J. Zhang and M. Ishii, "Isokinetic sampling probe and image processing system for droplet size measurement in two-phase flow," *International Journal of Heat and Mass Transfer*, vol. 38, Jul. 1995, pp. 2019-2027.
[104] R. Moissis and N.A. Radovcich, "Two phase flow through a vertical Venturi," *Heat transfer conference AIChE-ASME*, Boston: 1963.
[105] R.A. Herringe, "Slurry flow metering by pressure differential devices," *International Journal of Multiphase Flow*, vol. 3, 1977, pp. 285-298.
[106] N.T. Thang and M.R. Davis, "The structure of bubbly flow through venturis," *International Journal of Multiphase Flow*, vol. 5, 1979, pp. 17-37.
[107] N.T. Thang and M.R. Davis, "Pressure distribution in bubbly flow through venturis," *International Journal of Multiphase Flow*, vol. 7, 1981, pp. 191-210.
[108] B.J. Azzopardi and A.H. Govan, "The modelling of Venturi scrubbers," *Filtration and separation*, vol. 21, 1984, pp. 196-200.
[109] R. Kowe, J.C.R. Hunt, A. Hunt, B. Couet, and L.J.C. Bradbury, "The effects of bubbles on the volume fluxes and the pressure gradients in unsteady and non-uniform flow of liquids," *International Journal of Multiphase Flow*, vol. 14, 1988, pp. 587-606.
[110] B. Couët, J.C.R. Brown, and A. Hunt, "Two-phase bubbly-droplet flow through a contraction: Experiments and a unified model," *International Journal of Multiphase Flow*, vol. 17, 1990, pp. 291-307.
[111] A. Wolf, "Film structure of vertical annular flow," PhD, Imperial college, 1995.
[112] C. Boyer and H. Lemonnier, "Design of a flow metering process for two-phase dispersed flows," *International Journal of Multiphase Flow*, vol. 22, 1996, pp. 713-732.
[113] J.R. Fincke, "Performance Characteristics of an Extended Throat Flow Nozzle for the Measurement of High Void Fraction Multi-phase flows," *4th International Symposium Fluid Flow Measurement*, 1999.
[114] S. Guet, S. Decarre, V. Henriot, and A. Line, "Void fraction in vertical gas-liquid slug flow: influence of liquid slug content," *Journal of Chemical engineering science*, vol. 61, 2006, pp. 7336-7350.
[115] Frang Lide, Zhang Tao, and Jin Ningde, "A comparison of correlations used for venturi wet gas metering in oil and gas industry," *Journal of Petroleum science & engineering*, vol. 57, 2006, pp. 247-256.
[116] G.L. Shires, *A comparison of two-phase venturi measurements at high and low pressure*, UK: 1966.
[117] F.C. Lowell and F. Hirschfeld, "Acoustic flow meters for pipelines," *Mech. Eng.*, vol. 101, 1979, pp. 29–35.
[118] J.S. Gudmundsson and H.K. Celius, "Gas–liquid metering using pressure-pulse technology," Houston: SPE 56584 presented at the SPE Annual Technical Conference and Exhibition, 1999.
[119] M. Aritomi, S. Zhou, M. Nakajima, Y. Takeda, M. Mori, and Y. Yoshioka, "Measurement System of Bubbly Flow Using Ultrasonic Velocity Profile Monitor and Video Data Processing Unit.," *Journal of Nuclear Science and Technology*, vol. 33, 1996, pp. 915-923.
[120] D. Horvat, J. Mozina, I. zun, and M. Perpar, "Laser ultrasonics for bubbly flow detection," *Ultrasonics*, vol. 36, Feb. 1998, pp. 565-568.

[121] Y. Murai, Y. Tasaka, Y. Nambu, Y. Takeda, and S.R. Gonzalez A., "Ultrasonic detection of moving interfaces in gas-liquid two-phase flow," *Flow Measurement and Instrumentation*, vol. In Press, Corrected Proof, 2010.
[122] S. Rouhani, "Application of the turbine-type flowmeters in the measurement of steam quality and void," Oslo: Presented at the Symposium on In-Core Instrumentation, 1964.
[123] S. Rouhani, "Measuring techniques," Von Karman Institute of Fluid Dynamics, Lecture Series 71, Two-phase flows in application to Nuclear Reactor Design Problems., 1974.
[124] I. Aya, *A model to calculate mass flow rates and other quantities of two-phase flow in a pipe with a densitometer, a drag disc, and a turbine meter*, November, ORNL/TM-4759: 1975.
[125] N.O. Clark, "A Meter for the Measurement of the Properties and Quantity of Foam," *Journal of Scientific Instruments*, vol. 23, 1946, pp. 256-259.
[126] A.E. Arave and L.D. Goodrich, *Drag discs, turbine steam-water two-phase flow tests*, Nuclear Technology Division Annular Progress Report. ANCR-1177, pp. 252–255: 1974.
[127] P.N. Kamath and I. Lahey, *A turbine-meter evaluation model for two-phase transients (TEMT)*, Report prepared for EG & G Idaho Inc., #RPI Institute, Report NES-459: 1977.
[128] P. Mark, M. Johnson, J. Sproston, and B. Millington, "The turbine meter applied to void fraction determination in two-phase flow," *Flow Measurement and Instrumentation*, vol. 1, Oct. 1990, pp. 246-252.
[129] M.W. Johnson and S. Farroll, "Development of a turbine meter for two-phase flow measurement in vertical pipes," *Flow Measurement and Instrumentation*, vol. 6, Oct. 1995, pp. 279-282.
[130] J.M. Foussat and J.P. Hulin, "Vertical liquid–liquid and liquid–gas two phase flow
measurement with a vortex flowmeter," Nancy, France: IUTAM Symposium on Measuring Technique in Gas Liquid Two-Phase Flow, 1983.
[131] J. Hulin, C. Fierfort, and R. Coudol, "Experimental study of vortex emission behind bluff obstacles in a gas liquid vertical two-phase flow," *International Journal of Multiphase Flow*, vol. 8, Oct. 1982, pp. 475-490.
[132] R. Baxter and J.E. Deacon, "Tests on turbine, vortex and electromagnetic flowrates in two phase air–water upward flow," Coventry, England: International Conference on Physical Modelling of Multi-Phase Flow, 1983.
[133] Sun, Z. Q. et al, "On measurement property of vortex flowmeter in bubbly two-phase flows," China: Proceedings of the 5th International Symposium on Measurement Techniques for Multiphase Flows, 2006.
[134] M. Beck and A. Plaskowski, *Cross-correlation Flowmeters: Their Design and Applications*, Institute of Physics Publishing, 1987.
[135] L. Cimorelli and R. Evangelisti, "Experimental determination of the "slip ratio" in a vertical boiling channel, under adiabatic conditions at atmospheric pressure," *International Journal of Heat and Mass Transfer*, vol. 12, Jun. 1969, pp. 713-726.
[136] R.J.N. Bernier, *Unsteady two-phase flow instrumentation and measurement*, Report no: E200.4 Division of &gineering and Applied Science, California Institute of Technology.: 1981.
[137] W. Matthes and W. Riebold, "Measurement of the velocity of gas bubbles in

water by a correlation method," *Review of Scientific Instruments*, vol. 41, 1970, pp. 843-845.
[138] H. Murakawa, H. Kikura, and M. Aritomi, "Application of ultrasonic multi-wave method for two-phase bubbly and slug flows," *Flow Measurement and Instrumentation*, vol. 19, 2008, pp. 205-213.
[139] S. Jung, J. Kim, J. Kim, and T. Kwon, "Flow-rate measurements of a dual-phase pipe flow by cross-correlation technique of transmitted radiation signals," *Applied Radiation and Isotopes*, vol. 67, 2009, pp. 1254-1258.
[140] O.C. Jones Jr. and N. Zuber, "The interrelation between void fraction fluctuations and flow patterns in two-phase flow," *International Journal of Multiphase Flow*, vol. 2, Dec. 1975, pp. 273-306.
[141] Fang Lide and Zhang Tao, "Performance of a Horizontally Mounted Venturi in Low-pressure Wet Gas Flow," *Chinese Journal of Chemical Engineering*, vol. 16, 2008, pp. 320-324.
[142] J. Agar and D. Farchy, "Wet Gas Metering Using Dissimilar Flow Sensor: Theort and Field Trial Results," *SPE Annual Technical Conference and Exhibition*, San Antonio, Texas: Society of Petroleum Engineers, SPE 77349, 2002.
[143] R.W. Miller, *Flow measurement engineering handbook*, New York : McGraw-Hill, 1996.
[144] Abbas H. A. M. Hasan and G.P. Lucas, "Modeling of a homogenous gas-water two phase flow through a Venturi and vertical pipe; (A prediction of pressure drop sign change in two phase flow)," *School of Computing and Engineering AnnualResearchers' Conference*, University of Huddersfield, UK: School of Computing and Engineering, University of Huddersfield, 2007.
[145] Abbas H. A. M. Hasan and G.P. Lucas, "Simulation and Static Measurement of the Gas Volume Fraction in a Separated Flow Model Using a Conductance Multiphase Venturi Meter (CMVM)," *The proceedings of the Computing and Engineering Annual Conference*, Huddersfield, UK: University of Huddersfield, 2008, pp. 69-74.
[146] D. Halmi, "Metering Performance Investigation and Substantiation of the "Universal Venturi Tube" (UVT), Part 1- Hydraulic Shape and Discharge Coefficient.," *Journal of Fluid Engineering*, vol. 73-WA/FM-3, 1974, pp. 124-131.
[147] Q. Al-Yarubi, "Phase Flow Rate Measurements of Annular Flows," PhD (to be submitted in 2010), University of Huddersfield, 2010.
[148] M. Coney, "The theory and application of conductance probes for the measurement of liquid film thickness in two-phase flow," *Journal of Physics E: Scientific instruments.*, 1973.
[149] Abbas H. A. M. Hasan and G.P. Lucas, "Experimental and theoretical study of the gas-water two phase flow through a conductance multiphase Venturi meter in vertical annular (wet gas) flow," *Nuclear Engineering and Design Journal*, vol. (Accepted, under publication), 2010.
[150] yokogawa, "User's Manual: Model EJA110A, EJA120A and EJA130A Differential Pressure Transmitters," 2002.
[151] R.B. Benedict, *Fundamentals of Pipe Flow*, New York, U.S.A: John Wiley & Sons, 1980.
[152] B.S. Massey, *Mechanics of Fluids*, London, U.K: Chapman & Hall, 1989.
[153] Abbas H. A. M. Hasan and G.P. Lucas, "MODELLING AND

MEASUREMENT OF THE GAS FLOW RATE IN VERTICAL ANNULAR GAS-WATER FLOW USING A 'CONDUCTANCE MULTIPHASE VENTURI METER'," *What Where When Multi-dimensional Advances for Industrial Process Monitoring*, Leeds, UK: University of Leeds, 2009.

[154] Fang Lide, Zhang Tao, and Xu Ying, "Venturi Wet Gas Flow Modeling Based on Homogeneous and Separated Flow Theory," *Mathematical Problems in Engineering Journal*, vol. 2008 (2008), Article ID 807287, 2008, pp. 1-25.

[155] M.R. Malayeri, J.M. Smith, and H. Steinhagen, "The behaviour of gas-liquid and vapour-liquid upward bubbly flows passing through a vertical Venturi," *Trans. IChemE*, vol. 79, 2001, pp. 371-375.

[156] K.J. Zanker, *The influence of air on the performance of differential pressure water flowmeters*, Report RR870, British Hydro-mechanics Research Association: 1966.

[157] S.G. Bankoff, "A variable density single-fluid model for two phase flow with particular reference to steam-water flow," *Tran. A.S.M.E., Journal of Heat Transfer*, vol. series C, 82, 1960, p. 265.